Univerza v Ljubljani

Fakulteta za elektrotehniko

Aljaž Velikonja

Električne lastnosti hidriranih ravninskih lipidnih dvoslojev

DOKTORSKA DISERTACIJA

Mentor: izr. prof. dr. Alenka Maček Lebar

Somentor: prof. ddr. Aleš Iglič

Ljubljana, 2014

Operacijo je delno financirala Evropska unija iz Evropskega socialnega sklada. Operacija se je izvajala kot državna pomoč Operativnega programa razvoja človeških virov za obdobje 2007–2013. Vanjo sem bil vključen prek razvojnega oddelka podjetja SMARTEH Raziskave in razvoj procesne opreme d. o. o. iz Tolmina.

Lipidi kot umetnost

Fotografija, ki nosi naslov Apokalipsa, je nastala kot posnetek zaslona pri opazovanju dogajanja pod mikroskopom pri nanosu kemikalije z lipidom na že predhodno nanešeno kemikalijo za tvorjenje podpornega torusa na teflonsko folijo. Test je pomemben za študij obnašanja različnih kemikalij pri obdelavi teflonske folije. Pojav ne nastane vsakokrat, odvisen je od mešanice kemikalij, vrste uporabljenega lipida ter tipa teflonske folije. Ko nastane, traja približno 2 sekundi in potem izgine. Površina fotografije je približno 1 mm^2.

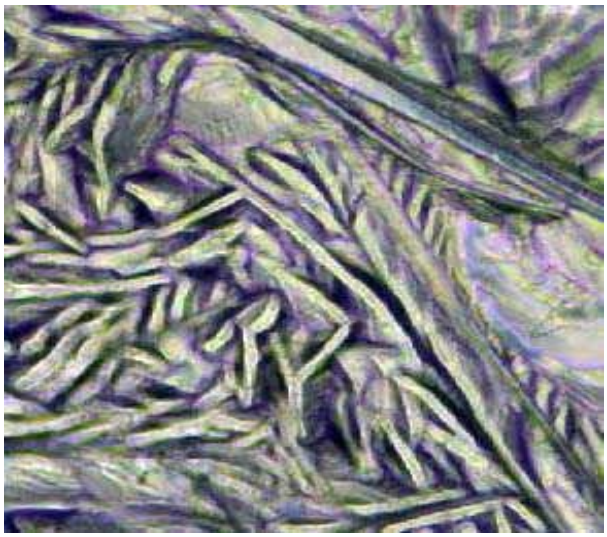

Zahvala

Hvala Evropski uniji oziroma Evropskemu socialnemu skladu in podjetju SMAR-TEH d. o. o. iz Tolmina za sofinanciranje doktorskega študija in za sofinanciranje objave prvega znanstvenega članka. Še posebej hvala direktorju Miroslavu Črvu, šefu razvoja Dragu Rijavcu ter vodji finančne službe Petri Marušič.

Hvala mentorici, izr. prof. dr. Alenki Maček Lebar, uni. dipl. inž. el., za ves trud in obilico vložene energije. Hvala za vse nasvete in še posebej za vse spodbude v trenutkih, ko ni šlo vse po zastavljenem načrtu.

Hvala somentorju, prof. ddr. Alešu Igliču, uni. dipl. inž. fiz., za dopolnitev študija s teoretičnimi modeli tako, da je študij skoraj postal način mojega življenja. Sedaj razumem tudi napis na podlogi računalniške miške v vašem kabinetu[1].

Hvala prof. dr. Damijanu Miklavčiču, uni. dipl. inž. el., predstojniku katedre za Biomedicinsko tehniko in Laboratorija za biokibernetiko na Fakulteti za elektrotehniko, da sem lahko gostoval v laboratoriju, še posebej se zahvaljujem za sofinanciranje objave prvega znanstvenega članka.

Hvala prof. dr. Nataši Poklar Ulrih, uni. dipl. kem., predstojnici Katedre za biokemijo in kemijo živil in Oddelka za živilstvo na Biotehniški fakulteti Univerze v Ljubljani, za ekstrakcijo arheolipidov iz termofilne arheje *Aeropyrum Pernix K1*.

Hvala prof. dr. Dejanu Križaju, uni. dipl. inž. el., predstojniku Laboratorija za bioelektromagnetiko na Fakulteti za elektrotehniko, za izposojo učila

[1] "Želim si, da bi bil tako nor, kot me vidijo moji sodelavci." Loesje

ploščatega kondenzatorja za luknjanje teflonske folije.

Hvala asist. dr. Šarki Perutková iz Laboratorija za biofiziko na Fakulteti za elektrotehniko za pomoč pri spoznavanju teoretičnih modelov, ki obravnavajo električno nabito površino v stiku z raztopino soli in njihovih enačb, prirejenih za programsko okolje Matlab.

Hvala asist. dr. Izidorju Sabotinu, uni. dipl. inž. el., iz Laboratorija za alternativne tehnologije ter dr. Goranu Mijuškoviću, uni. dipl. inž. str., nekdanjemu raziskovalcu iz Laboratorija za odrezavanje (LABOD) s Fakultete za strojništvo, Univerze v Ljubljani, za pomoč pri luknjanju/vrtanju teflonske folije.

Hvala dr. Andražu Polaku, uni. dipl. inž. el., za sprotno zagotavljane pomoči in odpravo napak na Sistemu za elektroporacijo ravninskih lipidnih dvoslojev druge generacije.

Hvala Davorju Obradoviću, uni. dipl. bioteh., za nadgradnjo protokola za čiščenje teflonske komore.

Hvala Mateju Trunku, uni. dipl. inž. el., za izdelavo držala iz pleksi stekla za teflonsko folijo, ki je služilo kot pomoč pri vrtanju/prebadanju teflonske folije.

Hvala sodelavcem Laboratorija za biokibernetiko – s svojimi idejami, nasveti in pripombami ste prispevali k hitrejšemu reševanju problemov, ki so nastajali v času študija.

Hvala Ines Lemut, univ. dipl. slov., za lektoriranje dela doktorske disertacije v slovenskem jeziku.

Vsebina

Seznam uporabljenih simbolov in kratic

Simbol	Ime
A	površina lipidnega dvosloja
A/D	analogno-digitalni
α	razmerje med pozitivno električno nabitimi deli zviterionskih glav in ostalimi delci (ioni, vodne molekule) v področju glav
a_0	površina na lipidno molekulo
Ag/AgCl	srebro/srebrov klorid
AGI	arhetidil(glukozil)inozitol
AI	arhetidilinozitol
α_p	tekoče-kristalna faza
β	obratna vrednost termične energije
b	razdalja približanja (debelina Sternove plasti)
β_p	gel-kristalna faza
C	električna kapacitivnost
$C_{12}E_8$	oktaetilen glikol monododecil eter
Ca^{++}	kalcijev ion
$CaCl_2$	kalcijev klorid
C_{blm}	kapacitivnost ravninskega lipidnega dvosloja
c_{blm}	specifična kapacitivnost ravninskega lipidnega dvosloja
CE1, CE2	merilna elektroda
C_{diff}	diferencialna kapacitivnost
C_{DL}	kapacitivnost difuzijske plasti

Simbol	Ime
Cl^-	klorov ion
c_p	podgel ali kristalna faza
C_p	toplotna kapaciteta
C_S	kapacitivnost Sternove plasti
C_{sis}	kapacitivnost sistema brez lipidnega dvosloja
C_{sisblm}	kapacitivnost sistema z lipidnim dvoslojem
d	debelina ravninskega lipidnega dvosloja
D	razdalja med električno nabitima deloma glave lipidne molekule
D/A	digitalno-analogni
D_{np}	razdalja nanodelca od negativno električno nabite lipidne plasti
DPhPC	1,2-diphitanoil-sn-glicero-3-fosfoholin
DPPC	1,2-dipalmitoil-sn-glicero-3-fosfoholin
E	velikost električnega polja
ε_0	dielektrična konstanta (dielektričnost vakuma)
e_0	osnovni naboj
EDL	električna dvojna plast
ε_r	relativna dielektričnost raztopine soli
ε_{rd}	relativna dielektričnost ravninskega lipidnega dvosloja
ε_S	relativna dielektričnost Sternove plasti
f	frekvenca
φ	električni potencial
GC	Gouy-Chapman
HEPES	4-(2-hidroksietil)-1-piperazinetansulfonska kislina
i	električni tok
k	Boltzmannova konstanta
KCl	kalijev klorid
k_i	naklon tokovnega signala
L	Langevinova funkcija
Λ	normalizacijski faktor
L	lamelirana (ang. *lamellar*) struktura dvosloja
L_α	(lamelirana nezasukana) tekoče-kristalna faza

Simbol	Ime
L_{β}	(lamelirana nezasukana) gel-kristalna faza
L_{β}'	(lamelirana) zasukana gel-kristalna faza
LB	Langevin-Bikerman
L_c	(lamelirana nezasukana) podgel ali kristalna faza
LCR meter	merilnik impedance
LPB	Langevin-Poisson-Boltzmann
L_x	nezasukana faza
L_x'	zasukana faza
M	število impulzov
m	številska gostota dvovalentnih ionov
m_0/N_A	koncentracija dvovalentnih ionov
MLB	nadgrajen Langevin-Bikerman
MLPB	nadgrajen Langevin-Poisson-Boltzmann
n	lomni količnik vode
N	število meritev
n_-	številska gostota negativno električno nabitih ionov (anionov)
$n_{i,w}$	številska gostota ionov in vodnih molekul
n_+	številska gostota pozitivno električno nabitih ionov (kationov)
n_0/N_A	koncentracija enovalentnih ionov
n_{0w}/N_A	koncentracija molekul vode
n_{0h}/N_A	koncentracija pozitivno električno nabitih delov zviterionskih lipidnih glav
NaCl	natrijev klorid
NaOH	natrijev hidroksid (natrijeva baza)
n_h	številska gostota pozitivno električno nabitih delov zviterionskih lipidnih glav
n_s	številska gostota mrežnih mest
n_w	številska gostota vodnih molekul
OHP	zunanja Helmholtzova ravnina
P	valovita (ang. *ripple*) struktura dvosloja
P	vektor polarizacije vodnih molekul

Simbol	Ime
$\|P\|$	velikost vektorja polarizacije vodnih molekul
PB	Poisson-Boltzmann
P_{β}'	valovita (ang. *ripple*) faza
P_{bulk}	tlak zunaj sistema
Π	osmotski tlak
P_{inner}	lokalni tlak
POPC	1-palmitil 2-oleil fosfatidilholin
POPS	1-palmitil 2-oleil fosfatidilserin
$P(x)$	gostota verjetnosti, da se pozitivno električno nabiti deli glav zviterionskih lipidnih molekul nahajajo na razdalji x od lipidne plasti
p_0	dipolni moment vodne molekule
R	ohmska upornost
RE1, RE2	referenčna elektroda
SFG	vibracijska spektroskopija
ρ_a	volumska gostota električno nabitih amino delov lipidnih glav
ρ_{as}	volumska gostota električno nabitih amino in serinskih delov lipidnih glav
ρ_{free}	volumska gostota električno nabitih delcev v sistemu
ρ_{ions}	volumska gostota ionov
ρ_s	volumska gostota električno nabitih serinskih delov lipidnih glav
ρ_{zw}	volumska gostota pozitivno električno nabitih delov glav zviterionskih lipidnih molekul
σ, σ_1	površinska gostota električnega naboja na površini lipidne plasti
σ_2	površinska gostota električnega naboja na površini nanodelca
T	temperatura
t_{br}	življenjska doba ravninskega lipidnega dvosloja
T_{komora}	temperatura v temperaturni komori
TLC	tankoplastna kromatografija
T_m	temperatura faznega prehoda lipida
T_{prekat}	temperatura v prekatu teflonske komore
u	električna napetost

Simbol	Ime
U_{br}	porušitvena napetost ravninskega lipidnega dvosloja
ω	kot med pozitivno električno nabitim delom glave zviterionske molekule in normalo na lipidno plast
∇	Laplaceov operator

Povzetek

Osnovni gradnik membrane biološke celice je dvojna plast lipidnih molekul, pretežno sestavljena iz glicerofosfolipidov, proteinov ter drugih molekul. Čeprav je celična membrana nehomogena struktura, lahko nekatere njene osnovne fizikalne lastnosti dovolj dobro opišemo s študijem hidriranega ravninskega lipidnega dvosloja, sestavljenega izključno iz lipidnih molekul. Nekatere od teh lastnosti (npr. dolžina in nasičenost maščobnih verig) so odvisne tudi od temperature, zato se s temperaturo spreminjajo tudi lastnosti hidriranega ravninskega lipidnega dvosloja. Zaradi različnih faznih prehodov uporabljenih lipidnih dvoslojev nas je zanimalo, ali imajo uporabljene vrste lipidnih dvoslojev zaradi tega tudi drugačne električne lastnosti, ki so odvisne od temperature. Poleg eksperimentalnega študija električnih lastnosti hidriranih ravninskih lipidnih dvoslojev v odvisnosti od temperature smo proučevali tudi teoretične modele električne dvojne plasti v dotiku z raztopino soli.

Pri eksperimentih smo z uporabo Montal-Muellerjeve metode ali metode dvigovanja gladine za vzpostavitev hidriranega ravninskega lipidnega dvosloja proučevali kapacitivnost hidriranega ravninskega lipidnega dvosloja kot parameter debeline ravninskega lipidnega dvosloja ter porušitveno napetost kot parameter stabilnosti v električnem polju. Kapacitivnost je parameter, s katerim ocenjujemo kvaliteto hidriranega ravninskega lipidnega dvosloja. Oba parametra sta odvisna od materialnih lastnosti lipidnih dvoslojev, torej tudi od temperature. V teoretičnih modelih pa smo z Langevin-Poisson-Boltzmannovim in Langevin-Bikermanovim modelom študirali elektrostatične razmere v bližini ele-

ktrične dvojne plasti v dotiku z raztopino soli.

Prvo poglavje opisuje fizikalne lastnosti in zgradbo lipidne molekule ter lipidnega dvosloja, metode, ki se uporabljajo pri njihovem proučevanju, teoretične modele za študij elektrostatičnih lastnosti v bližini električne dvojne plasti v dotiku z raztopino soli ter poda namen dela. V drugem poglavju so podrobneje predstavljeni uporabljeni materiali in metode, v tretjem poglavju pa so podani in pokomentirani dobljeni rezultati. Četrto poglavje predstavi zaključke doktorske disertacije, njeni glavni prispevki pa so podrobneje navedeni v petem poglavju.

Eksperimentalni rezultati so pokazali, da so električni parametri hidriranega ravninskega lipidnega dvosloja odvisni od temperature oziroma od temperature faznega prehoda lipidnega dvosloja. Pri lipidnih dvoslojih, zgrajenih iz lipidnih molekul, ki na merjenem temperaturnem področju nimajo faznega prehoda, so električni parametri neodvisni od temperature. Pri lipidnih dvoslojih, zgrajenih iz lipidnih molekul, ki na merjenem temperaturnem področju imajo fazni prehod, pa so vidne spremembe v merjenih električnih parametrih. Teoretični rezultati so pokazali, da je v bližini zviterionske lipidne plasti močno električno polje, zaradi katerega pride do nasičenja in orientacije vodnih molekul. Zaradi tega se spremeni relativna dielektričnost raztopine soli in številska gostota vseh prostih delcev.

Ključne besede: hidrirani ravninski lipidni dvosloj, temperatura, električni parametri, Langevin-Poisson-Boltzmannov model, Langevin-Bikermanov model

Abstract

The hydrated planar lipid bilayer is a basic building block of biologic cell membranes. Although the cell membrane is a highly heterogeneous structure, composed of lipids, proteins, carbohydrates and other components, a large number of physical properties of biological cell membrane which are important in physiological processes can be studied also in pure planar lipid bilayer systems. Some of these properties (lipid tail length and saturation) are dependent also on the temperature, therefore temperature dependent properties can be studied. Due to different phase transition of used lipid bilayers, the different electrical properties of hydrated planar lipid bilayers can be expected. Besides experimental work, the hydrated planar lipid bilayer was also studied theoretically as electric double layer in contact with electrolyte.

In experimental work the electrical capacitance as parameter of the hydrated planar lipid bilayer thickness and breakdown voltage as parameter of the stability of the hydrated planar lipid bilayer in the electric field, were measured using Montal-Mueller folding method. Both measured parameters are dependent on the lipid bilayer properties, therefore also dependent on the temperature. In theoretical work the hydrated planar lipid bilayer was studied using Langevin-Poisson-Boltzmann and Langevin-Bikerman models, where hydrated planar lipid bilayer was presented as negatively charged surface in contact with salt solution containing just monovalent or mixed (monovalent and divalent) ions.

First chapter of this thesis briefly describes the basic properties of lipid molecule and planar lipid bilayer, methods used in their experimental and theoretical

investigation and gives the purpose of the work. Second chapter describes in detail used materials and methods. Third chapter depicts the key results and gives their discussion. Fourth chapter contains the conclusion of the thesis, which its main contributions are stated in chapter five.

Experimental results showed that electrical parameters of hydrated planar lipid bilayer are temperature dependent, especially from the phase transition temperature. When planar lipid bilayers were made from lipids with no phase transition on measured temperature interval the measured electrical parameters were practically constant, in contrary, when planar lipid bilayers were made from lipids with phase transition on measured temperature interval, measured electrical properties showed temperature related changes. Theoretical results showed that due to the high electric field in the close vicinity of the hydrated zwitterionic planar lipid bilayer there is high concentration and orientation of water molecules resulting in changed electrical permittivity and concentration of all free particles in the model.

Key words: hydrated planar lipid bilayer, temperature, electrical parameters, Langevin-Poisson-Boltzmann model, Langevin-Bikerman model

1 Uvod

Osnovni gradnik celične membrane je dvojna plast lipidnih molekul, ki jo sestavljajo različne vrste fosfolipidov in molekule glicerola. Celična membrana ima asimetrično strukturo, ki je posledica različnih vrst proteinov, glikolipidov in drugih gradnikov celične membrane, vgrajenih v njeno notranjo in zunanjo plast. Skrbi za selektiven pretok materiala med citoplazmo in izvencelično tekočino. Čeprav je celična membrana nehomogena in ukrivljena struktura, lahko njene osnovne fizikalne lastnosti dovolj dobro opišemo s študijem ravninskega lipidnega dvosloja, sestavljenega izključno iz lipidnih molekul [1, 2].

1.1 Osnovne lastnosti lipidnih molekul

Molekula lipida sestoji iz hidrofilnega dela (hidrofilne glave) in hidrofobnega dela (hidrofobnega repa). Večino membranskih lipidov uvrščamo med fosfolipide. Ti imajo polarno glavo z notranjo porazdelitvijo električnega naboja ter nepolarni rep. Polarna glava lipidne molekule je lahko navzven električno nevtralna ali pa ima neto negativni električni naboj. Pri glicerofosfolipidih sestavljata rep dve maščobni kislini (verigi), polarno glavo pa tvori alkohol, najpogosteje holin, serin ali etanolamin, vezan na glicerol preko fosfatne skupine. Polarna glava na zunaj električno nevtralne lipidne molekule je sestavljena iz pozitivnega in negativnega pola. Taka dipolna glava se imenuje tudi zviterionska. Ena najpomembnejših lastnosti lipidov v celičnih membranah je amfifilnost. Ta je posledica atomske zgradbe lipidne molekule. Glede na lastnosti in obliko posameznih vrst lipidnih

molekul so v vodnem okolju možne različne lipidne tvorbe, ki nastanejo v procesu samozdruževanja lipidnih molekul, med drugim micele in ravninski lipidni dvosloji [1, 2].

1.2 Ravninski lipidni dvosloj

Ravninski lipidni dvosloj je zgrajen iz dveh plasti lipidnih molekul, orientiranih tako, da polarne glave lipidnih molekul tvorijo zunanji plasti lipidnega dvosloja. Tipična debelina lipidnega dvosloja je za lipidne molekule, katerih maščobne kisline so sestavljene iz 10 do 20 ogljikovih atomov, približno 5 nm [1]. Preprosti lipidni dvosloji so zgrajeni izključno iz ene vrste lipidnih molekul. Lipidni dvosloji, ki skušajo še bolje posnemati celično membrano, pa so zgrajeni iz mešanice različnih lipidov [3], vsebujejo v lipidni dvosloj vgrajene različne proteine [4] ali holesterol [5] (slika 1.1). V ravninski lipidni dvosloj z namenom proučevanja spremenjenih lastnosti vgrajujemo tudi druge primesi, kot so na primer surfaktanti (npr. oktaetilen glikol monododecil eter ($C_{12}E_8$)) [6, 7].

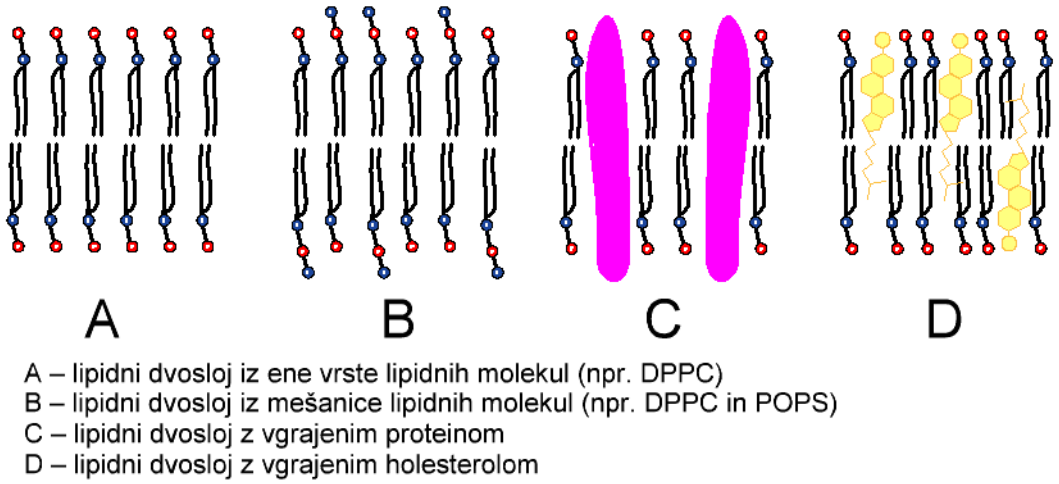

Slika 1.1: Lipidni dvosloj, zgrajen iz ene vrste lipidnih molekul (npr. DPPC) (A), mešanice lipidnih molekul (npr. DPPC in POPS) (B), z vgrajenim proteinom (C) in z vgrajenim holesterolom (D).

1.3 Faze lipidnih dvoslojev

Med lipidnimi molekulami delujejo vodikove vezi (med atomi vodika) ter privlačne ali odbojne London-Van der Waalsove in Coulombske sile [8]. Te sile so dovolj šibke, da lipidni dvosloj ni trdna, ampak elastična, lahko upogljiva struktura. Dolžina maščobnih verig in njihova nasičenost vplivata na temperaturo faznega prehoda lipidnega dvosloja in konfiguracijo lipidne molekule znotraj dvosloja. Daljša veriga maščobne kisline ima za posledico višjo temperaturo faznega prehoda med gel-kristalno in tekoče-kristalno fazo. Višja stopnja nasičenosti, ki jo določa število prisotnih dvojnih vezi, ima za posledico upognjenost verige maščobne kisline in s tem vpliv na konfiguracijo (prostorsko organiziranost) lipidne molekule. Omenjeni lastnosti maščobnih kislin, dolžina in nasičenost, poglavitno vplivata na elastične lastnosti lipidnega dvosloja in skupaj z elektrostatičnimi lastnostmi glav določajo različne faze lipidnih dvoslojev [2, 9]. Različne pozicije lipidnih molekul v lipidnem dvosloju, različne povprečne orientacije glav lipidnih molekul glede na daljšo (glavno) os glave, nagnjenosti oziroma zasuka-

nosti repov in glav lipidnih molekul (zaradi veliko prostostnih stopenj maščobnih kislin so tako možne različne postavitve lipidne molekule znotraj dvosloja) lahko pomembno znižajo prosto energijo sistema lipidnega dvosloja v stiku z raztopino soli pa tudi povečajo ali zmanjšajo površino na molekulo (površina, ki jo zasede ena lipidna molekula, gledano v smeri njene daljše osi) [2]. Ob upoštevanju vseh teh postavitev in konfiguracij lipidnih molekul znotraj dvosloja lahko dvosloj ob spreminjanju temperature prehaja skozi različne faze/podfaze [9] (slika 1.2). V grobem jih lahko razdelimo na tri faze (podgel (kristalno) fazo – c_p, gel-kristalno fazo – β_p in tekoče-kristalno fazo – α_p) in podfaze (nezasukano – L_x, zasukano – L_x' in valovito (ang. *ripple*) – P_β'). Oznaki L in P podajata, ali gre za lamelirano (ang. *lamellar*) ali pa za valovito (ang. *ripple*) strukturo dvosloja.

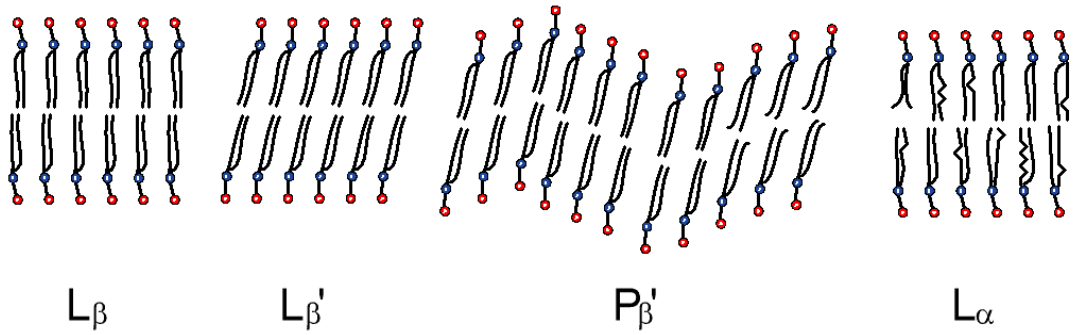

Slika 1.2: Faze lipidnih dvoslojev, predstavljene na dvoslojih, zgrajenih iz zvitterionskih molekul (npr.: DPPC). L_β predstavlja nezasukano gel-kristalno fazo, L_β' zasukano gel-kristalno fazo, P_β' valovito oziroma predfazo tekoče-kristalne faze in L_α predstavlja tekoče-kristalno fazo. Oznaki L in P podajata, ali gre za lamelirano (ang. *lamellar*) ali pa za valovito (ang. *ripple*) strukturo dvosloja.

Vsi lipidi pri spreminjanju temperature ne izkazujejo vseh faz. Nekateri lipidi kot npr. DPPC izkazujejo podgel ali kristalno fazo (L_c) pod posebnimi pogoji priprave in hrambe vzorca [10]. Za homogene lipidne dvosloje temperaturo faznega prehoda med gel-kristalno in tekoče-kristalno fazo imenujemo temperatura glavnega faznega prehoda lipida (T_m) (ang. *melting temperature*). Ta nastopi

takrat, ko sta v lipidnem dvosloju istočasno prisotni dve fazi. Nad to temperaturo ($T > T_m$) je dvosloj v tekoče-kristalni fazi (L_α). Lipidi se lahko prosto gibajo znotraj dvosloja. Čeprav so lipidi v tekoče-kristalni fazi bolj gibljivi, lahko vseeno prehajajo s površine membrane v raztopino, ki jo obdaja, kar je posledica hidrofobnosti repov. Po drugi strani pa je pod to temperaturo ($T < T_m$) lipidni dvosloj v gel-kristalni fazi (L_β). V tej fazi so lipidi bolj združeni, urejeni in togi. V bližini temperature faznega prehoda sta prisotni obe fazi, katerih rezultat so spremenjene lastnosti lipidnega dvosloja (debelina, večji odvod toplote ...) [11]. Za nehomogene lipidne dvosloje pa o temperaturi prehoda ne moremo govoriti, saj sta dve (ali več) fazi hkrati prisotni na večjem oziroma širšem temperaturnem območju. Pri mešanicah, sestavljenih iz lipidov, ki se razlikujejo le v razdalji maščobnih kislin, je mešanje skoraj idealno glede na teoretične modele. Pri mešanicah, sestavljenih iz lipidov, ki pa se razlikujejo v glavi lipida, mešanje postane manj idealno glede na teoretične modele [12]. Za ponazoritev prehajanja med fazami v odvisnosti od temperature se uporablja fazne diagrame. Poudariti je treba, da je temperatura faznega prehoda odvisna tudi od tega, ali lipidni dvosloj ogrevamo ali ohlajamo, saj nekateri lipidni sistemi izkazujejo histerezo [9, 13]. Na temperaturo faznega prehoda vpliva tudi hidracija lipidnega dvosloja. Bolj kot je lipidni dvosloj hidriran, bolj je zaradi amfifilnosti "vpet" v vodne molekule, zato ima temperaturo faznega prehoda pri višji temperaturi [14, 15].

1.4 Arheje in arheolipidi

Arheje predstavljajo eno najmanj raziskanih skupin mikroorganizmov. Večina znanih predstavnikov arhej je bila izoliranih iz ekstremnih okolij (slanih jezer, žveplenih vrelcev, kislih ali bazičnih vodà, močvirij ...) ali zelo specializiranih ekoloških niš. Membrane bakterij in evkariotov so sestavljene pretežno iz lipidov, ki so glicerolni estri, membrane arhej pa so sestavljene iz lipidov, ki so glicerolni etri, katerih vezi so enojne in zato kemijsko bolj odporne kot esterske vezi. Hidrofobni rep je v arheolipidih osnovan na dveh verigah izoprenoida, ki sta dolgi

verigi s stranskimi vejami. Te membrani arheje preprečujejo, da bi postala propustna oziroma bi se razgradila pri ekstremnih temperaturah. Arheje najpogosteje delimo med ekstremno halofilne, metanogene in hipertermofilne arheje. Slednje najbolje rastejo pri temperaturi nad 353 K, pod 333 K pa ne rastejo več. Njihov predstavnik je tudi *Aeropyrum pernix K1*, ki je prva nevtrofilna, hipertermofilna arheja. Večina hipertermofilnih arhej je anaerobnih, *Aeropyrum pernix K1* pa je eden redkih pravih aerobov. Optimalna temperatura rasti *A. pernix K1* je med 363 K in 368 K, optimalna pH vrednost okoli 7 in slanost 3,5 %. Arhejo *A. pernix K1* pridobivamo iz žveplenih vrelcev v bližini otoka Kodakarajima na Japonskem. Posebnost arheje *A. pernix K1* so lipidi, ki so drugačni od ostalih, do sedaj najdenih v hipertermofilih. *A. pernix K1* v membrani nima bipolarnega monosloja, ampak dvosloj, ki ga sestavljata dve vrsti lipidov: fosfolipid arhetidil(glukozil)inozitol (AGI) in arhetidilinozitol (AI). AGI ima za komponento polarne glave glukozo in inozitol, fosfat pa je povezan z inozitolom. Druga vrsta fosfolipida AI ima kot komponento polarne glave samo inozitol, ki je vezan na fosfat [16, 17, 18, 19].

1.5 Uporabljeni lipidi

Najpogosteje uporabljen lipid za proučevanje fizikalnih lastnosti lipidnih dvoslojev, odvisnih od temperature, je umetni lipid 1,2-dipalmitoil-sn-glicero-3-fosfoholin (DPPC) [20]. Omeniti velja še nekoliko modificiran lipid 1,2-diphitanoil-sn-glicero-3-fosfoholin (DPhPC), ki ima na maščobnih verigah še stranske veje in je zato – vsaj po strukturi repov – podoben nekaterim lipidom iz arhej. V skupini proučevanih lipidov najdemo tudi dva naravna lipida, lecitin in arheolipid iz arheje *Aeropyrum Pernix K1*. Iz literature je poznano, da je temperatura faznega prehoda (T_m) lipida DPPC pri 314 K, lecitina pri 327 K, arheolipid in lipid DPhPC pa še nimata potrjene temperature prehoda.

1.6 Metode za proučevanje lastnosti hidriranih lipidnih dvoslojev

Najpogosteje uporabljena metoda za proučevanje od temperature odvisnih lastnosti lipidnih dvoslojev je diferenčna dinamična kalorimetrija. Uporablja se za študij prehajanja toplote bodisi iz vzorca ali v vzorec pri njegovi fizikalni ali kemijski spremembi pri konstantnem tlaku. Obnašanje vzorca primerjamo z referenčnim vzorcem. Kalorimeter sestavljata dve celici, merilna in referenčna, ki ju običajno grejemo z električnim grelnikom z linearnim naraščanjem temperature. Ko pride do procesa, ki vključuje prehajanje toplote, inštrument prenese odvečno toploto v vzorec ali iz vzorca, da se ohrani ista temperatura kot v referenčni celici. Ta odvečna toplota je definirana kot toplotna kapaciteta vzorca C_p (pri konstantnem tlaku) [21]. Z metodo lahko detektiramo fazne prehode lipidnih dvoslojev v odvisnosti od temperature [17].

Metode sipanja rentgenskih žarkov (metode sipanja X-žarkov) omogočajo ugotavljanje strukturnih parametrov, kot so: površina na lipidno molekulo, debelina lipidnega dvosloja, razdalja med polarnimi glavami lipidov itn. [22]. Metode temeljijo na opazovanju jakosti sipanja rentgenskih žarkov na vzorcu. V splošnem jih delimo na elastične in neelastične. Elastične metode so pogosteje uporabljene, saj se pri neelastičnih pojavlja šum. Ker je debelina lipidnega dvosloja odvisna od povprečne dolžine ogljikovodikovih verig, ta pa od temperature, lahko ocenjujemo tudi stopnjo povprečne orientacije lipidnih molekul. Porazdelitvena funkcija povprečnega razmika med dvema glavama pa lahko služi kot mera za povprečno pozicijo lipidne molekule [9].

Poleg predhodno opisanih najpogosteje uporabljenih metod se za proučevanje temperaturno odvisnih lastnosti lipidnih dvoslojev uporablja tudi IR-spektroskopija [23], mikroskopija na atomsko silo (ang. *atomic force microscopy*) [11], elektronska mikroskopija [24], vibracijska spektroskopija SFG (ang. *sum-frequency generation Spectroscopy*) [14], kromatografija TLC (ang. *thin-layer*

Cromatography) [25], jedrska magnetna resonanca [26] in druge.

1.7 Meritev električnih lastnosti hidriranih lipidnih dvoslojev

Ravninski lipidni dvosloj lahko obravnavamo kot ploščati električni kondenzator [27, 28, 29, 30], zato lahko merimo njegovo kapacitivnost. Običajno jo podajamo kot kapacitivnost na enoto površine lipidnega dvosloja, zato jo definiramo kot specifična kapacitivnost lipidnega dvosloja ($\mu F/cm^2$). Kapacitivnost je parameter, ki se spreminja z debelino lipidnega dvosloja. Ker se ta spreminja s temperaturo, [13, 31] je od nje odvisna tudi kapacitivnost lipidnega dvosloja.

Začetki raziskovanj dvoslojev segajo v drugo polovico 17. in v začetek 18. stoletja, ko sta Robert Hooke [32] in Isaac Newton [33] opazovala odboj svetlobe na površini milnih mehurčkov. Newton je zapisal, da je v centru barvnih obročev videl rasti okroglo črno pego, znotraj nje pa kopico črnih pik, ki so bile videti boj črne oziroma temnejše od ostalega. Pri nadaljnjih poskusih je tako znotraj velike črne pege kot znotraj manjših peg opazil neizrazit odsev nekaterih predmetov, kot sta sonce in sveča. Sestavil je tudi tabelo, kjer je posamezni barvi pripisal določeno debelino mehurčka. Črna barva je ustrezala najdebelejši plasti.

Po Hookovi in Newtonovi analogni metodi je v začetku 60-tih let 20. stoletja Mueller s sodelavci [34, 35] tvoril črne membrane na odprtini med dvema prekatoma, ki sta bila napolnjena z raztopino soli. Na odprtino so nanesli lipidne molekule v mešanici topil. Odvečne molekule so se zaradi amfifilnosti lipidnih molekul zbirale na površini raztopine soli, dokler na odprtini ni ostal hidriran ravninski lipidni dvosloj (slika 1.3). Metoda je danes znana kot Mueller-Rudinova metoda za tvorjenje lipidnih dvoslojev oziroma kot metoda barvanja, saj lipide na odprtino med obema prekatoma nanašamo s čopičem. S pomočjo metode so lahko merili električne lastnosti tvorjene membrane. V 100 mM raztopini soli so izmerili specifično električno kapacitivnost 1 $\mu F/cm^2$, specifično upornost reda

velikosti $10^7\ \Omega\ cm^2$, pogosto tudi nad $10^8\ \Omega\ cm^2$ ter porušitveno napetost 150 mV–200 mV, ob kateri je prišlo do porušitve membrane. Ker lipide v mešanici topil nanašamo na odprtino, ki se nahaja v raztopini soli, je velika možnost, da se topila delno vgradijo v lipidni dvosloj in s tem spremenijo njegove lastnosti.

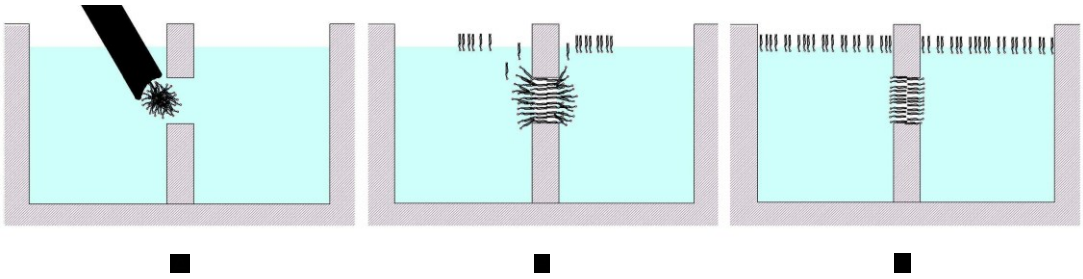

Slika 1.3: Mueller-Rudinova metoda za vzpostavitev hidriranega ravninskega lipidnega dvosloja ali metoda barvanja. (A) Na odprtino med obema prekatoma s čopičem pobarvamo oziroma nanesemo lipidne molekule. (B) Odvečne molekule se zaradi amfifilnosti lipidnih molekul zbirajo na površini, dokler na odprtini ne ostane hidriran ravninski lipidni dvosloj (C).

Leta 1970 je Stephen H. White [29] objavil študijo meritve specifične kapacitivnosti ravninskega lipidnega dvosloja, vzpostavljenega po metodi Mueller-Rudin. Pred njim so specifično kapacitivnost lipidnega dvosloja merili tudi drugi, vendar ne po isti metodi [36]. V študiji je med drugim ugotavljal, da je specifična kapacitivnost dvosloja odvisna tudi od temperature. Za lipidne dvosloje, zgrajene iz oksidiranega holesterola, raztopljenega v n-dekanu, je pokazal, da se kapacitivnost z naraščanjem temperature na temperaturnem intervalu med 291 K in 308 K zmanjšuje. To si je razlagal kot naraščanje debeline lipidnega dovosloja zaradi povečevanja volumna lipidnega dvosloja kot posledica višje temperature. Meritve je podkrepil tudi s teoretičnimi izračuni. V nadaljnjih študijah, v katerih je uporabljal glicerol monooleat, raztopljen v n-tetradekanu (z različnimi dolžinami verig), je dobil podobne rezultate [37, 38].

Leta 1972 sta Montal in Mueller [39] nadgradila Mueller-Rudinovo metodo.

Metoda je zmanjšala možnost za vgrajevanje topila v lipidni dvosloj. Danes je metoda poznana kot Montal-Muellerjeva metoda ali metoda dvigovanja gladine (slika 1.4). Pri tej metodi nanesemo lipide v mešanici topil na površino raztopine soli ter – še preden sta nivoja raztopine soli nad nivojem odprtine – še na odprtino. Po nekaj minutah naj bi topila izhlapela, tako se na odprtini med obema prekatoma ob vsakokratnem dvigu nivojev raztopine soli v obeh prekatih formira lipidni dvosloj, ki naj ne bi vseboval vgrajenih topil. Meritve specifične kapacitivnosti in porušitvene napetosti sta izvajala tako s tokovnimi kot z napetostnimi impulzi.

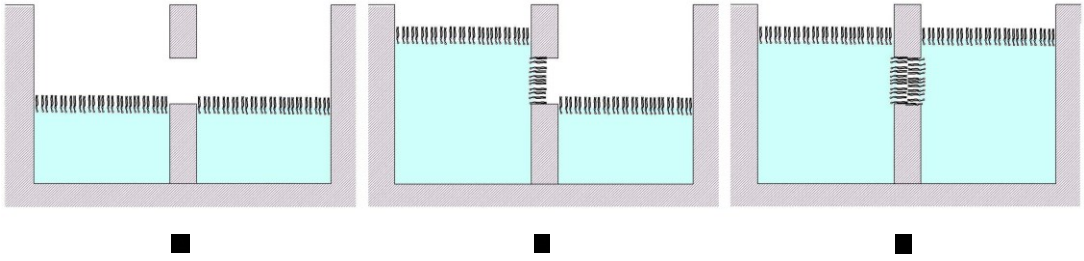

Slika 1.4: Montal-Muellerjeva metoda za vzpostavitev hidriranega ravninskega lipidnega dvosloja ali metoda dvigovanja gladine. (A) Na površini raztopine je v obeh prekatih plast lipidnih moleku. (B) Po dvigu prve gladine lipidi na odprtini tvorijo enosloj. (C) Po dvigu druge gladine se na odprtini med obema prekatoma tvori hidriran ravninski lipidni dvosloj.

Nadaljuje pa se tudi proučevanje električnih parametrov v odvisnosti od temperature. Leta 2003 Antonov in sodelavci [13] objavijo študijo meritve kapacitivnosti za lipidne dvosloje iz hidrogeniranega jajčnega lecitina. Študija je pokazala, da se pri ogrevanju kapacitivnost pri določeni temperaturi skokovito poveča, pri ohlajanju pa skokovito zmanjša. Ker temperaturi, pri katerih pride do skokovite spremembe kapacitivnosti, nista enaki, je med ohlajanjem in ogrevanjem opazna histereza, ki jo je prvi sicer opazil že White [38]. Raziskovalci pridejo do zaključka, da sta temperaturi približno enaki temperaturi faznega prehoda dveh glavnih lipidnih komponent hidrogeniranega jajčnega lecitina.

Raziskovalci so za določevanje električnih lastnosti lipidnih dvoslojev uporabljali tokovne ali napetostne impulze različnih amplitud, dolžin trajanj ter različnega števila [35, 39, 40]. Izkaže se, da uporaba impulzov za merjenje porušitvene napetosti ni najbolj primerna, saj nikoli vnaprej ne vemo, kakšno število impulzov moramo nastaviti in kakšna naj bo amplituda, da bo prišlo do porušitve lipidnega dvosloja. Dogajalo se je, da po vlaku M impulzov ni prišlo do porušitve, zato so vlaku dodali še en impulz (M+1) in poskusili znova. V kolikor je takrat prišlo do porušitve, ni nihče mogel oceniti, kakšno posledico je na lipidni dvosloj pri tem imel vlak prvih M impulzov in s tem kakšna je bila pri tem napaka izmerjene porušitvene napetosti. V izogib temu so leta 2007 Kramar in sodelavci [41] predlagali izboljšan protokol meritve porušitvene napetosti z uporabo linearno naraščajočega napetostnega signala. Tako so zagotovili, da je pri meritvi porušitvene napetosti lipidni dvosloj izpostavljen signalu le enkrat, ter da vsakokrat pride do porušitve lipidnega dvosloja.

V zadnjih letih se za študij električnih lastnosti lipidnih dvoslojev uporabljajo tudi druge metode, ki uporabljajo mikrostrukturo za tvorjenje večih lipidnih dvoslojev hkrati [42, 43] ali pa za stiskanje lipidnega mehurčka [44] v ravninski lipidni dvosloj, vendar te metode še niso uveljavljene.

1.8 Elektrostatični modeli ravninskega lipidnega dvosloja v dotiku z raztopino soli

V teoretičnih modelih površino ravninskega lipidnega dvosloja v stiku z raztopino soli obravnavamo kot sistem z električno nabito površino v stiku z raztopino soli. Pri lipidnih molekulah dipolno (zviterionsko) glavo v modelu predpostavimo tako, da je negativni pol glav prek glicerolnih skupin povezan s hidrofobnimi repi ter tvori negativno električno nabito površino, pozitivni deli glav pa so v stiku z raztopino soli, pri čemer je električni naboj pozitivnih delov glav volumsko porazdeljen. Površino zviterionskih lipidnih dvoslojev v stiku z raztopino soli lahko

opišemo tudi kot dipolno plast s spremenljivo orientacijo dipolov, ki je odvisna od zunanjih pogojev, kot so pH, temperatura ali koncentracija soli. Površino lipidnega sloja iz glicerofosfolipidnih molekul z neto negativnim električnim nabojem v stiku z raztopino soli obravnavamo kot naelektreno površino z negativno površinsko gostoto naboja [9, 27].

Prvi je sistem električno nabite površine v stiku z raztopino soli obravnaval Hermann von Helmholtz v začetku druge polovice 19. stoletja [45]. Opazil je, da se v bližini električno nabite elektrode, potopljene v raztopini soli, ioni, ki imajo isti predznak kot električno nabita elektroda, od elektrode odbijajo. Ioni, ki imajo nasproten predznak kot elektroda, pa se nabirajo pri elektrodi. Helmholtzov model je zagotovil dobro oceno potenciala pri električno nabiti površini, vendar je vseboval nekaj napačnih domnev kot na primer, da so ioni v sistemu homogeno porazdeljeni po vsej raztopini soli in da termično gibanje nanje nima vpliva [27].

Louis Gouy in David Leonard Chapman sta v začetku 20. stoletja z uporabo Poisson-Boltzmannove enačbe neodvisno drug od drugega nadgradila Helmholtzov model tako, da je predvideval odvisnost porazdelitve ionov znotraj raztopine soli v odvisnosti od razdalje od električno nabite površine [8, 46]. Desetletje kasneje sta Peter Joseph William Debye in Erich Hückel posplošila Gouy-Ghapmanov (GC) model [46].

Zgoraj navedeni modeli so predpostavljali, da je relativna dielektričnost v celotni raztopini soli konstantna. To naj bi bila posledica majhnih električnih polj ter konstantnega števila vodnih molekul v celotni raztopini soli. Vendar se zaradi naraščanja velikosti električnega polja ter zmanjšanja koncentracije vodnih molekul v bližini naelektrene površine relativna dielektričnost v bližini električno nabite površine lahko bistveno spremeni. Posledica tega je krajevna odvisnost električnega potenciala v bližini električno nabite površine. Problem so leta 2011 matematično opisali Gongadze in sodelavci [47] v Langevin-Poisson-Boltzmannovem (LPB) modelu. Model LPB obravnava vse delce v sistemu kot točkaste delce (delce brez volumna).

Vzporedno z modeli, ki obravnavajo vse delce v sistemu kot točkaste delce, so se začeli razvijati tudi modeli, ki vključujejo delce s končnimi volumni. Leta 1942 je Bikerman [48] objavil model, ki je vključeval končne volumne ionov ter nekatere njihove lastnosti (npr. dipolni moment zaradi hidracije ionov). Od takrat se je zvrstilo še mnogo objav modelov, ki vljučujejo končne volumne, vpeljane v model na več različnih načinov [49, 50, 51, 52, 53, 54, 55]. Leta 2012 sta Gongadze in Iglič [56] s pomočjo posplošene Langevin-Bikermanove (LB) teorije izpeljala Gongadze-Igličevo enačbo, ki je s pomočjo statističnega pristopa v model vključila končne volumne vseh delcev v sistemu.

Za reševanje tovrstnih modelov uporabljamo različne pristope, ki so odvisni predvsem od zahtevnosti modela. Za enostavne enodimenzijske modele lahko uporabimo funkcije za reševanje navadnih diferencialnih enačb, medtem ko se moramo za reševanje kompliciranih (stohastičnih) tridimenzionalnih modelov poslužiti metode Monte Carlo [57].

1.9 Namen dela

Zaradi različnih temperatur faznih prehodov uporabljenih lipidov, nas je zanimalo, ali imajo lipidni dvosloji, zgrajeni iz različnih vrst lipidnih molekul (DPPC, DPhPC in arheolipidov), drugačne električne lastnosti glede na to, da se nahajajo v različnih faznih stanjih, in ali so električne lastnosti ravninskega lipidnega dvosloja odvisne tudi od temperature. Preučevali smo kapacitivnost hidriranega ravninskega lipidnega dvosloja kot parameter debeline ravninskega lipidnega dvosloja ter porušitveno napetost kot parameter, ki vpliva na mehansko stabilnost ravninskega lipidnega dvosloja v električnem polju. Kapacitivnost in porušitvena napetost sta odvisni od materialnih lastnosti lipidnih dvoslojev, kot sta povprečna dolžina in nasičenost maščobnih verig lipidnih molekul, ki sta odvisni tudi od temperature. Zanimalo nas je tudi, ali lahko kapacitivnost in porušitveno napetost v odvisnosti od temperature primerjamo s parametri katerih drugih metod za proučevanje lastnosti lipidnih dvoslojev v odvisnosti od temperature.

Hidrirani ravninski lipidni dvosloj je zanimiv tudi s stališča elektrostatike, zato smo s teoretičnimi modeli proučevali elektrostatične lastnosti ravninskega lipidnega dvosloja v stiku z raztopino soli. V Langevin-Poisson-Boltzmannov (LPB) model [47] in Langevin-Bikermanov (LB) model [56] z že vključeno krajevno odvisno relativno dielektričnostjo raztopine soli v odvisnosti od električnega polja v bližini lipidnega dvosloja smo vključili enačbo, ki upošteva notranjo strukturo zviterionskih glav lipidnih molekul in gradient koncentracije vodnih molekul v bližini lipidnega dvosloja iz zviterionskih lipidnih molekul, ki imajo v glavi električno pozitivni in električno negativni del, kot je na primer 1,2-dipalmitoil-sn-glicero-3-fosfoholin (DPPC). Enačbe našega modela smo izpeljali s pomočjo uporabe gostote verjetnosti kota odmika pozitivnega dela zviterionske glave lipidne molekule iz normalne ravnine (ω).

2 Materiali in metode

2.1 Eksperimentalni del

2.1.1 Uporabljene kemikalije

Za elektrolitsko raztopino (raztopino soli) smo uporabljali 100 mM raztopino KCl in 10 mM 4-(2-hidroksietil)-1-piperazinetansulfonsko kislino (HEPES), ki smo ju namešali v enakem razmerju. Raztopini je bilo dodanih nekaj kapljic NaOH, da smo dosegli pH = 7.4. Lipide 1,2-dipalmitoil-sn-glicero-3-fosfoholin (DPPC) in 1,2-diphitanoil-sn-glicero-3-fosfoholin (DPhPC), proizvajalca Avanti Polar Lipids, ZDA, smo raztapljali v mešanici heksana (Sigma-Aldrich, ZDA) in absolutnega etanola (Sigma-Aldrich, ZDA) v razmerju 9 : 1 in v koncentraciji 10 mg/ml. Arheolipide, pridobljene iz arheje *A. Pernix K1*, so nam pripravljali na Oddelku za živilstvo na Biotehniški fakulteti Univerze v Ljubljani in smo jih raztapljali v enakih kemikalijah in v enakih razmerjih kot lipide DPPC oziroma DPhPC. Kemikalijo za tvorjenje podpornega torusa smo pripravljali iz mešanice heksadekana (Fluka, Nemčija) in pentana (Fluka, Nemčija) v razmerju 3 : 7.

2.1.2 Sistem za elektroporacijo hidriranih ravninskih lipidnih dvoslojev pri različnih temperaturah – lipidiporator druge generacije

Sistem za elektroporacijo hidriranih ravninskih lipidnih dvoslojev je bil razvit v Laboratoriju za Biokibernetiko na Fakulteti za elektrotehniko Univerze v Ljubljani [58]. Sestoji se iz petih glavnih komponent (slika 2.1):

- temperaturne komore s teflonsko komoro za vzpostavitev ravninskega lipidnega dvosloja,
- dveh črpalk (*Syringe pumps*) za dvigovanje nivojev raztopine soli v obeh prekatih komore,
- sistema za merjenje porušitvene napetosti lipidnega dvosloja,
- merilnika impedance Agilent 4284A za merjenje kapacitivnosti ravninskega lipidnega dvosloja,
- temperaturne celice *Thermo Cube*.

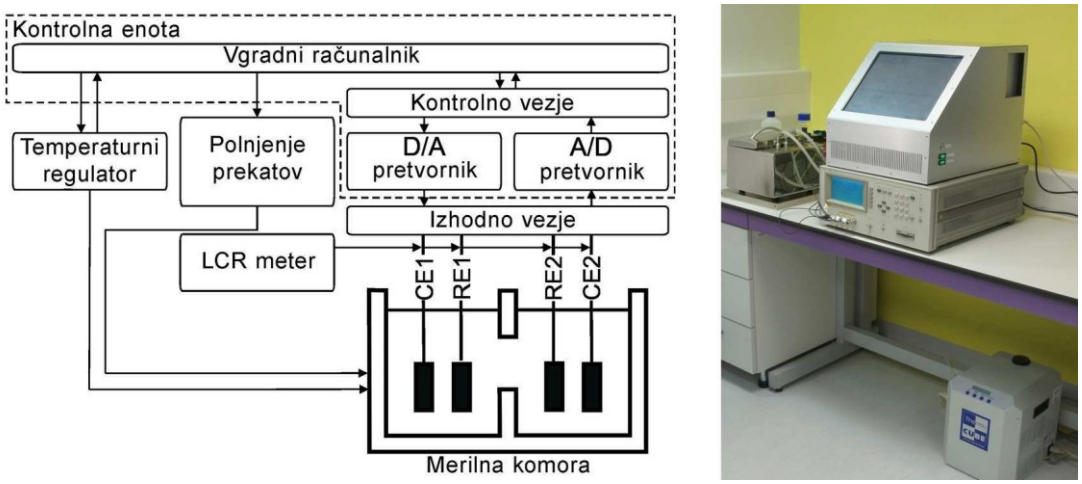

Slika 2.1: Blokovni diagram (levo) in fotografija sistema (desno) za elektroporacijo hidriranih ravninskih lipidnih dvoslojev v odvisnosti od temperature – lipidiporator druge generacije. Blokovni diagram je povzet po [58].

Temperaturna komora je narejena iz nerjavečega jekla z dvojno steno, v kateri je zrak, ki ščiti notranjost posode pred vplivom temperature okolice. V temperaturni komori je izmenjevalnik toplote (hladilno grelna tuljava) in teflonska komora za vzpostavitev hidriranega ravninskega lipidnega dvosloja. Posoda potrebuje približno 1 l navadne vode, ki služi kot medij za prenos toplote med izmenjevalnikom toplote in teflonsko komoro.

Teflonska komora (slika 2.2) sestoji iz dveh delov, ki vsebujeta prekat volumna približno $5,3\,cm^3$ in odprtino premera približno 2 mm. Na eno izmed odprtin postavimo teflonsko folijo debeline 25 μm, z manjšo luknjico premera med 80 μm in 200 μm. Ko oba dela komore združimo, sta oba prekata med seboj povezana le prek luknjice v teflonski foliji. Na tej luknjici se tvori ravninski lipidni dvosloj. Za lažje tvorjenje lipidnega dvosloja mora biti rob luknjice čim bolj oster, luknjica pa čim bolj okrogla. V prekata sta vstavljeni še silikonski cevki, ki sta prek injekcij povezani s črpalkama za avtomatsko spuščanje in dvigovanje nivojev raztopine soli v obeh prekatih. Za merjenje kapacitivnosti (C_{sisblm} in C_{sis}) in porušitvene napetosti (U_{br}) je v vsak prekat teflonske komore vstavljena ena Ag/AgCl elektroda. Za merjenje temperature pa je v enega izmed prekatov vstavljen merilni termočlen.

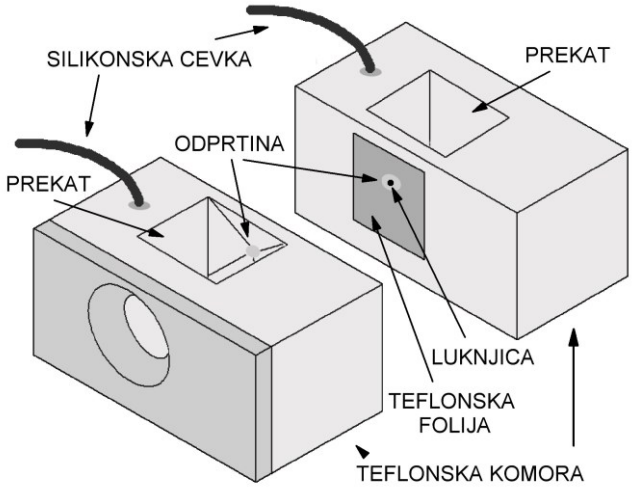

Slika 2.2: Shematski prikaz teflonske komore in njenih delov.

Črpalki za dvigovanje nivojev in temperaturna komora so povezani s sistemom za merjenje porušitvene napetosti, kar omogoča, da jih kontroliramo z uporabo enotnega uporabniškega vmesnika na sistemu za merjenje porušitvene napetosti lipidnega dvosloja.

Sistem za merjenje porušitvene napetosti lipidnega dvosloja je v grobem sestavljen iz vgrajenega računalnika, generatorja signala (D/A pretvornika) in vzorčevalnika signala (A/D pretvornika). Parametre generatorja signala lahko na enostaven način spreminjamo prek enotnega uporabniškega vmesnika.

Temperaturna celica *Thermo Cube* je zračno hlajena in deluje na termoelektričnem principu. Za hladilno grelni medij uporablja mešanico glikola in vode. Hladilno grelni medij kroži po cevi do hladilno grelne tuljave v temperaturni komori, od tam se hladilno grelni medij ponovno vrača v temperaturno celico. Temperaturna celica je povezana s sistemom za merjenje porušitvene napetosti, kar omogoča, da jo krmilimo s pomočjo enotnega uporabniškega vmesnika na sistemu za merjenje porušitvene napetosti lipidnega dvosloja.

2.1.3 Meritev kapacitivnosti hidriranega ravninskega lipidnega dvosloja

Hidrirani ravninski lipidni dvosloj lahko obravnavamo kot realni ploščati električni kondenzator [27]. Kapacitivnost lipidnega dvosloja je edini električni parameter, iz katerega lahko določimo oziroma ocenimo njegovo debelino. Kapacitivnosti ravninskega lipidnega dvosloja ne moremo direktno meriti, saj so v komori prisotne še druge parazitne kapacitivnosti (kapacitivnost raztopine soli, kapacitivnost na elektrodah, kapacitivnost med raztopino in lipidnim dvoslojem [8, 27]), ki jih s skupno besedo imenujemo kapacitivnost sistema (kapacitivnost sistema brez lipidnega dvosloja). Kapacitivnosti ravninskega lipidnega dvosloja računamo iz razlike kapacitivnosti sistema z lipidnim dvoslojem (C_{sisblm}) in kapacitivnosti sistema brez lipidnega dvosloja (C_{sis}) (slika 2.3).

Meritev izvedemo v dveh korakih: v prvem koraku, po postavitvi ravninskega lipidnega dvosloja, izmerimo kapacitivnost sistema z lipidnim dvoslojem (C_{sisblm}), po meritvi porušitvene napetosti pa v drugem koraku izmerimo še kapacitivnost sistema brez lipidnega dvosloja (C_{sis}). Razlika obeh kapacitivnosti predstavlja kapacitivnost ravninskega lipidnega dvosloja (C_{blm}). Zaradi lažje primerjave

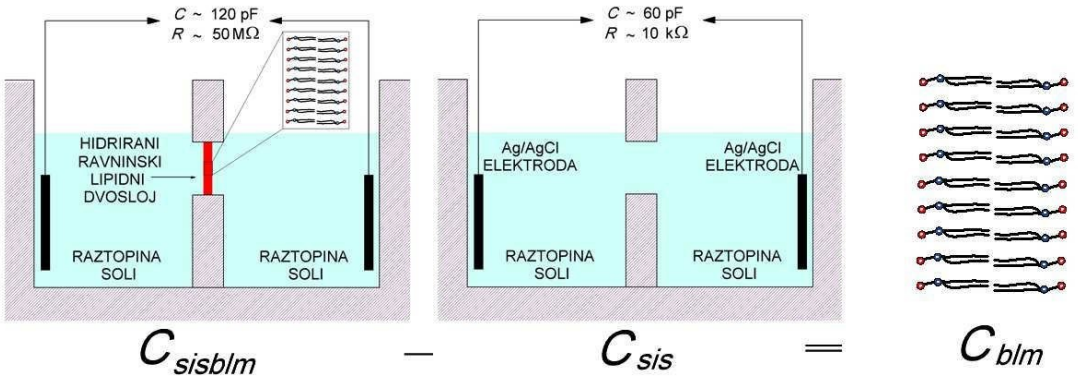

Slika 2.3: Shematski prikaz sistema, v katerem merimo kapacitivnost hidriranega lipidnega dvosloja. Slika levo: Merjenje kapacitivnosti sistema z lipidnim dvoslojem (C_{sisblm}). Slika sredina: Merjenje kapacitivnosti sistema (brez lipidnega dvosloja) (C_{sis}). Slika desno: Razlika obeh kapacitivnosti predstavlja kapacitivnost hidriranega ravninskega lipidnega dvosloja (C_{blm}).

med posameznimi poskusi in z drugimi študijami to kapacitivnost normiramo na površino lipidnega dvosloja, ki je približno enaka površini luknjice v teflonski foliji. Tako dobimo specifično kapacitivnost ravninskega lipidnega dvosloja (c_{blm}). Za merjenje kapacitivnosti smo uporabljali precizijski merilnik impedance Agilent 4284A z dvema Ag/AgCl elektrodama in nastavitvami: vzbujalna napetost $u = 25\,\mathrm{mV}$, frekvenca $f = 1\,\mathrm{kHz}$. Kapacitivnost ravninskega lipidnega dvosloja (C_{blm}) je glede na posplošeno Helmholtzovo teorijo električne dvojne plasti enaka [27]:

$$C_{blm} = \frac{\varepsilon_0 \varepsilon_{rd} A}{d}\,, \tag{2.1}$$

kjer je ε_0 dielektričnost vakuma, ε_{rd} relativna dielektričnost ravninskega lipidnega dvosloja, d in A pa sta debelina in površina ravninskega lipidnega dvosloja. Če enačbo delimo s površino lipidnega dvosloja (A), dobimo izraz za specifično kapacitivnost ravninskega lipidnega dvosloja [28]:

$$c_{blm} = \frac{\varepsilon_0 \varepsilon_{rd}}{d}\,. \tag{2.2}$$

Iz posplošene Helmholtzove teorije sledi, da je specifična električna kapacitivnost lipidnega dvosloja linearno proporcionalna recipročni vrednosti debeline lipidnega dvosloja [59].

2.1.4 Meritev porušitvene napetosti hidriranega ravninskega lipidnega dvosloja

Meritev porušitvene napetosti smo izvajali s tokovno metodo z uporabo sistema, opisanega v podpoglavju 2.1.2. V komoro smo dovajali linearno naraščajoči tokovni signal [41, 60] z naklonom k_i = 300 µA/s in merili napetost (slika 2.4). Z dovajanjem toka se na lipidnem dvosloju povečuje potencialna razlika, lahko rečemo, da gre za polnjenje ploščatega električnega kondenzatorja, ki smo ga definirali v prejšnjem podpoglavju (podpoglavje 2.1.3). Ko potencialna razlika toliko naraste, da pride do porušitve hidriranega ravninskega lipidnega dvosloja, merjena napetost drastično upade. Tik preden napetost na lipidnem dvosloju upade, je definirana porušitvena napetost ravninskega lipidnega dvosloja U_{br}, čas, pri katerem pride do porušitve, pa je definiran kot življenjska doba ravninskega lipidnega dvosloja (t_{br}).

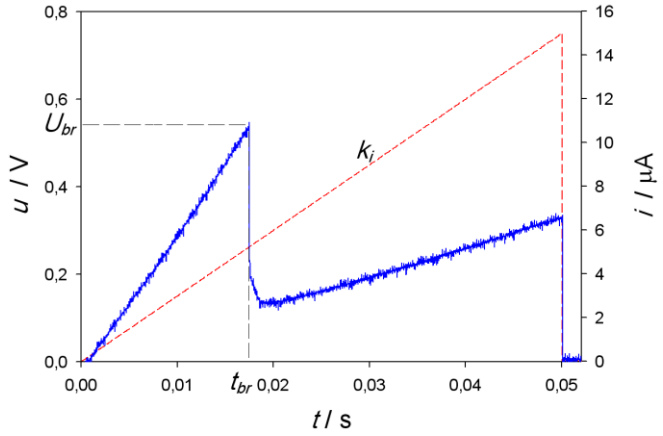

Slika 2.4: Meritev porušitvene napetosti z linearno naraščajočim tokovnim signalom (rdeča črtkana krivulja) z naklonom k_i = 300 µA/s. Tik preden napetost (modra polna krivulja) na lipidnem dvosloju drastično upade, je definirana porušitvena napetost (U_{br}) ravninskega lipidnega dvosloja, čas pa je definiran kot življenjska doba lipidnega dvosloja (t_{br}).

2.1.5 Priprava teflonske komore in obdelava folije

Ko smo med oba dela teflonske komore položili teflonsko folijo z luknjico tako, da je ta na odprtini med prekatoma, in vse skupaj trdno pričvrstili, smo na luknjici v teflonski foliji naredili obdelavo (ang. *pretreatment*). Teflonska folija je namreč glede na debelino lipidnega dvosloja približno 5000-krat debelejša, zato smo za lažje tvorjenje lipidnega dvosloja na luknjico nanesli kemikalijo za tvorjenje podpornega torusa in kemikalijo z lipidom. V vzporednih poskusih opazovanja nanašanja kemikalij za obdelavo pod mikroskopom se je izkazalo, da je uspešna obdelava odvisna od vrstnega reda nanašanja kemikalij ter od položaja in tipa uporabljene teflonske folije, zato smo za različne lipide uporabili različen pristop, ki je podrobneje opisan v naslednjih dveh podpoglavjih (podpoglavji 2.1.5.1 in 2.1.5.2). Po končani obdelavi smo s pomočjo črpalk iz injekcij iztisnili toliko raztopine soli, da sta bila oba nivoja v prekatih pod luknjico v teflonski foliji. Nato smo na površino raztopine soli v oba prekata nanesli po 2 µl raztopine lipida.

Pred prvim dvigovanjem gladine je bilo treba počakati določen čas, da iz raztopin lipida in podpornega torusa izhlapijo vsa topila, ter da se lipidi enakomerno razporedijo po vsej gladini raztopine soli.

2.1.5.1 Lipidni dvosloji, zgrajeni iz arheolipidov

Pri ravninskih lipidnih dvoslojih, zgrajenih iz arheolipidov, smo uporabili približno 1 leto star vzorec teflonske folije debeline 25 µm, proizvajalca Saint Gobain Performance Plastics. Obdelavo smo izvedli tako, da smo na luknjico v teflonski foliji najprej nanesli 1, 5 µl raztopine za tvorjenje podpornega torusa, šele nato pa 1 µl raztopine lipida. Raztopini smo na folijo nanašali z uporabo mikropipeterja na steklene cevke, pri tem je bila teflonska folija v ležečem položaju. Do prvega dviga nivojev smo čakali 10 min, nato smo nivoja dvignili, vklopili *Thermo Cube* in pričeli z meritvami. Pri poskusih z arheolipidi smo uporabili teflonske folije z luknjicami premerov 109 µm, 114 µm, 125 µm in 132 µm.

2.1.5.2 Lipidni dvosloji, zgrajeni iz DPPC in DPhPC

Pri lipidnih dvoslojih, sestavljenih iz lipida DPPC, DPhPC ter iz njune mešanice, smo uporabili približno 10 let star vzorec teflonske folije debeline 25 µm, proizvajalca Saint Gobain Performance Plastics. Obdelavo smo izvedli tako, da smo na luknjico v teflonski foliji najprej nanesli 1 µl raztopine lipida, nato pa 1, 5 µl raztopine za tvorjenje podpornega torusa. Raztopini smo na folijo nanašali z uporabo mikropipeterja na steklene cevke, pri tem je bila teflonska folija v pokončnem položaju. Do prvega dviga nivojev smo čakali 5 min, nato smo nivoja dvignili, vklopili *Thermo Cube* in čakali še 40 min. Pri poskusih smo uporabili teflonsko folijo z luknjico premera 124 µm.

2.1.6 Potek meritev

Po predvidenem času čakanja (glejte prejšnji podpoglavji 2.1.5.1 in 2.1.5.2) smo s pomočjo črpalk nivoja raztopine soli dvignili tik nad luknjico v teflonski foliji. Najprej smo dvignili en nivo, nato še drugega. Ko sta bila oba nivoja poravnana, smo nastavili parametre črpalk tako, da sta se nivoja dvigovala in spuščala le okrog luknjice v teflonski foliji. Potem smo nivoja spustili in nazaj dvignili. Na luknjici v teflonski foliji se je tvoril ravninski lipidni dvosloj. Najprej smo izmerili C_{sisblm} nato U_{br} ter nato še C_{sis}. Nato smo nivoja spustili in postopek ponavljali, dokler so se tvorili ravninski lipidni dvosloji. Ker se je med meritvami temperatura v prekatih teflonske komore spreminjala (za primer glejte sliko 2.5), smo morali meritve izvajati čim hitreje. Najmanjši čas vzorčenja na tem sistemu je z uporabo črpalk za dvigovanje nivojev znašal približno 20 s. Brez uporabe črpalk pa se je le-ta podaljšal na 30 s–40 s.

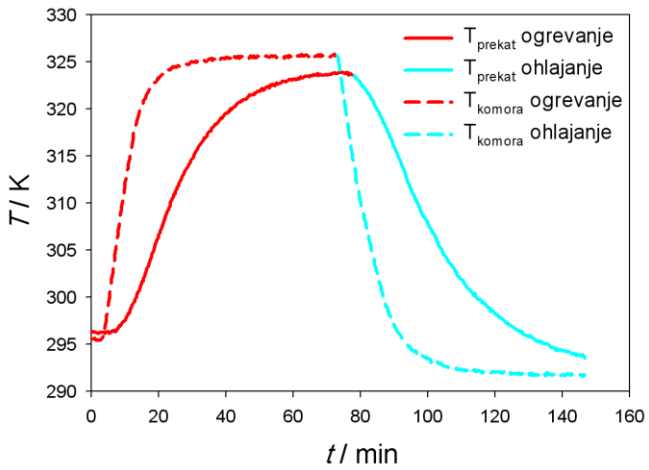

Slika 2.5: Potek temperature v temperaturni komori (T_{komora}) in v prekatu teflonske komore (T_{prekat}) med segrevanjem in ohlajanjem. Pri ogrevanju je bila v tem primeru na *Termo Cube* nastavljena temperatura 327 K, pri ohlajanju pa 291 K.

2.2 Teoretični del

2.2.1 Nadgrajen Langevin-Poisson-Boltzmannov (MLPB) model

Izhajali smo iz osnovnega (Poisson-Boltzmannovega (PB) ali Gouy-Chapmanovega (GC)) modela, ki obravnava negativno električno nabito površino s površinsko gostoto električnega naboja σ v stiku z raztopino soli. Grafično predstavitev modela prikazuje slika 2.6. Električni potencial in elek-

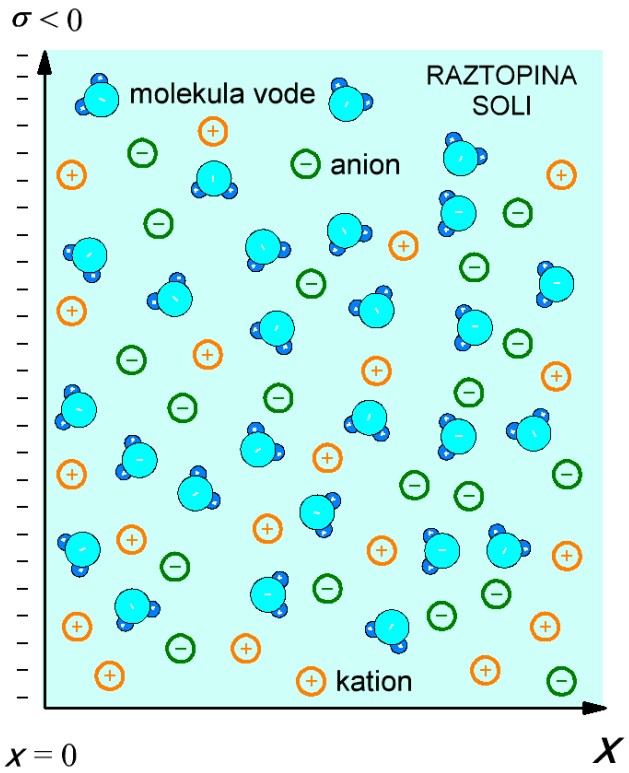

Slika 2.6: Grafična predstavitev Poisson-Boltzmannovega (PB) modela električno nabite površine v stiku z raztopino soli, ki vsebuje pozitivne (katione) in negativne (anione) enovalentne ione (npr.: KCl, NaCl). σ predstavlja površinsko gostoto električnega naboja negativno električno nabite površine pri x = 0.

trični naboj sta med seboj povezana s Poissonovo enačbo [27], ki je v sferičnem

koordinatnem sistemu zapisana kot:

$$\nabla [\varepsilon_0 \varepsilon_r(r) \nabla \varphi(r)] = -\rho_{free}(r) , \tag{2.3}$$

kjer je ∇ Laplaceov operator, $\varphi(r)$ električni potencial, ρ_{free} skupna volumska gostota električnega naboja sistema, ε_0 dielektričnost praznega prostora in $\varepsilon_r(r)$ krajevno odvisna relativna dielektričnost. Ker so premeri večine celic ali nanodelcev veliko večji, kot so prosti delci v sistemu (npr. ioni), lahko celice in nanodelce obravnavamo kot ravno ploskev s površinsko gostoto električnega naboja σ [27]. Zaradi te poenostavitve lahko Poissonovo enačbo (enačba 2.3) zapišemo v kartezičnem koordinatnem sistemu:

$$\nabla [\varepsilon_0 \varepsilon_r(x, y, z) \nabla \varphi(x, y, z)] = -\rho_{free}(x, y, z) . \tag{2.4}$$

Ob predpostavki, da je skupna volumska gostota električnega naboja sistema (ρ_{free}) homogena v obeh dimenzijah, ki sta vzporedni s površino celice [27], lahko enačbo 2.4, zapisano v tridimenzionalnem prostoru, poenostavimo z zapisom v eni dimenziji [27]:

$$\frac{d}{dx} \varepsilon_0 \varepsilon_r(x) \frac{d\varphi}{dx} = -\rho_{free}(x) , \tag{2.5}$$

kjer je $\varphi(x)$ električni potencial, ε_0 dielektričnost praznega prostora, $\varepsilon_r(x)$ krajevno odvisna relativna dielektričnost in $\rho_{free}(x)$ volumska gostota prostega električnega naboja sistema. Ker so edini prosti nosilci električnega naboja v PB modelu anioni in kationi, sta Gouy in Chapman $\rho_{free}(x)$ definirala kot [61, 62]:

$$\rho_{free}(x) = \rho_{ions}(x) = e_0 n_+(x) - e_0 n_-(x) , \tag{2.6}$$

kjer sta za opis številske gostote električnega naboja anionov ($n_-(x)$) in kationov ($n_+(x)$) uporabila Boltzmannovo porazdelitveno funkcijo [61, 62]:

$$n_+(x) = n_0 \exp(-e_0 \varphi(x) \beta) , \tag{2.7}$$

$$n_-(x) = n_0 \exp(e_0 \varphi(x) \beta) . \tag{2.8}$$

Iz enačb 2.6–2.8 sta tako izpeljala enačbo volumske gostote električnega naboja $\rho_{free}(x) = \rho_{ions}(x)$ v obliki:

$$\rho_{free}(x) = -2\, e_0\, n_0 \sinh e_0 \varphi \beta \ , \tag{2.9}$$

kjer je e_0 osnovni naboj, n_0 številska gostota raztopine soli (daleč stran od negativno naelektrene površine) in $\beta = 1/kT$, pri čemer je kT termična energija, k Boltzmannova konstanta in T absolutna temperatura.

Gouy-Chapmanov model električne dvojne plasti tudi predpostavlja, da je relativna dielektričnost po vsej raztopini soli konstantna ($\varepsilon_r(x) = \varepsilon_r = \text{konst.}$), zato iz enačb 2.5 in 2.9 sledi [61, 62]:

$$\frac{d}{dx}\left(\varepsilon_0\, \varepsilon_r \frac{d\varphi}{dx}\right) = 2\, e_0\, n_0 \sinh e_0 \varphi \beta \ . \tag{2.10}$$

Ustrezna robna pogoja sta:

$$\frac{d\varphi}{dx}(x = 0) = -\frac{\sigma}{\varepsilon_0\, \varepsilon_r} \ , \tag{2.11}$$

$$\frac{d\varphi}{dx}(x \to \infty) = 0 \ , \tag{2.12}$$

kjer prvi robni pogoj definira jakost električnega polja na električno nabiti površini pri $x = 0$, ki je posledica površinske gostote električnega naboja, drugi robni pogoj pa zahteva, da je električno polje daleč stran od električno nabite površine enako nič.

Predpostavka o konstantni dielektričnosti ε_r v celotni raztopini soli v splošnem ni sprejemljiva, saj v močnem električnem polju v bližini naelektrene površine ($x = 0$) pride do nasičenosti in orientacije vodnih molekul, zato so Gongadze in sodelavci [56, 47] z opisom vodnih molekul z Langevinovimi dipoli [63] izpeljali funkcijo za krajevno odvisnost relativne dielektričnosti $\varepsilon_r(x)$ kot sledi [47]:

$$\varepsilon_r(x) = 1 + \frac{|P(x)|}{\varepsilon^0 E(x)} = 1 + \frac{n_{0w}\, p_0\, L(p_0 E(x)\beta)}{\varepsilon^0 \qquad E(x)} \ , \tag{2.13}$$

kjer je $|P(x)|$ velikost vektorja polarizacije vodnih molekul, n_{0w} številska gostota vodnih molekul, p_0 amplituda zunanjega dipolnega momenta vodne molekule,

$L(u) = (\coth(u) - 1/u)$ je Langevinova funkcija in $E(x) = |\varphi(x)'|$ velikost električnega polja.

Enačbe 2.5, 2.9 in 2.13 tako tvorijo nov model, ki so ga Gongadze in sodelavci imenovali Langevin-Poisson-Boltzmannov model [47] (slika 2.7).

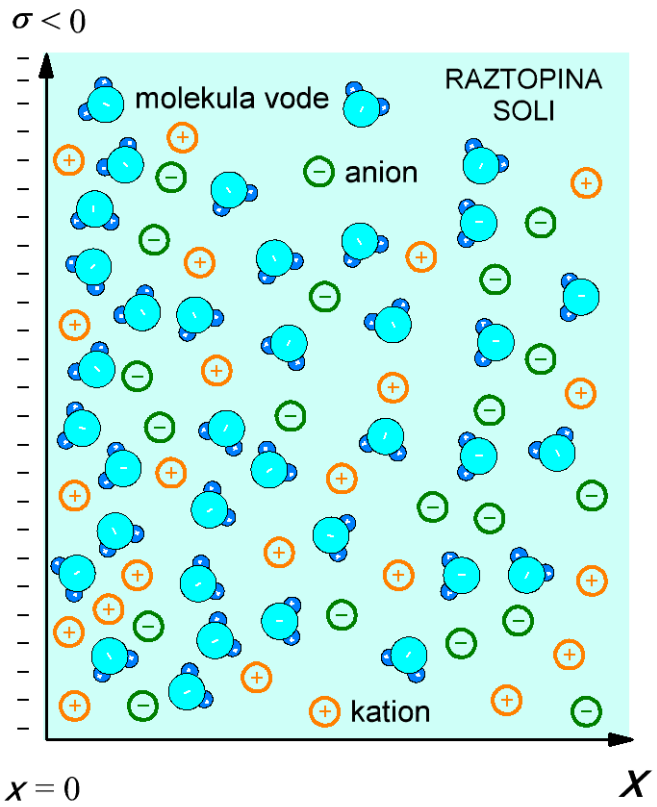

Slika 2.7: Grafična predstavitev Langevin-Poisson-Boltzmannovega (LPB) modela raztopine soli v bližini električno nabite površine, ki vsebuje pozitivne (katione) in negativne (anione) enovalentne ione (npr.: KCl, NaCl). Model napoveduje močno nasičeno koncentracijo vodnih molekul v bližini električno nabite površine. σ opisuje površinsko gostoto električnega naboja pri $x = 0$.

Z namenom izboljšati opis krajevno odvisne relativne dielektričnosti smo nadgradili Langevin-Poisson-Boltzmannov (LPB) model. V nadgrajenem Langevin-Poisson-Boltzmannovem modelu (MLPB) smo molekulo vode obravnavali kot

majhno kroglo z dielektričnostjo, ki je enaka kvadratu lomnega količnika vode (n^2) ter točkastim permanentnim dipolom z dipolnim momentom (p_0) v centru te krogle. Končna enačba za relativno dielektričnost $\varepsilon_r(x)$ je nadgradnja enačbe 2.13 in ima naslednjo obliko ([64] ali Priloga A):

$$\varepsilon_r(x) = n^2 + \frac{n_{0w} p_0}{\varepsilon_0} \frac{2+n^2}{3} \frac{L(\gamma p_0 E(x)\beta)}{E(x)} , \qquad (2.14)$$

kjer je $n = 1,33$ in $\gamma = (3/2)((2+n^2)/3)$. Ostali parametri so podani pri enačbi 2.13.

V sklopu MLPB modela smo dodali tudi zviterionsko lipidno plast. Zaradi amfifilnosti so negativno električno nabiti deli lipidnih glav (fosfatni deli glav) v stiku z raztopino soli in jih opišemo kot ravno negativno električno nabito površino z negativno površinsko gostoto električnega naboja ($\sigma < 0$), pozitivno električno nabiti deli lipidnih glav (amino deli glav) pa prodrejo v raztopino soli (glejte sliko 2.8). Prispevek pozitivnega električnega naboja lipidnih glav ($\rho_{Zw}(x)$) k skupni prosti volumski gostoti prostega električnega naboja sistema ($\rho_{free}(x)$) smo izpeljali iz gostote verjetnosti, da se pozitivni del zviterionske lipidne glave nahaja nekje znotraj področja glav ($0 \le x \le D$). D je razdalja med električno nabitimi deli v zviterionski lipidni glavi. Prispevek pozitivno električno nabitih delov lipidnih glav ($\rho_{Zw}(x)$) tako zapišemo kot ([64] ali Priloga A):

$$\rho_{Zw}(0 \le x \le D) = \frac{e_0 P(x)}{D a_0} \quad \text{in} \quad \rho_{Zw}(x > D) = 0 , \qquad (2.15)$$

kjer je a_0 površina na lipidno molekulo, D razdalja med električno nabitimi deli v zviterionski lipidni glavi in $P(x)$ gostota verjetnosti, da se pozitivni del glave lipidne molekule (amino del) nahaja na razdalji x ($0 \le x \le D$):

$$P(x) = \Lambda \exp(-e_0 \varphi(x)\beta) , \qquad (2.16)$$

kjer je Λ faktor normalizacije, ki nam zagotovi izpolnitev normalizacijskega pogoja (enačba 2.17).

Tako kot vse enačbe znotraj MLPB modela tudi enačba 2.16 upošteva, da so pozitivno električno nabiti deli zviterionskih glav točkasti delci. Z upoštevanjem

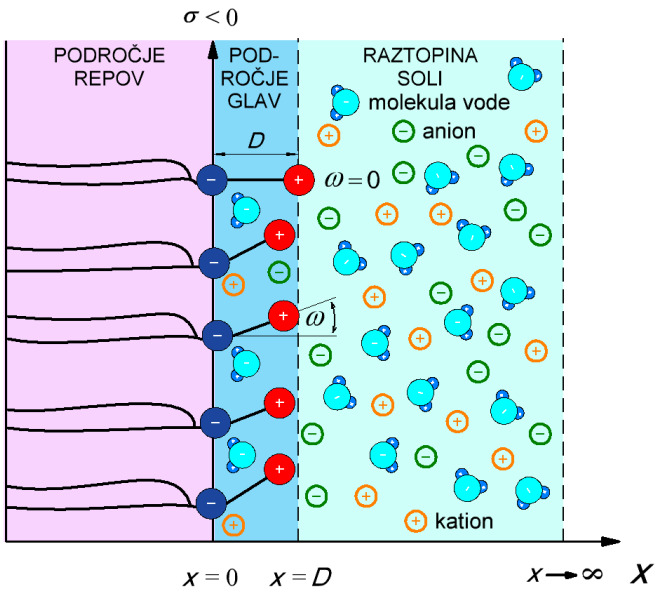

Slika 2.8: Grafična predstavitev nadgrajenega Langevin-Poisson-Boltzmannovega (MLPB) modela za študij elektrostatičnih lastnosti v bližini zviterionske lipidne plasti v stiku z raztopino soli. Model predvideva močno nasičenje in orientacijo vodnih molekul v bližini električno nabite površine in prispevek pozitivnih delov glav ($\rho_{Zw}(x)$) k skupni volumski gostoti prostega električnega naboja sistema $\rho_{free}(x)$. σ predstavlja površinsko gostoto električnega naboja pri $x = 0$, D je razdalja med električno nabitimi deli v zviterionski lipidni glavi in ω je kot med lipidno glavo in daljšo osjo lipidne molekule.

normalizacijskega pogoja:

$$\frac{1}{D}\int_0^D P(x)\,dx = 1\ , \tag{2.17}$$

dobimo vrednost za Λ:

$$\Lambda = \frac{D}{\int_0^D \exp(-e_0\varphi(x)\beta)\,dx}\ . \tag{2.18}$$

Enačba MLPB modela je sestavljena iz prispevka raztopine soli (enačba 2.9) in prispevka pozitivno električno nabitih delov glav lipidnih molekul (enačba 2.15)

k volumski gostoti električnega naboja sistema. V enačbi je upoštevana krajevna odvisnost relativne dielektričnosti $\varepsilon_r(x)$ vodnih molekul v bližini negativno električno nabite površine pri $x = 0$ (enačba 2.14). Če vse prispevke upoštevamo v enačbi 2.5, dobimo končno enačbo MLPB modela v obliki ([64] ali Priloga A):

$$\frac{d}{dx}\left(\varepsilon_0\,\varepsilon_r(x)\frac{d\varphi}{dx}\right) = 2\,e_0\,n_0\sinh e_0\varphi\beta - \frac{e_0\exp(-e_0\varphi(x)\beta)}{a_0\int_0^D \exp(-e_0\varphi(x)\beta)\,dx}, \qquad (2.19)$$

s pripadajočimi robnimi pogoji:

$$\frac{d\varphi}{dx}(x=0) = -\frac{\sigma}{\varepsilon_0\,\varepsilon_r(x=0)}, \qquad (2.20)$$

$$\frac{d\varphi}{dx}(x\to\infty) = 0, \qquad (2.21)$$

$$\varphi(x=D_-) = \varphi(x=D_+), \qquad (2.22)$$

$$\frac{d\varphi}{dx}(x=D_-) = \frac{d\varphi}{dx}(x=D_+), \qquad (2.23)$$

kjer enačba 2.20 določa, da je električno polje na površini $x = 0$ posledica površinske gostote električnega naboja lipidne površine $\sigma = -e_0/a_0$ in vrednosti relativne dielektričnosti $\varepsilon_r(x = 0)$. Enačba 2.21 upošteva, da je električno polje dovolj daleč od naelektrene lipidne površine enako nič. Enačbi 2.22 in 2.23 pa zagotavljata zveznost električnega polja in potenciala na koncu zviterionskih lipidnih glav v točki $x = D$ (slika 2.8). Indeksa $_-$ in $_+$ v enačbah 2.22 in 2.23 ponazarjata levo oziroma desno stran na meji $x = D$.

Enačbo 2.19 smo reševali v programu Matlab z uporabo vgrajene funkcije (*bvp4c*) za reševanje diferencialnih enačb s podanimi robnimi pogoji (enačbe 2.20–2.23). Funkcija *bvp4c* problem reševanja diferencialne enačbe drugega reda poenostavi v problem reševanja dveh enačb prvega reda z uporabo substitucije [65]. Vrednost integrala $\int_0^D \exp(-e_0\varphi(x)\beta)\,dx$ v enačbi 2.19 in $\varepsilon_r(x)$ (enačba 2.14) smo reševali v iterativnem procesu zunaj funkcije *bvp4c*. Za podrobnejše izpeljave enačb MLPB modela za uporabo v programu Matlab glejte Dodatek v Prilogi A. Rešitev modela je potek potenciala in električnega polja v raztopini soli v odvisnosti od oddaljenosti od električno nabite površine pri $x = 0$.

2.2.1.1 Izračun prispevka pozitivnih delov zviterionskih glav ($\rho_{Zw}(x)$) z upoštevanjem končnih volumnov glav

Prispevek za pozitivne lipidne glave $\rho_{Zw}(x)$ lahko izračunamo tudi s pomočjo posplošenega Langevin-Bikermanovega (LB) modela, ki upošteva končne volumne pozitivno električno nabitih delov glav lipidnih molekul. Če področje glav (slika 2.9) razdelimo na končno število enakih mrežnih mest in predpostavimo, da so vsa zasedena s pozitivno električno nabitimi deli zviterionskih glav ali raztopino soli (ioni, molekule vode), ki zasedajo eno mrežno mesto, lahko razmerje pozitivnih delov glav proti vsem delcem v področju glav izračunamo kot:

$$\frac{n_h}{n_h + n_{i,w}}\,, \tag{2.24}$$

kjer je n_h številska gostota pozitivnih delov zviterionskih glav in $n_{i,w}$ skupna številska gostota ionov in vodnih molekul. Če v enačbi 2.24 upoštevamo še

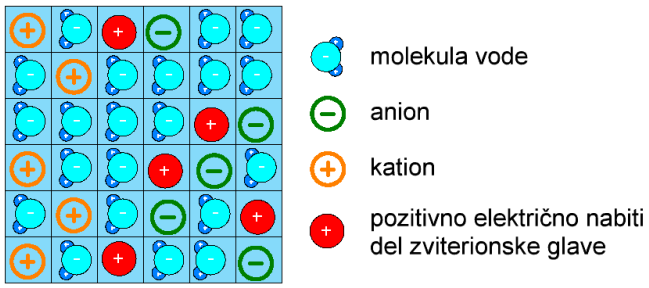

Slika 2.9: Grafična predstavitev posplošene Langevin-Bikermanove (LB) teorije. Teorija predpostavlja, da vsi delci zasedajo eno mrežno mesto.

Boltzmanovo porazdelitev za pozitivne dele glav zviterionskih molekul $n_h(x) = n_{0h}\exp(-e_0\varphi(x)\beta)$, lahko zapišemo:

$$\frac{n_{0h}\exp(-e_0\varphi(x)\beta)}{n_{0h}\exp(-e_0\varphi(x)\beta) + n_{i,w}}. \tag{2.25}$$

Deljenje enačbe 2.25 z $n_{i,w}$ pripelje enačbo 2.25 v obliko:

$$\frac{\frac{n_{0h}}{n_{i,w}}\exp(-e_0\varphi(x)\beta)}{\frac{n_{0h}}{n_{i,w}}\exp(-e_0\varphi(x)\beta)+1} = \frac{\alpha\exp(-e_0\varphi(x)\beta)}{\alpha\exp(-e_0\varphi(x)\beta)+1}, \tag{2.26}$$

kjer uvedemo parameter $\alpha = \frac{n_{0h}}{n_{i,w}}$. Na podlagi enačbe 2.26 lahko zapišemo gostoto verjetnosti za pozitivne dele zviterionskih glav $P(x)$ ([64] ali Priloga A):

$$P(x) = \Lambda \frac{\alpha \exp(-e_0\varphi(x)\beta)}{\alpha \exp(-e_0\varphi(x)\beta) + 1} . \quad (2.27)$$

Parameter α opisuje volumsko razmerje med pozitivnimi deli zviterionskih glav in raztopino soli v področju glav in na ta način upošteva končni volumen pozitivnih delov zviterionskih glav. Faktor normalizacije Λ pa določimo numerično, v iterativnem procesu, dokler ni izpolnjen normalizacijski pogoj (enačba 2.17).

Nadgrajena enačba MLPB modela, ki upošteva končne volumne zviterionskih glav, je tako:

$$\frac{d}{dx}\left(\varepsilon_0 \varepsilon_r(x) \frac{d\varphi}{dx}\right) = 2 e_0 n_0 \sinh e_0\varphi\beta - \Lambda \frac{e_0 \alpha \exp(-e_0\varphi(x)\beta)}{a_0 D(\alpha \exp(-e_0\varphi(x)\beta)+1)}, \quad (2.28)$$

s pripadajočimi robnimi pogoji v enačbah 2.20–2.23 in enačbo 2.14 za izračun $\varepsilon_r(x)$.

2.2.1.2 Izračun prispevka amino ($\rho_a(x)$) in serinske ($\rho_s(x)$) skupine lipidne molekule POPS k skupni volumski gostoti električnega naboja sistema ($\rho_{free}(x)$)

Lipidna molekula POPS ima v glavi molekule poleg negativne fosfatne skupine še pozitivno amino skupino ter negativno serinsko skupino. Zaradi poenostavitve modela predpostavimo, da ležijo vsi trije deli glav na isti osi, ter da so med seboj enako oddaljeni na razdalji D (slika 2.10). Iz danih predpostavk lahko enačbo 2.15 za volumsko gostoto zapišemo v nadgrajeni obliki ([66] ali Priloga C):

$$\rho_{as}(0 \le x \le 2D) = \rho_a(x) - \rho_s(x) = \frac{e_0 P(x)}{D a_0} - \frac{e_0 P(x)}{2D a_0} \quad (2.29)$$

in

$$\rho_{as}(x > 2D) = 0 ,$$

pri čemer prvi člen na desni strani predstavlja prispevek pozitivne (amino) skupine ($\rho_a(x)$), drugi člen pa predstavlja prispevek negativne (serinske) skupine

($\rho_s(x)$). Skupni prispevek amino in serinske skupine $\rho_{as}(x)$ je definiran le v področju glav ($0 \leq x \leq 2D$) (slika 2.10), izven njega ($x > 2D$) pa ima vrednost nič.

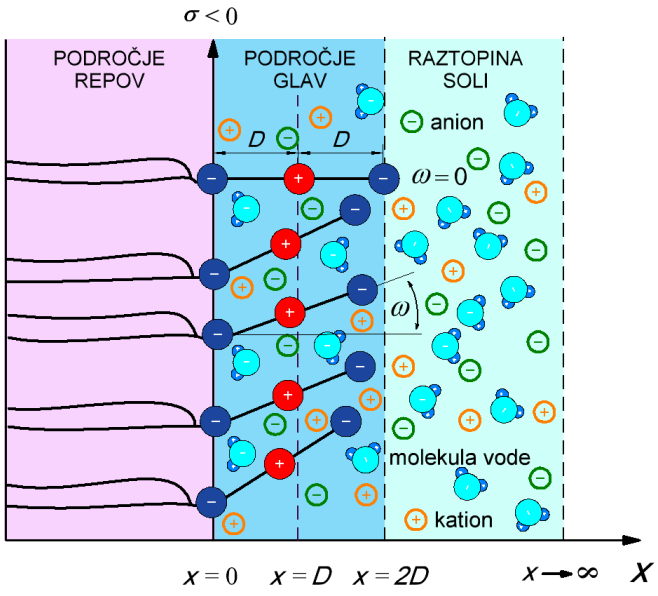

Slika 2.10: Grafična predstavitev nadgrajenega Langevin-Poisson-Boltzmannovega (MLPB) modela za študij elektrostatičnih lastnosti lipidne plasti, sestavljene iz lipida POPS v stiku z raztopino soli. D je razdalja pozitivne (amino) skupine od negativno naelektrene površine pri $x = 0$, $2D$ pa je razdalja negativne (serinske) skupine od negativno naelektrene površine pri $x = 0$. Razdalja $2D$ omejuje področje glav ($0 \leq x \leq 2D$). Za razlago ostalih parametrov glejte sliko 2.8.

2.2.1.3 Izračun prispevka raztopine soli iz pozitivnih dvovalentnih in negativnih enovalentnih ionov k volumski gostoti električnega naboja ($\rho_{ions}(x)$)

V vodni raztopini posamezna molekula kalcijevega klorida ($CaCl_2$) disocira na en dvovalentni kation Ca^{++} in dva enovalentna aniona $2Cl^-$ (slika 2.11), zato lahko

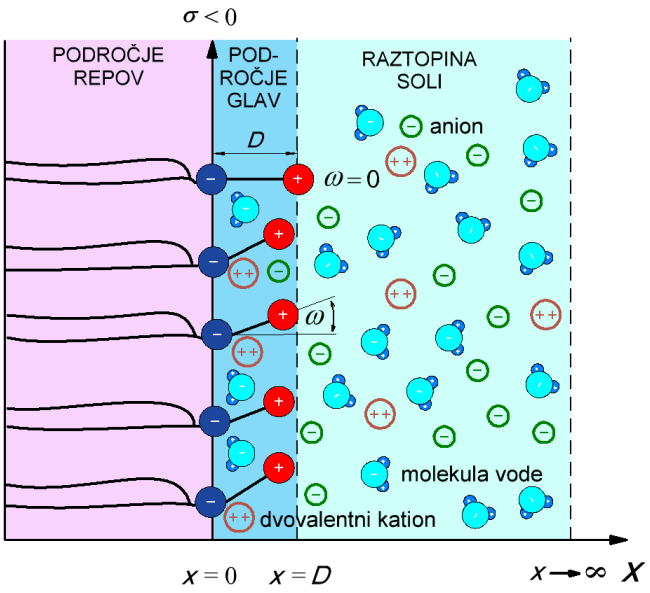

Slika 2.11: Grafična predstavitev nadgrajenega Langevin-Poisson-Boltzmannovega (MLPB) modela zviterionske lipidne plasti v stiku z raztopino soli, ki je sestavljena iz enovalentnih anionov in dvovalentnih kationov (npr.: $CaCl_2$). Ostali parametri so razloženi pri sliki 2.8.

volumsko gostoto električnega naboja za ione ($\rho_{ions}(x)$) zapišemo kot:

$$\rho_{ions}(x) = -e_0 n_-(x) + 2e_0 m(x) \,, \tag{2.30}$$

kjer je $n_-(x)$ številska gostota električnega naboja (porazdelitev) klorovih anionov (Cl^-) in $m(x)$ številska gostota električnega naboja (porazdelitev) kalcijevih kationov (Ca^{++}). Ob upoštevanju Boltzmannove porazdelitve za Cl^- in Ca^{++}:

$$n_-(x) = n_0 \exp(+e_0\varphi(x)\beta) \,,\; m(x) = m_0 \exp(-2e_0\varphi(x)\beta) \,, \tag{2.31}$$

kjer je n_0 številska gostota enovalentnih Cl^-, m_0 pa številska gostota dvovalentnih Ca^{++} daleč stran od lipidne plasti $x = 0$. Iz pogoja elektronevtralnosti daleč stran od lipidne plasti sledi:

$$-n_0 + 2m_0 = 0 \ . \tag{2.32}$$

Ob upoštevanju enačb 2.31 in 2.32 lahko enačbo 2.30 zapišemo v obliki ([67] ali Priloga E):

$$\rho_{ions}(x) = -2e_0 m_0 \left[\exp(+e_0\varphi(x)\beta) - \exp(-2e_0\varphi(x)\beta)\right] \ . \tag{2.33}$$

2.2.1.4 MLPB model za opis sistema lipidne plasti v stiku z nanodelci v raztopini soli

Vpliv električno nabitih nanodelcev na lipidno plast v dotiku z raztopino soli smo v MLPB model vpeljali s spremembo drugega robnega pogoja (enačba 2.21). Spremenjen robni pogoj je tako ([66, 68] ali Priloga C):

$$\frac{d\varphi}{dx}(x = D_{nd}) = +\frac{\sigma_2}{\varepsilon_0 \varepsilon_r(x = D_{nd})} \ , \tag{2.34}$$

kjer je σ_2 površinska gostota električnega naboja nanodelca s površino pri $x = D_{nd}$. D_{nd} predstavlja razdaljo nanodelca od lipidne plasti pri $x = 0$ (slika 2.12).

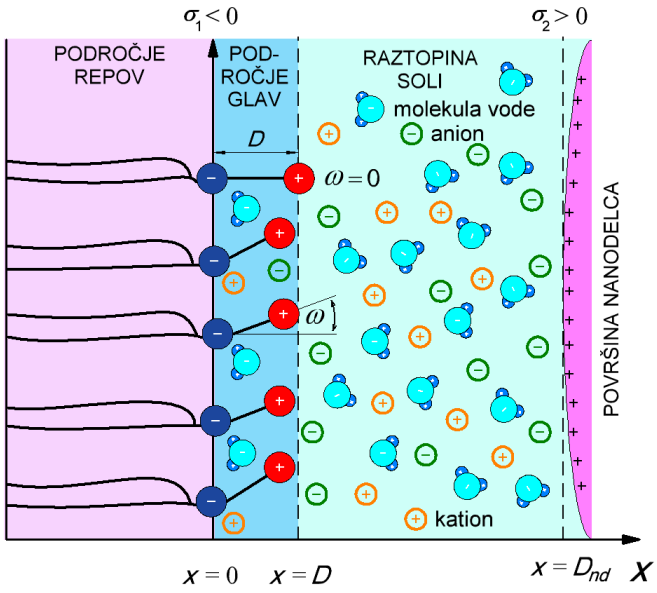

Slika 2.12: Grafična predstavitev nadgrajenega Langevin-Poisson-Boltzmannovega (MLPB) modela zviterionske lipidne plasti v stiku z raztopino soli in nanodelcem. D_{nd} je razdalja med negativno električno nabito lipidno površino pri $x = 0$ in nanodelcem, σ_1 predstavlja površinsko gostoto električnega naboja negativnih delov glav, σ_2 pa površinsko gostoto električnega naboja pozitivno nabitega nanodelca. Za razlago ostalih parametrov glejte sliko 2.8.

2.2.2 Osmotski tlak

Osmotski tlak med dvema naelektrenima površinama, v našem primeru zviterionsko lipidno plastjo pri $x = 0$ in nanodelcem pri $x = D_{np}$, smo izpeljali v okviru MLPB modela (enačba 2.28 z upoštevanjem robnih pogojev 2.20, 2.22, 2.23, 2.34). Enačbo 2.28 lahko prepišemo v obliko:

$$-\frac{d}{dx}\left[\varepsilon_0 n^2 \frac{d\varphi}{dx} + 2 e_0 n_0 \sinh e_0 \varphi \beta\right] - n_{0w} p_0 \frac{2+n^2}{3} \frac{d}{dx} L(\gamma p_0 E(x)\beta) - \frac{e_0 \Lambda}{D a_0} \frac{\alpha \exp(-e_0 \varphi(x)\beta)}{\alpha \exp(-e_0 \varphi(x)\beta) + 1} = 0 . \tag{2.35}$$

Zgornjo enačbo 2.35 pomnožimo z $\varphi' \equiv d\varphi/dx$ ter integriramo ob upoštevanju zvez:

$$\varphi'' \varphi' dx = \frac{1}{2} d(\varphi')^2 = \frac{1}{2} (\varphi')^2 , \qquad \frac{dL}{dx} \varphi' dx = L\varphi' - L d\varphi' ,$$

kjer je $\varphi'' \equiv d^2\varphi/dx^2$ in $d\varphi = \varphi' dx$, da dobimo izraz za lokalni tlak P_{inner}:

$$\begin{aligned} -\frac{1}{2}\varepsilon_0 n^2 E(x)^2 + 2 n_0 kT\ (\cosh(-e_0\varphi(x)\beta)) - \\ -E(x)\ \frac{2+n^2}{3}\ n_{0w} p_0 L(\gamma p_0 E(x)\beta) + \\ +\frac{\Lambda}{D a_0 \beta} \ln(1+\alpha \exp(-e_0\varphi(x)\beta)) + \\ +\ \frac{2+n^2}{3}\ \frac{n_{0w}}{\gamma\beta} \ln\ \frac{\sinh(\gamma p_0 E(x)\beta)}{\gamma p_0 E(x)\beta}\ = P_{inner} = \text{const} . \end{aligned} \tag{2.36}$$

Za izračun vrednosti osmotskega tlaka Π moramo lokalnemu tlaku P_{inner} (enačba 2.36) odšteti pripadajočo vrednost tlaka izven sistema P_{bulk}. Ker sta električno polje (E) in električni potencial (φ) izven sistema enaka nič, lahko posamezne prispevke P_{bulk} izračunamo tako, da vrednosti E in φ v enačbi 2.36 limitiramo proti nič. P_{bulk} je tako:

$$\begin{aligned} P_{bulk} = 0 + 2 n_0 kT + \\ +0 + \\ +0 + \\ +0 . \end{aligned} \tag{2.37}$$

Razlika tlakov $P_{inner} - P_{bulk}$ nam da vrednost osmotskega tlaka Π:

$$\begin{aligned} \Pi = -\frac{1}{2}\varepsilon_0 n^2 E(x)^2 + 2 n_0 kT\ (\cosh(-e_0\varphi(x)\beta) - 1) - \\ - E(x)\ \frac{2+n^2}{3}\ n_{0w} p_0 L(\gamma p_0 E(x)\beta) + \\ +\frac{\Lambda}{D a_0 \beta} \ln(1+\alpha \exp(-e_0\varphi(x)\beta)) + \\ +\ \frac{2+n^2}{3}\ \frac{n_{0w}}{\gamma\beta} \ln\ \frac{\sinh(\gamma p_0 E(x)\beta)}{\gamma p_0 E(x)\beta} , \end{aligned} \tag{2.38}$$

pri čemer je drugi člen enačbe prispevek zaradi raztopine soli (npr.: NaCl, KCl), tretji in peti člen sta prispevka zaradi krajevno odvisne relativne dielektričnosti $\varepsilon_r(x)$, četrti člen pa je prispevek zaradi pozitivnih delov zviterionskih lipidnih glav in je zato definiran le v področju glav ($0 \le x \le D$). Ker so bili vsi izračuni osmotskega tlaka Π narejeni daleč izven področja glav ($x >> D$), smo četrti prispevek izpustili ([68] ali Priloga B).

2.2.3 Nadgrajen Langevin-Bikermanov (MLB) model

Izhajali smo iz Gongazde-Igličeve (GI) enačbe ([56] ali Priloga D), ki temelji na Langevin-Bikermanovem (LB) modelu. Enačba tako predpostavlja končne volumne vseh delcev v sistemu, tj. ionov soli ter vodnih molekul. LB model predpostavlja, da vsi delci v sistemu zasedajo le eno mrežno mesto, ter da so vsa mrežna mesta zasedena (glejte tudi sliko 2.9). GI enačbi smo dodali prispevke za pozitivno električno nabite dele zviterionskih glav, zato je nadgrajen sistem enačb:

$$n_+(x) = n_s \frac{n_0 e^{-e_0\varphi\beta}}{n_0 e^{e_0\varphi\beta} + n_0 e^{-e_0\varphi\beta} + n_{0w}\left\langle e^{-\gamma p_o E\beta\cos(\omega)}\right\rangle_\omega + n_{0h} e^{-e_0\varphi\beta}}, \quad (2.39)$$

$$n_-(x) = n_s \frac{n_0 e^{e_0\varphi\beta}}{n_0 e^{e_0\varphi\beta} + n_0 e^{-e_0\varphi\beta} + n_{0w}\left\langle e^{-\gamma p_o E\beta\cos(\omega)}\right\rangle_\omega + n_{0h} e^{-e_0\varphi\beta}}, \quad (2.40)$$

$$n_w(x) = n_s \frac{n_{0w}\, e^{-\gamma p_o E\beta\cos(\omega)}}{n_0 e^{e_0\varphi\beta} + n_0 e^{-e_0\varphi\beta} + n_{0w}\left\langle e^{-\gamma p_o E\beta\cos(\omega)}\right\rangle_\omega + n_{0h} e^{-e_0\varphi\beta}}, \quad (2.41)$$

$$n_h(x) = n_s \frac{n_{0h} e^{-e_0\varphi\beta}}{n_0 e^{e_0\varphi\beta} + n_0 e^{-e_0\varphi\beta} + n_{0w}\left\langle e^{-\gamma p_o E\beta\cos(\omega)}\right\rangle_\omega + n_{0h} e^{-e_0\varphi\beta}}, \quad (2.42)$$

kjer je n_s številska gostota mrežnih mest, n_{0h} številska gostota glav vseh zviterionskih lipidnih molekul in

$$\left\langle e^{-\gamma p_o E\beta\cos(\omega)}\right\rangle_\omega = \frac{\sinh(\gamma p_0 E\beta)}{\gamma p_0 E\beta} \quad (2.43)$$

Boltzmanov faktor za dipol vodne molekule povprečen po vseh kotih ω. Enačbe 2.39–2.42 lahko prepišemo v obliko:

$$n_+(x) = n_0 e^{-e_0\varphi\beta}\frac{n_s}{D(\varphi,E)}, \tag{2.44}$$

$$n_-(x) = n_0 e^{e_0\varphi\beta}\frac{n_s}{D(\varphi,E)}, \tag{2.45}$$

$$n_w(x) = \frac{n_{0w}\, n_s}{D(\varphi,E)}\frac{\sinh(\gamma p_0 E\beta)}{\gamma p_0 E\beta}, \tag{2.46}$$

$$n_h(x) = n_{0h}\, e^{-e_0\varphi\beta}\frac{n_s}{D(\varphi,E)}, \tag{2.47}$$

kjer je:

$$D(\varphi,E) = 2n_0\cosh(e_0\varphi\beta) + n_{0w}\frac{\sinh(\gamma p_0 E\beta)}{\gamma p_0 E\beta} + n_{0h}\, e^{-e_0\varphi\beta}. \tag{2.48}$$

Poissonova enačba MLB modela je tako:

$$\frac{d}{dx}\varepsilon_0\,\varepsilon_r(x)\frac{d\varphi}{dx} = 2e_0 n_s n_0\frac{\sinh(e_0\varphi\beta)}{D(\varphi,E)} - e_0\, n_s n_{0h}\frac{e^{-e_0\varphi\beta}}{D(\varphi,E)}, \tag{2.49}$$

pri čemer je krajevna odvisnost relativne dielektričnosti $\varepsilon_r(x)$:

$$\varepsilon_r(x) = n^2 + n_{0w}\, n_s\frac{p_0}{\varepsilon_0}\frac{2+n^2}{3}\frac{L(\gamma p_0 E\beta)(\sinh(\gamma p_0 E\beta)/(\gamma p_0 E\beta))}{D(\varphi,E)\,E}. \tag{2.50}$$

Pripadajoči robni pogoji pa so enačbe 2.20–2.23. V primeru vključitve nanodelca v model, se enačbo 2.21 nadomesti z enačbo 2.34. Vsi členi v enačbah 2.44–2.50, ki pripadajo prispevku pozitivno električno nabitih delov zviterionskih glav, so definirani le v področju glav ($0 \le x \le D$).

Enačbo 2.49 MLB modela smo reševali v programu Matlab z uporabo vgrajene funkcije (*bvp4c*) za reševanje diferencialnih enačb s podanimi robnimi pogoji (enačbe 2.20–2.23). Izraz 2.50 za $\varepsilon_r(x)$ pa smo računali v iterativnem procesu zunaj funkcije *bvp4c*. Iterativni proces smo zaključili ob izpolnitvi narmalizacijskega pogoja:

$$\int_0^D a_0\, n_h(x)\,dx = 1. \tag{2.51}$$

2.2.4 Diferencialna kapacitivnost

Ob dotiku kovinske elektrode z raztopino soli se ustvari električna dvojna plast (EDL), ki jo sestavlja električno nabita površina elektrode ter plast nasprotno naelektrenih ionov. Ioni, ki so enako električno nabiti kot površina elektrode, pa se od nje odmaknejo. Rezultat je nastanek potencialne razlike na meji med elektrodo in raztopino soli. Pri izračunih diferencialne kapacitivnosti (C_{diff}) opisanega sistema smo privzeli Sternov model [69], ki je kombinacija GC modela in Helmholtzovega modela [27], kjer zunanja Helmholtzova ravnina (OHP) definira mejo med Sternovo in difuzijsko plastjo (slika 2.13). Diferencialna kapacitivnost

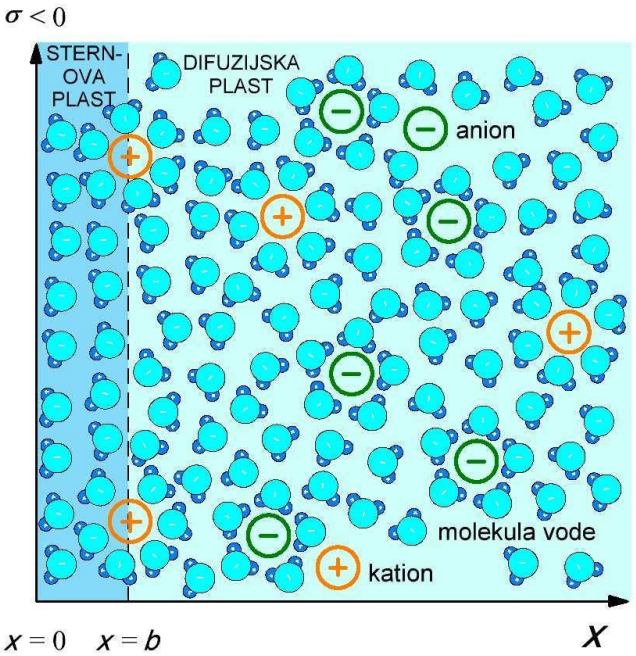

Slika 2.13: Grafična predstavitev Sternove in difuzijske plasti. Zunanja Helmholtzova ravnina (OHP) je locirana na razdalji b (razdalja približanja). Okoli posameznih anionov in kationov so vodne molekule močno orientirane. σ predstavlja površinsko gostoto električnega naboja na kovinski površini elektrode pri x = 0.

(C_{diff}) je [28]:

$$\frac{1}{C_{diff}} = \frac{1}{C_S} + \frac{1}{C_{DL}} \; ; \tag{2.52}$$

torej predvideva, da je plast med površino kovinske elektrode in raztopino soli vsota dveh kapacitivnosti: kapacitivnosti Sternove plasti (C_S) in kapacitivnosti difuzijske plasti (C_{DL}). Kapacitivnost Sternove plasti (C_S) je enaka kapacitivnosti ploščatega kondenzatorja:

$$C_S = \frac{\varepsilon_0 \varepsilon_S}{b}, \tag{2.53}$$

kjer je ε_0 dielektričnost vakuma, ε_S relativna dielektričnost Sternove plasti in b debelina Sternove plasti. Znotraj GC modela pa je kapacitivnost difuzijske plasti (C_{DL}) enaka [28, 70, 71]:

$$C_{DL} = \frac{d\sigma}{d\varphi(x=b)} = \left(2\beta e_0^2 n_0 \varepsilon_r \varepsilon_0\right)^{1/2} \cosh(\beta e_0 \varphi(x=b)/2) \; , \tag{2.54}$$

kjer je ε_r od kraja neodvisna dielektričnost difuzijske plasti ($b \leq x < \infty$). Skupna diferencialna kapacitivnost (C_{diff}) je tako:

$$\frac{1}{C_{diff}} = \frac{b}{\varepsilon_0 \varepsilon_S} + \frac{1}{(2\beta e_0^2 n_0 \varepsilon_r \varepsilon_0)^{1/2} \cosh(\beta e_0 \varphi(x=b)/2)} \; . \tag{2.55}$$

Sternov model predpostavlja, da sta ε_S in ε_r konstantni. Zaradi enostavnosti privzamemo za ε_r v difuzijski plasti konstantno vrednost. V Sternovi plasti je velikost jakosti električnega polja (E) konstantna, zato lahko relativno dielektričnost v Sternovi plasti (ε_S) izračunamo kot sledi. Če vodno molekulo obravnavamo kot v modelu MLPB (kot kroglo s točkastim permanentnim dipolom z dipolnim momentom (p_0) in dielektričnostjo, ki je enaka kvadratu lomnega količnika vode (n^2)) [64], lahko vektor polarizacije vodnih molekul v Sternovi plasti ($0 \leq x < b$) zapišemo kot [56, 64]:

$$P = -n_{0w} p_0 \left(\frac{2+n^2}{3}\right) L(\gamma p_0 E \beta) \; , \tag{2.56}$$

kjer je n_{0w} številska gostota molekul vode, E je velikost električnega polja, n je lomni količnik vode, p_0 amplituda zunanjega dipolnega momenta vodne molekule,

L je Langevinova funkcija in $\gamma = (2+n^2)/2$. Relativna dielektričnost v Sternovi plasti (ε_S) je tako:

$$\varepsilon_S = n^2 + \frac{|P|}{\varepsilon_0 E} = n^2 + \frac{n_{0w} p_0}{\varepsilon_0} \frac{2+n^2}{3} \frac{L(\gamma p_0 E \beta)}{E} , \tag{2.57}$$

od tod dobimo enačbo za kapacitivnost Sternove plasti ($0 \leq x \leq b$) ([59] ali Priloga F):

$$C_S = \frac{\varepsilon_0 n^2 + n_{0w} p_0 \frac{2+n^2}{3} \frac{L(\gamma p_0 E \beta)}{E}}{b} . \tag{2.58}$$

Za relativno dielektričnost difuzijske plasti (ε_r) privzamemo pri sobni temperaturi vrednost $\varepsilon_r = 78,5$.

Za izračun električnega potenciala $\varphi(x = b)$ ter relativne dielektričnosti Sternove plasti (ε_S) smo uporabili naslednje robne pogoje ([59] ali Priloga F):

$$\frac{d\varphi}{dx}(x = 0) = -\frac{\sigma}{\varepsilon_0 \varepsilon_S} , \tag{2.59}$$

$$\varepsilon_0 \varepsilon_S \frac{d\varphi}{dx}(x = b_-) = \varepsilon_0 \varepsilon_r \frac{d\varphi}{dx}(x = b_+) , \tag{2.60}$$

$$\varphi(x = b_-) = \varphi(x = b_+) , \tag{2.61}$$

kjer je σ površinska gostota električnega naboja na površini elektrode. Zaradi konstantne vrednosti električnega polja v Sternovi plasti ([59] ali Priloga F):

$$\frac{d\varphi}{dx}(x = 0) = \frac{d\varphi}{dx}(x = b_-) \tag{2.62}$$

lahko s pomočjo enačb 2.59–2.60 dobimo še pogoj:

$$\frac{d\varphi}{dx}(x = b_+) = -\frac{\sigma}{\varepsilon_0 \varepsilon_r} . \tag{2.63}$$

Indeksa $_-$ in $_+$ v enačbah 2.60–2.63 ponazarjata levo oziroma desno stran na meji $x = b$.

3 Rezultati in razprava

3.1 Meritev električnih lastnosti ravninskih lipidnih dvoslojev

3.1.1 Lipidni dvosloji, zgrajeni iz arheolipidov, pridobljenih iz arheje Aeropyrum Pernix K1

Specifično kapacitivnost (c_{blm}) in porušitveno napetost (U_{br}) v odvisnosti od temperature za lipidne dvosloje iz lipidnih molekul, pridobljenih iz arheje *A. Pernix K1*, prikazuje slika 3.1. Meritve so prikazane s srednjo vrednostjo s pripadajočim standardnim odklonom. Meritve ohlajanja in ogrevanja so bile opravljene v temperaturnem območju med 292 K in 329 K. Tako c_{blm} kot U_{br} sta praktično neodvisni od temperature v temperaturnem območju do nekje 323 K, nad to temperaturo je zaznati padec tako pri c_{blm} kot pri U_{br}. Padec so napovedali tudi Polak in sodelavci [72] v modelu molekularne dinamike. Pokazali so, da po 323 K površina na lipidno molekulo naraste, kar je analogno padcu c_{blm}, dipolni potencial membrane pa po 323 K upade, kar lahko interpretiramo kot padec U_{br}. Povprečna c_{blm} med ogrevanjem je $0,216\ \mu F/cm^2$, med ohlajanjem pa $0,253\ \mu F/cm^2$. Število meritev je pri posamezni temperaturi med ogrevanjem in ohlajanjem predstavljeno na sliki 3.2. Statistični t-test je zaradi velikih standardnih odklonov pokazal, da ni statističnih razlik med meritvami c_{blm} med ogrevanjem in ohlajanjem pri posamezni temperaturi. Prav tako zaradi istega vzroka ni statističnih razlik med meritvami U_{br}. Povprečna U_{br} na celotnem opazovanem temperaturnem območju

med ogrevanjem je 556 mV, med ohlajanjem pa 577 mV.

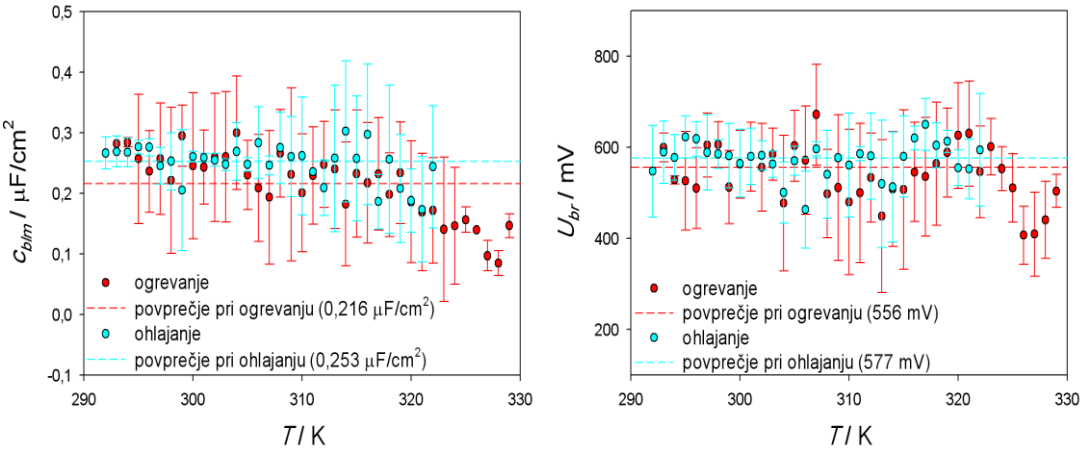

Slika 3.1: Specifična kapacitivnost (c_{blm}) (levi graf) in porušitvena napetost (U_{br}) (desni graf) v odvisnosti od temperature za lipidne dvosloje iz arheolipidov, pridobljenih iz arheje *A. Pernix K1*. Rdeče meritve predstavljajo c_{blm} in U_{br} med ogrevanjem, turkizne pa med ohlajanjem. Meritve so prikazane s srednjo vrednostjo s podanim standardnim odklonom. Horizontalni črtkani črti predstavljata povprečji c_{blm} in U_{br} med ogrevanjem (rdeča črtkana črta) in ohlajanjem (turkizna črtkana črta).

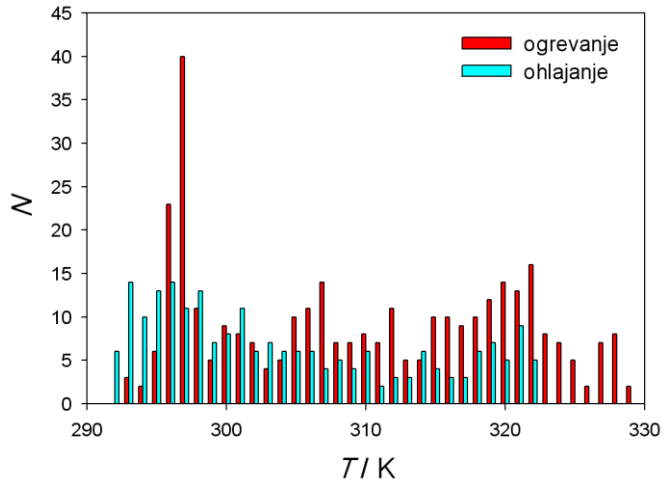

Slika 3.2: Število meritev (N) pri posamezni temperaturi (T) med ogrevanjem (rdeči stolpci) in ohlajanjem (turkizni stolpci) za lipidne dvosloje iz arheolipidov, pridobljenih iz arheje *A. Pernix K1*.

3.1.2 Lipidni dvosloji iz mešanice DPPC in DPhPC

Specifično kapacitivnost (c_{blm}) in porušitveno napetost (U_{br}) v odvisnosti od temperature za lipidne dvosloje iz mešanice lipida DPPC in DPhPC v razmerju 20 : 80 prikazuje slika 3.3. Meritve c_{blm} in U_{br} med ohlajanjem in ogrevanjem so bile opravljene v temperaturnem območju med 298 K in 325 K. Pri c_{blm} je opaziti močno odvisnost od temperature. Vrednost c_{blm} je pri temperaturi 298 K približno $0,3\ \mu F/cm^2$ in se z višanjem temperature linearno povečuje do vrednosti približno $0,5\ \mu F/cm^2$ ($T = 314$ K). Temperatura 314 K predstavlja temperaturo faznega prehoda (T_m) lipida DPPC. Nad temperaturo faznega prehoda c_{blm} linearno upade na vrednost približno $0,4\ \mu F/cm^2$. Število meritev je pri posamezni temperaturi med ogrevanjem in ohlajanjem predstavljeno na sliki 3.4. Razlika med posameznimi meritvami pri c_{blm} med ogrevanjem in ohlajanjem pri isti temperaturi ni statistično različna (t-test), saj so meritve znotraj območja standardnega odklona. Porušitvena napetost (U_{br}) v merjenem temperaturnem območju ne izkazuje odvisnosti od temperature, prav tako ni statistično določljive razlike

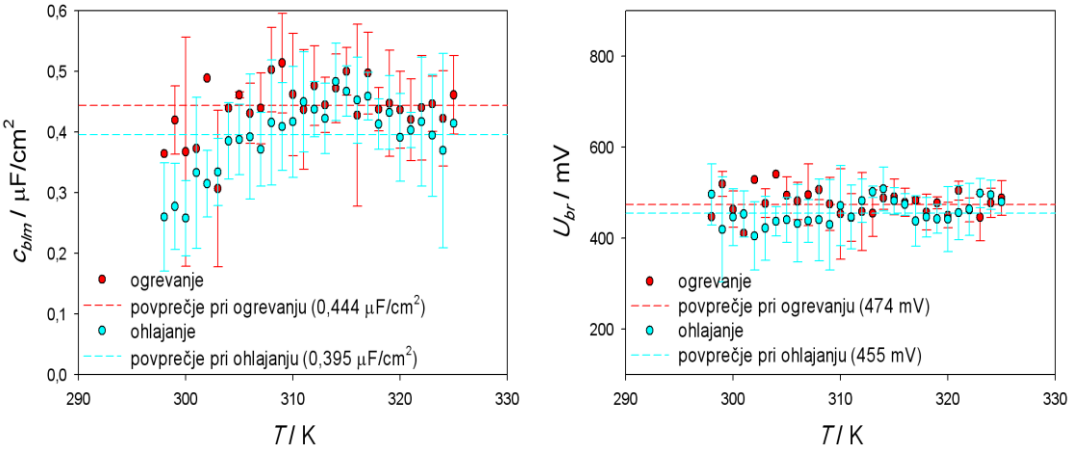

Slika 3.3: Specifična kapacitivnost (c_{blm}) (levi graf) in porušitvena napetost (U_{br}) (desni graf) v odvisnosti od temperature za lipidne dvosloje iz mešanice lipida DPPC in DPhPC v razmerju 20 : 80. Meritve so prikazane s srednjo vrednostjo s pripadajočim standardnim odklonom. Rdeče meritve predstavljajo izmerjene vrednosti med ogrevanjem, turkizne pa med ohlajanjem. Horizontalni črtkani črti predstavljata povprečji c_{blm} in U_{br} med ogrevanjem (rdeča črtkana črta) in ohlajanjem (turkizna črtkana črta).

pri U_{br} med ogrevanjem in ohlajanjem.

Specifična kapacitivnost (c_{blm}) in porušitvena napetost (U_{br}) v odvisnosti od temperature za lipidne dvosloje iz mešanice lipida DPPC in DPhPC v razmerju 20 : 80 v primerjavi s toplotno kapaciteto C_p (primerjava z U_{br}) in molekularnim volumnom (primerjava s c_{blm}) [73] je prikazana na sliki 3.5. Meritve so prikazane s srednjo vrednostjo s pripadajočim standardnim odklonom. Meritve c_{blm} in U_{br} so povprečje meritev med ogrevanjem in ohlajanjem. Pri U_{br} opazimo zelo dobro ujemanje s toplotno kapaciteto na celotnem primerjanem temperaturnem območju. Okrog temperature faznega prehoda lipida DPPC (T_m = 314 K) opazimo tudi rahlo povečanje porušitvene napetosti (U_{br}). Primerjava c_{blm} z molekularnim volumnom pa pokaže, da je pod temperaturo faznega prehoda lipida DPPC ($T < T_m$) pri c_{blm} in U_{br} trend naraščanja, nad temperaturo faznega prehoda ($T > T_m$) pa c_{blm} upade, molekularni volumen pa še naraste.

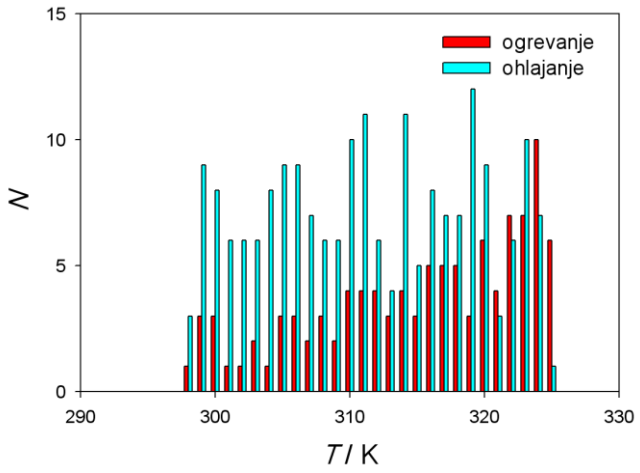

Slika 3.4: Število meritev (N) pri posamezni temperaturi (T) med ogrevanjem (rdeči stolpci) in ohlajanjem (turkizni stolpci) za lipidne dvosloje iz mešanice lipida DPPC in DPhPC v razmerju 20 : 80.

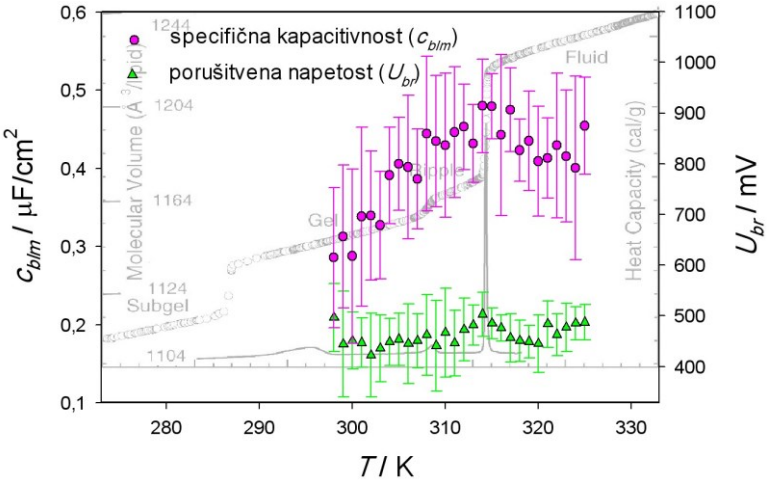

Slika 3.5: Specifična kapacitivnost (c_{blm}) (roza meritve) in porušitvena napetost (U_{br}) (zelene meritve) v odvisnosti od temperature za lipidne dvosloje iz mešanice lipida DPPC in DPhPC v razmerju 20 : 80 v primerjavi s toplotno kapaciteto (primerjava z U_{br}) in molekularnim volumnom (primerjava s c_{blm}) [73]. Meritve so prikazane s srednjo vrednostjo s pripadajočim standardnim odklonom. Opomba: Ujema se le temperaturno območje (os x), ujemanje osi y je le rezultat skaliranja.

3.1.3 Lipidni dvosloji iz DPhPC

Specifično kapacitivnost (c_{blm}) in porušitveno napetost (U_{br}) v odvisnosti od temperature za lipidne dvosloje iz lipida DPhPC prikazuje slika 3.6. Meritve ohlajanja in ogrevanja so bile opravljene na temperaturnem območju med 298 K in 321 K. Meritve so prikazane s srednjo vrednostjo s pripadajočim standardnim odklonom. Število meritev je pri posamezni temperaturi med ogrevanjem in ohlajanjem predstavljeno na sliki 3.7. Meritve smo uporabili kot referenčne meritve za meritve na sliki 3.3, saj smo vse meritve na ravninskih lipidnih dvoslojih, sestavljenih iz mešanic DPPC in DPhPC, ki so izkazovale enak trend kot meritve na sliki 3.6, zanemarili. Pri vrednostih c_{blm} je na videz opazna razlika med ohlajanjem in ogrevanjem pri posameznih temperaturah, vendar izvedba statističnega t-testa zaradi pomanjkanja meritev ni možna, zato tega ne moremo z gotovostjo trditi.

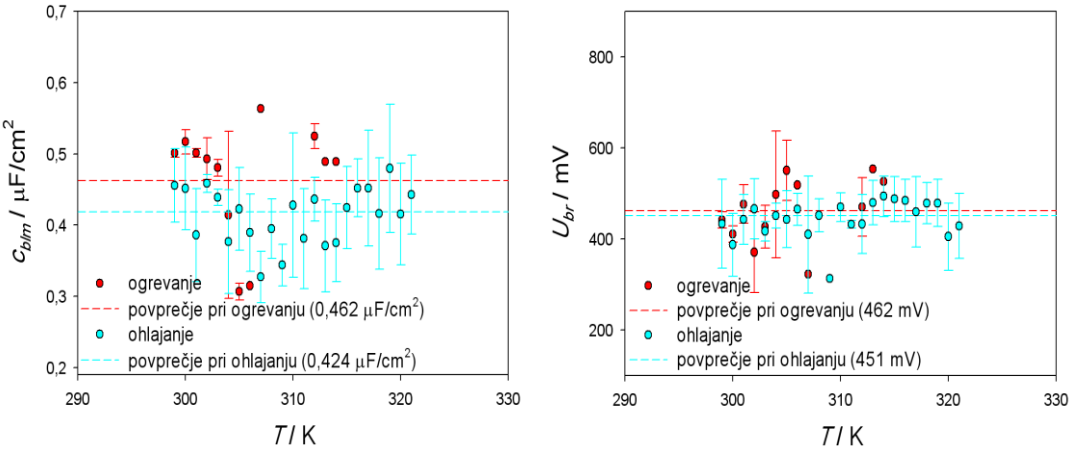

Slika 3.6: Specifična kapacitivnost (c_{blm}) (levi graf) in porušitvena napetost (U_{br}) (desni graf) v odvisnosti od temperature za lipidne dvosloje iz lipida DPhPC. Rdeče meritve predstavljajo meritve med ogrevanjem, turkizne pa med ohlajanjem. Meritve so prikazane s srednjo vrednostjo s pripadajočim standardnim odklonom. Horizontalni črtkani črti predstavljata povprečji c_{blm} in U_{br} med ogrevanjem (rdeča črtkana črta) in ohlajanjem (turkizna črtkana črta).

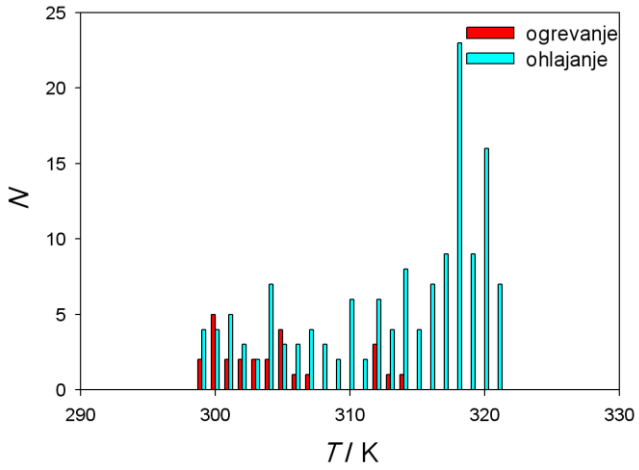

Slika 3.7: Število meritev (N) pri posamezni temperaturi (T) med ogrevanjem (rdeči stolpci) in ohlajanjem (turkizni stolpci) za lipidne dvosloje iz lipida DPhPC.

3.1.4 Lipidni dvosloji iz DPPC

Specifična kapacitivnost (c_{blm}) in porušitvena napetost (U_{br}) v odvisnosti od temperature za lipidne dvosloje iz DPPC v primerjavi s toplotno kapaciteto (primerjava z U_{br}) in molekularnim volumnom (primerjava s c_{blm}) [73] sta prikazani na sliki 3.8. Prikazane meritve c_{blm} in U_{br} so rezultat enega eksperimenta. Opazimo zelo dobro ujemanje vrednosti c_{blm} z molekularnim volumnom in U_{br} s toplotno kapaciteto na celotnem primerjanem temperaturnem območju. Pri c_{blm} se dobro odrazi tako gel-kristalna faza, predfaza (ang. *ripple*) faza ter tekoče-kristalna faza. V gel-kristalni fazi je povprečna specifična kapacitivnost $0,29\,\mu F/cm^2$, v predfazi naraste na povprečno vrednost $0,44\,\mu F/cm^2$, po faznem prehodu pa na $0,51\,\mu F/cm^2$. Povprečje porušitvene napetosti (U_{br}) je v gel-kristalni fazi 593 mV, po faznem prehodu pa naraste na 931 mV. Z meritvijo c_{blm} in U_{br} je mogoče detektirati območje prehoda lipida, ne moremo pa definirati točne temperature faznega prehoda (T_m) za dani lipid.

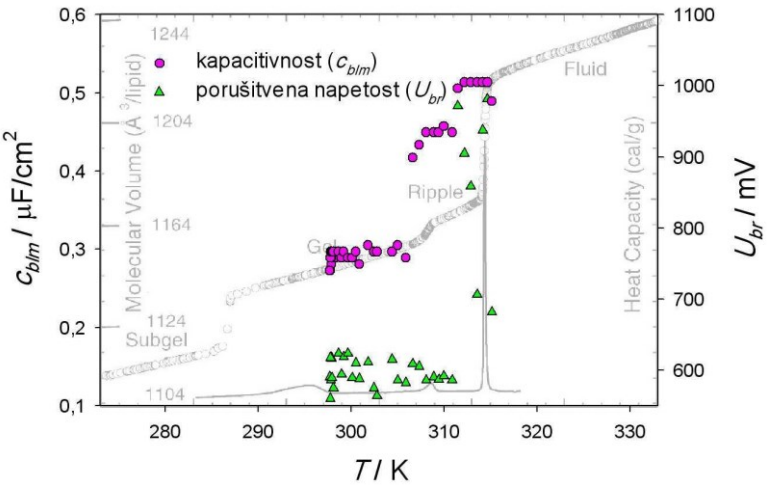

Slika 3.8: Specifična kapacitivnost (c_{blm}) (roza meritve) in porušitvena napetost (U_{br}) (zelene meritve) v odvisnosti od temperature za lipidne dvosloje iz lipida DPPC v primerjavi s toplotno kapaciteto (primerjava z U_{br}) in molekularnim volumnom (primerjava s c_{blm}) [73]. Opomba: Ujema se le temperaturno območje (os x), ujemanje osi y je le rezultat skaliranja.

3.2 Modeliranje lipidne dvojne plasti v stiku z raztopino soli in nanodelcem

3.2.1 MLPB model

Številsko gostoto električnega naboja anionov (n_-) in kationov (n_+) v odvisnosti od razdalje od zviterionske plasti pri $x = 0$, pri dveh temperaturah 310 K in 323 K prikazuje slika 3.9. V bližini zviterionske lipidne plasti pri $x = 0$ je vidna akumulacija kationov (n_+) in primanjkljaj anionov (n_-). Z naraščanjem razdalje x od negativne površine pri $x = 0$ proti pozitivnim delom zviterionskih glav se povečuje številska gostota anionov (n_-) in zmanjšuje številska gostota kationov (n_+). Od področja glav naprej ($x > D$) pa se trend spet obrne, vse dokler številski gostoti n_+ in n_- pri velikih razdaljah ne dosežeta ravnovesne koncentracije (pogoja elektronevtralnosti), ki odgovarja koncentraciji raztopine soli. Pri

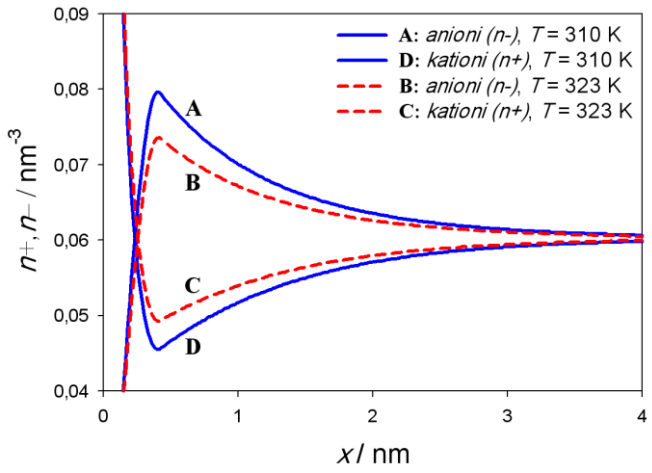

Slika 3.9: Številska gostota električnega naboja anionov (n_-) (A,B) in kationov (n_+) (C,D) v odvisnosti od razdalje od zviterionske plasti pri $x = 0$, računano pri dveh temperaturah 310 K (polna modra krivulja) in 323 K (črtkana rdeča krivulja) s pripadajočima vrednostima za površino na lipidno molekulo ($a_0 = 0,48\,\mathrm{nm}^2$ pod 314 K in $a_0 = 0,60\,\mathrm{nm}^2$ nad 314 K). Dipolni moment vodne molekule je $p_0 = 3,1$ Debye, $D = 0,42$ nm, koncentracija raztopine soli $n_0/N_A = 0,1$ mol/l in koncentracija vode $n_{0w}/N_A = 55$ mol/l, kjer je N_A Avogadrovo število.

višji temperaturi (323 K) zavzema lipidna molekula DPPC tudi večjo površino $a_0 = 0,60\,\mathrm{nm}^2$, zaradi tega je manjša površinska gostota električnega naboja zviterionske plasti (σ) pri $x = 0$, kar vodi v manjšo številsko gostoto električnega naboja ionov kot v primeru nižje temperature 310 K (Priloga A).

Električni potencial (φ) in relativno dielektričnost (ε_r) v odvisnosti od oddaljenosti od zviterionske lipidne plasti pri $x = 0$ za primer dveh temperatur in pripadajočih vrednosti za površino na lipidno molekulo (a_0): $T = 310$ K, $a_0 = 0,48\,\mathrm{nm}^2$ in $T = 323$ K, $a_0 = 0,60\,\mathrm{nm}^2$ prikazuje slika 3.10. Iz grafa je razvidno, da se relativna dielektričnost (ε_r) drastično zniža v bližini zviterionske lipidne plasti. Pri zviterionski plasti ($x = 0$) vrednost ε_r upade na 44 pri $T = 310$ K in na 55 pri $T = 323$ K. Vpliv zviterionske plasti na nižanje ε_r je skoraj zanemarljiv že na razdalji $x = D$. Daleč stran od zviterionske lipidne plasti

pri $x = 0$ je vrednost relativne dielektričnosti 75, 5 pri temperaturi $T = 310\,K$ in 72, 6 pri temperaturi $T = 323\,K$. Tudi električni potencial ($\varphi(x)$) je v bližini zviterionske plasti opazno negativnejši in znaša $-60\,mV$ pri temperaturi $T = 310\,K$ in $-54\,mV$ pri temperaturi $T = 323\,K$ (Priloga A).

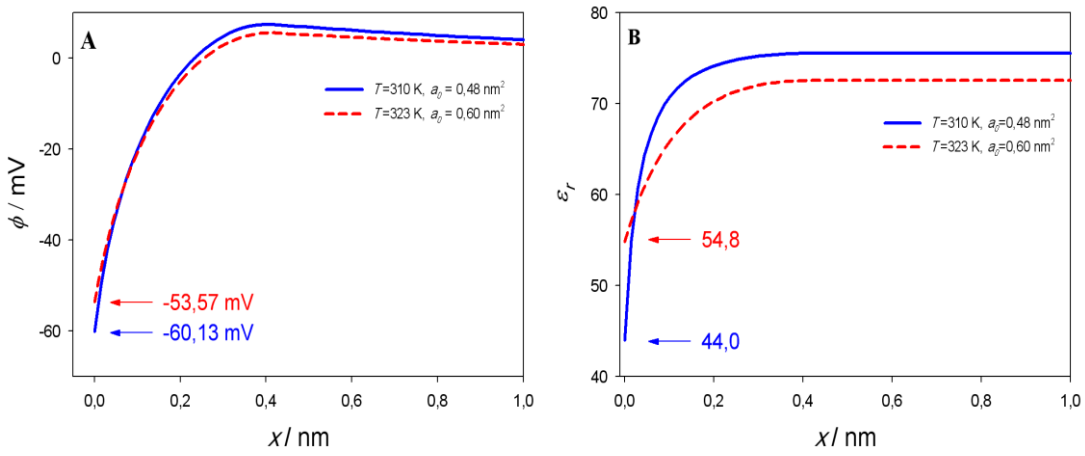

Slika 3.10: Električni potencial (φ) (graf A) in relativna dielektričnost (ε_r) (graf B) v odvisnosti od razdalje od zviterionske lipidne plasti pri $x = 0$ za primer dveh temperatur in pripadajočih vrednosti za površino na lipidno molekulo a_0: $T = 310\,K$, $a_0 = 0,48\,nm^2$ (polna modra krivulja) in $T = 323\,K$, $a_0 = 0,60\,nm^2$ (črtkana rdeča krivulja). Vrednosti a_0 odgovarjajo vrednostim za lipid DPPC v dveh fazah. Relativno dielektričnost (ε_r) kot funkcijo razdalje od zviterionske plasti pri $x = 0$ smo izračunali s pomočjo enačbe 2.19. Dipolni moment molekule vode je $p_0 = 3,1$ Debye, $D = 0,42\,nm$, koncentracija soli je $n_0/N_A = 0,1\,mol/l$, koncentracija molekul vode je $n_{0w}/N_A = 55\,mol/l$, kjer je N_A Avogadrovo število. Drugi robni pogoj (enačba 2.21) je bil zaradi poenostavitve postavljen pri 12 nm.

Povprečen kot orientacije glave zviterionske molekule ($< \omega >$) v odvisnosti od temperature T prikazuje slika 3.11. Pri temperaturi faznega prehoda 314 K lipidne molekule DPPC vrednosti $< \omega >$ nismo izračunali, ker fazni prehod ni bil vključen v MLPB model. Iz grafa vidimo, da je povprečen kot orientacije glave zviterionske molekule ($< \omega >$) neodvisen od temperature. Razlika v $< \omega >$ med gel-kristalno in tekoče-kristalno fazo pa je posledica različnih vrednosti površine

na lipidno molekulo a_0 med obema faznima stanjema (Priloga A).

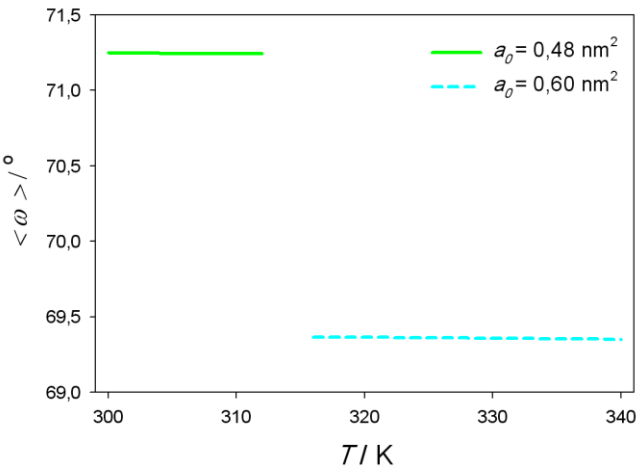

Slika 3.11: Povprečen kot orientacije glave zviterionske molekule ($< \omega >$) (glejte tudi sliko 2.8) v odvisnosti od temperature (T). Površina na lipidno molekulo je $a_0 = 0,48\,\mathrm{nm}^2$ pod temperaturo 314 K, kar odgovarja gel-kristalni fazi lipidne molekule DPPC (polna zelena črta) in $a_0 = 0,60\,\mathrm{nm}^2$ nad 314 K, kar odgovarja tekoče-kristalni fazi lipidne molekule DPPC (črtkana turkizna črta). Ker MLPB model ne vključuje faznega prehoda, krivulji v bližini temperature prehoda (314 K) med seboj nista povezani. Povprečen kot orientacije glave zviterionske molekule ($< \omega >$) smo izračunali iz $P(x)$ (glejte dodatek v Prilogi A). Vrednosti drugih parametrov so iste kot na sliki 3.10.

Gostoto verjetnosti za pozitivne dele zviterionskih lipidnih glav $P(x)$ v odvisnosti od razdalje od zviterionske lipidne plasti pri $x = 0$ za primer, ko so pozitivni deli zviterionskih lipidnih glav obravnavani kot točkasti delci, ter za tri različne parametre α, ko so pozitivni deli zviterionskih lipidnih glav obravnavani kot delci s končnim volumnom in z gostoto verjetnosti izračunano iz molekularne dinamike prikazuje slika 3.12. Površina na lipidno molekulo je $a_0 = 0,60\,\mathrm{nm}^2$ in temperatura 323 K, kar odgovarja tekoče-kristalni fazi lipidne molekule DPPC. Iz grafa vidimo, da je razlika med $P(x)$ v MLPB, ki ne upošteva končnih volumnov pozitivnih delov zviterionskih lipidnih glav (enačba 2.16) in $P(x)$ izračunan iz mo-

lekularne dinamike zelo velika in hkrati pričakovana, saj molekularna dinamika vključuje končne volumne vseh delcev v sistemu. Pri modificirani enačbi za $P(x)$ (enačba 2.27), ki upošteva končne volumne pozitivnih delov zviterionskih lipidnih glav, pa se z večanjem deleža pozitivnih delov zviterionskih lipidnih glav (α), približujemo vrednosti iz molekularne dinamika. V primeru, ko so vsa mrežna mesta zasedena samo s pozitivnimi deli zviterionskih lipidnih glav ($\alpha \to \infty$), postane $P(x)$ konstantna vrednost (Priloga A).

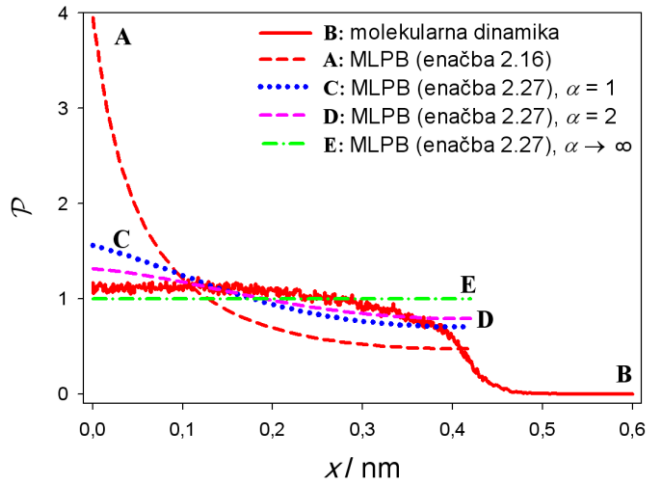

Slika 3.12: Gostota verjetnosti za pozitivne dele zviterionskih lipidnih glav $P(x)$ v odvisnosti od razdalje od zviterionske lipidne plasti pri $x = 0$ za primer, ko so pozitivni deli zviterionskih lipidnih glav obravnavani kot točkasti delci (A), ter za tri primere ($\alpha = 1$ (C), $\alpha = 2$ (D) in $\alpha = 1000$ (E)), ko so pozitivni deli zviterionskih lipidnih glav obravnavani kot delci s končnim volumnom in z gostoto verjetnosti izračunano iz molekularne dinamike (B). Površina na lipidno molekulo je $a_0 = 0,60\,\mathrm{nm}^2$, temperatura 323 K, kar odgovarja tekoče-kristalni fazi lipidne molekule DPPC, koncentracija soli je $n_0/N_A = 0,45$ mol/l, vrednosti ostalih parametrov pa so iste kot na sliki 3.10.

Povprečen kot orientacije glave zviterionske molekule ($<\omega>$) v odvisnosti od razdalje nanodelca (D_{np}) od lipidne plasti ($x = 0$) pri treh različnih parametrih α in za tri različno električno nabite površine nanodelca (σ_2) prikazuje slika 3.13. V

primeru negativnega nanodelca ($\sigma_2 = 0,5\,\sigma_1$) se povprečen kot orientacije glave zviterionske molekule ($<\omega>$) z manjšanjem razdalje D_{np} zmanjšuje, saj se pozitivni deli zviterionskih lipidnih glav pri $x = D$ in negativno električno nabiti nanodelec privlačijo. Za vse tri parametre α se kot $<\omega>$ približa vrednosti 57°. V primeru pozitivno električno nabitega nanodelca ($\sigma_2 = -0,5\,\sigma_1$) pa se pozitivni zviterionski deli lipidnh glav ($x = D$) odbijajo od nanodelca, zato se povprečen kot orientacije glave zviterionske molekule ($<\omega>$) povečuje. V primeru nevtralnega nanodelca ($\sigma_2 = 0$) pa je povprečen kot orientacije glave zviterionske molekule ($<\omega>$) praktično konstanten (Priloga B).

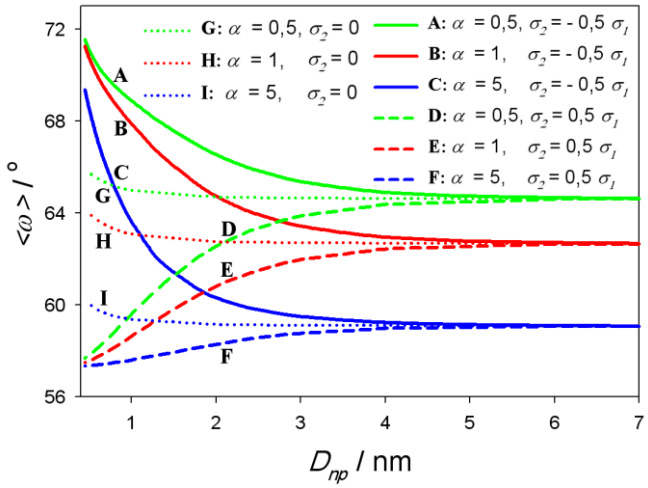

Slika 3.13: Povprečen kot orientacije glave zviterionske molekule ($<\omega>$) v odvisnosti od razdalje nanodelca (D_{np}) od zviterionske lipidne plasti ($x = 0$) (glejte tudi sliko 2.12) pri treh različnih vrednostih parametra α in za tri različne vrednosti električno nabite površine nanodelca (σ_2): negativno (črtkane krivulje), pozitivno (polne krivulje) in nevtralno površino (pikčaste krivulje). Ostali uporabljeni parametri so: $p_0 = 3,1$ Debye, $D = 0,42$ nm, $T = 298$ K, $\sigma_1 = -0,3$ As/m^2, koncentracija soli je $n_0/N_A = 0,1$ mol/l, koncentracija molekul vode je $n_{0w}/N_A = 55$ mol/l.

Osmotski tlak (Π) med zviterionsko lipidno plastjo ($x = 0$) ter pozitivno in negativno električno nabitim nanodelcem (glejte tudi sliko 2.12) kot funkcija

razdalje od nanodelca (D_{np}) je prikazan na sliki 3.14. V primeru pozitivnega nanodelca se z zmanjševanjem razdalje D_{np} osmotski tlak (Π) povečuje, saj se povečuje tudi povprečen kot orientacije glave zviterionske molekule ($< \omega >$) (slika 3.13). V primeru negativnega nanodelca pa se z zmanjševanjem razdalje D_{np} osmotski tlak (Π) zmanjšuje, saj se zaradi privlačnih elektrostatičnih sil med pozitivnimi deli zviterionskih glav in negativnim nanodelcem zmanšuje tudi povprečen kot orientacije glave zviterionske molekule ($< \omega >$) (slika 3.13)(Priloga B).

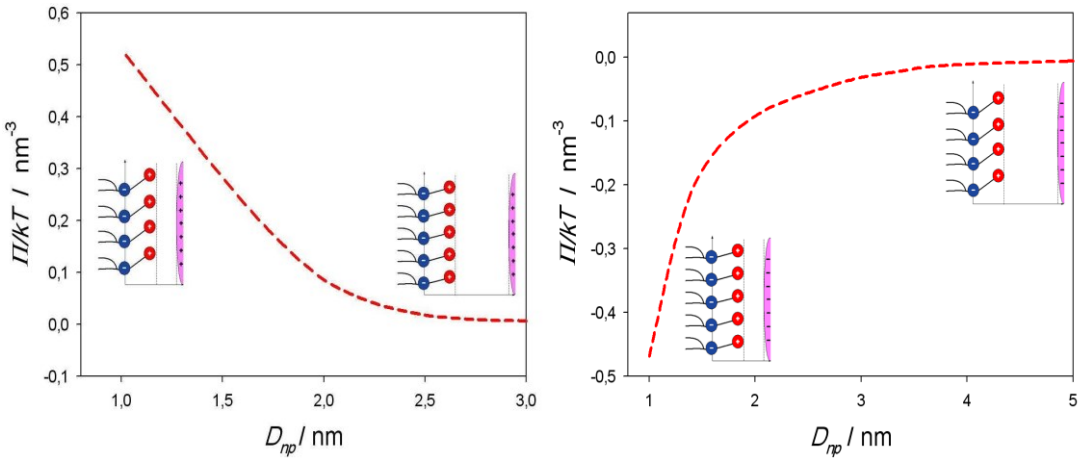

Slika 3.14: Osmotski tlak (Π) med negativno zviterionsko lipidno plastjo ($x = 0$) in pozitivno (levi graf) in negativno (desni graf) električno nabitim nanodelcem (glejte tudi sliko 2.12) kot funkcija razdalje D_{np}. Parametri modela so: $p_0 = 3,1$ Debye, $D = 0,42$ nm, $T = 298$ K, $a_0 = 0,60$ nm^2, $\alpha = 5$, koncentracija raztopine soli je $n_0/N_A = 0,01$ mol/l, koncentracija molekul vode je $n_{0w}/N_A = 55$ mol/l, kjer je N_A Avogadrovo število.

Povprečen kot orientacije glave molekule POPS ($< \omega >$) v odvisnosti od razdalje nanodelca (D_{np}) od zviterionske lipidne plasti ($x = 0$) pri treh različnih parametrih α in za tri različno električno nabite površine nanodelca (σ_2) prikazuje slika 3.15. V primeru negativnega nanodelca ($\sigma_2 = 0,5\,\sigma_1$) se povprečen kot orientacije glave molekule POPS ($< \omega >$) z manjšanjem razdalje D_{np} povečuje, saj se negativni (serinski) deli lipidnih glav ($x \leq 2D$) od negativno električno

nabitega nanodelca odbijajo. V primeru pozitivno električno nabitega nanodelca ($\sigma_2 = -0,5\,\sigma_1$) pa se negativni (serinski) deli lipidnih glav ($x \leq 2D$) privlačijo k nanodelcu proti povprečnemu kotu orientacije glave molekule POPS ($< \omega > = 57°$), kar predstavlja tudi izračunan povprečni kot orientacije. V primeru nevtralnega nanodelca ($\sigma_2 = 0$) je povprečen kot orientacije glave molekule POPS ($< \omega >$) praktično konstanten (Priloga C). V primerjavi s povprečnim kotom orientacije glave zviterionske molekule ($< \omega >$) (slika 3.13) vidimo, da je za dosego enakega kota rotacija lipidnih molekul ($< \omega >$) potrebno, da je v primeru POPS lipidnih molekul nanodelec bližje lipidni plasti. Iz tega lahko sklepamo, da pozitivni (amino) deli lipidnih glav ($x \leq D$) senčijo vpliv nanodelca na povprečen kot orientacije glave molekule POPS ($< \omega >$).

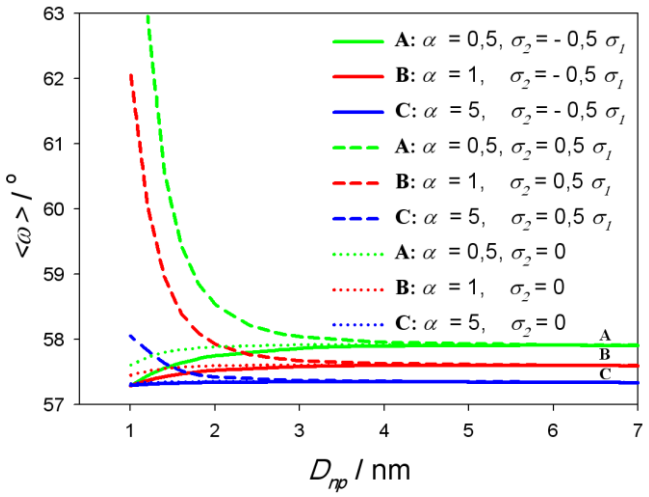

Slika 3.15: Povprečen kot orientacije glave molekule POPS ($< \omega >$) (glejte tudi sliko 2.10) v odvisnosti od razdalje nanodelca (D_{np}) od lipidne plasti ($x = 0$) pri treh različnih parametrih α in za tri različno električno nabite površine nanodelca (σ_2): negativne (polne krivulje), pozitivne (črtkane krivulje) in nevtralne površine (pikčaste krivulje). Ostali uporabljeni parametri so enaki kot na sliki 3.13.

Številsko gostoto električnega naboja enovalentnih anionov (n_-) in dvovalentnih kationov (m) v odvisnosti od razdalje od zviterionske lipidne plasti pri $x = 0$

prikazuje slika 3.16. Znotraj področja glav ($0 \leq x \leq D$) se številska gostota enovalentnih anionov (n_-) zmanjšuje, številska gostota pozitivnih dvovalentnih ionov (m) pa narašča s približevanjem zviterionski plasti ($x = 0$). V področju pozitivnih delov zviterionskih glav pa je prisotna velika številska gostota enovalentnih anionov (n_-) in primanjkljaj dvovalentnih kationov (m). Daleč proč od zviterionske plasti ($x = 0$) je številska gostota enovalentnih anionov (n_-) dvakrat večja od številske gostote dvovalentnih kationov (m), kar ustreza pogoju elektronevtralnosti (enačba 2.32) (Priloga E).

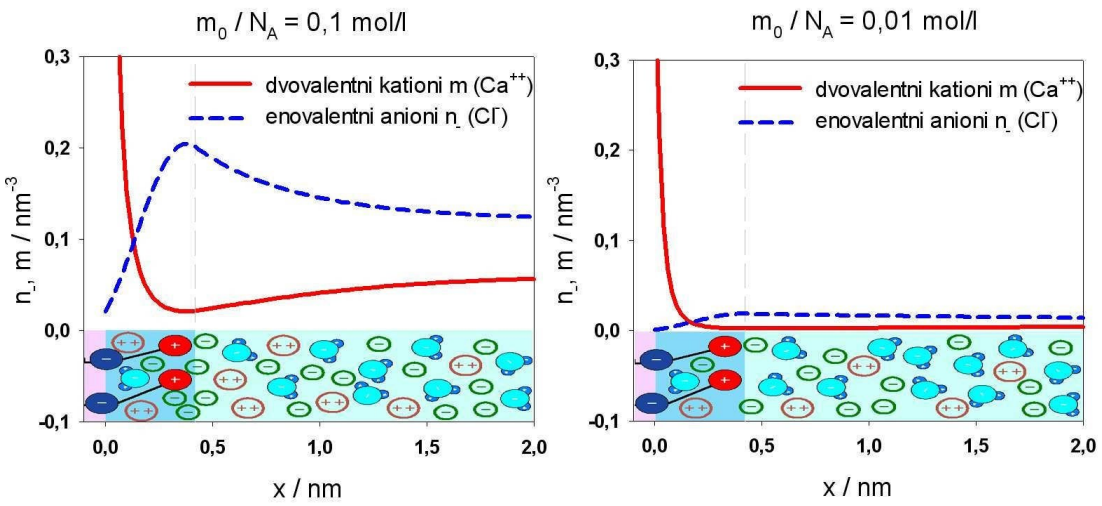

Slika 3.16: Številska gostota električnega naboja enovalentnih anionov (n_-: črtkna modra krivulja) in dvovalentnih kationov (m: polna rdeča krivulja) v odvisnosti od razdalje od zviterionske lipidne plasti pri $x = 0$. Izračun je bil narejen pri dveh različnih koncentracijah dvovalentnih kationov m_0/N_A: 0,1 mol/l (levi graf) in 0,01 mol/l (desni graf). Ostali parametri MLPB modela so: $p_0 = 3,1$ Debye, $D = 0,42$ nm, $T = 298$ K, $\sigma_1 = -e_0/a_0$, $a_0 = 0,60\,\mathrm{nm}^2$, $\alpha = 0,5$, koncentracija molekul vode je $n_{0w}/N_A = 55$ mol/l.

3.2.2 MLB model

Številska gostota električnega naboja kationov (n_+) in anionov (n_-) v odvisnosti od razdalje od zviterionske plasti pri $x = 0$, računano pri temperaturi 323 K s pripadajočo vrednostjo za površino na lipidno molekulo $a_0 = 0,60\,\mathrm{nm}^2$ je prikazana na sliki 3.17. Izračunan primer predstavlja lipid DPPC v tekoče-kristalni

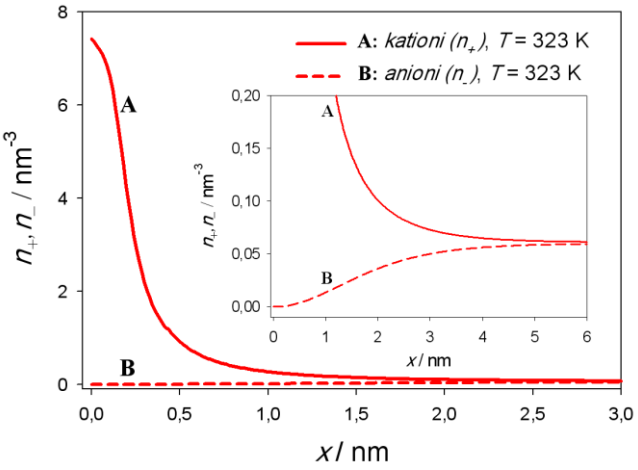

Slika 3.17: Številska gostota električnega naboja kationov (n_+) (A) in anionov (n_-) (B) v odvisnosti od razdalje od zviterionske površine pri $x = 0$, računano pri temperaturi 323 K s pripadajočo vrednostjo za površino na lipidno molekulo $a_0 = 0,60\,\mathrm{nm}^2$. Izračunani primer predstavlja lipid DPPC v tekoče-kristalni fazi. Vstavek prikazuje povečavo pri majhnih številskih gostotah. Dipolni moment vodne molekule je $p_0 = 3,1$ Debye, $D = 0,42$ nm, koncentracija soli $n_0/N_A = 0,1$ mol/l in koncentracija vode $n_{0w}/N_A = 55$ mol/l, kjer je N_A.

fazi. V bližini zviterionske lipidne plasti pri $x = 0$ je velika številska gostota kationov $n_+(x = 0) = 7,4\,\mathrm{nm}^{-3}$ in primankljaj anionov $n_-(x = 0) = 0$. Zaradi upoštevanja končnih volumnov so koncentracije navzgor omejene, zato pozitivni deli zviterionskih glav pri $x = D$ ne morejo spremeniti poteka številske gostote kationov (n_+) in anionov (n_-), kot vidimo na sliki 3.9, kjer je efekt končnih volumnov upoštevan le za pozitivne dele zviterionskih glav ne pa tudi za molekule

soli in vode. Daleč stran od zviterionske plasti sta številski gostoti kationov (n_+) in anionov (n_-) enaki, tako da je izpolnjen pogoj elektronevtralnosti.

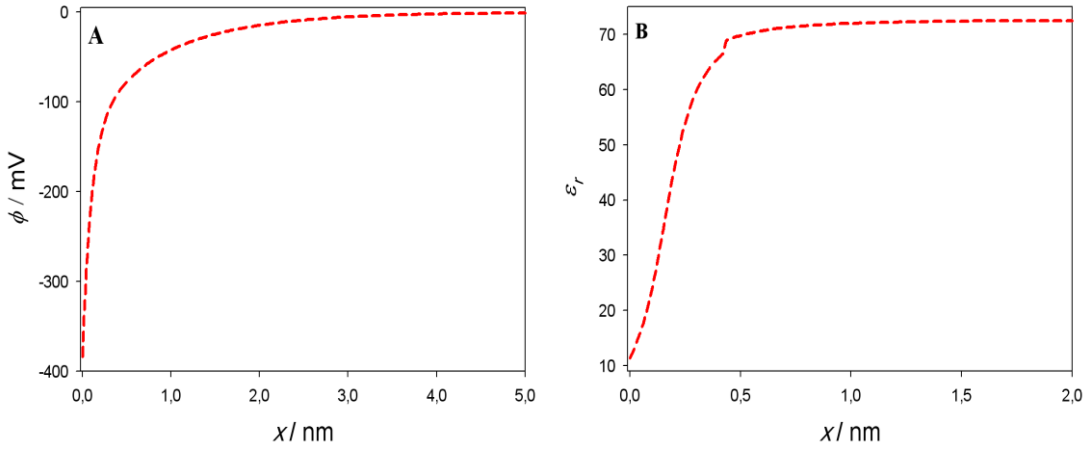

Slika 3.18: Električni potencial (φ) (graf A) in relativna dielektričnost (ε_r) (graf B) v odvisnosti od razdalje od zviterionske lipidne plasti pri $x = 0$, pri temperaturi $T = 323\,\mathrm{K}$ in pripadajoči vrednosti površine na lipidno molekulo $a_0 = 0,60\,\mathrm{nm}^2$, ki odgovarja lipidu DPPC v tekoče-kristalni fazi. Relativno dielektričnost (ε_r) kot funkcijo razdalje od zviterionske plasti pri $x = 0$ smo računali s pomočjo enačbe 2.50. Uporabljeni parametri so enaki kot na sliki 3.17. Drugi robni pogoj (enačba 2.21) je bil zaradi poenostavitve postavljen pri $x = 9\,\mathrm{nm}$.

Električni potencial (φ) in relativna dielektričnost (ε_r) v odvisnosti od razdalje od zviterionske lipidne plasti pri $x = 0$, pri temperaturi $T = 323\,\mathrm{K}$ in pripadajoči vrednosti površine na lipidno molekulo $a_0 = 0,60\,\mathrm{nm}^2$, ki odgovarja lipidu DPPC v tekoče-kristalni fazi, sta prikazani na sliki 3.18. Relativna dielektričnost (ε_r) se v bližini zviterionske lipidne plasti drastično zniža. Pri zviterionski plasti ($x = 0$) vrednost ε_r upade na približno 10. Vpliv zviterionske plasti na nižanje ε_r je skoraj zanemarljiv že na razdalji $x = D$. Daleč stran od zviterionske lipidne plasti je vrednost relativne dielektričnosti $72,6$. Tudi električni potencial (φ) je v bližini zviterionske lipidne plasti ($x = 0$) negativen in znaša približno $-400\,\mathrm{mV}$.

Številska gostota električnega naboja pozitivnih delov zviterionskih glav (n_h) v odvisnosti od razdalje od zviterionske lipidne plasti pri $x = 0$, pri temperaturi

323 K in površino na lipidno molekulo $a_0 = 0,60\,\mathrm{nm}^2$ je prikazana na sliki 3.19. Iz grafa se vidi, da se večina pozitivnih delov zviterionskih lipidnih glav nahaja bližje negativno električno nabiti plasti pri $x = 0$, saj jih ta privlači. Manjša kot je vrednost x, večja je vrednost ω. To tudi pomeni, da je zato povprečen kot orientacije glave zviterionske lipidne molekule $< \omega >$ večji v bližini zviterionske lipidne plasti pri $x = 0$ znotraj področja glav zviterionskih lipidnih molekul in se z oddaljenostjo zmanjšuje. Na meji $x = D = 0,42\,\mathrm{nm}$ je n_h tako najmanjši ($1,15\,\mathrm{nm}^{-3}$), kar pomeni, da je v področju glav zelo malo takšnih lipidnih molekul, ki imajo $\omega = 0$.

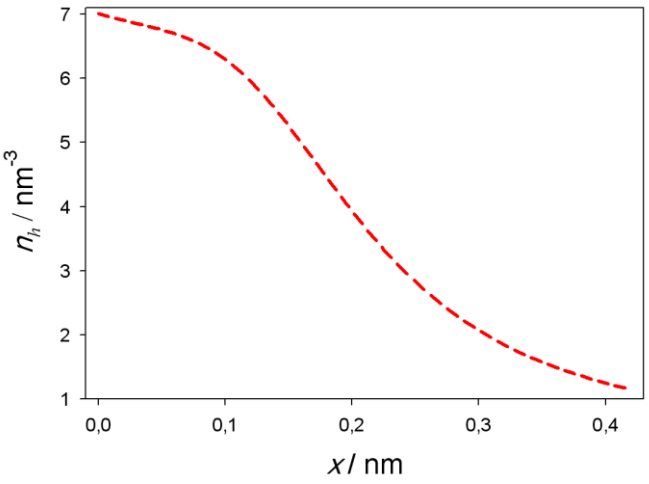

Slika 3.19: Številska gostota električnega naboja pozitivnih delov zviterionskih lipidnih glav (n_h) v odvisnosti od razdalje od zviterionske lipidne plasti pri $x = 0$ znotraj področja glav, računano pri temperaturi 323 K, s pripadajočo vrednostjo za površino na lipidno molekulo $a_0 = 0,60\,\mathrm{nm}^2$, kar predstavlja zviterionsko molekulo DPPC v tekoče-kristalni fazi. Uporabljeni parametri so enaki kot pri sliki 3.17.

Številska gostota električnega naboja vodnih molekul (n_w) v odvisnosti od razdalje od zviterionske lipidne plasti pri $x = 0$, pri temperaturi 323 K s pripadajočo vrednostjo za površino na lipidno molekulo $a_0 = 0,60\,\mathrm{nm}^2$, kar predstavlja lipid DPPC v tekoče-kristalni fazi, je prikazana na sliki 3.20. V področju glav

($0 \leq x \leq D$) se s približevanjem zviterionski lipidni plasti pri $x = 0$ številska gostota vodnih molekul zmanjšuje in doseže vrednost okoli $19\,\mathrm{nm}^{-3}$. V točki $x = D$ pride do skokovite spremembe v številski gostoti vodnih molekul na račun prisotnosti pozitivnih zviterionskih lipidnih glav (glejte tudi sliko 3.19). Daleč stran od zviterionske plasti ($x >> D$) pa je številska gostota vodnih molekul $33,1\,\mathrm{nm}^{-3}$, kar ustreza koncentraciji $n_{0w}/N_A = 55\,\mathrm{mol/l}$.

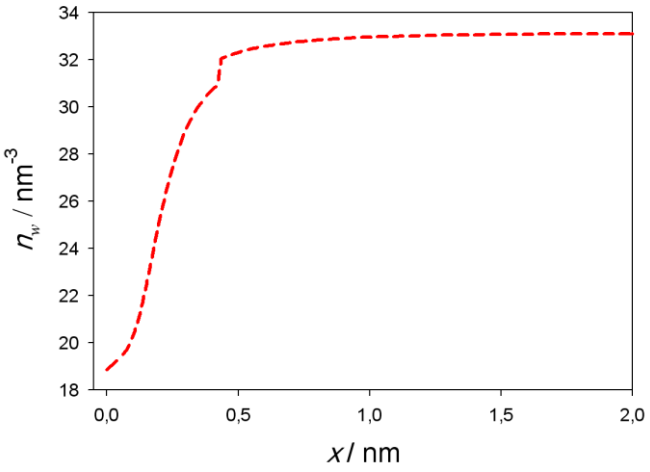

Slika 3.20: Številska gostota vodnih molekul (n_w) v odvisnosti od razdalje od lipidne plasti pri $x = 0$, računano pri temperaturi 323 K, s pripadajočo vrednostjo za površino na lipidno molekulo $a_0 = 0,60\,\mathrm{nm}^2$, kar predstavlja lipid DPPC v tekoče-kristalni fazi. Uporabljeni parametri so enaki kot pri sliki 3.17.

3.2.3 Spremenjen Sternov model

Relativno dielektričnost (ε_S) v Sternovi plasti ($0 \leq x < b$) kot funkcijo gostote električnega naboja na površini elektrode (σ) lahko vidimo na sliki 3.21. Zaradi močne orientacije in nasičenosti vodnih molekul v močnem električnem polju v bližini elektrode se pri velikih vrednostih σ močno zmanjša relativna dielektričnost ε_S (Priloga F).

Relativno dielektričnost ε_r v odvisnosti od oddaljenosti od površine elektrode pri $x = 0$ pri treh različnih vrednostih σ prikazuje slika 3.22. Znotraj posamezne

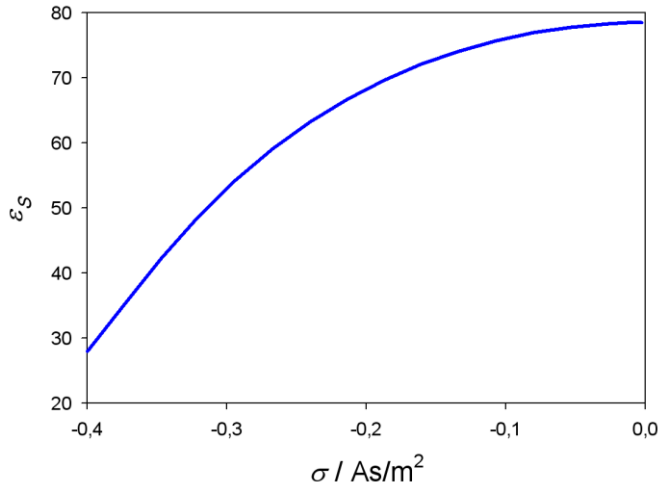

Slika 3.21: Relativna dielektričnost (ε_S) v Sternovi plasti ($0 \leq x < b$) kot funkcija gostote električnega naboja na površini elektrode (σ). Parametri modela so: razdalja približanja $b = 0,4\,\text{nm}$, $p_0 = 3,1$ Debye in koncentracija vode je $n_{0w}/N_A = 55\,\text{mol/l}$.

plasti je relativna dielektričnost konstantna, v Sternovi plasti ($0 \leq x < b$) pa je močno odvisna tudi od gostote električnega naboja na površini elektrode (Priloga F).

Električni potencial (φ) kot funkcija razdalje od površine elektrode pri $x = 0$ je prikazan na sliki 3.23. V Sternovi plasti ($0 \leq x < b$) je odvisnost potenciala linearna in izračunana s pomočjo integriranja robnega pogoja v enačbi 2.59. V vstavku na sliki 3.23 je prikazana medsebojna odvisnost električnega potenciala na površini elektrode $\varphi(x = 0)$ in električnega potenciala na meji med Sternovo in difuzijsko plastjo pri $x = b$. Slika 3.24 pa skupaj z vstavkom prikazuje odvisnost obeh električnih potencialov od površinske gostote električnega naboja na površini elektrode (σ) (Priloga F).

Slika 3.25 prikazuje kapacitivnost Sternove plasti (C_S), diferencialno kapacitivnost difuzijske plasti (C_{DL}) in skupne kapacitivnosti (C_{diff}) v odvisnosti od potenciala na površini elektrode ($\varphi(x = 0)$). Z naraščanjem velikosti potenciala

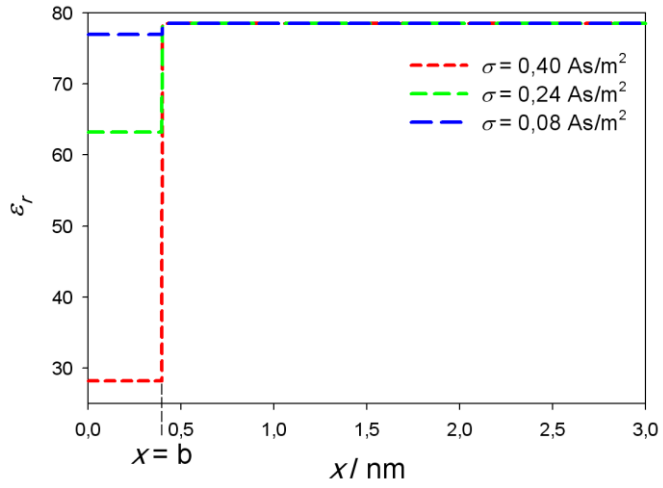

Slika 3.22: Relativna dielektričnost v Sternovi ($0 \leq x < b$) in difuzijski plasti ($b \leq x < \infty$) kot funkcija razdalje od površine elektrode pri $x = 0$, računana pri treh vrednostih površinske gostote električnega naboja na površini elektrode (σ). Parametri modela so enaki kot na sliki 3.21.

$\varphi(x=0)$ se kapacitivnost difuzijske plasti (C_{DL}) povečuje, kapacitivnost Sternove plasti (C_S) pa zmanjšuje. Pri velikih električnih potencialih na površini elektrode ($\varphi(x=0)$) je prispevek C_{DL} k skupni diferencialni kapacitivnosti (C_{diff}) (enačba 2.52) zanemarljiv, zato je prispevek kapacitivnosti Sternove plasti (C_S) približno enak skupni diferencialni kapacitivnosti ($C_S \approx C_{diff}$) (Priloga F).

Diferencialno kapacitivnost na stiku površine elektrode z raztopino soli (C_{diff}) kot funkcijo električnega potenciala na površini elektrode ($\varphi(x=0)$), izračunano za primer krajevno odvisne ($\varepsilon_S(\sigma)$) in konstantne (ε_S) relativne dielektričnosti v Sternovi plasti, prikazuje slika 3.26. V primeru $\varepsilon_S(\sigma)$ diferencialna kapacitivnost (C_{diff}) izkazuje maksimum in v nadaljevanju upadanje C_{diff} z naraščanjem velikosti električnega potenciala ($\varphi(x=0)$). V primeru konstantne relativne dielektričnosti (ε_S) vrednost C_{diff} z naraščanjem $\varphi(x = 0)$ narašča (Priloga F). Odvisnost C_{diff}, pri kateri nastopa maksimum, v primeru krajevno odvisnega $\varepsilon_S(\sigma)$, lahko opazimo tudi v modelih, ki upoštevajo končne volumne znotraj Bikermanovega modela ([71, 74, 75] ali Priloga D).

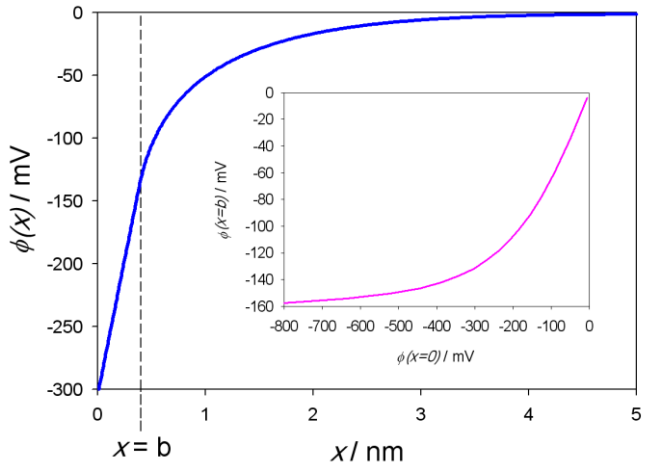

Slika 3.23: Električni potencial (φ) kot funkcija razdalje od površine elektrode pri $x = 0$. Uporabljeni parametri so: gostota električnega naboja na površini elektrode $\sigma = -0,2\,\mathrm{As/m^2}$, koncentracija ionov $n_0/N_A = 0,1\,\mathrm{mol/l}$, razdalja približanja $b = 0,4\,\mathrm{nm}$, $p_0 = 3,1\,\mathrm{Debye}$ in koncentracija vodnih molekul $n_{0w}/N_A = 55\,\mathrm{mol/l}$. Vstavek prikazuje odvisnost med potencialom $\varphi(x = b)$ in potencialom $\varphi(x = 0)$, računano za različne vrednosti σ.

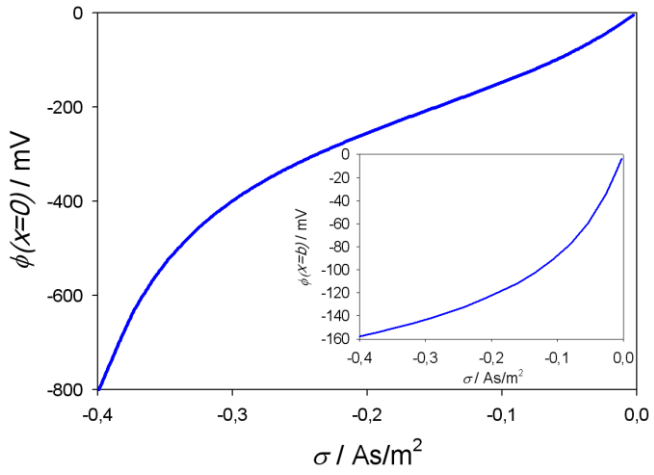

Slika 3.24: Električni potencial $\varphi(x = 0)$ v odvisnosti od gostote električnega naboja na površini elektrode (σ). Vstavek prikazuje odvisnost $\varphi(x = b)$ od σ. Parametri modela so enaki kot pri sliki 3.23.

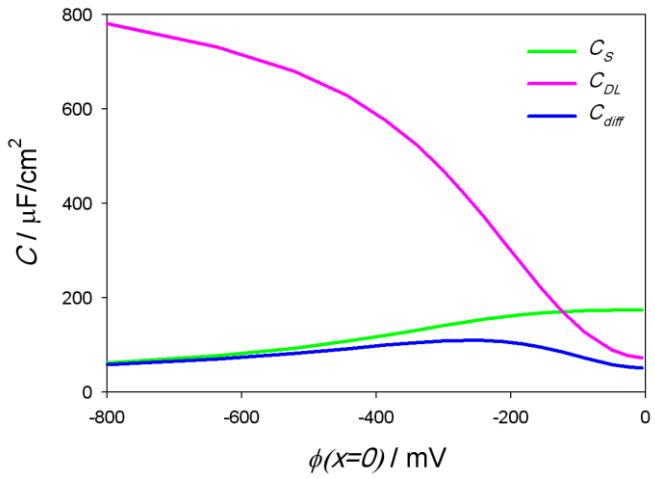

Slika 3.25: Kapacitivnosti Sternove plasti (C_S) in difuzijske plasti (C_{DL}) ter diferencialna kapacitivnost (C_{diff}) v odvisnosti od potenciala na površini elektrode ($\varphi(x=0)$). Uporabljeni parametri modela so enaki kot pri sliki 3.23.

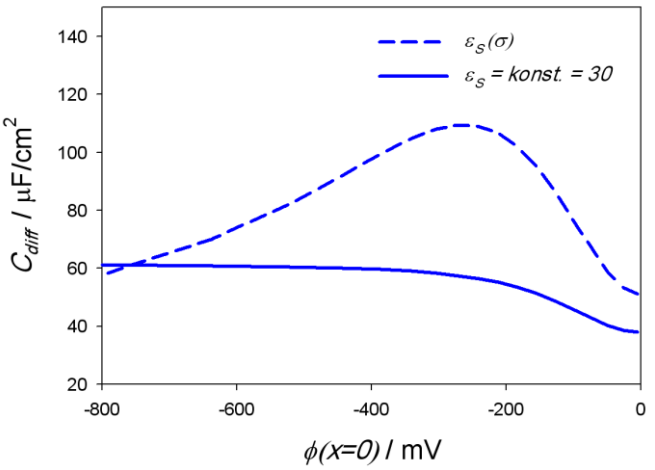

Slika 3.26: Diferencialna kapacitivnost na stiku površine elektrode z raztopino soli (C_{diff}) kot funkcija električnega potenciala na površini elektrode ($\varphi(x = 0)$), računana za primer krajevno odvisne ($\varepsilon_S(\sigma)$) in konstantne (ε_S) relativne dielektričnosti v Sternovi plasti. Parametri modela so enaki kot pri sliki 3.23.

4 Zaključek

Ravninski lipidni dvosloj predstavlja model membrane biološke celice, saj lahko z njim na dovolj dober in preprost način študiramo njene osnovne lastnosti. Lipidni dvosloj sestoji iz lipidnih molekul, lahko pa vanj vgrajujemo tudi druge gradnike, na primer proteine, in se tako skušamo še bolje približati nehomogeni strukturi membrane biološke celice.

Ravninske lipidne dvosloje smo eksperimentalno vzpostavljali na odprtini med dvema prekatoma po metodi dvigovanja gladine ali Montal-Muellerjevi metodi. Ker metoda predvideva vzpostavitev lipidnega dvosloja na meji raztopina soli-lipidni dvosloj-raztopina soli, je ta zato obdan z vodnimi molekulami in zaradi tega hidriran. Hidriranemu ravninskemu lipidnemu dvosloju se lahko zaradi interakcij z vodnimi molekulami spremenijo nekatere fizikalne lastnosti, kot je npr. temperatura faznega prehoda. Hidrirani ravninski lipidni dvosloj je zato še boljši model celične membrane, če vemo, da tudi membrano biološke celice obdaja znotraj citoplazma, zunaj pa izvencelična tekočina.

V eksperimentalnem delu doktorske disertacije smo se posvetili študiju električnih lastnosti, predvsem kapacitivnosti (c_{blm}) in porušitveni napetosti (U_{br}) hidriranega ravninskega lipidnega dvosloja v odvisnosti od temperature. Lipidni dvosloj je bil sestavljen iz različnih vrst lipidnih molekul. Predvsem smo primerjali električne lastnosti ravninskih lipidnih dvoslojev, sestavljenih iz lipidov, ki na merjenem temperaturnem področju nimajo faznega prehoda (arheolipidi), s takimi, ki na merjenem temperaturnem področju imajo fazni prehod (DPPC).

Rezultati so pokazali, da sta pri lipidnih dvoslojih, sestavljenih iz arheolipi-

dov, tako kapacitivnost (c_{blm}) kot porušitvena napetost (U_{br}) praktično neodvisni od temperature na celotnem merjenem temperaturnem intervalu (slika 3.1). Pri ravninskih lipidnih dvoslojih, ki so sestavljeni iz mešanice lipida DPPC in DPhPC v razmerju 20 : 80, pa se nepričakovano opazi izrazitejša sprememba samo pri meritvi kapacitivnosti (slika 3.3.A). Pričakovali bi namreč tudi spremembo v porušitveni napetosti, saj se lipidni dvosloj pod temperaturo prehoda nahaja v L_β fazi, v kateri so lipidne molekule (DPPC) bolj toge, nad temperaturo prehoda pa se nahaja v L_α fazi, v kateri so lipidne molekule (DPPC) bolj fleksibilne. Ta rezultat lahko pripišemo veliki koncentraciji lipida DPhPC, uporabljenega v mešanici, ki v merjenem temperaturnem intervalu nima faznega prehoda, zato sprememba v porušitveni napetosti v bližini temperature prehoda ni tako izrazita. Isti efekt lahko opazimo v študiji Gmajner in sodelavci [76], ki s pomočjo diferenčne dinamične kalorimetrije ugotavlja temperaturni prehod liposomov pri različnih mešanicah lipida DPPC in arheolipidov. Večji je bil delež arheolipidov, manjša je bila sprememba toplotne kapacitete (C_p) pri diferenčni dinamični kalorimetriji ob faznem prehodu, zato lahko sklepamo, da bi porušitvena napetost lahko bila analogna toplotni kapaciteti. Izmerjena specifična kapacitivnost pa je zelo podobna meritvi molekularnega volumna [73], saj se oba parametra s temperaturo povečujeta. Pri lipidnih dvoslojih, sestavljenih iz lipida DPhPC, pa pri meritvi specifične kapacitivnosti na temperaturnem območju med 298 K in 308 K opazimo padanje s temperaturo, kar skoraj sovpada z meritvami specifične kapacitivnosti pri White-u [29].

Na podlagi ugotovitev iz prejšnjega odstavka lahko sklepamo, da z meritvijo električnih lastnosti hidriranih ravninskih lipidnih dvoslojev, ki so zgrajeni iz mešanice različnih lipidnih molekul, ne moremo določiti temperature faznega prehoda ravninskega lipidnega dvosloja. Lahko pa to storimo v okviru študija električnih lastnosti lipidnih dvoslojev, ki so zgrajeni iz ene vrste lipidnih molekul (slika 3.8), in napovemo približno temperaturo faznega prehoda. Vendar, ker so bile naše meritve izvedene zgolj v okviru enega eksperimenta, ne moremo podati končnih zaključkov.

Poleg študija električnih lastnosti ravninskih lipidnih dvoslojev smo se v doktorski disertaciji posvetili tudi teoretičnim modelom, ki obravnavajo elektrostatične lastnosti ravninskih lipidnih dvoslojev v stiku z raztopino soli. Še posebej so bili v središču naše pozornosti ravninski lipidni dvosloji iz zviterionskih lipidnih molekul (npr. DPPC) ob uporabi nadgrajenega Langevin-Poisson-Boltzmannovega (MLPB) in nadgrajenega Langevin-Bikermanovega modela (MLB), ki smo ju v okviru doktorskega dela tudi izpeljali.

Rezultati nadgrajenega Langevin-Poisson-Boltzmannovega modela (MLPB) so pokazali, da je v bližini zviterionske lipidne plasti v stiku z raztopino soli zelo veliko električno polje, v katerem pride do močne orientacije in efekta končnih volumnov vodnih molekul, kar močno vpliva na krajevno odvisnost relativne dielektričnosti (slika 3.10.B) in številsko gostoto prostih električno nabitih nosilcev (ionov) v bližini površine zviterionske lipidne plasti ($x = 0$). Številska gostota ionov se spremeni tudi v bližini pozitivnih delov glav zviterionskih lipidnih molekul (slika 3.9). Z upoštevanjem končnih volumnov pozitivnih delov zviterionskih lipidnih glav, se je vrednost $P(x)$ približala vrednosti iz molekularne dinamike (slika 3.12). Z obravnavo električno nabitega nanodelca v bližini zviterionske lipidne plasti v okviru MLPB modela smo pokazali, da se z zmanjševanjem razdalje med zviterionsko lipidno površino in naelektrenim nanodelcem spreminja povprečni kot orientacije zviterionske lipidne molekule (slika 3.13), saj pride do privlačnih oziroma odbojnih sil med glavami zviterionskih lipidnih molekul in električno nabitimi nanodelci. Do podobnega zaključka smo prišli pri računanju osmotskega tlaka med lipidno površino in nanodelcem (slika 3.14). Pokazali smo tudi, da lahko prisotnost dvovalentnih kalcijevih ionov delno vpliva na povprečni kot orientacije glav zviterionskih lipidnih molekul.

Rezultati nadgrajenega Langevin-Bikermanovega (MLB) modela so pokazali, da je električno polje (slika 3.18.A) v bližini zviterionske plasti zelo močno in po velikosti za velikostni razred večje kot v primeru običajnega MLPB modela, kar je pričakovano, če vemo, da model MLB za razliko od modela MLPB upošteva končne volumne vseh prostih delcev v sistemu. Zaradi tega sta efekt končnega vo-

lumna in orientacij vodnih molekul še večja, kar vse pomembno vpliva na krajevno odvisnost relativne dielektričnosti v bližini in v področju glav lipidnih molekul. (slika 3.18.B). Iz rezultatov tudi sledi, da zaradi končnih volumnov (nasičenega sistema) ni opazne spremembe v koncentraciji ionov v bližini pozitivnih delov zviterionskih lipidnih glav pri $x = D$ (slika 3.17), kot je bilo to v primeru modela MLPB (slika 3.9), ki je obravnaval vse delce v sistemu kot točkaste delce, razen pozitivnih delov glav, ki so bili izpeljani kot končni volumni (enačba 2.27).

Rezultati spremenjenega Sternovega modela za računanje diferencialne kapacitivnosti v bližini naelektrene površine (elektrode ali lipidne plasti) so pokazali, da se kapacitivnost na meji naelektrene površine z raztopino soli manjša z večanjem potenciala na površini naelektrene površine (slika 3.26), in da je pri velikih potencialih diferencialna kapacitivnost (C_{diff}) odvisna le od kapacitivnosti Sternove plasti (C_S), saj je pri velikih potencialih prispevek kapacitivnosti difuzijske plasti (C_{DL}) praktično zanemarljiv (slika 3.25).

5 Izvirni prispevki k znanosti

5.1 Razvoj postopka določanja električnih lastnosti hidri- ranih ravninskih lipidnih dvoslojev in odvisnosti teh lastnosti od temperature

Kandidat je razvil metodo, ki omogoča vrednotenje električnih lastnosti lipidnih dvoslojev na osnovi meritev na modelnih hidriranih ravninskih dvoslojih, izgrajenih na luknjici v teflonski foliji, pri nadzorovani in nastavljivi temperaturi. Izvirnost kandidatovega prispevka je predvsem v poskusu določitve faznih prehodov z meritvijo električnih lastnosti dvosloja.

5.2 Izpopolnitev teoretičnega Langevin-Poisson-Boltzmannovega modela, ki opisuje elektrostatične lastnosti snovi v neposredni bližini hidriranega lipidnega dvosloja (tik ob električni dvojni plasti)

Kandidat se je v svojem delu lotil izpopolnitve Langevin-Poisson-Boltzmannovega (LPB) modela naelektrene površine s površinsko gostoto naboja v stiku z raztopino soli, ki so ga razvili Gongadze in sodelavci leta 2011. Kandidat je v tem izpopolnjenem modelu nadgradil opis molekul vode, za katere ni privzel enotne dielektričnosti, temveč je ločil med dielektričnostjo prostih molekul vode v širši okolici dvosloja in dielektričnostjo molekul vode tik ob dvosloju, upošteval pa je

tudi upadajočo koncentracijo molekul vode s približevanjem dvosloju. Dodatno je kandidat model izpopolnil še z upoštevanjem zwitterionske narave glav lipidnih molekul in končno (ne-ničelno) prostornino, ki jo zavzemajo te glave na stičišču z vodo.

Literatura

[1] R. Lipovsky in E. Sackmann, *Handbook of Biological Physics*, vol. 1. Elsevier: Amsterdam, The Netherlands, 1 st. izd., 1995.

[2] M. Luckey, "Membrane structural biology," *Cambridge University Press, Cambridge*, 2008.

[3] I. Sabotin, A. M. Lebar, D. Miklavcic in P. Kramar, "Measurement protocol for planar lipid bilayer viscoelastic properties," *Dielectrics and Electrical Insulation, IEEE Transactions on*, vol. 16, no. 5, str. 1236–1242, 2009.

[4] L. K. Tamm in S. A. Tatulian, "Infrared spectroscopy of proteins and peptides in lipid bilayers," *Quarterly reviews of biophysics*, vol. 30, no. 04, str. 365–429, 1997.

[5] J. H. Ipsen, O. G. Mouritsen in M. J. Zuckermann, "Theory of thermal anomalies in the specific heat of lipid bilayers containing cholesterol," *Biophysical journal*, vol. 56, no. 4, str. 661–667, 1989.

[6] G. C. Troiano, L. Tung, V. Sharma in K. J. Stebe, "The reduction in electroporation voltages by the addition of a surfactant to planar lipid bilayers," *Biophysical journal*, vol. 75, no. 2, str. 880–888, 1998.

[7] G. S. Smith in J. Majewski, "X-ray and neutron scattering studies of lipid monolayers and single bilayers," v *Lipid Bilayers*, str. 127–147, Springer, 2001.

[8] E. J. W. Verwey, J. T. G. Overbeek in J. T. G. Overbeek, *Theory of the stability of lyophobic colloids*. Courier Dover Publications, 1999.

[9] A. Lee, "Lipid phase transitions and phase diagrams i. lipid phase transitions," *Biochimica et Biophysica Acta (BBA)-Reviews on Biomembranes*, vol. 472, no. 2, str. 237–281, 1977.

[10] B. Tenchov, R. Koynova in G. Rapp, "New ordered metastable phases between the gel and subgel phases in hydrated phospholipids," *Biophysical journal*, vol. 80, no. 4, str. 1873–1890, 2001.

[11] F. Tokumasu, A. J. Jin in J. A. Dvorak, "Lipid membrane phase behaviour elucidated in real time by controlled environment atomic force microscopy," *Journal of electron microscopy*, vol. 51, no. 1, str. 1–9, 2002.

[12] A. Lee, "Lipid phase transitions and phase diagrams ii. mixtures involving lipids," *Biochimica et Biophysica Acta (BBA)-Reviews on Biomembranes*, vol. 472, no. 3, str. 285–344, 1977.

[13] V. F. Antonov, A. A. Anosov, V. P. Norik, E. A. Korepanova in E. Y. Smirnova, "Electrical capacitance of lipid bilayer membranes of hydrogenated egg lecithin at the temperature phase transition," *European Biophysics Journal*, vol. 32, no. 1, str. 55–59, 2003.

[14] W. Hung, F. Chen in H. W. Huang, "Order–disorder transition in bilayers of diphytanoyl phosphatidylcholine," *Biochimica et Biophysica Acta (BBA)-Biomembranes*, vol. 1467, no. 1, str. 198–206, 2000.

[15] J. F. Nagle, "Theory of the main lipid bilayer phase transition," *Annual Review of Physical Chemistry*, vol. 31, no. 1, str. 157–196, 1980.

[16] T. Benvegnu, M. Brard in D. Plusquellec, "Archaeabacteria bipolar lipid analogues: structure, synthesis and iyotropic properties," *Current opinion in Colloid and Interface Sciences*, vol. 8, str. 469–479, 2004.

[17] N. P. Ulrih, D. Gmajner in P. Raspor, "Structural and physicochemical properties of polar lipids from thermophilic archaea," *Applied microbiology and biotechnology*, vol. 84, no. 2, str. 249–260, 2009.

[18] M. De Rosa, A. Gambacorta in A. Gliozzi, "Structure, biosynthesis, and physicochemical properties of archaebacterial lipids.," *Microbiological reviews*, vol. 50, no. 1, str. 70, 1986.

[19] T. Anzelc, "Fizikalne lastnosti arheosomov pripravljenih iz lipidov hipertermofilne arheje *Aeropyrum pernix K1*." Diplomsko delo, Biotehniška fakulteta, Ljubljana, 2006.

[20] J. F. Nagle in S. Tristram-Nagle, "Structure and interactions of lipid bilayers: role of fluctuations," v *Lipid Bilayers*, str. 1–23, Springer, 2001.

[21] R. L. Biltonen in D. Lichtenberg, "The use of differential scanning calorimetry as a tool to characterize liposome preparations," *Chemistry and physics of lipids*, vol. 64, no. 1, str. 129–142, 1993.

[22] M. Rappolt, A. Hickel, F. Bringezu in K. Lohner, "Mechanism of the lamellar/inverse hexagonal phase transition examined by high resolution x-ray diffraction," *Biophysical journal*, vol. 84, no. 5, str. 3111–3122, 2003.

[23] H. Mantsch in R. McElhaney, "Phospholipid phase transitions in model and biological membranes as studied by infrared spectroscopy," *Chemistry and physics of lipids*, vol. 57, no. 2, str. 213–226, 1991.

[24] A. Gliozzi, A. Relini in P. L.-G. Chong, "Structure and permeability properties of biomimetic membranes of bolaform archaeal tetraether lipids," *Journal of membrane science*, vol. 206, no. 1, str. 131–147, 2002.

[25] Y. Matsuno, A. Sugai, H. Higashibata, W. Fukuda, K. Ueda, I. Uda, I. Sato, T. Itoh, T. Imanaka in S. Fujiwara, "Effect of growth temperature and growth phase on the lipid composition of the archaeal membrane from *Thermo-*

coccus kodakaraensis," *Bioscience, biotechnology, and biochemistry*, vol. 73, no. 1, str. 104–108, 2009.

[26] C.-H. Hsieh, S.-C. Sue, P.-C. Lyu in W. Wu, "Membrane packing geometry of diphytanoylphosphatidylcholine is highly sensitive to hydration: phospholipid polymorphism induced by molecular rearrangement in the headgroup region," *Biophysical journal*, vol. 73, no. 2, str. 870–877, 1997.

[27] M. E. Starzak, *The physical chemistry of membranes*. Academic Press London, UK:, 1984.

[28] V. Lockett, M. Horne, R. Sedev, T. Rodopoulos in J. Ralston, "Differential capacitance of the double layer at the electrode/ionic liquids interface," *Physical Chemistry Chemical Physics*, vol. 12, no. 39, str. 12499–12512, 2010.

[29] S. H. White, "A study of lipid bilayer membrane stability using precise measurements of specific capacitance," *Biophysical journal*, vol. 10, no. 12, str. 1127–1148, 1970.

[30] S. H. White in T. Thompson, "Capacitance, area, and thickness variations in thin lipid films," *Biochimica et Biophysica Acta (BBA)-Biomembranes*, vol. 323, no. 1, str. 7–22, 1973.

[31] Z. Leonenko, E. Finot, H. Ma, T. Dahms in D. Cramb, "Investigation of temperature-induced phase transitions in dopc and dppc phospholipid bilayers using temperature-controlled scanning force microscopy," *Biophysical journal*, vol. 86, no. 6, str. 3783–3793, 2004.

[32] T. Birch, *The history of the Royal society of London for improving of natural knowledge, from its first rise: In which the most considerable of those papers communicated to the society, which have hitherto not been published, are inserted in their proper order, as a supplement to the Philosophical transactions*, vol. 3. A. Millar, 1757.

[33] I. Newton, *Opticks: Or, a Treatise of the Reflections, Refractions, Inflections, and Colors of Light (1730)*. The Project Gutenberg eBook of Opticks, 2010.

[34] P. Mueller, D. O. Rudin, H. Ti Tien in W. C. Wescott, "Reconstitution of cell membrane structure in vitro and its transformation into an excitable system," *Nature*, vol. 194, str. 979–980, 1962.

[35] P. Mueller, D. O. RUDIN, H. T. Tien in W. C. WESCOTT, "Reconstitution of excitable cell membrane structure in vitro," *Circulation*, vol. 26, no. 5, str. 1167–1171, 1962.

[36] T. Hanai, D. Haydon in J. Taylor, "Polar group orientation and the electrical properties of lecithin bimolecular leaflets," *Journal of theoretical biology*, vol. 9, no. 2, str. 278–296, 1965.

[37] S. H. White, "Temperature-dependent structural changes in planar bilayer membranes: solvent "freeze-out"," *Biochimica et Biophysica Acta (BBA)-Biomembranes*, vol. 356, no. 1, str. 8–16, 1974.

[38] S. H. White, "Phase transitions in planar bilayer membranes," *Biophysical journal*, vol. 15, no. 2, str. 95–117, 1975.

[39] M. Montal in P. Mueller, "Formation of bimolecular membranes from lipid monolayers and a study of their electrical properties," *Proceedings of the National Academy of Sciences*, vol. 69, no. 12, str. 3561–3566, 1972.

[40] I. Abidor, V. Arakelyan, L. Chernomordik, Y. A. Chizmadzhev, V. Pastushenko in M. Tarasevich, "Electric breakdown of bilayer lipid membranes: I. the main experimental facts and their qualitative discussion," *Journal of Electroanalytical Chemistry and Interfacial Electrochemistry*, vol. 104, str. 37–52, 1979.

[41] P. Kramar, D. Miklavcic in A. M. Lebar, "Determination of the lipid bilayer breakdown voltage by means of linear rising signal," *Bioelectrochemistry*, vol. 70, no. 1, str. 23–27, 2007.

[42] B. Le Pioufle, H. Suzuki, K. V. Tabata, H. Noji in S. Takeuchi, "Lipid bilayer microarray for parallel recording of transmembrane ion currents," *Analytical chemistry*, vol. 80, no. 1, str. 328–332, 2008.

[43] S. Ota, H. Suzuki in S. Takeuchi, "Microfluidic lipid membrane formation on microchamber arrays," *Lab Chip*, vol. 11, no. 15, str. 2485–2487, 2011.

[44] K. Funakoshi, H. Suzuki in S. Takeuchi, "Lipid bilayer formation by contacting monolayers in a microfluidic device for membrane protein analysis," *Analytical chemistry*, vol. 78, no. 24, str. 8169–8174, 2006.

[45] H. v. Helmholtz, "Ueber einige gesetze der vertheilung elektrischer ströme in körperlichen leitern mit anwendung auf die thierisch-elektrischen versuche," *Annalen der Physik*, vol. 165, no. 6, str. 211–233, 1853.

[46] F. Fogolari, A. Brigo in H. Molinari, "The poisson–boltzmann equation for biomolecular electrostatics: a tool for structural biology," *Journal of Molecular Recognition*, vol. 15, no. 6, str. 377–392, 2002.

[47] E. Gongadze, U. van Rienen, V. Kralj-Iglič in A. Iglič, "Langevin poisson-boltzmann equation: Point-like ions and water dipoles near a charged surface," *General physiology and biophysics*, vol. 30, no. 2, str. 130, 2011.

[48] J. Bikerman, "Xxxix. structure and capacity of electrical double layer," *Philosophical Magazine*, vol. 33, no. 220, str. 384–397, 1942.

[49] P. Nielaba in F. Forstmann, "Packing of ions near an electrolyte-electrode interface in the hnc/lmsa approximation to the rpm model," *Chemical physics letters*, vol. 117, no. 1, str. 46–48, 1985.

[50] C. Caccamo, G. Pizzimenti in L. Blum, "An improved closure for the born–green–yvon equation for the electric double layer," *The Journal of chemical physics*, vol. 84, no. 6, str. 3327–3335, 1986.

[51] R. Kjellander in S. Marčelja, "Interaction of charged surfaces in electrolyte solutions," *Chemical physics letters*, vol. 127, no. 4, str. 402–407, 1986.

[52] M. Plischke in D. Henderson, "Pair correlation functions and density profiles in the primitive model of the electric double layer," *The Journal of Chemical Physics*, vol. 88, no. 4, str. 2712–2718, 1988.

[53] L. Mier-y Teran, S. Suh, H. S. White in H. Davis, "A nonlocal free-energy density-functional approximation for the electrical double layer," *The Journal of Chemical Physics*, vol. 92, no. 8, str. 5087–5098, 1990.

[54] V. Kralj-Iglič in A. Iglič, "A simple statistical mechanical approach to the free energy of the electric double layer including the excluded volume effect," *Journal de Physique II*, vol. 6, no. 4, str. 477–491, 1996.

[55] S. Lamperski in C. Outhwaite, "Exclusion volume term in the inhomogeneous poisson-boltzmann theory for high surface charge," *Langmuir*, vol. 18, no. 9, str. 3423–3424, 2002.

[56] E. Gongadze in A. Iglič, "Decrease of permittivity of an electrolyte solution near a charged surface due to saturation and excluded volume effects," *Bioelectrochemistry*, vol. 87, str. 199–203, 2012.

[57] J. Griesbauer, A. Wixforth, H. Seeger in M. Schneider, "Method for the monte carlo based simulation of lipid-monolayers including lipid movement," *arXiv preprint arXiv:1012.4973*, 2010.

[58] A. Polak, B. Mulej in P. Kramar, "System for measuring planar lipid bilayer properties," *The Journal of membrane biology*, vol. 245, no. 10, str. 625–632, 2012.

[59] A. Velikonja, E. Gongadze, V. Kralj-Iglič in A. Iglič, "Charge dependent capacitance of stern layer and capacitance of electrode/electrolyte interface," *Int. J. Electrochem. Sci*, vol. 9, str. 5885–5894, 2014.

[60] P. Kramar, L. Delemotte, A. M. Lebar, M. Kotulska, M. Tarek in D. Miklavčič, "Molecular-level characterization of lipid membrane electroporation using linearly rising current," *The Journal of membrane biology*, vol. 245, no. 10, str. 651–659, 2012.

[61] D. L. Chapman, "Li. a contribution to the theory of electrocapillarity," *The London, Edinburgh, and Dublin Philosophical Magazine and Journal of Science*, vol. 25, no. 148, str. 475–481, 1913.

[62] G. Gouy, "Constitution of the electric charge at the surface of an electrolyte," *J. phys*, vol. 9, no. 4, str. 457–467, 1910.

[63] C. Outhwaite, "A treatment of solvent effects in the potential theory of electrolyte solutions," *Molecular Physics*, vol. 31, no. 5, str. 1345–1357, 1976.

[64] A. Velikonja, Š. Perutkova, E. Gongadze, P. Kramar, A. Polak, A. Maček-Lebar in A. Iglič, "Monovalent ions and water dipoles in contact with dipolar zwitterionic lipid headgroups-theory and md simulations," *International journal of molecular sciences*, vol. 14, no. 2, str. 2846–2861, 2013.

[65] MathWorks, "bvp4c - solve boundary value problems for ordinary differential equations." Dosegljivo: http://www.mathworks.com/help/matlab/ref/bvp4c.html. [Dostopano: 10. 2. 2013].

[66] P. B. Santhosh, A. Velikonja, Š. Perutkova, E. Gongadze, M. Kulkarni, J. Genova, K. Eleršič, A. Iglič, V. Kralj-Iglič in N. P. Ulrih, "Influence of nanoparticle–membrane electrostatic interactions on membrane fluidity and bending elasticity," *Chemistry and physics of lipids*, vol. 178, str. 52–62, 2014.

[67] P. Budime Santhosh, A. Velikonja, E. Gongadze, A. Iglič, V. Kralj-Iglič in N. Poklar Ulrih, "Interactions of divalent calcium ions with head groups of zwitterionic phosphatidylcholine liposomal membranes," *Acta Chimica Slovenica*, vol. 61, str. 215–222, 2014.

[68] A. Velikonja, P. B. Santhosh, E. Gongadze, M. Kulkarni, K. Eleršič, Š Perutkova, V. Kralj-Iglič, N. P. Ulrih in A. Iglič, "Interaction between dipolar lipid headgroups and charged nanoparticles mediated by water dipoles and ions," *International journal of molecular sciences*, vol. 14, no. 8, str. 15312–15329, 2013.

[69] O. Stern, "The theory of the electrolytic double-layer," *Zeit. Elektrochem*, vol. 30, str. 508–516, 1924.

[70] H.-J. Butt, K. Graf in M. Kappl, *Physics and chemistry of interfaces*. John Wiley & Sons, 2006.

[71] E. Gongadze, A. Velikonja, Š Perutkova, P. Kramar, A. Maček-Lebar, V. Kralj-Iglič in A. Iglič, "Ions and water molecules in an electrolyte solution in contact with charged and dipolar surfaces," *Electrochimica Acta*, vol. 126, str. 42–60, 2014.

[72] A. Polak, M. Tarek, M. Tomšič, J. Valant, N. P. Ulrih, A. Jamnik, P. Kramar in D. Miklavčič, "Electroporation of archaeal lipid membranes using md simulations," *Bioelectrochemistry*, vol. 100, str. 18–26, 2014.

[73] S. Tristram-Nagle in J. F. Nagle, "Lipid bilayers: thermodynamics, structure, fluctuations, and interactions," *Chemistry and physics of lipids*, vol. 127, no. 1, str. 3–14, 2004.

[74] M. Z. Bazant, M. S. Kilic, B. D. Storey in A. Ajdari, "Towards an understanding of induced-charge electrokinetics at large applied voltages in concentrated solutions," *Advances in colloid and interface science*, vol. 152, no. 1, str. 48–88, 2009.

[75] A. A. Kornyshev, "Double-layer in ionic liquids: paradigm change?," *The Journal of Physical Chemistry B*, vol. 111, no. 20, str. 5545–5557, 2007.

[76] D. Gmajner in N. P. Ulrih, "Thermotropic phase behaviour of mixed liposomes of archaeal diether and conventional diester lipids," *Journal of thermal analysis and calorimetry*, vol. 106, no. 1, str. 255–260, 2011.

Priloge

A Članek 1: Monovalent Ions and Water Dipoles in Contact with Dipolar Zwitterionic Lipid Headgroups-Theory and MD Simulations

Polno ime revije:	International Journal of Molecular Sciences
Okrajšava:	Int. J. Mol. Sci.
ISSN (elektronska izdaja):	1422-0067
Založnik:	Multidisciplinary Digital Publishing Institute (MDPI)
Naslov založnika:	MDPI AG, Klybeckstrasse 64, 4057 Basel, Switzerland
Pogostost izdaje:	mesečno
Medij:	elektronska verzija
Spletna stran revije:	http://www.mdpi.com/journal/ijms
Prvo leto izdaje:	2000
Faktor vpliva:	2.464 (2012)
Faktor vpliva (5 let):	2.732 (2012)
Naslov članka:	Monovalent Ions and Water Dipoles in Contact with Dipolar Zwitterionic Lipid Headgroups-Theory and MD Simulations
Avtorji:	Velikonja, Aljaž; Perutkova, Šarka; Gongadze, Ekaterina; Kramar, Peter; Polak, Andraž; Maček-Lebar, Alenka; Iglič, Aleš
Izdaja:	14
Številka:	2
Strani:	2846–2861
Leto objave:	2013
DOI:	10.3390/ijms14022846

Int. J. Mol. Sci. 2013, *14*, 2846-2861; doi:10.3390/ijms14022846

OPEN ACCESS

International Journal of
Molecular Sciences
ISSN 1422-0067
www.mdpi.com/journal/ijms

Article

Monovalent Ions and Water Dipoles in Contact with Dipolar Zwitterionic Lipid Headgroups-Theory and MD Simulations

Aljaž Velikonja [1,2], Šarka Perutkova [3], Ekaterina Gongadze [3,4], Peter Kramar [1], Andraž Polak [1], Alenka Maček-Lebar [1] and Aleš Iglič [3,4,*]

[1] Laboratory of Biocybernetics, Faculty of Electrical Engineering, University of Ljubljana, Tržaška 25, SI-1000 Ljubljana, Slovenia; E-Mails: aljaz.velikonja@avelik.homeip.net (A.V.); peter.kramar@fe.uni-lj.si (P.K.); andraz.polak@fe.uni-lj.si (A.P.); alenka.macek-lebar@fe.uni-lj.si (A.M.-L.)

[2] SMARTEH Research and Development of Electronic Controlling and Regulating Systems, Trg tigrovcev 1, SI-5220 Tolmin, Slovenia

[3] Laboratory of Biophysics, Faculty of Electrical Engineering, Tržaška 25, University of Ljubljana, SI-1000 Ljubljana, Slovenia; E-Mails: sarka.perutkova@fe.uni-lj.si (S.P.); ekaterina.gongadze@fe.uni-lj.si (E.G.)

[4] Laboratory of Clinical Biophysics, Orthopaedic Clinics and Faculty of Medicine, University of Ljubljana, Vrazov trg 2, SI-1000 Ljubljana, Slovenia

* Author to whom correspondence should be addressed; E-Mail: ales.iglic@fe.uni-lj.si; Tel.: +386-1-4768-825; Fax: +386-1-4768-850.

Received: 22 December 2012; in revised form: 20 January 2013 / Accepted: 21 January 2013 / Published: 29 January 2013

Abstract: The lipid bilayer is a basic building block of biological membranes and can be pictured as a barrier separating two compartments filled with electrolyte solution. Artificial planar lipid bilayers are therefore commonly used as model systems to study the physical and electrical properties of the cell membranes in contact with electrolyte solution. Among them the glycerol-based polar phospholipids which have dipolar, but electrically neutral head groups, are most frequently used in formation of artificial lipid bilayers. In this work the electrical properties of the lipid layer composed of zwitterionic lipids with non-zero dipole moments are studied theoretically. In the model, the zwitterionic lipid bilayer is assumed to be in contact with aqueous solution of monovalent salt ions. The orientational ordering of water, resulting in spatial variation of permittivity, is explicitly taken into account. It is shown that due to saturation effect in orientational ordering of water dipoles the relative

Int. J. Mol. Sci. 2013, *14* 2847

permittivity in the zwitterionic headgroup region is decreased, while the corresponding electric potential becomes strongly negative. Some of the predictions of the presented mean-field theoretical consideration are critically evaluated using the results of molecular dynamics (MD) simulation.

Keywords: lipids; dipolar zwitterionic headgroups; relative permittivity; orientational ordering; water molecules; planar lipid bilayers

1. Introduction

The lipid bilayer is a basic building block of cell membranes. Although the cell membrane is a highly heterogeneous structure, composed of lipids, proteins, carbohydrates and other components [1–3], a large number of physical properties of biological (cell) membrane which are important in physiological processes [4,5] can be studied also in pure planar lipid bilayer systems [6,7]. Due to its double-sided accessability in experiments the planar lipid bilayer is suitable for experimental manipulation [8,9] even if some other pure lipids systems, like lipid vesicles, may mimic also three-dimensional geometry of the cell membrane.

Among others a planar lipid bilayer can be constructed on a small hole positioned on a barrier separating two compartments filled with electrolyte solution. Experimental setup usually consists of two teflon pieces with separate compartments and 100 μm–1 mm diameter hole in between. The diameter of the hole mostly depends on the procedure used in planar lipid bilayer formation [10]. In experiments, the electrodes are dipped into electrolyte solution approximately 1 cm away form the barrier. Electrolyte solution is basically an aqueous solution of salt composed of water molecules (Figure 1) and monovalent positively and negatively charged ions. Such experimental setup is ordinarily used to determine various mechanical and electrical properties of planar lipid bilayers [9,11,12].

Figure 1. A single water molecule is considered as a sphere with permittivity n^2 and point-like rigid (permanent) dipole with dipole moment p at the center of the sphere [13], where n is the optical refractive index of water.

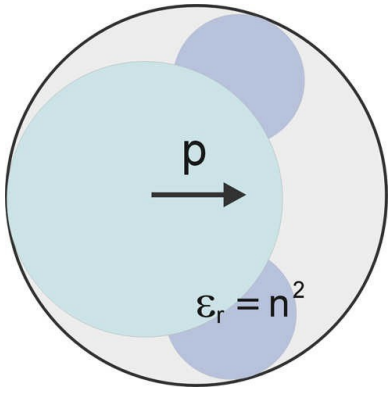

Most frequently used lipid molecules in the procedures of forming the planar lipid bilayers are glycerol-based phospholipids [6,7,14], which are major compound of cell membranes [15–18]: 1-palmitoyl-2-oleoyl-sn-glycero-3-phosphocholine (POPC), 1-palmitoyl-2-oleoyl-sn- glycero-3-phospho-L-serine (POPS), 1,2-dipalmitoyl-sn-glycero-3-phosphocholine (DPPC), L-α-phosphatidylcholine (PC), 1-palmitoyl-2-oleoyl-sn-glycero-3-phosphoethanolamine (POPE), 1,2-dipalmitoyl-sn-glycero-3-phosphoethanolamine (DPPE), and 1,2-dimyristo-yl(d54)-sn-glycero-3-phosphocholine (DMPC). The majority of these lipids can be made artificially, *i.e.*, without need to isolate them from natural cell membranes. Artificially made lipids are more than 99 percent pure, and easy to handle. They are available in powder state form or dissolved in chloroform [9].

In general, some of the lipid molecules bear net negative charge, while other lipids like glycerophospholipids are electrically neutral [14]. Glycerophospholipids (see Figure 2) are composed of dipolar (zwitterionic) headgroup and two nonpolar tails [1,2,6,7,14]. The tails are hydrophobic fatty acids. Due to its hydrophilic nature [14] the headgroups of lipids are in contact with aqueous solution. The negative charges of the dipolar lipid headgroup (Figure 2) are in contact with nonpolar tails on the one side (left side in Figure 2) and with electrolyte solution on the other (right side in Figure 2), thus its charge distribution is described in the model as negatively charged surface at $x = 0$ (Figure 2). The positive charges of the headgroups in planar bilayer of dipolar lipids protrude further in the electrolyte solution as depicted in Figure 2. In the headgroup region of planar dipolar lipid layer the cations are attracted towards the negatively charged surface at $x = 0$, while anions are depleted from this region. Using the MD simulations, the accumulation of sodium cations near the phosphate groups and accumulation of anions near the choline groups in the DOPC bilayer were predicted by [19]. These theoretical predictions were supported also by the results of fluorescence spectroscopy experiments on zwitterionic phospholipid bilayers which show that the addition of salt into the solution being in contact with the lipid bilayer restricts the mobility of the hydrated lipid headgroups and their lateral diffusion when compared to pure water solution [19]. In the high electric field of dipolar lipid headgroups (see [20] and the references therein) the water dipoles are expected to be oriented towards the charged plane at $x = 0$ (see for example [13,21]). Due to accumulation of cations and saturation effect in polarization the electric potential decreases towards the $x = 0$ plane [22].

Most of the electrostatic models of electrolyte solution in contact with lipid surfaces [20,23–26] assume that the dielectric permittivity in the electrolyte solution is constant. In the absence of an explicit consideration of orientational ordering of water molecules the assumption of constant permittivity is the consequence of the assumption of the constant number density of water molecules in the system [13]. But actually, close to the membrane surface the orientation and depletion of water molecules may result in strong spatial variation of permittivity [13,27–31].

In this paper the effect of the nonhomogeneous volume charge distribution in the headgroup region of the planar dipolar lipid layer on the space dependent electric potential and permittivity is presented. An analytical mean-field model, based on the previously developed Langevin-Poisson-Boltzman (LPB) model [21], is introduced. The relative (dielectric) permittivity, related to the electric field strength was analysed in the headgroup region and its close vicinity. To test the predictions of the model, the realistic values of the input model parameters, previously determined in measurements or simulations for DPPC

Int. J. Mol. Sci. 2013, *14* 2849

lipid molecules, were used. The results of an analytical model are compared with the results of molecular dynamic simulation (MD) of DPPC planar lipid bilayer.

Figure 2. Negative charges of dipolar (zwitterionic) lipid headgroups are described by negative surface charge density $\sigma = -e_0/a_0$ at $x = 0$, where a_0 is the area per lipid. D is the distance between charges within the single dipolar lipid headgroup, while ω describes orientation angle of the dipole within the single headgroup. MD model of DPPC lipid molecule is presented at the bottom.

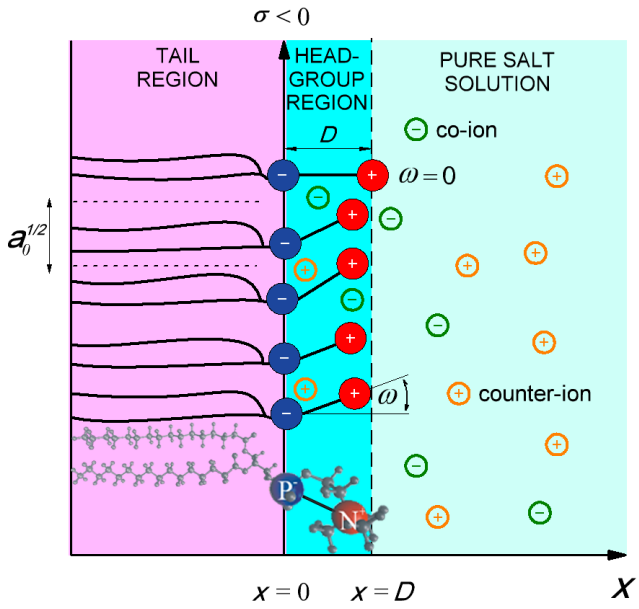

2. Model

2.1. Modified Langevin-Poisson-Boltzmann (MLPB) Model

The Langevin-Poisson-Boltzmann (LPB) model [21] is generalized to take into account the cavity field [13] in the saturation regime. In addition, the electronic polarization of the water is taken into account by assuming that the point-like rigid (permanent) dipole embedded in the center of the sphere with a volume equal to the average volume of a water molecule in the electrolyte solution (Figure 1) [13,32]. The permittivity of the sphere is taken to be n^2, where $n = 1.33$ is the optical refractive index of water. The relative (effective) permittivity of the electrolyte solution ε_r can be then expressed as [13,32]:

$$\varepsilon_r(x) = n^2 + \frac{P(x)}{\varepsilon_0 E(x)} \quad (1)$$

where $P = |P|$ is the magnitude of the polarization vector due to a net orientation of permanent point-like water dipoles having dipole moment p, ε_0 is the permittivity of the free space, while $E = |E|$ is the magnitude of the electric field strength. The absolute value of polarization $P(x)$ is given by [13] :

$$P(x) = n_w(x) \frac{2+n^2}{3} p_0 L(\gamma p_0 E \beta) \tag{2}$$

where $n_w(x)$ is the space dependency of the number density of water molecules, p_0 is the magnitude of the external dipole moment $p_e = (3/(2 + n^2))\, p$ (see also Figure 1) [13,32], $L(u) = (\coth(u) - 1/u)$ is the Langevin function, $\beta = 1/kT$, kT is thermal energy, while γ is [13] :

$$\gamma = \frac{3}{2} \frac{2+n^2}{3} \tag{3}$$

In the following, for the sake of simplicity the finite volume of ions and water molecules is not taken into account as in [13] and consequently the number density of water molecules is considered to be constant all over the solution and equal to its bulk value n_{w0}, *i.e.*, $n_w(x) = n_{0w}$ from where it follows :

$$P(x) = n_{0w} \frac{2+n^2}{3} p_0 L(\gamma p_0 E \beta) \tag{4}$$

Combining Equations 1 and 4 yields space dependency of permittivity within modified Langevin-Poisson-Boltzmann model (MLPB model) in the form:

$$\varepsilon_r(x) = n^2 + \frac{n_{0w} p_0}{\varepsilon_0} \frac{2+n^2}{3} \frac{L(\gamma p_0 E(x) \beta)}{E(x)} \tag{5}$$

or

$$\varepsilon_r(x) = n^2 + \frac{3}{2} \frac{2+n^2}{3} \frac{n_{0w} p_0^2 \beta}{\varepsilon_0} \frac{L(\gamma p E(x) \beta)}{\gamma p_0 E(x) \beta} \tag{6}$$

In the limit of vanishing electric field strength ($E(x) \longrightarrow 0$ everywhere in the solution) the above equation for relative permittivity $\varepsilon_r(x)$ gives the classical Onsager expression:

$$\varepsilon_x \cong n^2 + \frac{2+n^2}{3} \frac{n_{0w} p_0^2 \beta}{2\varepsilon_0} \tag{7}$$

At room temperature (298 K) the above Equation 7 gives $\varepsilon_r = 78.5$ for bulk solution. The parameters p_0 and n_{0w}/N_A are 3.1 Debye and 55 mol/l, respectively.

2.2. Poisson Equation

In the model the dipolar lipid headgroup is described by two charges at fixed distance D, *i.e.*, it is assumed that the headgroup has non-zero dipole moment. The negative charges of the phosphate groups of dipolar (zwitterionic) lipids are described by negative surface charge density $\sigma = -e_0/a_0$ at $x = 0$ (see Figure 2), where a_0 is the area per lipid. The orientational ordering of water is taken into account assuming the spatial dependence of permittivity $\varepsilon_r(x)$ as described by Equation 6.

Int. J. Mol. Sci. 2013, *14* 2851

The corresponding Poisson equation in planar geometry can thus be written in the form (see e.g., [22]) :

$$\frac{d}{dx}\left(\varepsilon_0 \varepsilon_r(x)\frac{d\varphi}{dx}\right) = -\rho_{ions}(x) - \rho_{Zw}(x) \quad (8)$$

where $\varphi(x)$ is the electric potential, $\rho_{Zw}(x)$ is the macroscopic (net) volume charge density of positive charges of dipolar (zwitterionic) headgroups, $\rho_{ions}(x)$ is the macroscopic (net) volume charge density of co-ions (n_-) and counter-ions (n_+) of the electrolyte solution (see Figure 3). Since we neglect the finite volumes of the salt ions and water molecules [21,22] the co-ions and counter-ions are assumed to be distributed according to Boltzmann distribution functions [20,22–26]) :

$$n_+(x) = n_0 \exp(-e_0\varphi(x)\beta) \quad (9)$$

$$n_-(x) = n_0 \exp(e_0\varphi(x)\beta) \quad (10)$$

therefore

$$\rho_{ions}(x) = e_0 n_+(x) - e_0 n_-(x) = -2 e_0 n_0 \sinh e_0\varphi\beta \quad (11)$$

where e_0 is the unit charge and n_0 bulk number density of salt co-ions and counter-ions. The lipid headgroups can be oriented at various angles ω relative to the normal vector to the planar lipid layer (Figure 2), hence the volume charge density due to the positive charges of the lipid dipolar headgroups can be written in the form:

$$\rho_{Zw}(0 < x \le D) = \frac{e_0 P(x)}{D a_0} \quad \text{and} \quad \rho_{Zw}(x > D) = 0 \quad (12)$$

where a_0 is the area per lipid, while $P(x)$ is the probability density function indicating the probability that the positive charge of the dipolar lipid headgroup is located at the distance x from the negatively charged surface at $x = 0$:

$$P(x) = \Lambda \exp(-e_0\varphi(x)\beta) \quad (13)$$

where $x \le D$. Equation 13 neglects the finite volume of lipid headgroups. The normalization condition

$$\frac{1}{D}\int_0^D P(x)\,dx = 1 \quad (14)$$

yields :

$$\Lambda = \frac{D}{r_D \int_0^D \exp(-e_0\varphi(x)\beta)\,dx} \quad (15)$$

Using Equations 11–13 and 15 it follows from Equation 8 :

$$\frac{d}{dx}\left(\varepsilon_0 \varepsilon_r(x)\frac{d\varphi}{dx}\right) = 2 e_0 n_0 \sinh e_0\varphi\beta - \frac{e_0 \exp(-e_0\varphi(x)\beta)}{a_0 \int_0^D \exp(-e_0\varphi(x)\beta)\,dx} \quad (16)$$

The boundary conditions are (see for example [22]) :

$$\frac{d\varphi}{dx}(x=0) = -\frac{\sigma}{\varepsilon_0 \varepsilon_r(x=0)} \quad (17)$$

$$\frac{d\varphi}{dx}(x \to \infty) = 0 \quad (18)$$

$$\varphi(x=D_-) = \varphi(x=D_+) \quad (19)$$

$$\frac{d\varphi}{dx}(x=D_-) = \frac{d\varphi}{dx}(x=D_+) \quad (20)$$

where in Equation 17 the surface charge density $\sigma = -e_0/a_0$. Note that the area per lipid a_0 is different in gel and liquid phase. $E = |\phi'|$.

Figure 3. The calculated charge density profile of co-ions (n_-) (A,B) and counter-ions (n_+) (C,D) of the electrolyte solution for two temperatures 310 K (full blue line) and 323 K (dashed red line) and corresponding DPPC values of the area per lipid ($a_0 = 0.48\,nm^2$ below 314 K and $a_0 = 0.60\,nm^2$ above 314 K). The dipole moment of water was $p_0 = 3.1$ Debye, $D = 0.42$ nm, bulk concentration of salt $n_0/N_A = 0.1$ mol/l and concentration of water $n_{0w}/N_A = 55$ mol/l, where N_A is Avogadro number.

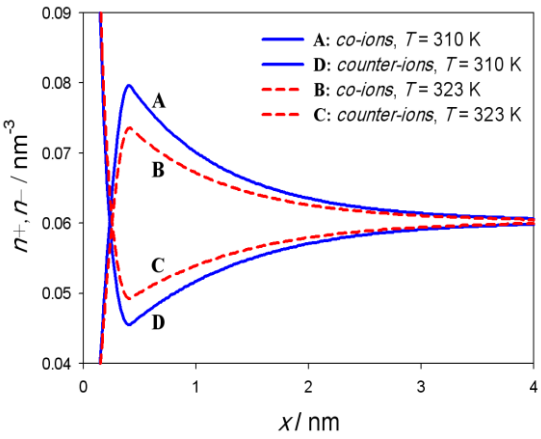

In numerical calculations the distance from the negatively charged surface x was limited to 12 nm, where the boundary condition stated in Equation 18 was applied. The modified LPB equation (Equation 16) was solved numerically as described in the Appendix A. All the results were obtained using $a_0 = 0.48\,nm^2$ and $a_0 = 0.60\,nm^2$ corresponding to DPPC lipid in gel-crystalline (below 314 K) and liquid-crystalline phase (above 314 K), respectively [33]. Other values of model parameters were: the dipole moment of water $p_0 = 3.1$ Debye, bulk concentration of salt $n_0/N_A = 0.1$ mol/l and concentration of water $n_{0w}/N_A = 55$ mol/l. N_A is Avogadro number.

2.3. Molecular Dynamics Simulations (MD)

The molecular dynamics (MD) model of DPPC planar lipid bilayer was constructed in NAMD program using all molecule performance CHARMM 36 force field. The model consists of 256 lipid

units and 20174 water molecules. The solvent was 450 mM KCl modeled by 153 K^+ and 153 Cl^- ions [34,35]. Chemical bonds between hydrogen and heavy atoms were constrained to their equilibrium value. Long-range electrostatic forces were taken into account using a fast implementation of the particle mesh Ewald (PME) method [36,37]. The model was examined at constant pressure (1.013×10^5 Pa) and constant temperature (232 K) employing Langevin dynamics and the Langevin piston method. The equations of motion were integrated using the multiple time-step algorithm. A time step of 2.0 fs was employed. Short- and long-range forces were calculated every one and two time steps, respectively.

The model was equilibrated and followed 30 ns. The last 15 ns of the simulation were used for extraction of dipole orientation angle. From the P and N atoms positions the dipole was determined for all 256 lipids in each of 1500 simulation frames and exported to Matlab2012b. The distribution of vector amplitude corresponding to distance D between charges was extracted as well as distribution of the angle ω between the dipole and normal vector to the planar lipid bilayer plane (Figure 2). To obtain the probability density $P(x)$, projection of each headgroup dipole on the normal vector to the planar lipid bilayer plane was calculated. The average distance between P and N atoms (0.42 nm) was used as a parameter D in MLPB model (Equation 16).

3. Results

Electric potential ϕ and relative permittivity ε_r as a function of the distance from the charged planar surface ($x = 0$) is presented in Figure 4. The results are presented for two values of the temperature: $T = 310$ K ($a_0 = 0.48$ nm^2) and $T = 323$ K ($a_0 = 0.60$ nm^2). It can be seen in Figure 4 that the relative permittivity $\varepsilon_r(x)$ is considerably decreased in the vicinity of charged planar surface. At the charged planar surface ($x = 0$) the value of $\varepsilon_r(x)$ drops to 44 at $T = 310$ K and to 55 at $T = 323$ K. The effect of the charged planar surface at $x = 0$ is very weak already at the distance $x = D$. Far away from the surface ($x = 0$) the values of $\varepsilon_r(x)$ is 75.5 at temperature $T = 310$ K and 72.6 for temperature $T = 323$ K. The electric potential in the vicinity of the charged planar surface is considerably negative. It is -60 mV for temperature $T = 310$ K and -54 mV for temperature $T = 323$ K.

Charge density profile of co-ions (n_-) and counter-ions (n_+) of the electrolyte solution for two temperatures 310 K and 323 K can be seen in Figure 3. Near the negatively charged planar surface at $x = 0$ one can observe strong accumulation of positively charged counter-ions and depletion of the negatively charged co-ions. With increasing distance from the headgroup region ($0 < x \leq D$), *i.e.*, for x larger than D, the number density of co-ions (n_-) decreases and the number density of counter-ions (n_+) increases. Far away from the charged planar surface, the concentration of counter-ions (n_+) equals the concentration of co-ions (n_-) corresponding to electroneutrality condition in bulk solution. At higher temperature (323 K) the DPPC has increased area per lipid $a_0 = 0.60$ nm^2 resulting in lower area density of the lipid molecules and hence less negative surface charge density at $x = 0$ plane as in the case of lower temperature (310 K). Consequently, also the calculated ion number density profiles are lower for $x > D$ (Figure 3).

The average headgroup orientation angle $< \omega >$ as a function of the temperature T can be seen on Figure 5. At DPPC phase transition temperature (314 K) the value of $< \omega >$ can not be calculated as phase transition effect is not included in MLPB model. The average dipole orientation angle $< \omega >$, calculated from $P(x)$ as described in Appendix B, is not temperature dependent. At DPPC liquid-crystalline phase average headgroup orientation angle $< \omega > = 69.36$ degrees, which agrees with median angle $< \omega >$ between N and P dipole and normal vector obtained in MD simulation ($< \omega > = 68$ degrees). The difference of $< \omega >$ between liquid-crystalline and gel-crystalline phase is a consequence of a different values of area per lipid a_0 in gel-crystalline phase and liquid-crystalline phase.

Figure 4. Electric potential ϕ and relative permittivity ε_r as a function of the distance from the charged planar surface at $x = 0$ calculated for two temperatures and corresponding values of a_0: $T = 310$ K, $a_0 = 0.48$ nm^2 (full blue lines) and $T = 323$ K, $a_0 = 0.60$ nm^2 (dashed red lines). These values of a_0 correspond to DPPC in two different phases. Relative permittivity ε_r as the function of the distance from the charged planar surface x (panel B) was calculated from Equation 6. The MLPB equation was solved numerically as described in the Appendix A. The dipole moment of water $p_0 = 3.1$ Debye, $D = 0.42$ nm bulk concentration of salt $n_0/N_A = 0.1$ mol/l, concentration of water $n_{0w}/N_A = 55$ mol/l, where N_A is Avogadro number. For simplicity the second boundary condition was applied at a distance of 12 nm.

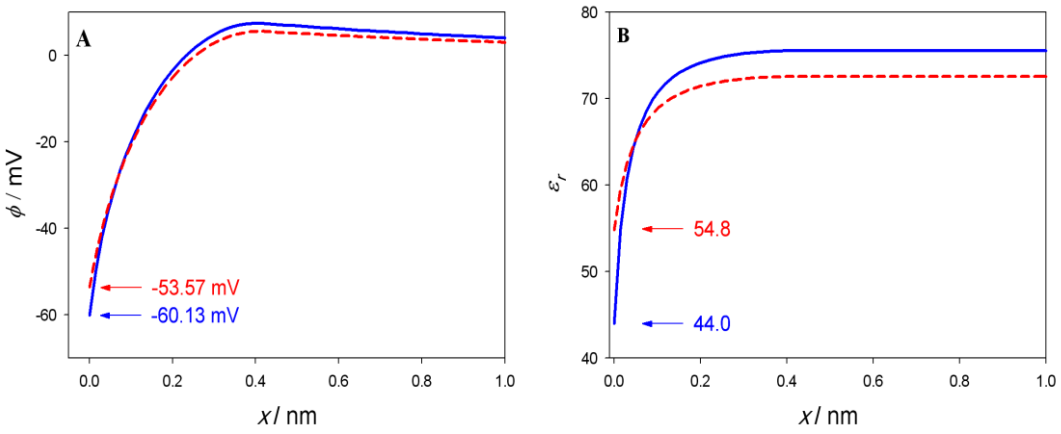

Int. J. Mol. Sci. 2013, *14* 2855

Figure 5. Average headgroup dipole orientation angle $< \omega >$ (see also Figure 2) as a function of the temperature T. Area per lipid $a_0 = 0.48\ nm^2$ below 314 K, corresponding to DPPC lipid gel-crystalline phase (full line) and $a_0 = 0.60\ nm^2$ above 314 K, corresponding to DPPC lipid liquid-crystalline phase (dashed line). A gap near the phase transition temperature (314 K) is present, because phase transition effect is not included in MLPB model. Average dipole orientation angle $< \omega >$ was calculated from $P(x)$ as described in Appendix B. The values of other model parameters are the same as in Figure 4.

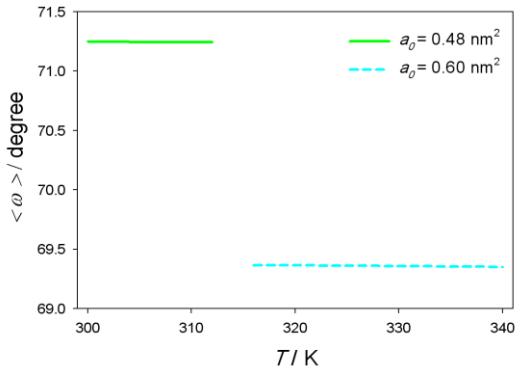

4. Discussion and Conclusions

The comparison between the probability density $P(x)$ calculated within MLPB model (Equation 13) and $P(x)$ obtained in MD simulations, can be seen on Figure 6. In MLPB model the function $P(x)$ is steeply increasing in the vicinity of $x = 0$ plane (Figure 6, plot A) which is a consequence of the exponential Boltzmann factor in the function $P(x)$ (Equation 13). This result is clearly not in accordance with MD simulation (Figure 6, plot B), where the function $P(x)$ is saturated. The discrepancy between the predictions of MLPB model and MD simulations arises due to the fact that the finite volumes of lipid headgroups and finite volumes of ions and water molecules are not considered in MLPB model. Taking into account the finite volume of lipid headgroups within the lattice statistics approach (see also [13,24]) yields for probability density that the positive charge of the dipolar lipid headgroup is located at certain distance x from the $x = 0$ surface in the form :

$$P(x) = \Lambda \frac{\alpha \exp(-e_0 \phi(x) \beta)}{\alpha \exp(-e_0 \phi(x) \beta) + 1} \tag{21}$$

where Λ is determined from normalization Equation 14. The parameter α is equal to the ratio between the average volume of the positively charged parts of dipolar (zwitterionic) headgroups and the average volume of the salt solution in the headgroup region. Equation 21 predicts the saturation of the probability density function $P(x)$, corresponding to the close packing of the lipid headgroups in accordance with the results of MD simulations. Figure 6 thus shows the dependence of $P(x)$ calculated by using Equation 21 for the values of the parameter α. It can be seen that taking into account the finite volume of lipid headgroups leads to better agreement between the predicted $P(x)$ dependencies within MLPB model and MD simulations. In the limit of $\alpha \to \infty$ (when all lattice sites are occupied by the headgroups) the probability density function $P(x)$ becomes constant as expected. On the other hand, in the limit of

small values of α (*i.e.*, negligible volume of the headgroups) the probability density P(x), calculated by using Equation 21, approaches to the probability denisty P(x) determined by Equation 13 (curve A in Figure 6).

Figure 6. Probability density P(x) that the positive charge of the lipid dipolar headgroup (see also Figure 2) is located at the distance x from the negatively charged surface calculated from MLPB model (A,C,D,E) and obtained from MD simulations (B). The values of MLPB model parameters are the same as in Figure 4.

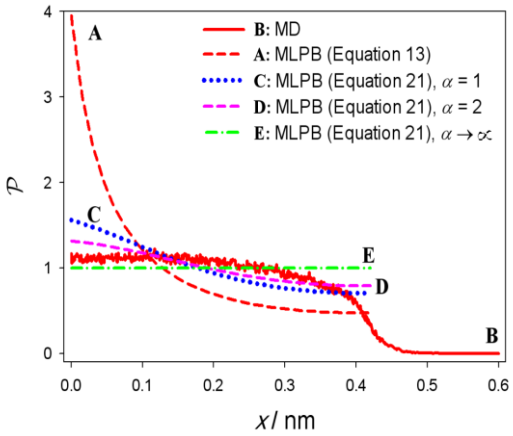

Although the relative permittivity ε_r is usually considered as a constant, it is shown in present paper that ε_r can considerably change within the dipolar (zwitterionic) lipid headgroup region. Consequently, the electric potential in this region is substantially decreased.

To conclude, our model shows that the effect of decreasing potential and permittivity has an impact only in the headgroup region of dipolar zwitterionic lipids and its close vicinity. The average orientation angle of the zwitterionic lipid headgroup dipole ($< \omega >$) predicted within the presented MLPB model is comparable with the results obtained in MD simulation.

Acknowledgements

This work was in part supported by the Slovenian Research Agency. The research was conducted in the scope of the EBAM European Associated Laboratory (LEA). Molecular Dynamics Simulations were performed using HPC resources from Arctur Slovenia. First author was mainly supported by European social fund and SMARTEH.

A. Derivation of Equations for Matlab

A.1. Variant A

Equation 16 can be rewritten as :

$$\frac{d^2\psi(x)}{dx^2} = \kappa^2(x)\sinh(\psi(x)) - \frac{\kappa^2(x)\exp(-\psi(x))}{2n_0a_0\int_0^r \exp(-\psi(x))dx} - \frac{1}{\varepsilon_r(x)}\frac{d\varepsilon_r(x)}{dx}\frac{d\psi(x)}{dx} \quad (22)$$

where $\psi(x)$ is reduced electric potential :

$$\psi(x) = e_0\beta\varphi(x) \quad (23)$$

and

$$\kappa^2(x) = \frac{2e_0^2n_0\beta}{\varepsilon_0\varepsilon_r(x)} \quad (24)$$

The boundary conditions (Equations 17–20) can be rewritten as :

$$\frac{d\psi(x)}{dx}(x=0) = -\frac{e_0\beta\sigma}{\varepsilon_0\varepsilon_r(x=0)} \quad (25)$$

$$\frac{d\psi}{dx}(x\to\infty) = 0 \quad (26)$$

$$\psi(x=D_-) = \psi(x=D_+) \quad (27)$$

$$\frac{d\psi}{dx}(x=D_-) = \frac{d\psi}{dx}(x=D_+) \quad (28)$$

Equation 22 was solved in Matlab using the standard function for the boundary value problems (bvp4c). The second part of the right hand side of Equation 22 is defined only within headgroup region, therefore it is equal to zero for $x > D$. The value of $\varepsilon_r(x)$ (Equation 6) and the integral $\int_0^r \exp(-\psi(x))dx$ and $d\varepsilon_r(x)/dx$ in Equation 22 were calculated outside of bvp4c function. The $d\varepsilon_r(x)/dx$ was derived from Equation 6, where the Langevin function $L(x)$ was expanded for small values of electric field into Taylor series up to the cubic term $L(x) \approx x/3 - x^3/45$. Considering $E(x) = \left|\frac{d\psi(x)}{dx}\right|$, can be written :

$$\varepsilon_r(x) = K_1 + \frac{K_2}{45}\left(15 - (K_3E(x))^2\right) \quad (29)$$

$$\frac{d\varepsilon_r(x)}{dx} = -\frac{2K_2K_3^2}{45}\frac{d\psi(x)}{dx}\frac{d^2\psi(x)}{dx^2} \quad (30)$$

where the constants are :

$$K_1 = n^2 \quad (31)$$

$$K_2 = \frac{3}{2}\left(\frac{2+n^2}{3}\right)^2\frac{n_{0w}p^2\beta}{\varepsilon_0} \quad (32)$$

$$K_3 = \frac{\gamma p_0}{e_0} \quad (33)$$

For high values of electric field the $\varepsilon_r(x)$ and the $d\varepsilon_r(x)/dx$ are derived from Equation 6 with non-expanded Langevin function :

$$\varepsilon_r(x) = K_1 + K_2 \left(\frac{(K_3 E(x)) \coth(K_3 E(x)) - 1}{(K_3 E(x))^2} \right) \tag{34}$$

$$\frac{d\varepsilon_r(x)}{dx} = \frac{K_2}{\frac{d\psi(x)}{dx}} \left(\frac{1}{\sinh^2(K_3 E(x))} - \frac{(K_3 E(x)) \coth(K_3 E(x)) - 2}{(K_3 E(x))^2} \left(\frac{d^2\psi(x)}{dx^2} \right) \right) \tag{35}$$

where constants are the same as above (Equations 31–33).

A.2. Variant B

By inserting the Equation 6 and its derivative into Equation 8, the Equation 8 can be rewritten as :

$$\frac{d^2\psi(x)}{dx^2} = \left[\frac{\frac{2e_0^2 n_0}{\varepsilon_0 \beta} \sinh(\psi(x)) - \frac{e_0^2 \exp(-\psi(x))}{a \varepsilon_0 \beta \int_0^D \exp(-\psi(x))dx}}{K_2 \left(\frac{1}{(K_3 E(x))^2} - \frac{1}{\sinh^2(K_3 E(x))} \right) + K_1} \right] \tag{36}$$

where the constants K1, K2, K3 are defined as above (Equations 31–33). Equation 36 was solved in Matlab using standard function for boundary value problem (bvp4c) with multipoint boundary values (Equations 25–28). The value of the integral $\int_0^D \exp(-\psi(x))dx$ in Equation 36 was calculated in iteration process outside of bvp4c function.

B. Average Orientation of Lipid Head-Groups

From Equations (13 and 15) it follows:

$$P(x) = \frac{D \exp(-\psi(x))}{\int_0^D \exp(-\psi(x))dx} \tag{37}$$

Average orientation angle of the headgroup dipole ($< \omega >$) can be then written as normalized distribution function:

$$< \omega > = \frac{\int_0^D \omega P(x)dx}{\int_0^D P(x)dx} \tag{38}$$

where the dipole orientation angle is (see also Figure 2) :

$$\omega = \arccos \frac{x}{D} \tag{39}$$

References

1. Sackmann, E. Molecular and global structure and dynamics of membranes and lipid bilayers. *Can. J. Phys.* 1990, *68*, 999–1012.

2. Sackmann, E. Biological Membranes Architecture and Function. In *Structure and Dynamics of Membranes*; Lipowsky, R., Sackmann, E., Eds.; Elsevier: Amsterdam, The Netherlands, 1995; pp. 1–63.
3. Šuštar, V.; Zelko, J.; Lopalco, P.; Lobasso, S.; Ota, A.; Ulrih, N.P.; Corcelli, A.; Kralj-Iglič, V. Morphology, biophysical properties and protein-mediated fusion of archaeosomes. *PLoS One* 2012, *7*, e39401.
4. Kralj-Iglič, V. Stability of membranous nanostructures: A possible key mechanism in cancer progression. *Int. J. Nanomed.* 2012, *7*, 3579–3596.
5. Šuštar, V.; Bedina Zavec, A.; Štukelj, R.; Frank, M.; Bobojevič, G.; Janša, R.; Ogorevc, E.; Kruljc, P.; Mam, K.; Šimunič, B.; *et al*. Nanoparticles isolated from blood: A reflection of vesiculability of blood cells during the isolation process. *Int. J. Nanomed.* 2011, *6*, 2737–2748.
6. Rappolt, M.; Pabst, G. Flexibility and Struture of Fluid Bilyer Interfaces. In *Structure and Dynamics of Membranous Interfaces*; Nag, K., Ed.; John Wiley and Sons, Inc.: Hoboken, NJ, USA, 2008; pp. 45–81.
7. Yaghmur, A.; Rappolt, M. Structural characterization of lipidic systems under nonequilibrium conditions. *Eur. Biophys. J.* 2012, *41*, 831–840.
8. Tien, H.T.; Ottova-Leitmannova, A. The Lipid Bilayer Concept: Experimental Realization and Current Application. In *Planar Lipid Bilayers (BLMs) And Their Application*; Tien, H.T., Ottova-Leitmannova, A., Eds.; Elsevier: Amsterdam, The Netherlands, 2003; pp. 1–73.
9. Luckey, M. *Membrane Structural Biology*, 1st ed.; Cambridge University Press: New York, NY, USA, 2008; pp. 1–67.
10. Kramar, P.; Miklavčič, D.; Kotulska M; Maček Lebar, A. Voltage- and Current-clamp Methods for Determination of Planar Lipid Bilayer Properties. In *Advances in Planar Lipid Bilayers and Liposomes, Volume 11*; Iglič, A., Ed.; Elsevier: Amsterdam, The Netherlands, 2010; pp. 29–69.
11. Polak, A.; Mulej, B.; Kramar, P. System for measuring planar lipid bilayer properties. *J. Membrane Biol.* 2012, *24*, 625–632.
12. Kramar, P.; Miklavčič, D.; Maček Lebar, A. A system for the determination of planar lipid bilayer breakdown voltage and its applications. *IEEE Trans. Nanobiosci.* 2009, *8*, 132–138.
13. Gongadze, E.; Iglič, A. Decrease of permittivity of an electrolyte solution near a charged surface due to saturation and excluded volume effects. *Bioelectrochemistry* 2012, *87*, 199–203.
14. Cevc, G. *Phospholipid Handbook*, 1st ed.; Marcel Dekker: New York, NY, USA, 1993.
15. Rappolt, M.; Laggner, P.; Pabst, G. Structure and Elasticity of Phospholipid Bilayers in the L_α Phase: A Comparison of Phosphatidylcholine and Phosphatidylethanolamine Membranes. In *Recent Research Development in Biophysics*; Pandalai, S.G., Ed.; Trivandrum-Transworld Research Network: Kerala, India, 2004; Volume 3, pp. 363–392.
16. Kramar, P.; Miklavčič, D.; Maček Lebar, A. Determination of the lipid bilayer breakdown voltage by means of a linear rising signal. *Bioelectrochemistry* 2007, *70*, 23–27.
17. Kramar, P.; Delemotte, L.; Maček Lebar, A.; Kotulska, M.; Tarek, M.; Miklavčič, D. Molecular-level characterization of lipid membrane electroporation using linearly rising current. *J. Membrane Biol.* 2012, *245*, 651–659.

18. Sabotin, I.; Maček Lebar, A.; Miklavčič, D.; Kramar, P. Measurement protocol for planar lipid bilayer viscoelastic properties. *IEEE Trans. Diel. El. Insul.* 2009, *15*, 1236–1242.
19. Vácha, R.; Siu, S.W.I.; Petrov, M.; Böckmann, R.A.; Barucha-Kraszewska, J.; Jurkiewicz, P.; Hof, M.; Berkowitz, M.L.; Jungwirth, P. Effects of alkali cations and halide anions on the DOPC lipid membrane. *J. Chem. Phys. A* 2009, *113*, 7235–7243.
20. McLaughlin, S. The electrostatic properties of membranes. *Ann. Rev. Biophys. Chem.* 1989, *18*, 113–136.
21. Gongadze, E.; van Rienen, U.; Kralj-Iglič, V.; Iglič, A. Langevin Poisson-Boltzmann equation: Point-like ions and water dipoles near a charged surface. *Gen. Physiol. Biophys.* 2011, *30*, 130–137.
22. Gongadze, E.; van Rienen, U.; Kralj-Iglič, V.; Iglič, A. Spatial variation of permittivity of an electrolyte solution in contact with a charged metal surface: A mini review. *Comput. Meth. Biomech. Biomed. Eng.* 2012, 1–18. doi: 10.1080/10255842.2011.624769. Available online: http://dx.doi.org/10.1080/10255842.2011.624769 (accessed on 18 September 2012).
23. Cevc, G. Memrane electrostatics. *Biochim. Biophys. Acta.* 1990, *1031*, 311–382.
24. Kralj-Iglič, V.; Iglič, A. A simple statistical mechanical approach to the free energy of the electric double layer including the excluded volume effect. *J. Phys. II France* 1996, *6*, 477–491.
25. Lamperski, S.; Outhwaite, C.W. Exclusion volume term in the inhomogeneous poisson-boltzmann theory for high surface charge. *Langmuir* 2002, *18*, 3423.
26. Bazant, M.Z.; Kilic, M.S.; Storey, B.; Ajdari, A. Advances in colloid and interface science. *Adv. Colloid Interface Sci.* 2009, *152*, 48.
27. Butt, H.J.; Graf, K.; Kappl, M. *Physics and Chemistry of Interfaces*, 2nd ed.; Wiley-VCH Verlag: Weinheim, Germany, 2003.
28. Outhwaite, C.W. A treatment of solvent effects in the potential theory of electrolyte solutions. *Mol. Phys.* 1976, *31*, 1345–1357.
29. Outhwaite, C.W. Towards a mean electrostatic potential treatment of an ion-dipole mixture or a dipolar system next to a plane wall. *Mol. Phys.* 1983, *48*, 599–614.
30. Iglič, A.; Gongadze, E.; Bohinc, K. Excluded volume effect and orientational ordering near charged surface in solution of ions and Langevin dipoles. *Bioelectrochemistry* 2010, *79*, 223.
31. Das, S; Chakraborty, S.; Mitra, S.K. Redefining electrical double layer thickness in narrow confinements: Effect of solvent polarization. *Phys. Rev. E* 2012, *85*, 051508.
32. Fröhlich, H. *Theory of Dielectrics*, 1st ed.; Clarendon Press: Oxford, UK, 1964.
33. Marsh, D. An incteracting spin label study of lateral expansion in dipalmitoyllecithin-cholesterol bilayers. *Biochim. Biophys. Acta.* 1974, *363*, 373–386.
34. Kale, L.; Skeel, R.; Bhandarkar, M.; Brunner, R.; Gursoy, A.; Krawetz, N.; Phillips, J.; Shinozaki, A.; Varadarajan, K.; Schulten, K. NAMD2: Greater scalability for parallel molecular dynamics. *J. Comp. Phys.* 1999, *151*, 283–312.
35. Phillips, J.C.; Braun, R.; Wang, W.; Gumbart, J.; Tajkhorshid, E.; Villa, E.; Chipot, C.; Skeel, R.D.; Kale, L.; Schulten, K. Scalable molecular dynamics with NAMD. *J. Comp. Chem.* 2005, *26*, 1781–1802.

36. Dardenn, T.; York, D.; Pedersen, L. Particle mesh Ewald: An N·log(N) method for Ewald sums in large systems. *J. Chem. Phys.* 1993, *98*, 10089.
37. Essmann, U.; Perera, L.; Berkowitz, M.L. The origin of the hydration interaction of lipid bilayers from MD simulation of dipalmitoylphosphatidylcholine membranes in gel and liquid crystalline phases. *Langmuir* 1995, *11*, 4519–4531.

B Članek 2: Interaction between Dipolar Lipid Headgroups and Charged Nanoparticles Mediated by Water Dipoles and Ions

Polno ime revije:	International Journal of Molecular Sciences
Okrajšava:	Int. J. Mol. Sci.
ISSN (elektronska izdaja):	1422-0067
Založnik:	Multidisciplinary Digital Publishing Institute (MDPI)
Naslov založnika:	MDPI AG, Klybeckstrasse 64, 4057 Basel, Switzerland
Pogostost izdaje:	mesečno
Medij:	elektronska verzija
Spletna stran revije:	http://www.mdpi.com/journal/ijms
Prvo leto izdaje:	2000
Faktor vpliva:	2.464 (2012)
Faktor vpliva (5 let):	2.732 (2012)
Naslov članka:	Interaction between Dipolar Lipid Headgroups and Charged Nanoparticles Mediated by Water Dipoles and Ions
Avtorji:	Velikonja, Aljaž; Santhosh, Poornima Budime; Gongadze, Ekaterina; Kulkarni, Mukta; Eleršič, Kristina; Perutkova, Šarka; Kralj-Iglič, Veronika; Poklar Ulrih, Nataša; Iglič, Aleš
Izdaja:	14
Številka:	8
Strani:	15312–15329
Leto objave:	2013
DOI:	10.3390/ijms140815312

Int. J. Mol. Sci. 2013, *14*, 15312-15329; doi:10.3390/ijms140815312

OPEN ACCESS

International Journal of
Molecular Sciences
ISSN 1422-0067
www.mdpi.com/journal/ijms

Article

Interaction between Dipolar Lipid Headgroups and Charged Nanoparticles Mediated by Water Dipoles and Ions

Aljaž Velikonja [1], Poornima Budime Santhosh [2], Ekaterina Gongadze [3], Mukta Kulkarni [3], Kristina Eleršič [4], Šarka Perutkova [3,5], Veronika Kralj-Iglič [6,7], Nataša Poklar Ulrih [2] and Aleš Iglič [3,7,*]

[1] SMARTEH Research and Development of Electronic Controlling and Regulating Systems, Trg tigrovcev 1, Tolmin SI-5220, Slovenia; E-Mail: aljaz.velikonja@avelik.homeip.net

[2] Department of Food Science and Technology, Biotechnical Faculty, University of Ljubljana, Jamnikarjeva 101, Ljubljana SI-1000, Slovenia; E-Mails: poornima.budimesanthosh@bf.uni-lj.si (P.B.S.); natasa.poklar@bf.uni-lj.si (N.P.U.)

[3] Laboratory of Biophysics, Faculty of Electrical Engineering, University of Ljubljana, Tržaška 25, Ljubljana SI-1000, Slovenia; E-Mails: ekaterina.gongadze@fe.uni-lj.si (E.G.); mukta.kulkarni@fe.uni-lj.si (M.K.); sarka.perutkova@fe.uni-lj.si (S.P.)

[4] Jožef Stefan Institute, Jamova 39, Ljubljana SI-1000, Slovenia; E-Mail: kisstinca@hotmail.com

[5] Institute of Cell Biology, Faculty of Medicine, University of Ljubljana, Lipičeva 2, Ljubljana SI-1000, Slovenia

[6] Laboratory of Clinical Biophysics, Faculty of Health Studies, University of Ljubljana, Zdravstvena 5, Ljubljana SI-1000, Slovenia; E-Mail: veronika.kralj-iglic@fe.uni-lj.si

[7] Laboratory of Clinical Biophysics, Chair of Orthopaedic Surgery, Faculty of Medicine, University of Ljubljana, Zaloška 9, Ljubljana SI-1000, Slovenia

* Author to whom correspondence should be addressed; E-Mail: ales.iglic@fe.uni-lj.si; Tel.: +386-1-4768-825; Fax: +386-1-4768-850.

Received: 10 April 2013; in revised form: 24 May 2013 / Accepted: 25 June 2013 / Published: 24 July 2013

Abstract: In this work, a theoretical model describing the interaction between a positively or negatively charged nanoparticle and neutral zwitterionic lipid bilayers is presented. It is shown that in the close vicinity of the positively charged nanoparticle, the zwitterionic lipid headgroups are less extended in the direction perpendicular to the membrane surface, while in the vicinity of the negatively charged nanoparticle, the headgroups are more extended. This result coincides with the calculated increase in the osmotic pressure between the

Int. J. Mol. Sci. 2013, *14* 15313

zwitterionic lipid surface and positively charged nanoparticle and the decrease of osmotic pressure between the zwitterionic lipid surface and the negatively charged nanoparticle. Our theoretical predictions agree well with the experimentally determined fluidity of a lipid bilayer membrane in contact with positively or negatively charged nanoparticles. The prospective significance of the present work is mainly to contribute to better understanding of the interactions of charged nanoparticles with a zwitterionic lipid bilayer, which may be important in the efficient design of the lipid/nanoparticle nanostructures (like liposomes with encapsulated nanoparticles), which have diverse biomedical applications, including targeted therapy (drug delivery) and imaging of cancer cells.

Keywords: charged nanoparticles; lipids; osmotic pressure; dipolar zwitterionic headgroups; relative permittivity of water; orientational ordering

1. Introduction

The basic building block of a cell membrane is a bilayer of lipid molecules with embedded carbohydrates and proteins [1–6]. The mechanical and electrical properties of a lipid bilayer [1,7–12] play an important role in many processes of the cell [1,13–17]. In experimental systems, the membrane lipid bilayer is usually in contact with an electrolyte solution composed of water molecules and positively and negatively charged salt ions [13,14]. Some of the lipids, like 1-palmitoyl-2-oleoyl-sn-glycero-3-phospho-L-serine (POPS), bears net negative electric charge, while the others, like glycerophospholipid 1,2-dipalmitoyl-sn-glycero-3-phosphocholine (DPPC), having dipolar (zwitterionic) headgroups, are electrically neutral [1–3,8]. The negatively charged lipid bilayer (headgroups) in contact with an electrolyte solution attracts cations and repels anions, and thus, an electric double layer is formed [18,19]. In the electric double layer, a strong variation of electric potential close to the negatively charged membrane was predicted [13,14,20–25]. In the case of a lipid bilayer composed of dipolar (zwitterionic) lipids, a substantial drop of the electric potential takes place within the headgroup region [13,26]. In the high electric field of dipolar lipid headgroups (see [13] and the references therein), the water dipoles are oriented towards the negatively charged plane (see, for example, [23,26–32]). Recently, it was shown that within a simple mean-field approach, due to the saturation effect in the orientational ordering of water dipoles, the relative permittivity in the zwitterionic headgroup region is decreased, while the corresponding electric potential becomes more negative [26].

Liposomes encapsulated with the nanoparticles find enormous applications in various biomedical fields, such as cancer diagnosis, therapy and drug delivery [33]. As the usage of the nanoparticles is rapidly increasing, it becomes important to study the effect of differently charged nanoparticles on the cell membrane. The interaction of the nanoparticles with the lipid bilayer can alter the physical properties of the membrane, such as membrane fluidity, permeability and elasticity, and biological functions, such as cell signaling and transduction [34,35]. The biological and/or liposome membrane can be locally or globally deformed by the charged organic and inorganic nanoparticles attached to the membrane surface [36–39]. Among the charged organic nanoparticles, proteins are the biologically most

important [38,40]. A number of proteins have been identified that directly bind and deform biological membranes [37,41–43]. The binding of proteins and other charged nanoparticles to the lipid bilayer of the cell membrane or membrane of liposomes is partially driven by electrostatic forces. Therefore, in this paper, the interaction between a negatively charged or dipolar flat lipid layer and positively or negatively charged nanoparticles (Figure 1) mediated by water dipoles and ions is studied within the mean-field approach using the modified Langevin-Poisson-Boltzmann (LPB) model [26,30]. An analytical expression for the osmotic pressure between the lipid headgroups and nanoparticles is derived, and the change of the average orientation lipid headgroups, due to the charged nanoparticle, is predicted. Through experimental study of the nanoparticle-induced changes in lipid bilayer fluidity, we intend to establish a correlation between the theoretical calculations and experimental results.

Figure 1. Schematic figure of dipolar zwitterionic lipid bilayer membrane in contact with the positively and negatively charged nanoparticles.

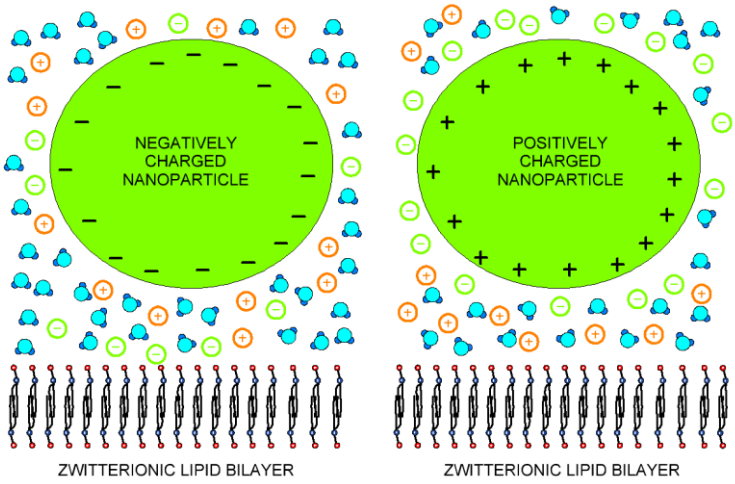

2. Interaction between Lipid Headgroups and Charged Nanoparticle

2.1. Space Dependence of Relative Permittivity within the Modified Langevin-Poisson-Boltzmann (MLPB) Model

Recently, the Langevin-Poisson-Boltzmann (LPB) model [30] was generalized to take into account the cavity field [31] in the saturation regime [26]. In this modified Langevin-Poisson-Boltzmann (MLPB) model [26], the electronic polarization of the water is taken into account by assuming that the point-like rigid (permanent) water dipole is embedded in the center of the sphere with a volume equal to the average volume of a water molecule in the electrolyte solution [31,44,45]. The permittivity of the single molecule's water sphere is $n^2 = 1.33^2$, where n is the optical refractive index of water. The space dependency of permittivity within the MLPB model has the form [26,30]:

$$\varepsilon_r(x) = n^2 + \frac{n_{0w}p_0}{\varepsilon_0}\frac{\left(2+n^2\right)}{3}\frac{L(\gamma p_0 E(x)\beta)}{E(x)} \quad (1)$$

where n_{0w} is the constant number density of water molecules, p_0 is the magnitude of the water external dipole moment [31], $E(x)$ is the magnitude of the electric field strength, ε_0 is the permittivity of the free space, $\beta = 1/kT$, kT is the thermal energy and $L(u) = (\coth(u) - 1/u)$ is the Langevin function, while $\gamma = \frac{3}{2}\frac{2+n^2}{3}$ [31]. In the limit of $E(x) \longrightarrow 0$, Equation (1) for $\varepsilon_r(x)$ gives the well-known Onsager expression: $\varepsilon_{r,b} \cong n^2 + (2+n^2/3)^2 n_{0w} p_0^2 \beta / 2\varepsilon_0$. At room temperature (298 K), the above equation predicts $\varepsilon_r = 78.5$ for the bulk solution. The parameters, p_0 and n_{0w}/N_A, are 3.1 Debye and 55 mol/L, respectively.

2.2. Osmotic Pressure between Two Planar Charged Surfaces

In this subsection, we derive the expression for the osmotic pressure of electrolyte solution confined by two charged planar surfaces described in the model by surface charge density, σ_1, at $x = 0$ and surface charge density, σ_2, at $x = H$ (see Figure 2). The space dependency of permittivity, $\varepsilon_r(x)$, is taken into account by Equation (1). The corresponding Poisson equation, *i.e.*, the MLPB equation, in a planar geometry can, thus, be written as: [26,30]:

$$\frac{d}{dx}\left[\varepsilon_0 \varepsilon_r(x) \frac{d\phi}{dx}\right] = 2 e_0 n_0 \sinh e_0 \phi \beta \tag{2}$$

where $\phi(x)$ is the electric potential, e_0 is the unit charge, n_0 is the bulk number density of salt anions and cations and $\varepsilon_r(x)$ is defined by Equation (1). The boundary conditions are (see, for example, [30]):

$$\frac{d\phi}{dx}(x=0) = -\frac{\sigma_1}{\varepsilon_0 \varepsilon_r(x=0)} \quad \frac{d\phi}{dx}(x=H) = +\frac{\sigma_2}{\varepsilon_0 \varepsilon_r(x=H)} \tag{3}$$

By integrating the MLPB Equation (2) and subtracting the corresponding bulk values from the local pressure between the lipid bilayer and nanoparticle surface, we obtain the expression for the osmotic pressure difference, $\Pi = P_{inner} - P_{bulk}$ in the form (see Appendix):

$$\Pi = -\frac{1}{2}\varepsilon_0 n^2 E(x)^2 + 2 n_0 kT \left(\cosh(-e_0\phi(x)\beta) - 1\right) - \\ - E(x)\left(\frac{2+n^2}{3}\right) n_{0w} p_0 L(\gamma p_0 E(x)\beta) + \left(\frac{2+n^2}{3}\right)\frac{n_{0w}}{\gamma\beta}\ln\left(\frac{\sinh(\gamma p_0 E(x)\beta)}{\gamma p_0 E(x)\beta}\right) \tag{4}$$

Substituting the spatial number density distributions for cations and anions of electrolyte solution:

$$n_+(x) = n_0 \exp(-e_0\phi(x)\beta) \ , \ n_-(x) = n_0 \exp(e_0\phi(x)\beta) \tag{5}$$

Equation (4) reads :

$$\Pi = -\frac{1}{2}\varepsilon_0 n^2 E(x)^2 + kT\left(n_-(x) + n_-(x) - 2n_0\right) - \\ -E(x)\left(\frac{2+n^2}{3}\right) n_{0w} p_0 L(\gamma p_0 E(x)\beta) + \left(\frac{2+n^2}{3}\right)\frac{n_{0w}}{\gamma\beta}\ln\left(\frac{\sinh(\gamma p_0 E(x)\beta)}{\gamma p_0 E(x)\beta}\right) \tag{6}$$

For small $\gamma p_0 E(x)\beta$, we can expand the third and fourth term in Equation (6) into a Taylor series to get:

$$\Pi = -\frac{1}{2}\varepsilon_0 n^2 + \left(\frac{2+n^2}{3}\right)^2 \frac{n_{0w} p_0^2 \beta}{2\varepsilon_0} E(x)^2 + kT\left(n_-(x) + n_-(x) - 2n_0\right) \tag{7}$$

Using the Onsager expression for bulk relative permittivity, the above Equation (7) can be rewritten in the usual Poisson-Boltzmann (PB) form for osmotic pressure within the electric double layer theory [46]:

$$\Pi = -\frac{1}{2}\varepsilon_0 \varepsilon_{r,b} E(x)^2 + kT\,(n_-(x) + n_-(x) - 2n_0) \quad (8)$$

In thermodynamic equilibrium, the value of the osmotic pressure is equal everywhere in the space between two charged surfaces (Figure 2); therefore we can calculate it at $x = H/2$ or at $x = H$. Using the boundary condition 3 Equation (8) becomes [46]:

$$\Pi(x = H) = -\frac{\sigma_2^2}{2\varepsilon_0 \varepsilon_{r,b}} + kT\,(n_-(x) + n_-(x) - 2n_0) \quad (9)$$

Figure 2. Schematic figure of the model of a negatively charged surface characterized by surface charge density, σ_1, at $x = 0$ and a positively charged surface with surface charge density, σ_2, at $x = H$.

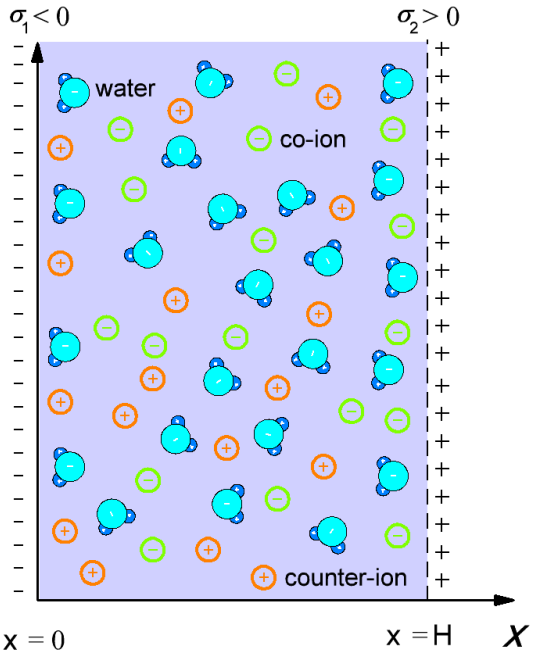

The MLPB equation (*i.e.*, Equation (2)) was solved numerically using MATLAB 2012a [26]) and COMSOL Multiphysics 4.3a [31]. Figure 3 shows the osmotic pressure between the negatively charged surface at $x = 0$ and the positively charged surface at $x = H$ as a function of the decreasing distance between them (H). It can be seen that the decrease of $\Pi(H)$ is more pronounced for the smaller values of the bulk concentration of salt. The predicted values of the osmotic pressure within the MLPB model differs from the corresponding values within the standard PB model, only at small distances, H. Within the MLPB model, the influence of the space variation of permittivity at both charged surfaces (see also [30,31]) on the osmotic pressure is not negligible.

Figure 3. Osmotic pressure between between a negatively and positively surface (see Figure 2) as a function of the distance between both surfaces (H), calculated within the modified Langevin-Poisson-Boltzmann (MLPB) model for two values of the bulk salt concentration, $n_0/N_A = 0.1$ mol/L (dashed line) and $n_0/N_A = 0.01$ mol/L (full line). Other model parameters are : $\sigma_1 = -0.3$ As/m^2, $\sigma_2 = 0.3$ As/m^2, $T = 298$ K, concentration of water, $n_{0w}/N_A = 55$ mol/L, and dipole moment of water, $p_0 = 3.1$ Debye, where N_A is the Avogadro number.

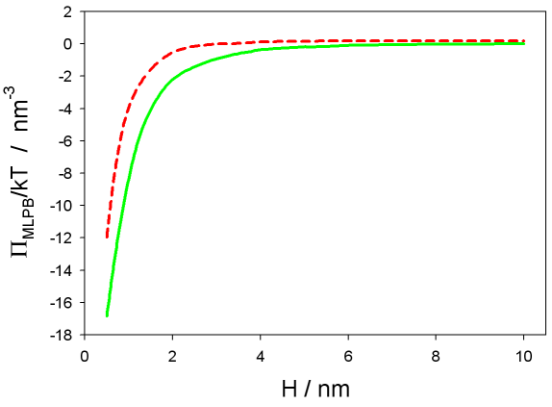

3. Interaction between Dipolar Zwitterionic Lipid Headgroups and Charged Nanoparticle

In the model, the zwitterionic dipolar lipid headgroup composed of a positively charged trimethylammonium group and a negatively charged carboxyl group (at neutral pH) is described by two charges at fixed distance, D (Figure 4) [26]. The negative charges of the phosphate groups of dipolar (zwitterionic) lipids are described by negative surface charge density, σ_1 at $x = 0$, while the positive surface charge of the nanoparticle (Figure 1) is approximated by the planar charged surface at $x = H$ with the surface charged density, σ_2. The corresponding Poisson equation in a planar geometry can be then written in the form [26]:

$$-\frac{d}{dx}\left[\varepsilon_0 \varepsilon_r(x) \frac{d\phi}{dx}\right] = 2 e_0 n_0 \sinh e_0 \phi \beta - \rho_{Zw}(x) \quad (10)$$

where $\rho_{Zw}(x)$ is the macroscopic (net) volume charge density of positive charges of dipolar (zwitterionic) headgroups [26]:

$$\rho_{Zw}(0 < x \leq D) = \frac{|\sigma_1| P(x)}{D} \quad \text{and} \quad \rho_{Zw}(x > D) = 0 \quad (11)$$

where $P(x)$ is the probability density function [26]:

$$P(x) = \Lambda \frac{\alpha \exp(-e_0 \phi(x) \beta)}{\alpha \exp(-e_0 \phi(x) \beta) + 1} \quad (12)$$

where Λ is determined from normalization condition, $\frac{1}{D}\int_0^D P(x)\,dx = 1$. The corresponding boundary conditions, as described in [25,26], should be taken into account.

Figure 4. Negative charges of dipolar (zwitterionic) lipid headgroups are described by the surface charge density, σ_1, at $x = 0$. The positive charges of the headgroups of dipolar lipids protrude in the electrolyte solution. Here, D, is the distance between the charges within the single dipolar lipid headgroup, and ω describes the orientation angle of the dipole within the single headgroup. The positive charge of the interacting nanoparticle is described by the surface charge density, σ_2.

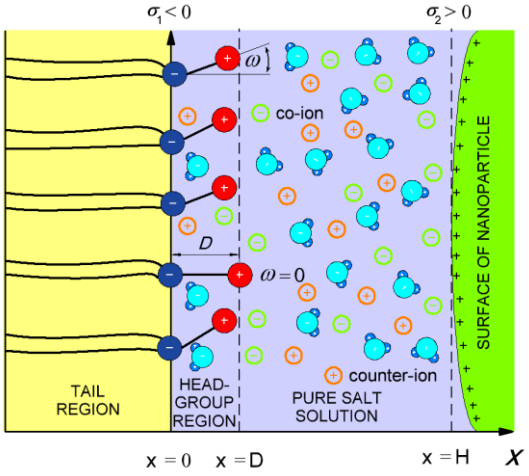

Figure 5. Average lipid dipolar headgroup orientation angle, $< \omega >$ (see, also, Figure 4), as a function of the distance (H) between the plane of the phosphate groups of dipolar (zwitterionic) headgroups and the surface of positively (left panel) and negatively (right panel) charged nanoparticle for the bulk concentration of salt, n_0/N_A = 0.1 mol/L, and two values of parameter, α: 0.5 (full line) and five (dashed line). The values of the model parameters are: the dipole moment of water, p_0 = 3.1 Debye, and concentration of water, n_{0w}/N_A = 55 mol/L.

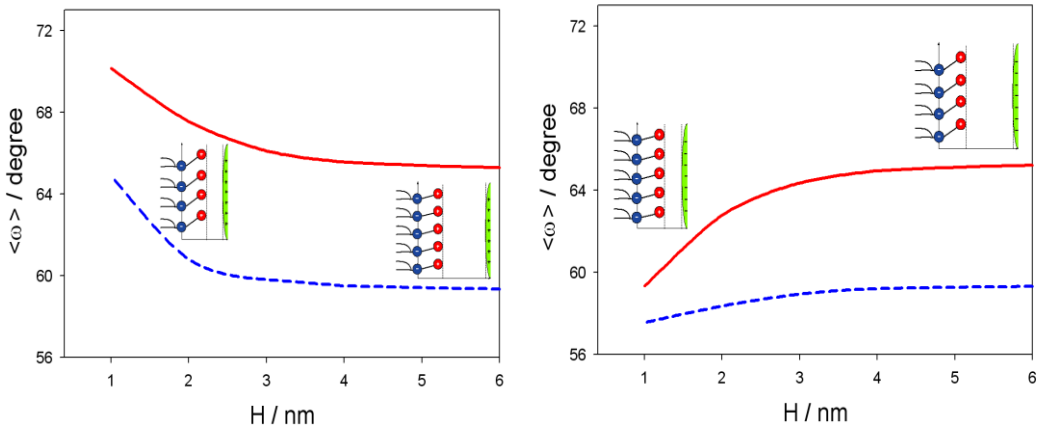

Figure 5 shows the influence of approaching positively and negatively charged nanoparticles on the average orientation of the lipid dipolar headgroup angle ($< \omega >$). As expected, the value of $< \omega >$ increases with decreasing H, due to electrostatic repulsion between the positive charged parts of the lipid headgroups and the positively charged nanoparticles. In accordance, also, the osmotic pressure between the headgroups and nanoparticle is increased with decreased H in the case of a positively charged nanoparticle and decreased in the case of a negatively charged nanoparticle, as presented in Figure 6.

Figure 6. Osmotic pressure between the plane of the phosphate groups of dipolar (zwitterionic) headgroups and the surface of positively (left panel) and negatively (right panel) charged nanoparticle, as a function of the distance (H) (see, also, Figures 4 and 5) calculated for $\alpha = 5$ and the bulk concentration of salt, $n_0/N_A = 0.01$ mol/L, by using Equation (9). The values of other model parameters are the same as in Figure 5.

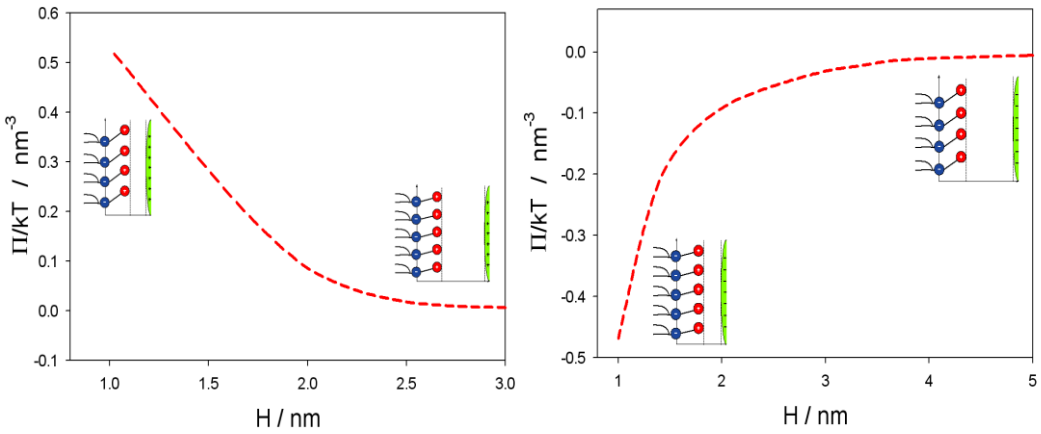

4. Experimental Results

Membrane fluidity denotes the viscosity of the phospholipid bilayer of a cell, and fluidity enables the free mobility of the lipids and protein molecules in a cell membrane [47]. Alteration in the membrane fluidity can affect various membrane associated functions of the cell. Fluidity of a cell membrane is affected by various factors, such as temperature, osmotic pressure, length of membrane fatty acid chains, cholesterol, nanoparticles and the degree of saturation of the lipids in the membrane [48]. In this work, small unilamellar vesicles were prepared to measure the bilayer fluidity in the presence of positively and negatively charged nanoparticles (NPs). The fluidity of the lipid bilayer membrane of small unilamellar vesicles was determined by measuring the fluorescence anisotropy, which is directly proportional to the lipid ordering in the membrane and inversely proportional to the membrane fluidity. As the membrane becomes more fluid, the mobility of the fluorescent dye (DPH) incorporated into the bilayer also increases, whereas the intensity of the fluorescence emission from the dye decreases. Hence, increased anisotropy values indicate that the membrane fluidity is decreased, and the lipids are in a more

ordered (liquid) phase. On the other hand, decreased anisotropy values denote increased membrane fluidity, and the bilayer lipids are in a less ordered (liquid) phase.

4.1. Synthesis of Nanoparticles

Superparamagnetic maghemite nanoparticles ($\gamma - Fe_2O_3$) were synthesized through a controlled chemical co-precipitation method. An aqueous solution of iron (II) sulfate heptahydrate ($FeSO_4 \cdot 7H_2O$) and iron (III) sulphate hydrate ($Fe_2(SO_4)_3 \cdot H_2O$) was prepared at acidic conditions (purchased from Alfa Aesar). The co-precipitation method has been used as a two step process. In the first step, iron hydroxides were precipitated in an alkaline medium during the reaction between the aqueous solution of metal salts and an aqueous solution of ammonium hydroxide. The corresponding metal hydroxides were precipitated during the reaction between the alkaline precipitating reagent and the mixture of metal salts and, subsequently, oxidized in air to form $\gamma - Fe_2O_3$ in the second step of the process. The temperature for this process was set constant at 25 °C for 1 h. After the reaction, nanoparticles were washed with diluted ammonia solution at pH 10 several times and 5 mg/mL of a solution of citric acid (purchased from Sigma-Aldrich) during stirring to prepare stable aqueous suspension. Particles were additionally coated with SiO_2 cover and functionalized with different groups. In order to stabilize the aqueous suspension of the magnetic nanoparticles, the particles were coated with a silica layer prepared by hydrolysis and polycondensation of tetraethyl orthosilicate (TEOS, purchased from Alfa Aesar) using alkaline medium. TEOS was added to the mixture by dropwise addition for 1 h and, after that, rigorously stirred for 3 h at room temperature. Using silica cover helps to prevent agglomeration, as well as provides an easily modifiable surface for creating different charges or groups on the surface of the nanoparticles. As shown in recent publications the cover is also biocompatible regarding cell viability studies [49]. Additional amino [NH_3^+] groups were added to their surface to create a positive charge using grafting with 3-(2-aminoethylamino) propylmethyldimethoxysilane (APMS, 97 %), purchased from Alfa Aesar. The similarly charged particles reduce the rate of aggregation, due to strong electrostatic repulsions, thereby ensuring increased stability. The nanoparticles were characterized for size and morphology using Transmission Electron Microscopy (TEM) model JEM 2100 at 200 kV from JEOL. The size of the synthesized $\gamma - Fe_2O_3$ nanoparticles was found to be 10 ± 2 nm, observed by TEM analysis, as shown in Figure 7.

The negatively charged cobalt ferrite nanoparticles were synthesized by co-precipitating the stoichiometric mixtures of $Fe(NO_3)_6 \cdot 9H_2O$ and $Co(NO_3)_2 \cdot 6H_2O$ in aqueous solutions. The pH was maintained between 9.5–11 using 10 % NaOH solution, and the temperature was set between 70–95 °C for 4–5 h under vigorous magnetic agitation. The resulting mixture was then centrifuged for fifteen minutes at 3,000 rpm. The supernatant was then decanted and centrifuged rapidly, until a thick black precipitate was obtained. The precipitate was then washed thoroughly with water and acetone for purification and dried overnight at 100 °C in hot air oven. The dried samples were then dispersed in double distilled water. The cobalt ferrite NPs were coated with citric acid to impart a negative charge to their surface. The size of $CoFe_2O_4$ NPs was found to be in the range of 10–15 nm by TEM, and the zeta potential value was estimated to be ± 34 mV using DLS.

Figure 7. TEM image of superparamagnetic maghemite nanoparticles ($\gamma - Fe_2O_3$), covered with 20 nm thick silica.

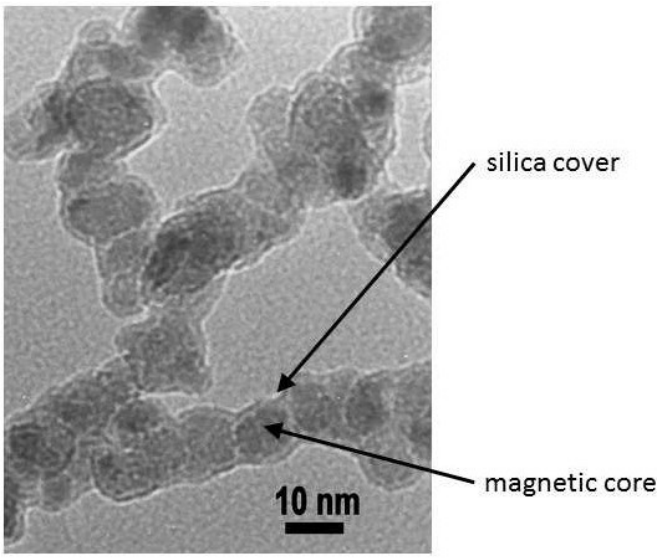

4.2. Preparation of Liposome—Nanoparticle Conjugates

Small unilamellar vesicles were prepared by the thin film method. 1 mg of the SOPC lipid was dissolved in 1 ml of chloroform and transferred into a round-bottomed flask. The solvent from the lipid samples was evaporated using a Rotavapor under reduced pressure (1.7 kPa). The dried lipid films were then hydrated with the aqueous iron oxide and cobalt ferrite nanoparticle solutions dispersed in distilled water with the concentration of 1 mg/mL. The final concentration of the lipids was made up to 1 mg/mL. Multilamellar vesicles (MLV) were prepared in our lab by vortexing the lipid suspensions vigorously with glass beads for 10 min. The MLV were further transformed into small unilamellar vesicles (SUV) by sonication for 30 min with 10 s on-off cycles at 50 % amplitude with a Vibracell Ultrasonic Disintegrator VCX 750 (Sonics and Materials, Newtown, CT, USA). To separate the debris from SUV after sonication, the sample was centrifuged for 10 min at 14,000 rpm (Eppendorf Centrifuge 5415C). The control lipid vesicles were prepared in a similar way by dissolving 1 mg of the SOPC lipid in 1 ml of chloroform to form a thin lipid film and the film was hydrated with 1 ml of 20 mM HEPES buffer instead of the nanoparticle solution.

4.3. Fluorescence Anisotropy Measurements: Anisotropy and Fluidity

Depending upon the surface charge of the liposomes and the charge of the nanoparticle, the degree of membrane fluidity is altered. The effect of charged nanoparticles in altering the bilayer fluidity of the liposomes can be studied using fluorescent anisotropy probes, such as DPH (diphenyl hexatriene) [50]. The fluorescent dye, DPH, is one of the widely used fluorescent probes to measure the fluidity in native

membranes, as well as in artificial membranes and was also used in this work. DPH is a rod-like hydrophobic molecule, which incorporates itself between the fatty acid tails in the core of the lipid bilayer [51]. The optical properties of the DPH largely depends on its environment; it is non-fluorescent in aqueous solutions, whereas after binding to the hydrophobic regions of the bilayer, it shows an intense fluorescence signal [11,52]. A unique feature of the DPH is that its rotational motion and emission intensities are largely dependent on the lipid ordering, and hence, its anisotropy results correlate well with the packing order of the lipids in the bilayer and their fluidity.

In this work, the temperature-dependent fluorescence anisotropy measurements of DPH in control liposomes and liposome-nanoparticle conjugates of zwitterionic SOPC and negatively charged SOPC-POPS liposomes were performed in a 10 mm-path-length cuvette using a Cary Eclipse fluorescence spectrophotometer (Varian, Mulgrave, Australia). The anisotropy values were measured within the temperature range from 15 °C to 50 °C by increasing the temperature 5 °C for every measurement with a time interval of 7 min, with constant mixing at pH 7.0. Varian autopolarizers were used, with slit widths, with a nominal band-pass of 5 nm for both excitation and emission. Ten liters of DPH was added to 2.5 mL of 100 μM solutions of SUV to reach a final concentration of 0.5 μM. DPH fluorescence anisotropy was measured at the excitation wavelength of 358 nm, with the excitation polarizer oriented in the vertical position, while the vertical and horizontal components of the polarized emission light were recorded through a monochromator at 410 nm for both probes. The emission fluorescence of DPH in aqueous solution is negligible. The anisotropy, <r>, was calculated using the built-in software of the instrument using the below formula:

$$< r >= \frac{I_{\parallel} - I_{\perp}}{I_{\parallel} + 2I_{\perp}} \tag{13}$$

where, $I_{\parallel}$ and $I_{\perp}$ represent the parallel and perpendicular fluorescence emission intensities, respectively.

The values of the G-factor (the ratio of the sensitivities of the detection system for vertically (I_{HV}) and horizontally polarized light (I_{HH})) were determined for each sample separately. The lipid-order parameter, S, was calculated from the anisotropy value using the following analytical expression [53]:

$$S = \frac{1 - 2\left(\frac{r}{r_0}\right) + 5\left(\frac{r}{r_0}\right)^{2\,\frac{1}{2}} - 1 + \left(\frac{r}{r_0}\right)}{2\left(\frac{r}{r_0}\right)} \tag{14}$$

where r_0 is the fluorescence anisotropy of DPH in the absence of any rotational motion of the probe. The theoretical value of r_0 of DPH is 0.4, while the experimental values of r_0 lie between 0.362 and 0.394 [53].

4.4. Influence of Nanoparticle-Membrane Interactions on Membrane Fluidity

Small unilamellar zwitterionic vesicles were prepared to measure the bilayer fluidity in the presence of positively and negatively charged nanoparticles (NPs). The fluidity of the lipid bilayer membrane of small unilamellar vesicles was determined by measuring the fluorescence anisotropy, which is directly proportional to the lipid ordering in the membrane and inversely proportional to the membrane fluidity. As the membrane becomes more fluid, the mobility of the dye incorporated into the bilayer also increases,

whereas the intensity of the fluorescence emission from the dye decreases. Increased anisotropy values indicate that the membrane fluidity is decreased and that the lipids are in a more ordered (liquid) phase. On the other hand, decreased anisotropy values denote increased membrane fluidity, meaning that the bilayer lipids are in a less ordered (liquid) phase (see [54,55]). A decrease in the anisotropy values may also indicate that the dye is incorporated in the liquid state of the bilayer [56].

Figure 8 shows the fluorescence anisotropy measurements of positively and negatively charged NPs in liposomes prepared with the zwitterionic (neutral) lipid (SOPC) surface of liposomes. The anisotropy values are gradually reduced with the temperature in all the cases. The fluidity of zwitterionic SOPC lipid bilayer is increased in the presence of negatively charged NPs, while it is similar to the control in the presence of positively charged nanoparticles (Figure 8). This result coincides well with the theoretically predicted decrease of average lipid dipolar headgroup orientation angle, $< \omega >$, in the vicinity of a negatively charged particle (Figure 5, right panel), leading to increased rotational mobility of the lipids, *i.e.*, increased fluidity, as shown in Figure 8. The influence of negatively charged nanoparticles on the average orientation angle, $< \omega >$, is possible, due to the attraction between negatively charged nanoparticles and the zwitterionic lipid surface, as presented in Figure 6 (right panel).

On the contrary, the fluidity of the zwitterionic lipid bilayer remains nearly intact in the presence of positively charged nanoparticles (*i.e.*, practically the same as the control values without the nanoparticle), due repulsion between positive nanoparticles and the zwitterionic lipid surface, as shown in the Figure 6 (left panel). The electrostatic repulsion between the zwitterionic surface and positively charged nanoparticles diminishes the probability of the close approach of the nanoparticles to the lipid bilayer surface, and consequently, the average lipid headgroup orientation angle, $< \omega >$, is not changed.

Figure 8. Temperature-dependent fluorescence anisotropy measurement of zwitterionic SOPC bilayer membranes in the presence of negatively or positively charged nanoparticles (NPs). The control curve corresponds to the absence of the nanoparticles.

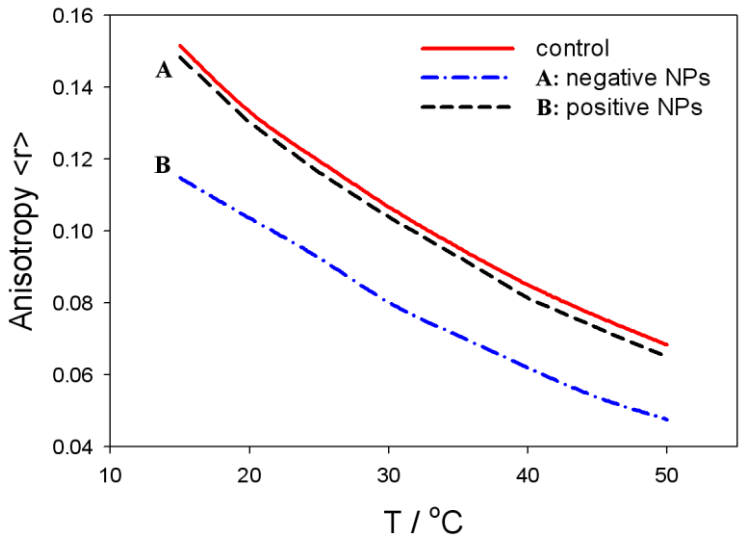

5. Conclusions

Electrostatic interactions play an important role in determining the efficiency of NP interaction with the lipid bilayer membrane. If attractive electrostatic forces exist between the liposome/cell membrane and the NP surface, a greater amount of NPs will be adsorbed to the membrane, leading to enhanced encapsulation [57,58]. This, in turn, will have a significant effect on the biophysical properties of the membrane. On the other hand, if electrostatic repulsions occur between the liposome/membrane surface and the NPs, a much lesser quantity of NPs will be encapsulated in the liposomes or enter into the cells. When some charged proteins or NPs are adsorbed onto the biological cell surface, the membrane undergoes deformation, and lipids in the constituent bilayers will be reorganized, due to electrostatic interaction between the lipids and NPs/proteins [59–61]. As the cell membrane is negatively charged, positively charged NPs are attracted more towards the surface of the membrane (Figure 3) and show higher levels of internalization when compared to the neutral (zwitterionic) and negatively charged particles [3,62].

The temperature changes induce the phase transition of the membrane lipids [63]. As a result, the NPs, which are incorporated between the fatty acid tails in the membrane, will start to move and vibrate rapidly throughout the bilayer. This dynamic motion of NPs fastens the phase transition of the membrane lipids by reducing the melting temperature and increases the bilayer fluidity. Bothun *et al*. reported that increasing the concentration of silver NPs increases the fluidity of the zwitterionic lipid bilayer membrane. The presence of NPs in the bilayer reduces the pre-transition and melting temperature of the membrane lipids through bilayer disruption [64].

In this paper, we presented within the modified MLPB model an analytical expression for the osmotic pressure between two planar charged surfaces mediated by ions and the ordering of water dipoles. It is shown that in close vicinity to the positively and negatively charged nanoparticles, the average orientation of the lipid headgroups (described by the angle, $< \omega >$) is changed, due to electrostatic repulsion/attraction between the positively/negatively nanoparticle and the positively charged trimethylammonium groups of the zwitterionic lipid headgroups, *i.e.*, the lipid headgroups that are in close vicinity to the positively/negatively charged nanoparticle are less/more extended in the direction perpendicular to the membrane surface (Figure 5). It can be further seen in Figures 5 and 6 that the distance between the lipid layer and the nanoparticle (H), where the lipid headgroups begin to change their average orientation (Figure 5), coincides well with the distance, H, where the osmotic pressure between the lipid monolayer (bilayer) starts to grow/decrease (Figure 6).

The presented theoretical predictions of the influence of charged nanoparticles on the average orientation of the lipid headgroups agree well with the measured fluidity of the zwitterionic lipid bilayer in the presence of positively or negatively charged nanoparticles, as presented in Figure 8. The enhanced interactions between the nanoparticles and zwitterionic liposomes increases the membrane fluidity (Figure 8), which is connected to considerable variation in the lipid ordering [65]. On the other hand, electrostatic repulsions between nanoparticle and the zwitterionic liposome/cell surface leads to much less interaction of the nanoparticles with the membrane lipids, and hence, membrane fluidity is not affected to a considerable extent, as indicated in Figure 8.

Acknowledgments

This work was in part supported by the Slovenian Research Agency (ARRS). A.V. was also supported by the European Social Fund and SMARTEH. E.G. and P.B.S. were partially supported by the grant from the Slovenian Human Resources Development and Scholarship Fund.

Conflict of Interest

The authors declare no conflict of interest.

Appendix

A. Derivation of Osmotic Pressure by Integration of the MLPB Equation

In this Appendix, the expression for osmotic pressure (Equation (4)) between the charged surfaces (as schematically presented in Figure 2) is derived. Using the method of the integration of the Poisson equation to get the osmotic pressure in between the two charged surfaces (see, for example, [32,46,66]), the MLPB Equation (2) will be first integrated, and then, in the second step, the corresponding bulk value of the pressure will be subtracted from the local pressure to get the osmotic pressure, Π. The modified MLPB Equation (2) can be rewritten as (see, also, [30]):

$$-\frac{d}{dx}\left[\varepsilon_0 n^2 \frac{d\varphi}{dx}\right] + 2 e_0 n_0 \sinh e_0\varphi\beta - n_{0w} p_0 \left(\frac{2+n^2}{3}\right) \frac{d}{dx} L(\gamma p_0 E\beta) = 0 \quad (15)$$

where Equation (1) was taken into account and $E(x)$ is the magnitude of electric field strength, as before. Equation (15) is multiplied by $\varphi' \equiv d\phi/dx$ and integrated to get the first integral equivalent to the contact theorem:

$$\frac{1}{2}\varepsilon_0 n^2 E(x)^2 + 2 n_0 kT \left(\cosh(-e_0\phi(x)\beta)\right) - \quad (16)$$
$$-E(x)\left(\frac{2+n^2}{3}\right) n_{0w} p_0 L(\gamma p_0 E(x)\beta) + \left(\frac{2+n^2}{3}\right)\frac{n_{0w}}{\gamma\beta}\ln\left(\frac{\sinh(\gamma p_0 E(x)\beta)}{\gamma p_0 E(x)\beta}\right) = \text{const.}$$

where const is osmotic pressure. In the derivation of Equation (16), we used the relations:

$$\phi'' \phi' dx = \frac{1}{2} d(\phi')^2 = \frac{1}{2}(\phi')^2 , \qquad \frac{dL}{dx}\phi' dx = L\phi' - L d\phi'$$

where $\phi'' \equiv d^2\phi/dx^2$ and $d\phi = \phi' dx$. By subtracting the corresponding bulk values from the local pressure, we obtain the expression for the osmotic pressure difference, $\Pi = P_{inner} - P_{bulk}$:

$$\Pi = -\frac{1}{2}\varepsilon_0 n^2 E(x)^2 + 2 n_0 kT \left(\cosh(-e_0\phi(x)\beta) - 1\right) - \quad (17)$$
$$- E(x)\left(\frac{2+n^2}{3}\right) n_{0w} p_0 L(\gamma p_0 E(x)\beta) + \left(\frac{2+n^2}{3}\right)\frac{n_{0w}}{\gamma\beta}\ln\left(\frac{\sinh(\gamma p_0 E(x)\beta)}{\gamma p_0 E(x)\beta}\right)$$

References

1. Sackmann, E. Biological Membranes Architecture and Function. In *Structure and Dynamics of Membranes*; Lipowsky, R., Sackmann, E., Eds.; Elsevier: Amsterdam, The Netherlands, 1995; pp. 1–63.
2. Rappolt, M.; Pabst, G. Flexibility and Struture of Fluid Bilyer Interfaces. In *Structure and Dynamics of Membranous Interfaces*; Nag, K., Ed.; John Wiley and Sons, Inc.: Hoboken, NJ, USA, 2008; pp. 45–81.
3. Yaghmur, A.; Rappolt, M. Structural characterization of lipidic systems under nonequilibrium conditions. *Eur. Biophys. J.* 2012, *41*, 831–840.
4. Tien, H.T.; Ottova-Leitmannova, A. The Lipid Bilayer Concept: Experimental Realization and Current Application. In *Planar Lipid Bilayers (BLMs) And Their Application*; Tien, H.T., Ottova-Leitmannova, A., Eds.; Elsevier: Amsterdam, The Netherlands, 2003; pp. 1–73.
5. Luckey, M. *Membrane Structural Biology*, 1st ed.; Cambridge University Press: New York, NY, USA, 2008; pp. 1–67.
6. Bagatolli, L.A.; Ipsen, J.H.; Simonsen, A.C.; Mouritsen, O.G. An outlook on organization of lipids in membranes: Searching for a realistic connection with the organization of biological membranes. *Prog. Lip. Res.* 2010, *49*, 378–389.
7. Rappolt, M.; Laggner, P.; Pabst, G. Structure and elasticity of phospholipid bilayers in the Lalpha phase: A comparison of phosphatidylcholine and phosphatidylethanolamine membranes. In *Recent Research Developments in Biophysics, Part II*; Pandalai, S.G., Ed.; Trivandrum - Transworld Research Network: Kerala, India, 2004; Volume 3, pp. 363–392.
8. Cevc, G. *Phospholipid Handbook*, 1st ed.; Marcel Dekker: New York, NY, USA, 1993.
9. Bivas, I. Electrostatic and mechanical properties of a flat lipid bilayer containing ionic lipids. *Coll. Surf. A* 2006, *282–283*, 423–434.
10. Boulbitch, A.A. Deflection of a cell membrane under application of a local force. *Phys. Rev. E* 1998, *75*, 2123–2128.
11. Kulkarni, C.V. Lipid crystallization: From self-assembly to hierarchical and biological ordering. *Nanoscale* 2012, *4*, 5779–5791.
12. Hianik, T.; Passechnik, V.I. *Bilayer Lipid Membranes: Structure and Mechanical Properties*; Kluwer Academic Publishers: London, UK, 1995.
13. McLaughlin, S. The Electrostatic properties of membranes. *Ann. Rev. Biophys. Chem.* 1989, *18*, 113–136.
14. Cevc, G. Memrane electrostatics. *Biochim. Biophys. Acta* 1990, *1031*, 311–382.
15. Šuštar, V.; Bedina Zavec, A.; Štukelj, R.; Frank, M.; Bobojevič, G.; Janša, R.; Ogorevc, E.; Kruljc, P.; Mam, K.; Šimunič, B.; *et al*. Nanoparticles isolated from blood: A reflection of vesiculability of blood cells during the isolation process. *Int. J. Nanomed.* 2011, *6*, 2737–2748.
16. Kralj-Iglič, V. Stability of membranous nanostructures: A possible key mechanism in cancer progression. *Int. J. Nanomed.* 2012, *7*, 3579–3596.
17. Shlomovitz, R.; Gov, N.S. Pysical model of contractile ring initiation in dividing cells. *Biophys. J.* 2008, *94*, 1155–1168.

18. Gouy, M.G. Sur la constitution de la charge electrique a la surface d'un electrolyte. *J. Phys.* 1910, *9*, 457–468.
19. Chapman, D.L. A Contribution to the theory of electrocapillarity. *Philos. Mag.* 1913, *25*, 475–481.
20. Kralj-Iglič, V.; Iglič, A. A simple statistical mechanical approach to the free energy of the electric double layer including the excluded volume effect. *J. Phys. II* 1996, *6*, 477–491.
21. Lamperski, S.; Outhwaite, C.W. Exclusion volume term in the inhomogeneous poisson-boltzmann theory for high surface charge. *Langmuir* 2002, *18*, 3423–3424.
22. Butt, H.J.; Graf, K.; Kappl, M. *Physics and Chemistry of Interfaces*, 2nd ed.; Wiley-VCH Verlag: Weinheim, Germany, 2003.
23. Bazant, M.Z.; Kilic, M.S.; Storey, B.; Ajdari, A. Towards an understanding of induced-charge electrokinetics at large applied voltages in concentrated solution. *Adv. Colloid Interface Sci.* 2009, *152*, 48–88.
24. Gongadze, E.; Van Rienen, U.; Iglič, A. Generalized Stern models of an electric double layer considering the spatial variation of permittivity and finite size of ions in saturation regime. *Cell. Mol. Biol. Lett.* 2011, *16*, 576–594.
25. Gongadze, E.; Van Rienen, U.; Kralj-Iglič, V.; Iglič, A. Spatial variation of permittivity of an electrolyte solution in contact with a charged metal surface: A mini review. *Comput. Meth. Biomech. Biomed. Eng.* 2013, *16*, 463–480.
26. Velikonja A.; Perutkova Š.; Gongadze E.; Kramar P.; Polak A.; Maček-Lebar A.; Iglič A. Monovalent ions and water dipoles in contact with dipolar zwitterionic lipid headroups theory and MD simulations. *Int. J. Mol. Sci.* 2013, *14*, 2846–2861.
27. Outhwaite, C.W. A treatment of solvent effects in the potential theory of electrolyte solutions. *Mol. Phys.* 1976, *31*, 1345–1357.
28. Outhwaite, C.W. Towards a mean electrostatic potential treatment of an ion-dipole mixture or a dipolar system next to a plane wall. *Mol. Phys.* 1983, *48*, 599–614.
29. Iglič, A.; Gongadze, E.; Bohinc, K. Excluded volume effect and orientational ordering near charged surface in solution of ions and Langevin dipoles. *Bioelectrochemistry* 2010, *79*, 223–227.
30. Gongadze, E.; Van Rienen, U.; Kralj-Iglič, V.; Iglič, A. Langevin Poisson-Boltzmannn equation: point-like ions and water dipoles near a charged surface. *Gen. Physiol. Biophys.* 2011, *30*, 130–137.
31. Gongadze, E.; Iglič, A. Decrease of permittivity of an electrolyte solution near a charged surface due to saturation and excluded volume effects. *Bioelectrochemistry* 2012, *87*, 199–203.
32. Misra, R.P.; Das, S.; Mitra S.K. Electric double layer force between charged surfaces: Effect of solvent polarization. *J. Chem. Phys.* 2013, *138*, 114703.
33. Torchilin, VP. Recent advances with liposomes as pharmaceutical carriers. *Nat. Rev. Drug Discov.* 2005, *4*, 145–160.
34. Bhandary, S.; Sultana, P.; Basu, R.; Das, S.; Nandy, P. A Study on the modulation of the phase behavior of lipid aggregates-effect of some metal nanoparticles, *Adv. Sci. Eng. Med.* 2011, *3*, 1–6.
35. Roiter, Y.; Ornatska, M.; Rammohan, A.R.; Balakrishnan, J.; Heine; D.R.; Minko S. Interaction of nanoparticles with lipid membrane. *Nano Lett.* 2008, *8*, 941–944.

36. Michel, R.; Gradzielski, M. Experimental aspect of colloidal interactions in mixed systems of liposome and inorganic nanoparticle and their applications. *Int. J. Mol. Sci.* 2013, *13*, 11610–11642.
37. Zimmerberg, J.; Kozlov, M.M. How proteins produce cellular curvature. *Nature Rew. Mol. Cell Biol.* 2006, *7*, 9–19.
38. Tian, A.; Baumgart, T. Sorting of lipids and proteins in membrane curvature gradients. *Biophys. J.* 2009, *96*, 2676–2688.
39. Iglič, A.; Slivnik, T.; Kralj-Iglič, V. Elastic properties of biological membranes influenced by attached proteins. *J. Biomech.* 2007, *40*, 2492–2500.
40. Powel, K. Ahead of the curve. *Nature* 2009, *460*, 318–320.
41. Bouma, B.; de Groot, P.G.; van den Elsen, J.M.H.; Ravelli, R.B.G.; Schouten, A.; Simmelink, J.A.; Derksen, M.J.A.; Kroon, J.; Gros, P. Adhesion mechanism of human β_2-glycoprotein I to phospholipids based on its crystal structure. *EMBO J.* 1999, *18*, 5166–5174.
42. Farsad, K.; De Camilli, P. Mechanisms of membrane deformation. *Curr. Opin. Cell Biol.* 2003, *15*, 372–381.
43. Sorre, B.; Callan-Jones, A.; Manneville, J.B.; Nassoy, P.; Joanny J.F.; Prost, J.; Goud, B.; Bassereau, P. Curvature-driven lipid sorting needs proximity to a demixing point and is aided by proteins. *PNAS* 2009, *106*, 5622–5626.
44. Fröhlich, H. *Theory of Dielectrics*, 1st ed.; Clarendon Press: Oxford, UK, 1964.
45. Booth, F. The dielectric constant of water and the saturation effect. *J. Chem. Phys.* 1951, *19*, 391–395.
46. Evans, D.F.; Wennerström H. *The Colloidal Domain*, 1st ed.; Wiley-VCH: New York, NY, USA, 1999; pp. 223–238.
47. Lee, A.G. How lipids affect the activities of integral membrane proteins. *Biochim. Biophys. Acta* 2004, *1666*, 62–87.
48. Casadei, M.A.; Manas, P.; Niven, G.; Needs, E.; Mackey; B.M. Role of membrane fluidity in pressure resistance of Escherichia coli NCTC 8164 Appl. *Environ. Microbiol.* 2002, *68*, 5965–5972.
49. Gandhi S.; Venkatesh S.; Sharma U.; Jagannathan N.R.; Sethuramana S.; Krishnan U.M. Superparamagnetic nanosystems based on iron oxide nanoparticles & mesoporous silica: Synthesis & evaluation of their magnetic, relaxometric and biocompatability properties. *J. Mater. Chem.* 2011, *21*, 15698.
50. Wanten, G.J.; Naber, A.H. Human neutrophil membrane fluidity after exposure to structurally different lipid emulsions. *JPEN J. Parenter. Enteral. Nutr.* 2001, *25*, 352–355.
51. Aricha, B.; Fishov, V; Cohen, V.; Sikron, N.; Pesakhov, S.; Khozin-Goldberg, I.; Dagan, R.; Porat N. Differences in membrane fluidity and fatty acid composition between phenotypic variants of streptococcus pneumoniae. *J. Bacteriol.* 2004, *186*, 4638–4644.
52. Gmajner, V.; Ota, A.; Šentjurc, M.; Poklar Ulrih, N. Stability of diether C25,25 liposomes from the hyperthermophilic archaeon Aeropyrum pernix K1. *Chem. Phys. Lipids* 2011, *164*, 236–245.

53. Pottel, H.; van der Meer, V.; Herreman, W. Correlation between the order parameter and the steady-state fluorescence anisotropy of 1,6-diphenyl-1,3,5-hexatriene and an evaluation of membrane fluidity. *Biochim. Biophys. Acta* 1983, *730*, 181–186.
54. Poklar Ulrih, N.; Gmajner, D.; Raspor, P. Structural and physicochemical properties of polar lipids from thermophilic archaea. *Appl. Microbiol. Biotechnol.* 2009, *84*, 249–260.
55. Marczak A. Fluorescence anisotropy of membrane fluidity probes in human erythrocytes incubated with anthracyclines and glutaraldehyde. *Bioelectrochemistry* 2009, *74*, 236–239.
56. Wrobel, D.; Kłys, A.; Ionov, M.; Vitovic, P.; Waczulikowa, I.; Hianik, T.; Gomez-Ramirez, R.; de la Mata, J.; Klajnert, B.; Bryszewska, M. Cationic carbosilane dendrimers-lipid membrane interactions. *Chem. Phys. Lipids* 2012, *165*, 401–407.
57. Michel, R.; Gradzielski, M. Experimental aspects of colloidal interactions in mixed systems of liposome and inorganic nanoparticle and their applications. *Int. J. Mol. Sci.* 2012, *13*, 11610–11642.
58. Eleršič, K; Pavlič, J.I.; Iglič, A.; Vesel, A; Mozetič, M. Electric-field controlled liposome formation with embedded superparamagnetic iron oxide nanoparticles. *Chem. Phys. Lipids* 2012, *165*, 120–124.
59. Hayden, S.C.; Zhao, G.; Saha, K.; Phillips, R.L.; Li, X.; Miranda, O.R.; Rotello, V.M.; El-Sayed, M.A.; Schmidt-Krey, I.; Bunz, U.H.F. Aggregation and interaction of cationic nanoparticles on bacterial surfaces. *J. Am. Chem. Soc.* 2012, *134*, 6920–6923.
60. Shlomovitz, R.; Gov, N.S. Membrane-mediated interactions drive the condensation and coalescence of FtsZ rings. *Phys. Biol.* 2009, *6*, 046017.
61. Kabaso, D.; Gongadze, E.; Elter, P.; van Rienen, U.; Gimsa, J.; Kralj-Iglič, V.; Iglič, A. Attachment of rod-like (BAR) proteins and membrane shape. *Mini Rev. Med. Chem.* 2011, *11*, 272–282.
62. Verma, A.; Stellacci, F. Effect of surface properties on nanoparticlecell interactions. *Small* 2010, *6*, 12–21.
63. Veksler, A.; Gov, N.S. Phase transitions of the coupled membrane-cytoskeleton modify cellular shape. *Biophys. J.* 2007, *93*, 3798–3810.
64. Bothun, G.D. Hydrophobic silver nanoparticles trapped in lipid bilayers: Size distribution, bilayer phase behavior, and optical properties. *J. Nanobiotechnol.* 2008, *6*, 13.
65. Alexandre, H.; Mathieu, B.; Charpentier, C. Alteration in membrane fluidity and lipid composition, and modulation of H+-ATPase activity in Saccharomyces cerevisiae caused by decanoic acid. *Microbiology* 1996, *142*, 469–475.
66. Abrashkin, A.; Andelman, D.; Orland, H. Dipolar Poisson-Boltzmannn equation: Ions and dipoles close to charge interfaces. *Phys. Rev. Lett.* 2007, *99*, 077801.

C Članek 3: Influence of nanoparticle-membrane electrostatic interactions on membrane fluidity and bending elasticity

Polno ime revije:	Chemistry and Physics of Lipids
Okrajšava:	Chem. Phys. Lipids
ISSN (tiskana izdaja):	0009-3084
Založnik:	Elsevier Science Ireland Ltd
Naslov založnika:	Elsevier Science Ireland Ltd, Limerick, Ireland
Pogostost izdaje:	mesečno
Medij:	tiskana izdaja
Spletna stran revije:	http://sciencedirect.com/science/journal/00093084
Prvo leto izdaje:	1966
Faktor vpliva:	2.147 (2012)
Faktor vpliva (5 let):	2.401 (2012)
Naslov članka:	Influence of nanoparticle-membrane electrostatic interactions on membrane fluidity and bending elasticity
Avtorji:	Santhosh, Poornima Budime; Velikonja, Aljaž; Perutkova, Šarka; Gongadze, Ekaterina; Kulkarni, Mukta; Genova, Julia; Eleršič, Kristina; Iglič, Aleš; Kralj-Iglič, Veronika; Poklar Ulrih, Nataša
Izdaja:	178
Številka:	-
Strani:	52–62
Leto objave:	2014
DOI:	10.1016/j.chemphyslip.2013.11.009

Chemistry and Physics of Lipids 178 (2014) 52–62

Contents lists available at ScienceDirect

Chemistry and Physics of Lipids

journal homepage: www.elsevier.com/locate/chemphyslip

Influence of nanoparticle–membrane electrostatic interactions on membrane fluidity and bending elasticity

Poornima Budime Santhosh [a], Aljaž Velikonja [b,c], Šarka Perutkova [d,e], Ekaterina Gongadze [d], Mukta Kulkarni [d], Julia Genova [f], Kristina Eleršič [g], Aleš Iglič [d], Veronika Kralj-Iglič [h], Nataša Poklar Ulrih [a,i,*]

[a] Department of Food Science and Technology, Biotechnical Faculty, University of Ljubljana, Jamnikarjeva 101, SI-1000 Ljubljana, Slovenia
[b] Laboratory of Biocybernetics, Faculty of Electrical Engineering, University of Ljubljana, Tržaska 25, SI-1000 Ljubljana, Slovenia
[c] SMARTEH Research and Development of Electronic Controlling and Regulating Systems, Trg Tigrovcev 1, SI-5220 Tolmin, Slovenia
[d] Laboratory of Biophysics, Faculty of Electrical Engineering, University of Ljubljana, Tržaska 25, SI-1000 Ljubljana, Slovenia
[e] Institute of Cell Biology, Faculty of Medicine, University of Ljubljana, Lipičeva 2, SI-1000 Ljubljana, Slovenia
[f] Institute of Solid State Physics, Bulgarian Academy of Sciences, 1784 Sofia, Bulgaria
[g] Jožef Stefan Institute, Jamova 39, SI-1000 Ljubljana, Slovenia
[h] Laboratory of Clinical Biophysics, Faculty of Health Sciences, University of Ljubljana, Vrazov trg 2, SI-1000 Ljubljana, Slovenia
[i] Centre of Excellence for Integrated Approaches in Chemistry and Biology of Proteins (CipKeBiP), Jamova 39, SI-1000 Ljubljana, Slovenia

article info

Article history:
Received 22 August 2013
Received in revised form
21 November 2013
Accepted 22 November 2013
Available online 2 December 2013

Keywords:
Nanoparticles
Liposomes
Membrane fluidity
Bending elasticity
Membrane electrostatics

abstract

The aim of this work is to investigate the effect of electrostatic interactions between the nanoparticles and the membrane lipids on altering the physical properties of the liposomal membrane such as fluidity and bending elasticity. For this purpose, we have used nanoparticles and lipids with different surface charges. Positively charged iron oxide (γ-Fe_2O_3) nanoparticles, neutral and negatively charged cobalt ferrite ($CoFe_2O_4$) nanoparticles were encapsulated in neutral lipid 1-stearoyl-2-oleoyl-sn-glycero-3-phosphocholine and negatively charged 1-palmitoyl-2-oleoyl-sn-glycero-3-phospho-L-serine lipid mixture. Membrane fluidity was assessed through the anisotropy measurements using the fluorescent probe 1,6-diphenyl-1,3,5-hexatriene. Though the interaction of both the types of nanoparticles reduced the membrane fluidity, the results were more pronounced in the negatively charged liposomes encapsulated with positively charged iron oxide nanoparticles due to strong electrostatic attractions. X-ray photoelectron spectroscopy results also confirmed the presence of significant quantity of positively charged iron oxide nanoparticles in negatively charged liposomes. Through thermally induced shape fluctuation measurements of the giant liposomes, a considerable reduction in the bending elasticity modulus was observed for cobalt ferrite nanoparticles. The experimental results were supported by the simulation studies using modified Langevin–Poisson–Boltzmann model.

1. Introduction

Liposomes with the potential to encapsulate the nanoparticles (NPs) find extensive applications in biomedical and pharmaceutical fields due to their ability to carry huge payload, improved stability, targeted delivery of the encapsulated material and to minimize the NPs toxicity (Torchilin, 2005; Uhumwangho and Okorr, 2005). For instance, liposomes encapsulated with ultrasmall superparamagnetic iron oxide NPs are gaining popularity in magnetic resonance imaging of cancer cells, diagnosis as well as treatment (Weinstein et al., 2010; Laurent and Mahmoudi, 2011). Since the NPs usage for in vivo applications are gradually increasing, it is crucial to investigate the various modes of NPs interaction with the bilayer lipids. Depending on the NPs concentration, their interaction with the bilayer lipids may alter the membrane properties and their functions (Albanese et al., 2012).

High density encapsulation of NPs in the liposomes is preferred in many clinical applications such as drug delivery and hyperthermia to achieve better results. Electrostatic interactions based on the surface charge of the liposomes and NPs plays an important role in determining the efficiency of NPs encapsulation in liposomes (Sipai Altaf Bhai et al., 2012). The surface charge of the liposomes can be altered by varying the lipid composition, pH and the external environment during liposome preparation. When charged lipids are used to prepare liposomes, they are more stable due to electrostatic repulsions which can prevent the aggregation and fusion of

* Corresponding author at: Department of Food Science and Technology, Biotechnical Faculty, University of Ljubljana, Jamnikarjeva 101, SI-1000 Ljubljana, Slovenia. Tel.: +386 13203780.
E-mail address: natasa.poklar@bf.uni-lj.si (N.P. Ulrih).

0009-3084/$ – see front matter © 2013 Elsevier Ireland Ltd. All rights reserved.
http://dx.doi.org/10.1016/j.chemphyslip.2013.11.009

neighbouring vesicles (Sybachin et al., 2012). Frokjaer et al. (1982) has demonstrated increased stability of phosphatidylcholine liposomes by decreasing the ionic strength and increasing the surface charge. The surface charge of the NPs can be modified by changing the functional groups attached to the NPs surface or by changing the coating material (Jiang et al., 2009). The NPs are coated with different materials such as polyethylene glycol, citric acid and dextran to increase their stability. The nature of the coating material greatly influences the zeta potential value of NPs. High zeta potential values of the NPs are a key factor to stabilize them in suspensions and to reduce their cytotoxicity (Wu et al., 2008).

To study the effect of surface charges and electrostatic interactions in detail, we have used a neutral lipid 1-stearoyl-2-oleoyl-sn-glycero-3-phosphocholine (SOPC) and its mixture with negatively charged 1-palmitoyl-2-oleoyl-sn-glycero-3-phospho-L-serine (POPS) to prepare the liposomes. Similarly we have used NPs with varying surface charges by adding different functional groups to their surface. Neutral and negatively charged $CoFe_2O_4$ NPs and positively charged γ-Fe_2O_3 NPs were encapsulated in both the type of liposomes. We have chosen magnetic NPs such as iron oxide and cobalt ferrite NPs for our work as they have vast expanding applications such as magnetofection, cell labeling, immunoassays and cancer therapy (Akbarzadeh et al., 2012). By the application of an external magnetic field, they can be easily manipulated to reach the target region for diagnosis, drug delivery and treatment (Santhosh and Ulrih, 2013).

The interaction of NPs with the phospholipid membrane affects the fluidity which can be studied through the anisotropy measurements using the fluorescent probes such as 1,6-diphenyl-1,3,5 hexatriene (DPH) (Hianik and Passechnik, 1995). Bilayer fluidity is related to the viscosity of the lipid membrane which is an important feature of the cell membrane. Increased fluidity enhances the free movement of phospholipid molecules and protein moieties in the membrane to facilitate various biological functions like ion transport, cell signaling and cell growth (Park et al., 2005). The fluidity of the bilayer/membrane can be affected by the membrane bound or encapsulated NPs (Roiter et al., 2008). Similarly the NPs adsorbed to the membrane surface or entrapped in the bilayer have a significant effect on the elastic properties of the membrane which is essential for the cell to perform the fundamental functions like adhesion, migration and interaction (Lai et al., 2013). Hence in order to better understand the influence of NPs in membranes, it is necessary to study the various effects of NPs interactions on cell membranes and model membranes.

Recent studies on the effects of NPs on membrane stability have revealed that the incorporation of metal NPs within the membrane alters the phase behavior of the lipids by decreasing the phase transition temperature and increasing the bilayer fluidity (Bhandary et al., 2011). Since the polymorphic phase behavior of lipids influence different membrane related processes, it has become important to study the effect of NPs interaction with different lipid membranes. Enormous research has been carried out with homogeneous bilayers consisting of zwitterionic phospholipids, but very less work has been done to understand the electrostatic attraction between the negatively charged lipid bilayers and differently charged NPs and its influence on the physical and chemical properties of membranes. Therefore the aim of our work is to study these interactions in detail through simulation studies and to establish a correlation between the theoretical calculations and the experimental results.

2. Materials and methods

SOPC and POPS lipids were purchased from Avanti Polar Lipids Inc., USA. DPH and HEPES [4-(2-Hydroxyethyl)piperazine-1-ethanesulfonic acid] were obtained from Sigma Aldrich Chemie GmbH, Steinheim, Germany. All the chemicals obtained have high purity (>99%) and used without any further purification. Negatively charged lipid vesicles were prepared by mixing SOPC and POPS lipids in the molar ratio of 4:1, respectively. Iron oxide and cobalt ferrite NPs were purchased from Nanotesla Institute, Ljubljana, Slovenia.

2.1. Synthesis of magnetic nanoparticles

Co-precipitation method was used to synthesize both the magnetic iron oxide and cobalt ferrite NPs. An aqueous mixture of ferric, ferrous salts and sodium hydroxide was prepared as an alkali stock solution (Wu et al., 2008; Mahnaz et al., 2013). The corresponding metal hydroxides were precipitated during the reaction between the alkaline precipitating reagent and the mixture of metal salts and subsequently oxidized in air to form γ-Fe_2O_3. The iron oxide NPs were coated with silica to ensure stability (Bumb et al., 2008) and attached with amino [NH_3^+] groups on their surface to impart positive charge. The dried iron oxide NPs were then dispersed in 20 mM HEPES buffer. The NPs were characterized using X-ray diffractometry and transmission electron microscopy (TEM) (see Fig. 2). The size of the synthesized γ-Fe_2O_3 NPs were found to be 10 ± 2 nm by TEM analysis and their zeta potential was found to be +40 mV using dynamic light scattering (DLS).

Aqueous $Fe(NO_3)_6 \cdot 9H_2O$ and $Co(NO_3)_2 \cdot 6H_2O$ solutions were mixed in stoichiometric ratios and served as precursors for the synthesis of cobalt ferrite NPs. To get the micelle solution, sodium dodecile sulfate was added and the resulting mixture was heated between 60 and 90 °C. To this mixture 10% NaOH solution was added to the mixture to set the pH between 9.5 and 11 and the synthesis temperature was maintained between 70 and 95 °C for about 4–5 h with continuous magnetic stirring. The mixture was centrifuged at a speed of 3000 rpm for 15 min. The supernatant was discarded and the remaining sample was centrifuged rapidly till a black precipitate was obtained. The precipitate was purified by washing thoroughly with water and acetone and dried in hot air oven at 100 °C for 2 h. The dried cobalt ferrite NPs were then dispersed in 20 mM HEPES buffer. To impart negative charge to their surface, the cobalt ferrite NPs were coated with citric acid. The size of the neutral and negatively charged cobalt ferrite NPs were found to be in the size range of 10–15 nm using TEM and their zeta potential values were found to be ±34 mV and −40 mV for neutral and negatively charged cobalt ferrite NPs respectively using DLS instrument.

2.2. Preparation of nanoparticles encapsulated liposomes

Small unilamellar vesicles in the size range of 30–50 nm, encapsulated with iron oxide and cobalt ferrite NPs were prepared using thin film method. The lipids SOPC and SOPC–POPS mixture were dissolved in sufficient quantity of chloroform and then transferred into round bottomed flasks (Bangham et al., 1967). The organic solvent was evaporated completely under reduced pressure (1.7 kPa) using rotavapor to form a thin lipid film. The thin film was hydrated with a suspension of positively charged iron oxide, neutral and negatively charged cobalt ferrite NPs (1 mg/ml) suspended in 20 mM HEPES buffer at pH 7.0. The lipid suspension was then vortexed vigorously with glass beads for 10 min to prepare multilamellar vesicles (MLVs) and sonicated using a vibracell ultrasonic disintegrator VCX 750 (Sonics and Materials, Newtown, USA) with 50% amplitude and 10 s on-off cycles for 30 min to obtain small unilamellar vesicles (SUVs). The sample was then centrifuged at a speed of 14,000 rpm for 10 min to separate the debris formed after sonication (Eppendorf Centrifuge 5415C). The control SUVs were also prepared in a similar method but instead of NP suspension they were diluted with 1 mL of 20 mM HEPES buffer.

2.3. Anisotropy measurements

Anisotropy was measured using the incorporation of the fluorescent dye DPH (Li et al., 2013; Repakova et al., 2005) in the control liposomes and liposomes with encapsulated NPs using the Cary Eclipse fluorescence spectrophotometer (Varian, Mulgrave, Australia). The sample was transferred into a 10 mm-path-length cuvette. 10 μL of DPH (Sigma–Aldrich Chemie GmbH, Steinheim, Germany) in dimethyl sulphoxide (MerckKGaA, Darmstadt, Germany) was added to 2.5 mL 100 μM solutions of SUVs prepared from SOPC and SOPC–POPS mixture to reach a final concentration of 0.5 μM DPH. The anisotropy measurements were performed within the temperature range from 15 °C to 50 °C by gradually increasing the temperature 5 °C for every measurement with a time interval of 7 min with constant mixing at pH 7.0. Varian autopolarizers having slit widths with a nominal band-pass of 5 nm was used for both the excitation and emission spectra. The fluorescent probe DPH was excited at 358 nm with the excitation polarizer oriented in the vertical position. The emitted polarized light in both vertical and horizontal planes were recorded by a monochromator and measured at 410 nm. The anisotropy (r) values were measured using the built-in software of the instrument by applying the below formula:

$$(r) = \frac{I_{\parallel} - GI_{\perp}}{I_{\parallel} + 2GI_{\perp}} \quad (1)$$

where, $I_{\parallel}$ and $I_{\perp}$ denotes the parallel and perpendicular fluorescence emission intensities. G is the correction factor for the scattered light and background fluorescence during fluorescence anisotropy measurements. The G-factor value for all the samples were determined individually by calculating the ratio of fluorescence intensities of vertically (I_{HV}) and horizontally polarized light (I_{HH}). From the anisotropy values, the lipid-order parameter S was calculated using the below formula (Pottel et al., 1983):

$$S = \frac{[1 - 2(r/r_0) + 5(r/r_0)^2]^{1/2} - 1 + r/r_0}{2(r/r_0)} \quad (2)$$

where r_0 denotes the fluorescence anisotropy measurements of DPH in the absence of any rotational motion of the probe. The theoretical value of r_0 of DPH is 0.4, and the experimental values of r_0 lie between the range of 0.362 and 0.394 (Pottel et al., 1983).

2.4. Preparation of giant unilamelar vesicles

The giant unilamellar liposomes were prepared with SOPC lipid through a modified electroformation technique (Angelova et al., 1992). 1 mg of the lipid was dissolved in 1 ml of chloroform and few drops of the resulting solution were placed on the surface of glass conductors coated with indium tin oxide (thickness of 100 ± 20 nm, sheet resistance of 100 □) which act as electrodes in the electroformation chamber. The glasses containing the lipid droplets were kept under high vaccum for 30 min to remove the chloroform completely. Once the dry lipid depots were formed, spacers were placed on the glass plates and filled with double distilled water. An alternative voltage of 1.5 V_{pp} and a low frequency of 10 Hz was applied to the conducting glass plates and kept overnight to form the giant vesicles.

2.5. Bending elasticity modulus

The analysis of thermally induced shape fluctuations of giant vesicles were used to study the influence of cobalt ferrite NPs on the bending elasticity of the membrane of giant neutral SOPC vesicles (Mitov et al., 1992). The giant vesicles were observed under a phase contrast microscope (Axiovert 100, Zeiss, Germany, oil immersion objective Ph3 100× magnification) to evaluate the fluctuations in the shape of the liposomes. The experimental equipment was improved by home-assembled stroboscopic illumination comprising an L6604 Xenon flash lamp, an E7289-01 external main discharge capacitor and a C6096 power supply, all from Hamamatsu, Japan. The images of the fluctuating GUVs were obtained with a C2400-60 camera (Hamamatsu, Japan) and the flash of the stroboscopic illumination was synchronized with the vertical pulses coming from the camera, with the light pulses lesser than 3–4 μs duration (full width at half maximum) at 2 J input energy. The data was recorded in the PC, analyzed with the AIS2 software (Genova and Mitov, 2013) and the bending elasticity modulus (k_c) values were measured by the thermal fluctuation method (Genova and Pavlic, 2012) as the weighted average value of about 7–8 vesicles. All of the experiments were performed in double distilled water environment.

2.6. X-ray photoelectron spectroscopy

The chemical composition of the control liposomes without NPs and liposomes encapsulated with the NPs were determined from the X-ray photoelectron spectroscopy (XPS) spectra. The samples were analyzed using the XPS instrument TFA XPS Physical Electronics. Since this analysis has to be carried out in high vacuum environment, a drop of the liposomes in buffer solution (10 μL) was placed onto a flat mica surface (110 Orientation) and dried completely. The dried sample was then placed in the XPS chamber and subsequently excited by the X-rays with a spot area over 400 μm^2 using a monochromatic Al $K_{1,2}$ radiation at 1486.6 eV, with the pressure about 60 μPa. The photoelectrons were identified with a hemispherical analyzer which was positioned at an angle of 45° with respect to the normal to the sample surface. The spectral energy resolution was found to be about 0.6 eV. The individual elemental composition of the sample was measured from the spectra using the MultiPak v7.3.1 built-in software of the instrument.

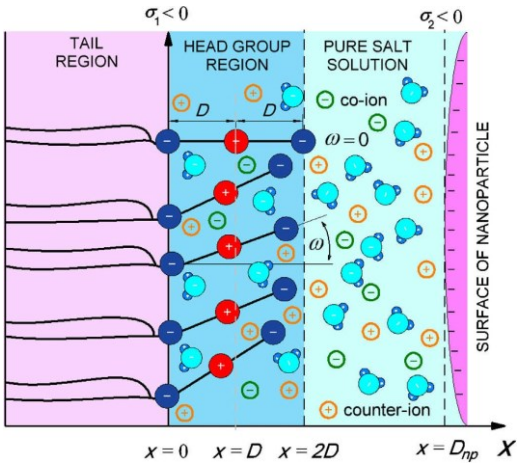

Fig. 1. Schematic presentation of the model to study the interaction between negatively charged POPS lipid and negatively charged NP suspended in salt solution. Negative charges at x = 0 are described as negative surface charge density a_1. D is the distance between opposite charges within the head region, a_2 is the surface charge density of charged NP, while ω describes the orientation angle of the single head group.

2.7. Analysis of encapsulation efficiency

The encapsulation efficiency (EE%) of NPs in the liposomes represents the percentage of NPs encapsulated into a liposome (Huang et al., 2005). The EE% value was calculated by measuring the ratio of the NPs concentration in the liposomes before and after the purification process. After sonication, the unbound $CoFe_2O_4$ and Fe_2O_3 NPs in the suspension were removed by centrifugation for 10 min at 12,000 ×g to obtain pure SUVs encapsulated with NPs. The obtained SUVs were treated with methanol (1:10, v/v) and sonicated for 10 min to release the encapsulated NPs into the suspension. The concentration of the released NPs can be determined by using the UV-visible spectrophotometer at 300 nm. The encapsulation efficiency was determined using the following equation:

$$\text{Encapsulation efficiency}(\%) = \left(1 - \frac{\text{Amount of NPs in the encapsulated liposome}}{\text{Total amount of the NPs added during liposome preparation}}\right) \times 100. \quad (3)$$

2.8. Theoretical model

Contact of zwitterionic lipid layer with salt solution containing NPs was theoretically described using modified Langevin–Poisson–Boltzmann (MLPB) model (Velikonja and Perutkova, 2013; Gongadze et al., 2011a). MLPB model takes into account the cavity field in saturation regime, electronic polarization of water dipoles (Gongadze et al., 2011a,b; Gongadze and Iglič, 2012; Fröhlich, 1964) and the finite volumes of lipid head groups (Velikonja and Perutkova, 2013). The finite volume effect of other particles was not taken into account. The corresponding Poisson equation can be written as:

$$\frac{d}{dx}\left(\varepsilon_0 \varepsilon_r(x)\frac{d\phi(x)}{dx}\right) = 2e n_0 \sinh(e\phi(x)\breve{}) - \frac{e_0 P(x)}{Da_0} + \frac{e_0 P(x)}{2Da_0}, \quad (4)$$

where $\phi(x)$ is the electric potential, ε_0 is permittivity of vacuum, $a_r(x)$ is relative permittivity of salt solution, e_0 is elementary charge, n_0 is bulk concentration of salt, $\breve{} = 1/kT$, kT is the thermal energy, $P(x)$ is the probability density function for angle ω (see Fig. 1), D is the distance between opposite charges in dipolar lipid head group and a_0 is the area per lipid molecule.

The boundary conditions are:

$$\frac{d\phi}{dx}(x = 0) = -\frac{a_1}{\varepsilon_0 \varepsilon_r(x = 0)}, \quad (5)$$

$$\frac{d\phi}{dx}(x = D_{np}) = \frac{a_2}{\varepsilon_0 \varepsilon_r(x = D_{np})}, \quad (6)$$

$$\phi(x = 2D_-) = \phi(x = 2D_+), \quad (7)$$

$$\frac{d\phi}{dx}(x = 2D_-) = \frac{d\phi}{dx}(x = 2D_+), \quad (8)$$

where in Eq. (5) the surface charge density at $x = 0$ is a_1, while in Eq. (6) the surface charge density at $x = D_{np}$ is a_2 corresponding to the surface charge density of NP (see also Fig. 1).

Eq. (4) was solved using standard implemented function for multi-boundary value problems (bvp4c) in Matlab2012b where the values $a_r(x)$ and $P(x)$ were calculated in iteration process outside of bvp4c function. The $\varepsilon_r(x)$ within MLPB model is (Velikonja and Perutkova, 2013; Gongadze et al., 2011a):

$$\varepsilon_r(x) = n^2 + \frac{n_{0w} p_0}{\varepsilon_0}\left(\frac{2 + n^2}{3}\right)\left(\frac{L(y p_0 E(x)\breve{})}{E(x)}\right), \quad (9)$$

where n is reffractive index of water, n_{0w} is concentration of water, p_0 is the dipole moment of water, $L(u) = (\coth(u) - 1/u)$ is Langevin function, $y = (3/2)((2 + n^2)/3)$ and $E(x) = |\phi(x)'|$ is the magnitude of the electric field, while the probability density function $P(x)$ also takes into account the finite volumes of lipid headgroups and can be written as (Velikonja and Perutkova, 2013):

$$P(x) = A\left(\frac{\lambda \exp(-e_0\phi(x)\breve{})}{(\exp(-e_0\phi(x)\breve{}) + 1)}\right), \quad (10)$$

where λ is ratio between charged lipid head groups in the salt solution and all particles inside the head group region (see Fig. 1) and the value lambda (A) is calculated iteratively until the normalization condition is met (Fig. 2):

$$\frac{1}{D}\int_0^D P(x)dx = 1. \quad (11)$$

3. Results and discussion

3.1. Bilayer fluidity

The influence of surface charge of the NPs and lipids ordering parameter and on bilayer fluidity of the liposomes was studied by the incorporation of fluorescent probe DPH into the liposomal bilayer and measuring the steady state fluorescent anisotropy values (Aricha et al., 2004; Kulkarni, 2012). The fluorescent probe DPH, as well as its derivatives are widely used to study the membrane properties such as polarity, fluidity and lipid ordering in the

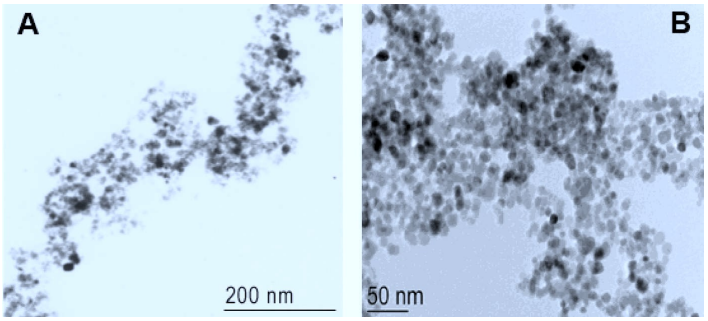

Fig. 2. TEM image of (A) neutral cobalt ferrite NPs and (B) iron oxide NPs.

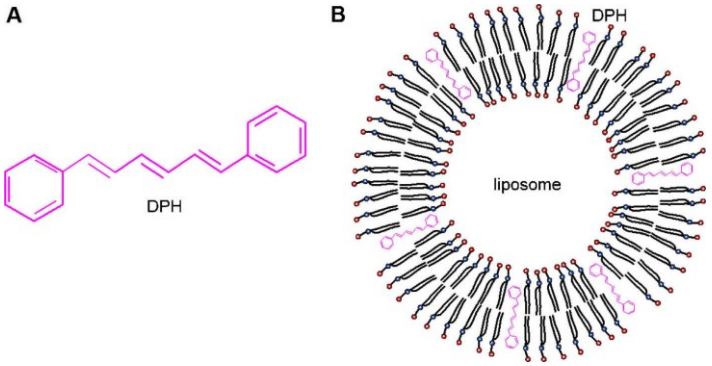

Fig. 3. (A) Structure of DPH molecule. (B) Schematic diagram illustrating the proposed incorporation of DPH in liposomes.

cell membranes as well as in liposomes (Perez-Berna et al., 2008; Spelios and Savva, 2008). The incorporation of DPH between the fatty acid tails in the bilayer is shown in Fig. 3. A notable feature of DPH is their ability to change their fluorescent properties depending on the environment. The dye is non-fluorescent in polar environment but after incorporating into the non-polar region of the bilayer, they emit strong fluorescence signals (Gmajner et al., 2011). They orient at various locations in the apolar tail region of the membrane and hence useful to study the entire organization and dynamics of the cell membranes as well as liposomes. The fluorescent anisotropy values of DPH correlate well with the rotational diffusion movement of the probe distributed throughout the bilayer and hence they are very sensitive in determining the packing order of the lipid chains and the membrane fluidity.

To study the effect of different NPs concentration and surface charge on the fluorescence anisotropy, positively charged Fe_2O_3 NPs, neutral and negatively charged $CoFe_2O_4$ NPs of varying concentrations such as 0.5, 1.0, 2.0, 3.0 and 5.0 mg were encapsulated in liposomes prepared with 1 mL of SOPC and SOPC–POPS lipids. The anisotropy values decreased gradually with decreasing NPs concentration in both the type of liposomes but the values decreased significantly in SOPC–POPS liposomes encapsulated with positively charged Fe_2O_3 NPs (data not shown). The result could be due to the strong electrostatic attractions between the oppositely charged surfaces leading to enhanced NPs encapsulation and the consequent disturbances in lipid ordering.

Anisotropy measurements are directly proportional to the ordering of membrane lipids and inversely proportional to the membrane fluidity; therefore reduced anisotropy values indicate increased membrane fluidity (Ulrih et al., 2009; Wrobel et al., 2012). The temperature changes induces the phase transition of the membrane lipids (Veksler and Gov, 2009). When the temperature increases, there is a transition from the rigid gel phase of the membrane lipids to the liquid phase. In such a phase, the mobility of the NPs in the membrane increases rapidly which disturbs the lipid ordering, induces the phase transition leading to decreased anisotropy values and increased membrane fluidity (Rappolt and Pabst, 2008).

The lipid-order parameter of neutral, positive and negatively charged NPs in the liposomes prepared with neutral lipid (SOPC) and negatively charged lipid (SOPC–POPS) mixture were shown in Fig. 4. The initial anisotropy and the corresponding order parameter values of DPH at 15 ° C in case of SOPC liposomes were: 0.152 and 0.475 for control liposomes without NPs; 0.135 and 0.420 for neutral $CoFe_2O_4$ encapsulated liposome; and 0.116 and 0.357 for negatively charged $CoFe_2O_4$ encapsulated liposomes; and 0.150 and 0.468 for positively charged Fe_2O_3 incorporated liposomes. In SOPC–POPS mixtures the anisotropy values and corresponding order parameter values at 15 ° C were: 0.136 and 0.423, 0.126 and 0.390, 0.135 and 0.420, 0.116 and 0.357 for control, neutral, negative and positively charged NPs loaded liposomes respectively. The standard error was ± 0.01 for all these measurements. In case of SOPC liposomes, the difference between the control and γ-Fe_2O_3 NPs was almost negligible due to the electrostatic repulsion

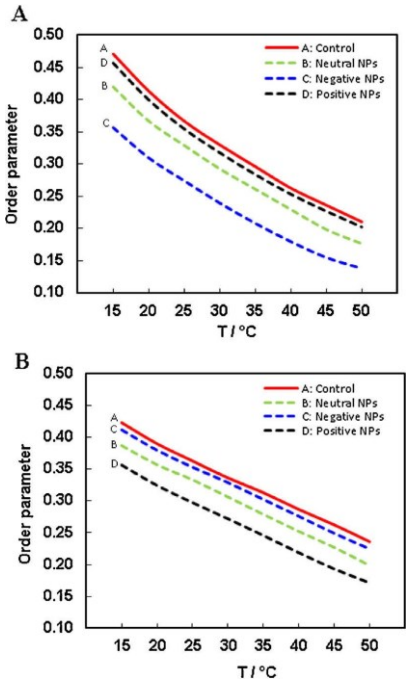

Fig. 4. Temperature dependent lipid-order parameter measurements of DPH following their incorporation into the liposomal membranes prepared from (A) SOPC, (B) SOPC–POPS lipid mixture. The liposomes were prepared at pH 7.0 and encapsulated with neutral and negatively charged cobalt ferrite NPs and positively charged iron oxide NPs.

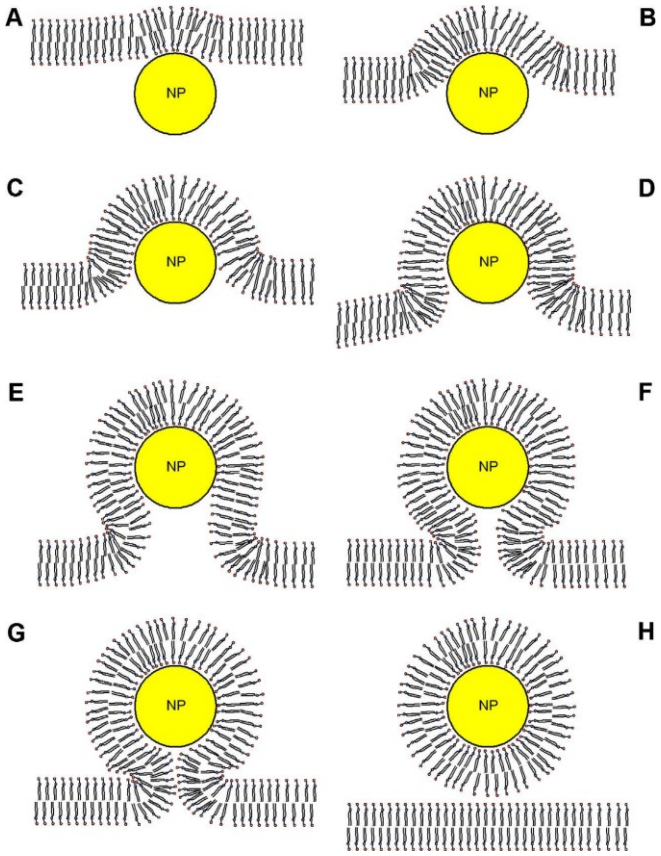

Fig. 5. Schematic figure showing the internalisation of larger NP inside the cell membrane. (A) NP adhesion to the membrane due to electrostatic attractive forces (B) initiation of membrane bending (C–E) membrane wrapping of the NP (F) neck formation (G) constriction of neck region (H) clevage of neck resulting in the internalisation of membrane encapsulated NP.

between the positively charged groups present in the lipid head and positively charged amino groups on the NP surface.

A similar effect was observed between the negatively charged SOPC–POPS mixture and negatively charged $CoFe_2O_4$ NPs. On the contrary, the difference was comparatively significant in the case of negatively charged SOPC–POPS and positively charged γ-Fe_2O_3 NPs. The attractive electrostatic forces between the cationic γ-Fe_2O_3 NPs and negatively charged SOPC–POPS lipid membrane enabled increased entrapment of NPs in the bilayer. These results indicate that electrostatic interactions play an important role in determining the efficiency of NPs encapsulation in liposomes as well as the interaction of NPs with the lipid membrane. If strong attractive electrostatic forces exists between the membrane and NPs surface, more amount of NPs will be encapsulated or adsorbed to the membrane leading to enhanced interactions (Michel and Gradzielski, 2012). This in turn will have a significant effect on the biophysical properties of the membrane. Some research groups have reported that even a small change in the fluorescence anisotropy values (up to 10%) caused a considerable change in the membrane viscosity (up to 25%) (Shinitzky and Barenholz, 1978). On the other hand, if electrostatic repulsions occur between the similarly charged liposome/membrane surface and the NPs, very less quantity of NPs will be encapsulated in the liposomes or enter into the cells. The obtained result is consistent with the findings of Bothun (2008) who demonstrated the encapsulation of silver NPs in liposomes decreased the anisotropy values and increased bilayer fluidity. Therefore our result coincides with the theoretical data, experimental results as well as with the simulations.

The adsorption of charged particles on the cell membrane due to strong electrostatic attractions leads to membrane deformation and alteration in the cell morphology (Hayden et al., 2012; Shlomovitz and Gov, 2009). Due to the negative surface charge of the cell membrane, NPs with the positive charge are attracted and internalised more compared to the neutral and negative NPs (Verma and Stellacci, 2010; Yaghmur and Rappolt, 2012). Though the size of the NPs exceed the width of the bilayer, due to membrane elasticity and flexibility the smaller NPs can be trapped partly or entirely into the bilayer. This entrapment of NPs disturbs the ordering of the lipids in the membrane leading to the changes in membrane fluidity. This result is supported by the fact that the cell membrane accommodates smaller intracellular proteins within itself and larger extracellular proteins partly embedded (encapsulated) in the lipid bilayer.

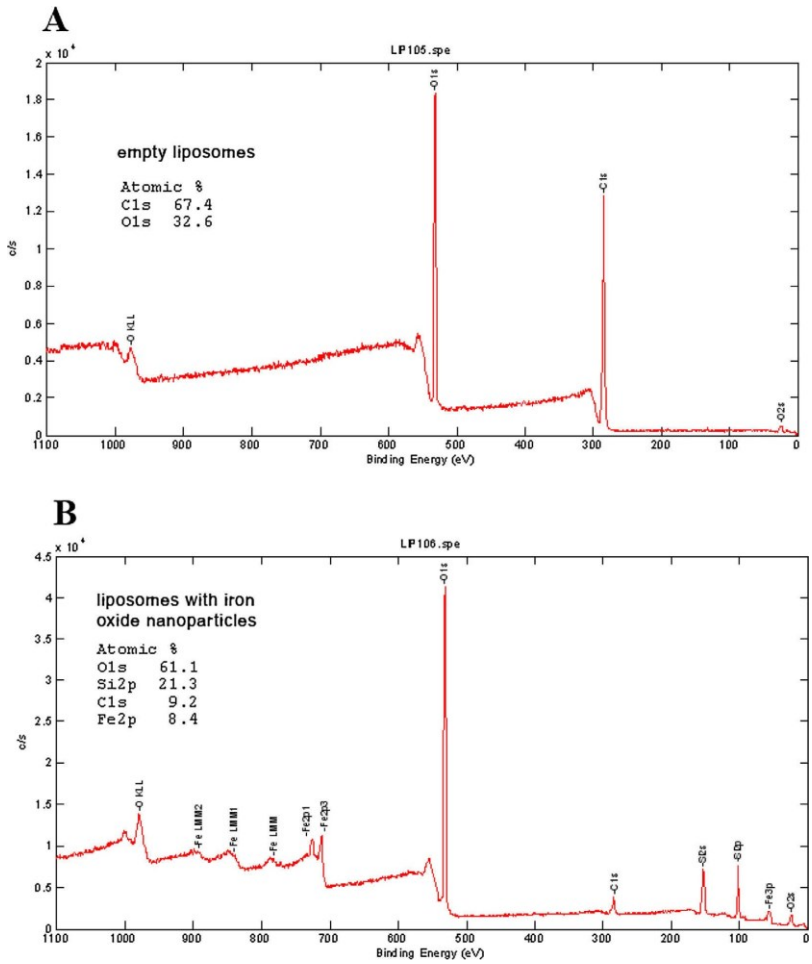

Fig. 6. XPS survey depicting the difference in chemical composition (at.%) between 2 spectrums. (A) Control liposomes without Fe_2O_3 NPs and (B) liposomes encapsulated with Fe_2O_3 NPs (Eleršič et al., 2012).

The cell membrane adopts different mechanisms for the NPs to pass through them and get internalised into the cell (Liu et al., 2009; Gladnikoff et al., 2009). A possible mode of encapsulation of a larger NP is shown in Fig. 5. Due to electrostatic attractive forces, the NPs approach and adhere to the membrane surface followed by membrane bending (Fig. 5(A and B)). If the adhesive forces between the NP and the membrane surface are strong enough to compensate the bending energy of the membrane, the membrane bends further forming a neck region to wrap the NP completely (Fig. 5(C–F)). Later the neck region constricts (Fig. 5G) further and cleave from the membrane due to thermal fluctuations, resulting in the formation of a bud in which the NP is entirely surrounded by the membrane and the encapsulated NP is subsequently released into the interior of the cell (Fig. 5H). Ruiz-Herrero et al. (2012) reported that the duration of membrane budding can be variable and the neck configurations during their observations lasted between 500 and 5000 r_0.

3.2. XPS analysis

XPS is a widely used spectroscopic technique to analyze the surface chemistry of a sample using X-ray beams (Eleršič et al., 2012). The X-ray spectrum enables to determine the elemental composition, empirical formula and the electronic state of the individual elements in the sample. Since we anticipated that the positively charged NPs will be encapsulated more in the negatively charged liposomes due to strong electrostatic attractions, we used XPS to prove the NPs encapsulation in liposomes by determining the difference in the chemical composition between the control liposomes without NPs and SOPC–POPS liposomes encapsulated with the γ-Fe_2O_3 NPs.

The XPS spectra showing the difference between the empty liposomes and NPs encapsulated liposomes is shown in Fig. 6. The XPS spectra in the upper panel shows the chemical composition of the pure liposomes where one can observe the peaks depicting the presence of carbon and oxygen. The atomic composition of carbon

Table 1
Bending elasticity modulus (k_c) measurements of pure SOPC membrane and SOPC membrane with $CoFe_2O_4$ NPs.

System	Weighted mean value of the bending elasticity modulus $k_c/10^{-19}$ J	Number of vesicles
Pure SOPC membrane	2.1 ± 0.1	8
SOPC membrane with $CoFe_2O_4$ NPs	1.6 ± 0.1	7

Table 2
Encapsulation efficiency of neutral SOPC liposomes and negatively charged SOPC–POPS liposomes encapsulated with iron oxide and cobalt ferrite NPs (n = 4).

Sample	Encapsulation efficiency (%)
SOPC – Neutral $CoFe_2O_4$ NPs	79 ± 2.6
SOPC – Negative $CoFe_2O_4$ NPs	86 ± 1.7
SOPC – Positive Fe_2O_3 NPs	75 ± 4.2
SOPC–POPS – Neutral $CoFe_2O_4$ NPs	81 ± 2.2
SOPC–POPS – Negative $CoFe_2O_4$ NPs	65 ± 3.7
SOPC–POPS – Positive Fe_2O_3 NPs	94 ± 2.3

(C) in the prepared liposomes was found to be 67.4% whereas the oxygen (O) composition was 32.6%. The lower panel corresponds to the liposomes encapsulated with iron oxide NPs. Apart from the carbon and oxygen peaks, new peaks corresponding to iron (Fe) and silica (Si) were observed in the lower panel. By the appearance of Fe2p and Si2p signals in the XPS spectra, the presence of silica coated iron oxide NPs in the liposomes were confirmed. The chemical composition of the iron oxide NPs was also shown by the XPS results; higher concentration of oxygen (from 32.6 to 61.1 at.%) and the presence of Fe (8.4%) and Si (21.3%) were observed. The XPS measurement is very sensitive surface analysis method and the escape depth of photoelectrons is only a few nm. This is also the reason for higher concentration of silica which corresponds to the cover layer of iron oxide NPs.

3.3. Bending elasticity measurements

Bending elasticity is an important parameter that controls the membrane fluctuations or alterations in the shape of the vesicles mainly due to adhesion or interaction with different substances such as proteins, NPs or drugs. The analysis of thermally induced shape fluctuations of giant liposomes is a classical method for studying the elastic properties of lipid membranes. It is based on the fact that under the Brownian motions of water molecules, the lipid membrane in water environment constantly changes its shape due to the fluctuation. Such fluctuations of the biological or model membranes are a part of the phenomena, describing the deviation of some physical properties from their equilibrium state.

The obtained experimental data for the bending elasticity modulus (k_c) for pure SOPC membrane and for SOPC membrane with NPs are presented in Table 1. As it can be seen from the obtained results, the bending elasticity modulus decreases in the presence of neutral cobalt ferrite NPs in comparison with that of pure lipid membrane. This result is in good agreement with the theoretical predictions showing that lipid bilayers containing additives as different inclusions or attached molecules have at certain conditions reduced bending elastic modulus, which is mainly due to entropic effect (Kralj-Iglič et al., 1999; Bivas and Méléard, 2003; Iglič et al., 2007; Fošnarič et al., 2006; Meleard et al., 2011; Ramakrishnan et al., 2011).

3.4. Encapsulation efficiency

The lipid composition, surface charge of NPs, nature of the coating material and variation in the size of magnetic core of NPs are some of the important factors that influence the efficiency of NPs encapsulation in liposomes. Electrostatic interactions between the NPs surface and the liposomes are important to be considered to increase the NPs load in the vesicles. Our results (Table 2) showed the highest encapsulation efficiency of 94% between the negatively charged SOPC–POPS liposomes and positively charged Fe_2O_3 NPs due to strong electrostatic attractive forces between them. On the contrary, a lower EE% of 65% was obtained between the negatively charged SOPC–POPS liposomes and negatively charged $CoFe_2O_4$ NPs due to the electrostatic repulsions among the similar charges. To check the influence of varying NPs concentration on the encapsulation efficiency of liposomes, 0.5, 1.0, 2.0, 3.0 and 5.0 mg of NPs/mL of the lipid was used during the liposome preparation. In both the neutral and negatively charged liposomes, the EE% reached the highest for the vesicles with the lowest NPs concentration of 0.5 mg/mL such as of 89% and 93% respectively. The EE% gradually decreased with the increased NPs concentration in both the type of liposomes. This result is consistent with the findings of Sabate et al. (2008) and Frascione et al. (2012) who showed that EE% is inversely proportional to the initial NPs concentration. Increasing the NPs concentration above 3.0 mg/mL did not bring significant increase in EE%.

3.5. Theoretical discussion

POPS consists of two negative groups (phosphate and serine group) and one positive group (amino group) in the head region contributing a net negative surface charge to the lipid. Due to amphiphilic effect, the negative part of the head group bounded to lipid tails (phosphate group) is in contact with salt solution forming negatively charged surface. The positive part of lipid head group (amino group) and the outer negative part of the lipid head group (serine group) penetrates into the salt solution (see Fig. 1). The average orientation angle of the lipid head group (ω) as a function of the distance of the NP (D_{np}) from the negatively charged part of lipid head groups at x = 0 can be seen in Fig. 7. The results were presented for three different values of parameter α and NPs with three

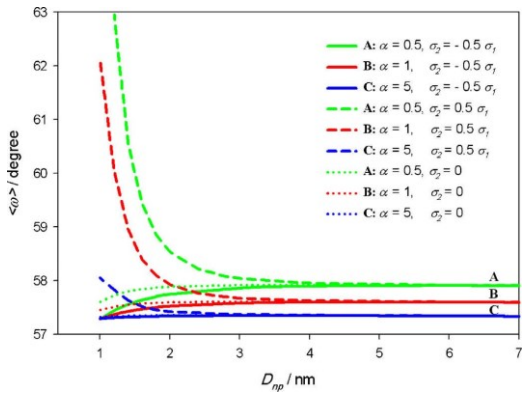

Fig. 7. The average orientation angle of the head group (ω) as a function of the distance of NP (D_{np}) from negatively charged lipid surface at x = 0 for three different values of parameter α and NPs with three different charges: negative (solid plots), positive (dashed plots) and neutral (dotted plots). The values of used parameters were: T = 298 K, $a_1 = -0.3$ As/m^2, dipole moment of water $p_0 = 3.1$ Debye, D = 0.42 nm, bulk concentration of salt $n_0/N_A = 0.1$ mol/L, concentration of water $n_{0w}/N_A = 55$ mol/L, where N_A is Avogadro number.

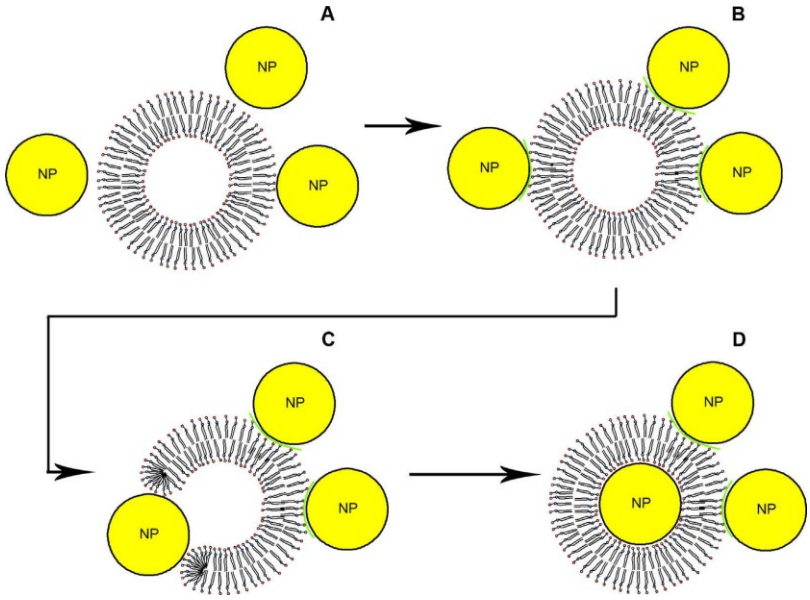

Fig. 8. Schematic diagram showing various possible modes of NPs interaction with the lipid membranes and their subsequent encapsulation. (A) approach of the charged NPs to the surface of the lipid membranes (B) attachment/adhesion of the NPs to the membrane surface and membrane bending (C) membrane pore formation by the NP (D) encapsulation of the NP in the core of the liposomes.

different charges (positive, neutral and negative). For negatively charged NP, it can be seen that with the decreasing distance D_{np} the average orientation angle of the lipid head group (ω) increases significantly. For positively charged NP, weak attractive forces exist between the negatively charged part of lipid head group at x = 2D and positively charged NP resulting in decreased average orientational angle (ω) towards 57 degrees. For the neutral NP, the average orientation angle is practically constant.

3.6. Different possible modes of nanoparticle interaction with the membrane

Based on the results presented in Fig. 7 and the results of many previous studies we conclude that the surface charge of the lipid vesicles and NPs play an important role in determining the encapsulation ratio of the NPs in the liposomes (Arsov et al., 2009; Husen et al., 2012; Bernchou et al., 2011). Fig. 8A depicts the approach of NPs to the surface of the vesicles and in case of strong electrostatic attractions, the particles adsorb to the bilayer surface and may induce membrane bending as shown in Fig. 8B. A possible mode of NPs encapsulation inside the liposomes is through pore formation. Roiter et al. (2008) reported the formation of membrane pores by silica NPs in the size range of 1.2–22 nm in the phosphatidylcholine membranes. Fig. 8C depicts the NPs induced pore formation in membranes and Fig. 8D demonstrates their subsequent encapsulation in the aqueous core of the liposomes.

4. Conclusion

Small unilamellar vesicles encapsulated with neutral, negative and positively charged NPs were prepared with SOPC (neutral), SOPC-POPS lipid mixture (negatively charged) to study the influence of electrostatic interactions on fluidity and elasticity of liposomal membranes. The fluorescent anisotropy measurements showed a significant reduction in the fluidity of negatively charged SOPC-POPS liposomal membranes caused by the positively charged iron oxide NPs. The results from XPS spectra also confirmed that γ-Fe_2O_3 NPs were successfully encapsulated in the interior of the liposomes. The increased adhesion of positive NPs on the negatively charged liposomes was also suggested from theoretical MLPB model, where we predicted the stronger average orientation of lipid headgroups in direction perpendicular to the liposome membrane surface, corresponding to the attractive forces between the negatively charged serine groups of the POPS lipid and positively charged iron oxide NPs. The encapsulation of $CoFe_2O_4$ NPs in the SOPC membrane bilayer of giant unilamellar vesicles reduced the bending elasticity modulus of the lipid membrane. Our findings are consistent with our understanding that the electrostatic attractions between the membrane and NPs surface promote the encapsulation efficiency of NPs in liposomes and enhance their interactions with the membrane. These results will contribute to gain knowledge about the effect of magnetic NPs on the physical properties of the membrane and the significance of electrostatic forces in order to increase the NPs load in the vesicles which in turn is desirable for various clinical applications such as drug delivery and magnetic hyperthermia. Since the application of NPs in the biomedical field is tremendously increasing, our results describing the effect of magnetic NPs on physical properties of the membrane gains importance.

Conflicts of interest

The authors have no conflicts of interest to disclose in this work.

Acknowledgements

This work was in part supported by the Slovenian Research Agency (ARRS). P.B.S., E.G., and J.G. were mainly supported by the

grants from Slovenian Human Resources Development and Scholarship Fund, while A.V. by European social fund and SMARTEH. J.G. was also supported by the Internal Grant VK-02-13 of the Institute of Solid State Physics, Bulgarian Academy of Sciences.

References

Akbarzadeh, A., Samiei, M., Davaran, S., 2012. Magnetic nanoparticles: preparation, physical properties, and applications in biomedicine. Nanoscale Res. Lett. 7, 144.

Albanese, A., Tang, P.S., Chan, W.C.W., 2012. The effect of nanoparticle size, shape, and surface chemistry on biological systems. Annu. Rev. Biomed. Eng. 14, 1–16.

Angelova, M., Soléau, S., Méléard, P., Faucon, F., Bothorel, P., 1992. Preparation of giant vesicles by external AC electric fields. Kinetics and applications. In: Helm, C., Lösche, M., Möhwald, H. (Eds.), Trends in Colloid and Interface Science VI, Progress in Colloid and Polymer Science. Springer, Berlin/Heidelberg, Germany, pp. 127–131.

Aricha, B., Fishov, I., Cohen, Z., Sikron, N., Pesakhov, S., Khozin-Goldberg, I., Dagan, R., Porat, N., 2004. Differences in membrane fluidity and fatty acid composition between phenotypic variants of Streptococcus pneumoniae. J. Bacteriol. 186, 4638–4644.

Arsov, Z., Rappolt, M., Grdodolnik, J., 2009. Weakened hydrogen bonds in water confined between lipid bilayers: the existence of a long-range attractive hydration force. Chem. Phys. Chem. 10, 1438–1441.

Bangham, A., De Gier, J., Greville, G., 1967. Osmotic properties and water permeability of phospholipid liquid crystals. Chem. Phys. Lipids 1, 225–246.

Bumb, A., Brechbiel, M.W., Choyke, P.L., Fugger, L., Eggeman, A., Prabhakaran, D., Hutchinson, J., Dobson, P.J., 2008. Synthesis and characterization of ultra-small superparamagnetic iron oxide nanoparticles thinly coated with silica. Nanotechnology 19, 335601.

Bernchou, U., Midtiby, H., Ipsen, J.H., Simonsen, A.C., 2011. Correlation between the ripple phase and stripe domains in membranes. Biochim. Biophys. Acta 1808, 2849–2858.

Bhandary, S., Sultana, P., Basu, R., Das, S., Nandy, P., 2011. A study on modulation of phase behavior of lipid aggregates-effect of some metal NPs. Adv. Sci. Eng. Med. 3, 1–6.

Bivas, I., Méléard, P., 2003. Bending elasticity and bending fluctuations of lipid bilayer containing an additive. Phys. Rev. E 67, 012901.

Bothun, G.D., 2008. Hydrophobic silver NPs trapped in lipid bilayers: size distribution, bilayer phase behavior, and optical properties. J. Nanobiotechnol. 6, 13.

Eleršič, K., Pavlič, J., Iglič, A., Vesel, A., Mozetič, M., 2012. Electric-field controlled liposome formation with embedded superparamagnetic iron oxide NPs. Chem. Phys. Lipids 165, 120–124.

Fošnarič, M., Iglič, A., May, S., 2006. Influence of rigid inclusions on the bending elasticity of a lipid membrane. Phys. Rev. E 74, 051503.

Frokjaer, S., Hjorth, E.L., Worts, O., 1982. Stability and storage of liposomes. In: Bundgard, H., Hansen, A., Kofod, H. (Eds.), Optimization of Drug Delivery. Munkgaard, Copenhagen, p. 384.

Frascione, D., Diwoky, C., Almer, G., Opriessnig, P., Vonach, C., Gradauer, K., Leitinger, G., Mangge, H., Stollberger, R., Prassl, R., 2012. Ultrasmall superparamagnetic iron oxide (USPIO)-based liposomes as magnetic resonance imaging probes. Int. J. Nanomed. 7, 2349–2359.

Fröhlich, H., 1964. Theory of Dielectrics. Clarendon Press, Oxford, UK.

Genova, J., Mitov, M., 2013. Lectures: measuring bending elasticity of lipid bilayers. In: Iglič, A., Genova, J. (Eds.), Advances in Planar Lipid Bilayers and Liposomes. Elsevier, Amsterdam, pp. 1–27.

Gladnikoff, M., Shimoni, E., Gov, N.S., Rousso, I., 2009. Retroviral assembly and budding occur through an actin-driven mechanism. Biophys. J. 97, 2419–2428.

Gongadze, E., Iglič, A., 2012. Decrease of permittivity of an electrolyte solution near a charged surface due to saturation and excluded volume effects. Bioelectrochemistry 87, 199–203.

Gongadze, E., van Rienen, U., Kralj-Iglič, V., Iglič, A., 2011a. Langevin Poisson–Boltzmann equation: point-like ions and water dipoles near charged membrane surface. Gen. Physiol. Biophys. 30, 130–137.

Gongadze, E., van Rienen, U., Iglič, A., 2011b. Generalized Stern models of an electric double layer considering the spatial variation of permittivity and finite size of ions in saturation regime. Cell. Mol. Biol. Lett. 16, 549–576.

Genova, J., Pavlic, J.I., 2012. Realization of Marin Mitov idea for the stroboscopic illumination used in optical microscopy. Bulg. J. Phys. 39, 65–71.

Gmajner, D., Ota, A., Šentjurc, M., Ulrih, N.P., 2011. Stability of diether C25,25 liposomes from the hyperthermophilic archaeon Aeropyrum pernix K1. Chem. Phys. Lipids 164, 236–245.

Hayden, S.C., Zhao, G., Saha, K., Phillips, R.L., Li, X., Miranda, O.R., Rotello, V.M., El-Sayed, M.A., Schmidt-Krey, I., Bunz, U.H.F., 2012. Aggregation and interaction of cationic NPs on bacterial surfaces. J. Am. Chem. Soc. 134, 6920–6923.

Hianik, T., Passechnik, V.I., 1995. Bilayer Lipid Membranes: Structure and Mechanical Properties. Kluwer Academic Publishers, Dordrecht, Netherlands, pp. 138–157.

Huang, Y.Z., Gao, J.Q., Liang, W.Q., Nakagawa, S., 2005. Preparation and characterization of liposomes encapsulating chitosan nanoparticles. Biol. Pharm. Bull. 28, 387–390.

Husen, P., Fidorra, M., Haertel, S., Bagatolli, L., Ipsen, J.H., 2012. A method for analysis of lipid vesicle domain structure from confocal image data. Eur. Biophys. J. Biophys. 41, 161–175.

Iglič, A., Slivnik, T., Kralj-Iglič, V., 2007. Elastic properties of biological membranes influenced by attached proteins. J Biomech. 40, 2492–2500.

Jiang, J., Oberdorster, G., Biswas, P., 2009. Characterization of size, surface charge, and agglomeration state of nanoparticle dispersions for toxicological studies. J. Nanopart. Res. 11, 77–89.

Kralj-Iglič, V., Heinrich, V., Svetina, S., Žekš, B., 1999. Free energy of closed membrane with anisotropic inclusions. Eur. Phys. J. B 10, 5–8.

Kulkarni, C.V., 2012. Lipid crystallization: from self assembly to hierarchical and biological ordering. Nanoscale 4, 5779–5791.

Lai, K., Wang, B., Zhang, Y., Zheng, Y., 2013. Computer simulation study of nanoparticle interaction with a lipid membrane under mechanical stress. Phys. Chem. Chem. Phys. 15, 270–278.

Laurent, S., Mahmoudi, M., 2011. Superparamagnetic iron oxide nanoparticles: promises for diagnosis and treatment of cancer. Int. J. Mol. Epidemiol. Genet., 367–390.

Li, Q., Tang, G., Xue, S., He, X., Miao, P., Li, Y., Wang, J., Xiong, L., Wang, Y., Zhang, C., Yang, G.Y., 2013. Silica-coated superparamagnetic iron oxide nanoparticles targeting of EPCs in ischemic brain injury. Biomaterials 34, 4982–5499.

Liu, J., Sun, Y., Drubin, D.G., Oster, G.F., 2009. The mechanochemistry of endocytosis. PLoS Biol. 7, e1000204.

Mahnaz, M., Ahmad, M.B., Haron, M.J., Namvar, F., Behzad, N., Rahman, M.Z.A., Amin, J., 2013. Synthesis, surface modification and characterisation of biocompatible magnetic iron oxide nanoparticles for biomedical applications. Molecules 18, 7533–7548.

Meleard, P., Pott, T., Bouvrais, H., Ipsen, J.H., 2011. Advantages of statistical analysis of giant vesicle flickering for bending elasticity measurements. Eur. Phys. J. E Soft Matter 34, 1–14.

Michel, R., Gradzielski, M., 2012. Experimental aspects of colloidal interactions in mixed systems of liposome and inorganic nanoparticle and their applications. Int. J. Mol. Sci. 13, 11610–11642.

Mitov, M.D., Faucon, J.F., Méléard, P., Bothorel, P., 1992. Thermal fluctuations of membranes. In: Gokel, G.W. (Ed.), Adv. Supramol. Chem. JAI Press, Greenwich, pp. 93–139.

Park, S.H., Oh, S.G., Mun, J.Y., Han, S.S., 2005. Effects of silver NPs on the fluidity of bilayer in phospholipid liposome. Colloids Surf. B 44, 117–122.

Perez-Berna, A.J., Guillen, J., Moreno, M.R., Bernabeu, A., Pabst, G., Laggner, P., Villalain, J., 2008. Identification of the membrane-active regions of hepatitis C virus p7 protein: biophysical characterization of the loop region. J. Biol. Chem. 283, 8089–8101.

Pottel, H., van der Meer, W., Herreman, W., 1983. Correlation between the order parameter and the steady-state fluorescence anisotropy of 1,6-diphenyl-1,3,5-hexatriene and an evaluation of membrane fluidity. Biochim. Biophys. Acta 730, 181–186.

Ramakrishnan, N., Kumar, P.B.S., Ipsen, J.H., 2011. Modeling anisotropic elasticity of fluid membranes. Macromol. Theor. Simul. 20, 446–450.

Rappolt, M., Pabst, G., 2008. Flexibility and structure of fluid bilayer interfaces. In: Nag, K. (Ed.), Structure and Dynamics of Membranous Interfaces. John Wiley and Sons, Inc., Hoboken, NJ, USA, pp. 45–81.

Repakova, J., Holopainen, J.M., Morrow, M.R., McDonald, M.C., Capkova, P., Vattulainen, I., 2005. Influence of DPH on the structure and dynamics of a DPPC bilayer. Biophys. J. 88, 3398–3410.

Roiter, Y., Ornatska, M., Rammohan, A.R., Balakrishnan, J., Heine, D.R., Minko, S., 2008. Interaction of NPs with lipid membrane. Nano Lett. 8, 941–944.

Ruiz-Herrero, T., Velasco, E., Hagan, M.F., 2012. Mechanisms of budding of nanoscale particles through lipid bilayers. J. Phys. Chem. B 116, 9595–9603.

Sabate, R., Barnadas-Rodriguez, R., Callejas-Fernandez, J., Hidalgo-Alvarez, R., Estelrich, J., 2008. Preparation and characterization of extruded magnetoliposomes. Int. J. Pharm. 347, 156–162.

Santhosh, P.B., Ulrih, N.P., 2013. Multifunctional superparamagnetic iron oxide nanoparticles: Promising tools in cancer theranostics. Cancer Lett. 336, 8–17.

Shinitzky, M., Barenholz, Y., 1978. Fluidity parameters of lipid regions determined by fluorescence polarization. Biochim. Biophys. Acta 515, 367–394.

Shlomovitz, R., Gov, N.S., 2009. Membrane-mediated interactions drive the condensation and coalescence of FtsZ rings. Phys. Biol. 6, 046017.

Sipai Altaf Bhai, M., Vandana, Y., Mamatha, Y., Prasanth, V.V., 2012. Liposomes: an overview. J. Pharm. Sci. Innov. 1, 13–21.

Spelios, M., Savva, M., 2008. Novel N,N-diacyl-1,3-diaminopropyl-2-carbamoyl bivalent cationic lipids for gene delivery – synthesis, in vitro transfection activity, and physicochemical characterization. FEBS J. 275, 148–162.

Sybachin, A.V., Ballauff, M., Yaroslavov, A.A., 2012. Composition and properties of complexes between spherical polycationic brushes and anionic liposomes. Langmuir 28, 16108–16114.

Torchilin, V.P., 2005. Recent advances with liposomes as pharmaceutical carriers. Nat. Rev. Drug. Discov. 4, 145–160.

Uhumwangho, M.U., Okorr, R.S., 2005. Current trends in the production and biomedical applications of liposomes: a review. J. Biomed. Sci. 4, 9–21.

Ulrih, N.P., Gmajner, D., Raspor, P., 2009. Structural and physicochemical properties of polar lipids from thermophilic archaea. Appl. Microbiol. Biotechnol. 84, 249–260.

Veksler, A., Gov, N.S., 2009. Phase transitions of the coupled membrane-cytoskeleton modify cellular shape. Biophys. J. 93, 3798–3810.

Velikonja, A., Perutkova, š., Gongadze, E., Kramar, P., Polak, A., Maček-Lebar, A., Iglič, A., 2013. Monovalent ions and water dipoles in contact with dipolar zwitterionic lipid headroups—theory and MD simulations. Int. J. Mol. Sci. 14, 2846–2861.

Verma, A., Stellacci, F., 2010. Effect of surface properties on nanoparticle–cell interactions. Small 6, 12–21.
Weinstein, J.S., Varallyay, C.G., Dosa, E., Gahramanov, S., Hamilton, B., Rooney, W.D., Muldoon, L.L., Neuwelt, E.A., 2010. Superparamagnetic iron oxide nanoparticles: diagnostic magnetic resonance imaging and potential therapeutic applications in neurooncology and central nervous system inflammatory pathologies, a review. J. Cereb. Blood Flow Metab. 30, 15–35.
Wrobel, D., Kłys, A., Ionov, M., Vitovic, P., Waczulikowa, I., Hianik, T., Gomez-Ramirez, R., de la Mata, J., Klajnert, B., Bryszewska, M., 2012. Cationic carbosilane dendrimers-lipid membrane interactions. Chem. Phys. Lipids 165, 401–407.
Wu, W., He, Q., Jiang, C., 2008. Magnetic iron oxide nps: synthesis and surface functionalization strategies. Nanoscale Res. Lett. 3, 397–415.
Yaghmur, A., Rappolt, M., 2012. Structural characterization of lipidic systems under nonequilibrium conditions. Eur. Biophys. J. 41, 831–840.

D Članek 4: Ions and water molecules in an electrolyte solution in contact with charged and dipolar surfaces

Polno ime revije:	Electrochimica Acta
Okrajšava:	Electrochim. Acta
ISSN (tiskana izdaja):	0013-4686
Založnik:	Oxford, New York, Pergamon Press
Naslov založnika:	Oxford, New York, United States
Pogostost izdaje:	mesečno s posebnimi izdajami v februarju, maju in septembru
Medij:	tiskana verzija
Spletna stran revije:	http://sciencedirect.com/science/journal/00134686
Prvo leto izdaje:	1959
Faktor vpliva:	3.777 (2012)
Faktor vpliva (5 let):	4.088 (2012)
Naslov članka:	Ions and water molecules in an electrolyte solution in contact with charged and dipolar surfaces
Avtorji:	Gongadze, Ekaterina; Velikonja, Aljaž; Perutkova, Šarka; Kramar, Peter; Maček-Lebar, Alenka; Kralj-Iglič, Veronika; Iglič, Aleš
Izdaja:	126
Številka:	-
Strani:	42—60
Leto objave:	2014
DOI:	10.1016/j.electacta.2013.07.147

Electrochimica Acta 126 (2014) 42–60

Contents lists available at ScienceDirect

Electrochimica Acta

journal homepage: www.elsevier.com/locate/electacta

Review

Ions and water molecules in an electrolyte solution in contact with charged and dipolar surfaces

Ekaterina Gongadze [a], Aljaž Velikonja [b,c], Šarka Perutkova [a], Peter Kramar [b], Alenka Maček-Lebar [b], Veronika Kralj-Iglič [d], Aleš Iglič [a,*]

[a] Laboratory of Biophysics, Faculty of Electrical Engineering, University of Ljubljana, Tržaška 25, SI-1000 Ljubljana, Slovenia
[b] Laboratory of Biocybernetics, Faculty of Electrical Engineering, University of Ljubljana, Tržaška 25, SI-1000 Ljubljana, Slovenia
[c] SMARTEH Research and Development of Electronic Controlling and Regulating Systems, Trg tigrovcev 1, SI-5220 Tolmin, Slovenia
[d] Laboratory of Clinical Biophysics, Faculty of Health Studies, University of Ljubljana, Zdravstvena 5, SI-1000 Ljubljana, Slovenia

article info

Article history:
Received 12 May 2013
Received in revised form 17 July 2013
Accepted 18 July 2013
Available online 2 August 2013

Keywords:
Water molecules
Permittivity
Orientational ordering
Attractive forces
Electric double layer

abstract

The electrolyte-charged surface interface is described within the Langevin–Poisson–Boltzmann (LPB) and Langevin–Bikerman models. It is shown that in the saturation regime close to the charged surface, water dipole ordering and depletion of water molecules may result in a strong local decrease of permittivity. Analytical expressions for the space dependence of relative permittivity are derived for both models. The differential capacitance as a function of the surface potential is calculated within the modified Langevin–Bikerman model and compared to the prediction of the classical Gouy–Chapman theory. As an example of the application of the models described, a zwitterionic lipid surface with non-zero dipole moments in contact with an electrolyte solution of monovalent salt ions and water dipoles is studied within the LPB model. An analytical expression for the osmotic pressure of the electrolyte solution between the zwitterionic lipid surface and a charged particle (macroion) is derived. Some of the predictions of the described electric double layer mean-field theoretical considerations are evaluated using the results of a molecular dynamics simulation. At the end a theoretical description of the possible origin of the attractive interactions between like-charged surfaces mediated by charged macroions with distinctive internal charge distribution is given.

Contents

* Corresponding author. Tel.: +386 1 4768 825; fax: +386 1 4768 850.
E-mail address: ales.iglic@fe.uni-lj.si (A. Iglič).

0013-4686/$ – see front matter © 2013 Elsevier Ltd. All rights reserved.
http://dx.doi.org/10.1016/j.electacta.2013.07.147

1. Introduction

In the complex interface between a charged surface and a surrounding electrolyte (Fig. 1), the electric double layer (EDL) plays a crucial role [1–11]. It causes the ions and water molecules to rearrange near the charged surface and thus to screen the electric potential [12–16]. Due to electrostatic forces between the charged surface and the ions in the electrolyte solution, the counterions (ions with a charge of the sign opposite to the charged surface) are accumulated close to the surface and the co-ions (ions with a charge of the same sign as the surface) are depleted from the surface.

Study of the EDL was begun in 1879 by Hermann von Helmholtz who treated the double layer as a simple capacitor, assuming that the surface charge density is neutralized by the counterions located at a distance equal to their hydrated radius. Gouy [17] and Chapman [18] considered the thermal motion of ions and pictured a diffuse double layer composed of counterions and co-ions. Within the so-called Poisson–Boltzmann (PB) theory [6,12,13,17–20], the ions in electrolyte solution are treated as dimensionless, the surfaces are considered as uniformly charged and uniform permittivity of the electrolyte solution is assumed. The Stern model [21] was the first attempt to incorporate the finite size of ions in EDL theory by combining the Helmholtz [22] and Gouy–Chapman [17,18] models [12,23,24]. Later Bikerman introduced the first complete modified Poisson–Boltzmann (MPB) model which took into consideration the finite size of molecules in the electrolyte solution [25]. This approach was continued by Grimley and Mott [26,27], Freise [28] and Wicke and Eigen [29–31]. Also more recently, the finite size of the molecules was incorporated into EDL theory using lattice statistics models [3,32,33], by functional density approaches [34–36] and by a modified PB theory where the ions and solvent molecules were treated as hard spheres [14,15,37].

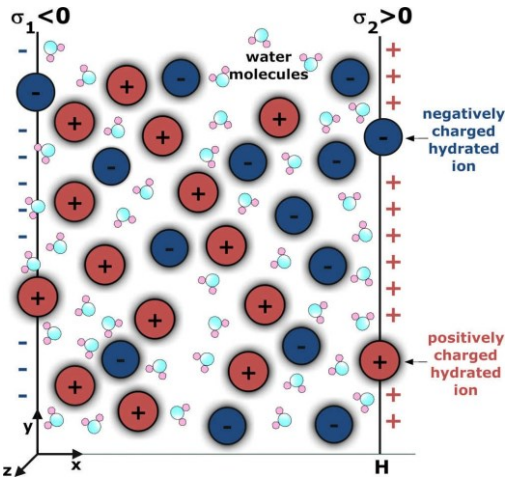

Fig. 1. Schematic figure of an electrolyte solution confined between negatively and positively charged surfaces characterized by surface charge densities a_1 at x = 0 and a_2 at x = H. The water dipoles in the vicinity of both charged surfaces are partially oriented towards the surfaces.

Most of the EDL models published to date are based on the concept that the relative permittivity is constant throughout the whole system [2,12,17,18,38,39]. The dipole moment vectors of water molecules at the charged metal surface are predominantly oriented in an orthogonal direction with respect to the charged surface. This results in a strong local decrease of permittivity [4,5,7,9,14–16,37,40–43], whereas all orientations of water dipoles further away from the charged surface are equally probable.

Considering simultaneously the orientational ordering of water and the finite size of molecules, Outhwaite and co-workers developed a modified PB (MPB) theory of the electrical double layer composed of a mixture of hard spheres with point dipoles and finite sized ions [14,15,37]. Later, Szalai et al. [44] published a mean spherical approximation-based theory [45] that can reproduce simulation results for the electric field dependence of the dielectric permittivity of a dipolar fluid in the saturation regime. The problem was also considered within lattice statistics [16,42,46]. It was shown that due to accumulation of counterions near the charged metal surface, the permittivity in this region is additionally reduced [46].

The Gouy–Chapman (GC) mean-field theory and its Poisson–Boltzmann (PB) equation may be used to estimate the interactions between like-charged surfaces in an electrolyte solution [12,13,47]. For a monovalent salt, it predicts repulsion between like-charged surfaces [58] in agreement with the experimental results and computer simulations. Therefore at first glance, an attractive interaction between two like-charged surfaces would seem impossible. However, the presence of ions with internal charge distribution (mediators) in the intermediate solution between the like-charged surfaces may change the repulsive interaction into an attractive one – not predicted by the mean-field GC approach. The mediators can be charged particles with a quadrupolar internal charge distribution [49–51]. This attraction is currently the subject of much interest because it is observed in a number of biologically relevant processes such as condensation of DNA [52], or the interactions between like-charged lipid membranes that occur during membrane adhesion [53] and fusion [54,55]. Electrostatic attraction between like-charged surfaces is also possible due to direct ion–ion correlations [56,57] in the limit of a high surface charge density and high ion charges [58].

In this review we present a lattice statistics approach to the theory of the EDL. First, we upgrade the description of GC theory and its PB equation by considering the orientational ordering of water molecules near a highly charged surface, the electronic polarizability and the cavity field of water molecules within the Langevin–Poisson–Boltzmann (LPB) model for point-like molecules in electrolyte solution. It is shown that the dielectric permittivity of an electrolyte close to a charged surface is decreased due to the increased orientational ordering of water dipoles. An expression for the osmotic pressure difference between the charged surfaces (Fig. 1) is also derived. The next section is devoted to the effects of ion size of the EDL within the Langevin–Bikerman

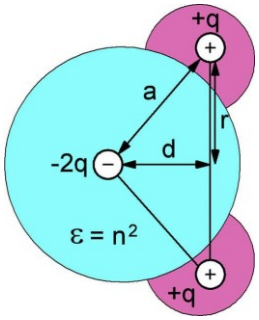

Fig. 2. A schematic figure of the charge distribution of a single water molecule within a triangular atomic model. In the model a single water molecule is considered as a sphere with permittivity n^2 and a point-like rigid (permanent) dipole/quadrupole at the centre of the sphere. Here n is the optical refractive index of water.
Adapted from [59].

(LB) model. It is shown that the dielectric permittivity close to the charged surface is additionally decreased due to the finite size of ions and dipoles in the electrolyte solution. We also shed light on the effect of finite-sized ions and water molecules on the osmotic pressure between charged surfaces in contact with the intermediate electrolyte solution. In the last part of this section we show that unlike the unphysical prediction of the GC model, the calculated differential capacitance within the MLB model, after reaching its maximum, decreases with increasing surface potential in accordance with experimental observations. In the next section the LPB model is generalized to describe the zwitterionic lipid layer in contact with an electrolyte solution where some of the model predictions are critically evaluated using the molecular dynamics (MD) simulation. The end of this section is dedicated to study of the interaction of positively and negatively charged macroions with the zwitterionic lipid layer. At the end of the article, we discuss the possible origins of attractive interactions between two like-charged surfaces immersed in a solution of macroions with spatially distributed internal charge. The final section rounds off the work by drawing final inferences, and pointing to future work and possible applications of the models described.

2. Energy of a single water molecule within a triangular atomic model

In the triangular atomic model of water, electronic polarization is taken into account by assuming that the point-like and rigid (permanent) dipole/quadrupole is embedded in the centre of a sphere with a volume equal to the average volume of a water molecule in an electrolyte solution, as shown schematically in Fig. 2. The permittivity of the sphere is taken to be n^2, where n = 1.33 is the optical refractive index of water [46,59,60]. The energy of a single water molecule can be written as (see Fig. 3):

$$W(x) = -2q\phi_c\left(x - \frac{d}{2}\cos\omega\right) + q\phi_c\left(x - \frac{d}{2}\cos\omega + a\cos(\omega+\phi)\right) + q\phi_c\left(x - \frac{d}{2}\cos\omega + a\cos(\omega-\phi)\right), \quad (1)$$

where +q and −q are point charges, ϕ_c is the local (cavity) electric potential, d and a are the distances and ω and ϕ the angles as denoted in Figs. 2 and 3.

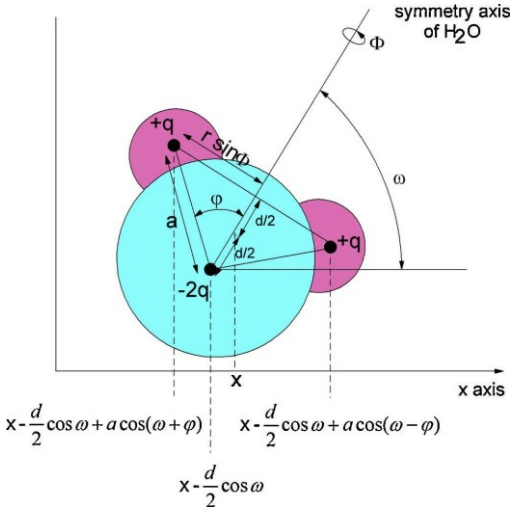

Fig. 3. Geometrical parameters of the triangular atomic model of a water molecule. Adapted from [59].

For small d and a, we can expand the energy W(x) in Eq. (1) into a Taylor series up to the quadratic terms [59]:

$$W(x) = p\cos\omega\,|\phi_c'(x)| + qr^2\sin^2\omega\,|\phi_c''(x)|, \quad (2)$$

where $d = a\cos\phi$, $a\sin\phi = r\sin^2$, $p = 2qd$ is the magnitude of the internal dipole, qr^2 characterizes the internal quadrupole, while ω is the angle between the gradient of the electric potential $\phi_d'(x)$ and the vector of the water dipole moment.

Fig. 4 shows the dependence of the average cosine $\langle\cos(\omega)\rangle_B$ (Eq. (11)) and the magnitude of the electric field strength E(x) as a function of the distance from the charged surface at x = 0. The spatial dependence of E(x) is determined within the Langevin–Bikerman model from the spatial dependence of the electric potential calculated from the Gongadze–Iglič (GI) equation (Eq. (43)), as described later in Section 4 of this review. It can be seen that the magnitude of $\langle\cos(\omega)\rangle_B$ increases with decreasing distance from the charged surface and increasing magnitude of the surface charge density a. This is because the magnitude of the electric field E(x) is strongly increased in the vicinity of the charged surface (Fig. 4). The tendency to increasing E(x) in the direction towards the charged surface is more pronounced for larger magnitudes of a.

3. Point-like molecules in an electrolyte solution

3.1. ModifiedLangevin–Poisson–Boltzmannequation

In this section we describe the modified Langevin–Poisson–Boltzmann (MLPB) model of the EDL [42,61] considering molecules of the electrolyte solution as point-like particles. For reasons of simplicity we neglect the internal quadrupole energy term (i.e. the second term in Eq. (2)) so that the energy of a single water molecule in the local field W(ω) is given by:

$$W(\omega) = pE_c\cos\omega, \quad (3)$$

where E_c is the magnitude of the local cavity electric field $\phi_c'(x)$. If the short range interactions between water molecules are neglected, the local electric field strength at the centre of the single

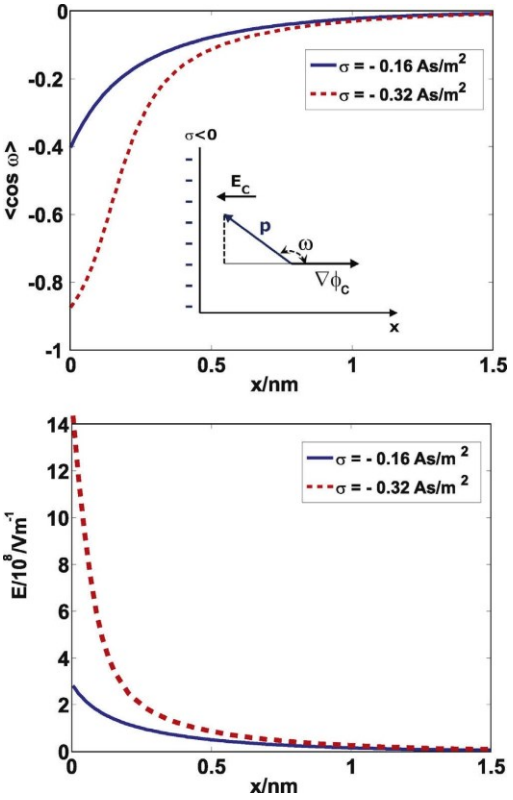

Fig. 4. Average orientation of water molecules described by $(\cos(\omega))_B$ (upper panel) and the magnitude of the electric field strength E(x) (lower panel) as a function of the distance from the charged plate (x) calculated within the LB model using the GI for two values of the surface charge density a: $e_0/nm^2 = -0.16$ As/m² (full lines) and $2e_0/nm^2 = -0.32$ As/m² (dashed lines). Values of parameters: bulk concentration of salt $n_0/N_A = 0.5$ mol/l, dipole moment of water $p_0 = 3.1$ D, optical refractive index $n = 1.33$, bulk concentration of water $n_{ow}/N_A = 55$ mol/l.

water molecule sphere (cavity) with dielectric permittivity n^2 at the location of the permanent (rigid) point-like dipole is [60]:

$$E_c = \frac{3\varepsilon_r}{2\varepsilon_r + n^2} E, \tag{4}$$

where E is the magnitude of the external field. The water molecules are embedded in a medium with permittivity ε_r. Eq. (4) is further simplified to the form (strictly valid for $\varepsilon_r \gg n^2$ only): $E_c = (3/2)E$. The energy of the point-like dipole p in the local cavity field of magnitude E_c may then be rewritten as:

$$W_i = y p_0 E \cos(\omega), \tag{5}$$

where p_0 is the magnitude of the external dipole moment $p_e = (3/(2 + n^2))\,p$ [46,60] and y is given by [46]:

$$= \frac{3}{2} \quad \frac{2 + n^2}{3} \quad . \tag{6}$$

In the LPB and MLPB models described in this section, the dielectric permittivity is consistently related to the orientational ordering of water molecules, while the finite volume of ions and water, i.e. the excluded volume effect, is not taken into account. The volume density of water ($n_w(x)$) is therefore constant over the whole electrolyte solution [3,42], while the number densities of counterions ($n_+(x)$) and coions ($n_-(x)$ are described by the Boltzmann distribution functions [3,17,18]:

$$n_+(x) = n_0 e^{-e_0 \phi \check{}}, \tag{7}$$

$$n_-(x) = n_0 e^{e_0 \phi \check{}}, \tag{8}$$

$$n_w(x) = n_{0w}, \tag{9}$$

where n_{0w} is the constant (bulk) number density of water and n_0 the bulk number density of counterions and coions of electrolyte solution, and $\check{} = 1/kT$, where kT is the thermal energy. The polarization in the vicinity of a negatively charged surface (see Fig. 1) is then given by [42]:

$$P(x) = n_{0w} \quad \frac{2 + n^2}{3} \quad p_0 (\cos(\omega))_B$$

$$= -n_{0w} \quad \frac{2 + n^2}{3} \quad p_0 L(y p_0 E\check{}), \tag{10}$$

where L(u) is Langevin function and $(\cos(\omega))_B$ is (see [60]):

$$(\cos(\omega))_B = \frac{\int_0^{n} \cos\omega P(x,\omega) 2n \sin\omega d\omega}{\int_0^{n} P(x,\omega) 2n \sin\omega d\omega} = -L(y p_0 E\check{}). \tag{11}$$

Combining the definition of the relative (effective) permittivity $\varepsilon_r(x) = n^2 + |P|/\varepsilon_0 E$ and Eq. (10) gives [42,61]:

$$\varepsilon_r(x) = n^2 + \frac{|P|}{\varepsilon_0 E} = n^2 + \frac{n_{0w} p_0}{\frac{E(x)\check{}}{\varepsilon_0}} \frac{2 + n^2}{3} \quad \frac{L(y p_0}{E(x)}, \tag{12}$$

Using Eq. (12) for the space-dependent relative permittivity $\varepsilon_r(x)$, we can rewrite the MLPB equation in the form [42,61]:

$$\frac{d}{dx} \varepsilon_0 \varepsilon_r(x) \frac{d\phi}{dx} = 2e_0 n_0 \sinh(e_0 \phi \check{}), \tag{13}$$

where the macroscopic (net) volume charge density of coions and counterions in the form:

$$\rho_{free}(x) = -e_0 n_+(x) - e_0 n_-(x) = -2e_0 n_0 \sinh(e_0 \phi \check{}), \tag{14}$$

was taken into account. The boundary conditions are [42,61] (see also Fig. 1):

$$\frac{d\phi}{dx}(x = 0) = -\frac{a_1}{\varepsilon_0 \varepsilon_r(x = 0)}, \tag{15}$$

$$\frac{d\phi}{dx}(x = H) = +\frac{a_2}{\varepsilon_0 \varepsilon_r(x = H)}. \tag{16}$$

Fig. 5 shows the spatial dependence of the electric potential $\phi(x)$ and relative permittivity ε_r in planar geometry for two values of the bulk number density of counterions and coions n_0. A considerable decrease of relative permittivity can be observed in the close vicinity of the charged surface.

In the limit of a vanishing electric field strength ($E(x) \to 0$) everywhere in the solution, Eq. (12) for the relative permittivity $\varepsilon_{r,b}(x)$ gives the classical Onsager expression [62]:

$$\varepsilon_{r,b} \cong n^2 + \frac{2 + n^2}{3} \quad \frac{2n_{0w} p_0^{2}\check{}}{2\varepsilon_0}. \tag{17}$$

At room temperature (298 K), $p_0 = 3.1$ Debye (the Debye is 3.336×10^{-30} C/m) and $n_{0w}/N_A = 55$ mol/l, Eq. (17) gives $\varepsilon_{r,b} = 78.5$ for bulk solution. The value $p_0 = 3.1$ Debye is considerably smaller than the corresponding value in previous similar models ($p_0 = 4.79$ D) [42,63,64] which did not take into account the cavity field and electronic polarizability of water molecules.

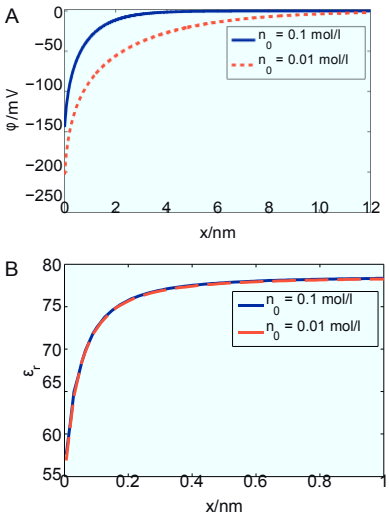

Fig. 5. Electric potential $\phi(x)$ (upper panel) and relative permittivity $\varepsilon_r(x)$ (lower panel) as a function of the distance from a negatively charged surface $x=0$ (see Fig. 1) and large H calculated within the MLPB model for two values of the bulk concentration of counterions and coions n_0/N_A: 0.1 mol/l and 0.01 mol/l. The model parameters are: $a_1 = -0.3$ As/m^2, $T = 298$ K, $p_0 = 3.1$ Debye, concentration of water $n_{0w}/N_A = 55$ mol/l, where N_A is the Avogadro number. The MLPB Eq. (13) was solved numerically as described in [42,46]).

3.2. Langevin–Poisson–Boltzmann equation

Neglecting the influence of the cavity field, the MLPB equation (Eq. (13)) [61] transforms into LPB equations [42] valid in the limit of $y \to 1$ and $n \to 1$ to obtain [16,42]:

$$\frac{d}{dx}\left(\varepsilon_0 \varepsilon_r(x) \frac{d\phi}{dx}\right) = 2 e_0 n_0 \sinh(e_0 \phi/kT), \tag{18}$$

where the space dependent relative permittivity $\varepsilon_r(x)$ is [16,42]:

$$\varepsilon_r(x) = 1 + \frac{n_{0w} p_0 L(p_0 E/kT)}{\varepsilon_0 E}. \tag{19}$$

Eq. (18) differs from Eq. (13) in the expression for $\varepsilon_r(x)$ which is not the same in the two cases. In the limit of vanishing electric field strength ($E \to 0$), Eq. (19) predicts:

$$\varepsilon_{r,b} \cong 1 + \frac{n_{0w} p_0^2/kT}{3\varepsilon_0}. \tag{20}$$

At room temperature (298 K), $p_0 = 4.79$ D and $n_{0w}/N_A = 55$ mol/l Eq. (20) gives $\varepsilon_{r,b} = 78.5$ for bulk solution. The value of the dipole moment $p_0 = 4.79$ D [42,63,64] is considerably larger than the corresponding value in the above described MLPB model ($p_0 = 3.1$ D) which takes into account the cavity field and electronic polarizability of water molecules [46,61].

3.3. Limiting Poisson–Boltzmann equation

Assuming a constant bulk value of the permittivity everywhere in the electrolyte solution, including the close vicinity of charged surfaces, the LPB equation transforms into the PB equation [17,18]:

$$\varepsilon_0 \varepsilon_{r,b} \frac{d^2\phi}{dx^2} = 2 e_0 n_0 \sinh(e_0 \phi/kT). \tag{21}$$

3.4. Osmotic pressure

In the following we derive an expression for the osmotic pressure difference between the charged surfaces as presented in Fig. 1. To this end Eq. (13) of the MLPB is first integrated (see also [47]) and then in the second step the corresponding bulk value of the pressure is subtracted from the local pressure to get the osmotic pressure Π. Prior to its integration, Eq. (13) is rearranged in the form (see also [42]):

$$-\frac{d}{dx}\left(\frac{1}{2}\varepsilon_0 n^2 \frac{d\phi}{dx}\right) + 2e_0 n_0 \sinh\frac{e_0\phi}{kT} - n_{0w} p_0 \frac{2+n^2}{3} \frac{d}{dx}(L(p_0 E/kT)) = 0. \tag{22}$$

Eq. (22) is multiplied by $\phi' \equiv d\phi/dx$ and integrated [47] to get the first integral equivalent to the contact theorem:

$$\frac{1}{2}\varepsilon_0 n^2 E(x)^2 + 2n_0 kT(\cosh(-e_0\phi(x)/kT)) - E(x)\frac{2+n^2}{3} n_{0w} p_0 L(p_0 E(x)/kT) + \frac{2+n^2}{3} \frac{n_{0w}}{y} kT \ln\frac{\sinh(p_0 E(x)/kT)}{p_0 E(x)/kT} = \text{const}, \tag{23}$$

where const is the local pressure between the charged surfaces (as defined in Fig. 1). In the derivation of Eq. (23) the relations

$$\phi'' \phi' dx = \frac{1}{2} d(\phi')^2, \quad \frac{dL}{dx}\phi' dx = L' d\phi,$$

are used. Here $\phi'' \equiv d^2\phi/dx^2$ and $d\phi = \phi' dx$. By subtracting the corresponding bulk values from the local pressure we obtain the expression for the osmotic pressure difference within the MLPB model [65]:

$$\Pi_{MLPB} = -\frac{1}{2}\varepsilon_0 n^2 E(x)^2 + 2n_0 kT(\cosh(-e_0\phi(x)/kT) - 1) - E(x)\frac{2+n^2}{3} n_{0w} p_0 L(p_0 E(x)/kT) + \frac{2+n^2}{3} \frac{n_{0w}}{y} kT \ln\frac{\sinh(p_0 E(x)/kT)}{p_0 E(x)/kT}. \tag{24}$$

Substituting the spatial number density distributions for cations and anions of the electrolyte solution:

$$n_+(x) = n_0 \exp(-e_0\phi(x)/kT), \quad n_-(x) = n_0 \exp(e_0\phi(x)/kT), \tag{25}$$

Eq. (24) reads:

$$\Pi_{MLPB} = -\frac{1}{2}\varepsilon_0 n^2 E(x)^2 + kT(n_+(x) + n_-(x) - 2n_0) - E(x)\frac{2+n^2}{3} n_{0w} p_0 L(p_0 E(x)/kT) + \frac{2+n^2}{3} \frac{n_{0w}}{y} kT \ln\frac{\sinh(p_0 E(x)/kT)}{p_0 E(x)/kT}. \tag{26}$$

For small $p_0 E(x)/kT$ we can expand the 3rd and 4th terms in Eq. (26) into Taylor series to get:

$$\Pi_{MLPB} \approx -\frac{1}{2}\varepsilon_0 n^2 + \frac{2+n^2}{3}\frac{2n_{0w} p_0^2/kT}{2\varepsilon_0} E(x)^2 + kT(n_+(x) + n_-(x) - 2n_0). \tag{27}$$

Using the Onsager expression for bulk relative permittivity (Eq. (17)), Eq. (27) can be rewritten in the usual PB form for the osmotic

pressure within the EDL theory [58]:

$$\breve{\pi}_{PB} = -\frac{1}{2}\varepsilon_0 \varepsilon_{r,b} E(x)^2 + kT(n_+(x) + n_-(x) - 2n_0)$$
$$= -\frac{1}{2}\varepsilon_0 \varepsilon_{r,b} E(x)^2 + 2n_0 kT(\cosh(e_0 \phi(x)\breve{}) - 1). \quad (28)$$

Following a procedure similar to that in the case of derivation of Eq. (24), one can also derive the corresponding expression for osmotic pressure by integrating Eq. (18) of the LPB (see also [47]) to get:

$$\breve{\pi}_{LPB} = -\frac{1}{2}\varepsilon_0 n^2 E(x)^2 + kT(n_+(x) + n_-(x) - 2n_0)$$
$$-E(x)n_{0w} p_0 L(p_0 E(x)\breve{}) + \frac{n_{0w}}{\breve{}} \ln \frac{\sinh(p_0 E(x)\breve{})}{p_0 E(x)\breve{}}. \quad (29)$$

One can also derive Eq. (29) directly from Eq. (24) in the limit of $y \to 1$ and $n \to 1$. For small $p_0 E(x)\breve{}$ we can expand the 3rd and 4th terms in Eq. (29) into Taylor series to get:

$$\breve{\pi}_{LPB} \approx -\frac{1}{2}\varepsilon_0 \left(1 + \frac{n_{0w} p_0^2 \breve{}}{3\varepsilon_0}\right) E(x)^2 + kT(n_+(x) + n_-(x) - 2n_0). \quad (30)$$

Taking into account Eq. (20), the above Eq. (30) attains the PB form of the equation for osmotic pressure, i.e. the form of Eq. (28).

The osmotic pressure is constant everywhere in the solution between the charged plates. In the case of like charged surfaces where a_1 at $x = 0$ and a_2 at $x = H$ (Fig. 1) are both negative or positive and equal ($a_1 = a_2$), the electric field strength at $x = H/2$ is zero, therefore the expression for osmotic pressure within the PB (Eq. (28)), LPB (Eq. (29)) and MLPB model (Eq. (26)) simplifies to:

$$\breve{\pi}_i(x = H/2) = \frac{2n_0}{\breve{}}(\cosh(e_0 \phi_i(x = H/2)\breve{}) - 1),$$
$$i = PB, LPB, MLPB. \quad (31)$$

where $\phi_{PB}(x = H/2)$, $\phi_{LPB}(x = H/2)$ and $\phi_{MLPB}(x = H/2)$ are calculated from the PB, LPB and MLPB equations, respectively.

Fig. 6 shows the osmotic pressure between negatively and positively charged surfaces (upper panel) and between two negatively charged surfaces (lower panel) (see also Fig. 1) as a function of the decreasing distance (H) between them, calculated within the MLPB model (Eq. (24)). The decrease of the osmotic pressure $\breve{}(H)$ is more pronounced for smaller values of the bulk concentration of salt. The predicted values of the osmotic pressure within the MLPB model differ from the corresponding values within the standard PB model only at very small distances H, where within the MLPB model the influence of the space variation of permittivity at both charged surfaces (see Eq. (12)) on the osmotic pressure is not negligible.

4. Finite-sized molecules in an electrolyte solution

Unlike in the LPB model, in this section the finite volume of the molecules is taken into account.

4.1. Gongadze–Iglič equation

Since in bulk solution the number densities of water molecules (n_{0w}), counterions (n_0) and co-ions (n_0) are constant, their number densities can be expressed in a simple way by calculating the corresponding probabilities that a single lattice site in the bulk solution is occupied by one of the three kinds of particles in the electrolyte solution (counterions, co-ions and water molecules) [16,20,24]. However, in the vicinity of a charged surface the number densities of ions and water molecules are influenced by the charged surface

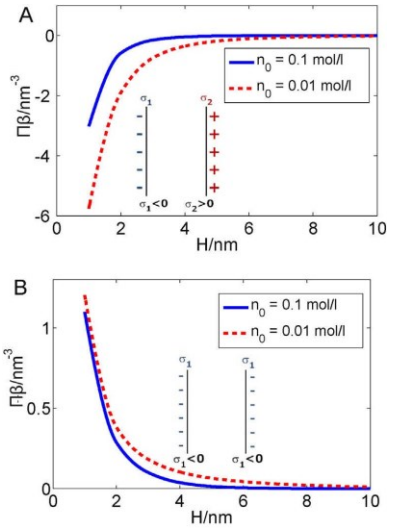

Fig. 6. Osmotic pressure between negatively and positively charged surfaces (upper panel) and between two negatively charged surfaces (lower panel) as a function of the distance between the two surfaces (H) (see Fig. 1), calculated within the MLPB model (Eq. (24)) for two values of the bulk salt concentration $n_0/N_A = 0.01$ mol/l (dashed lines) and $n_0/N_A = 0.1$ mol/l (full lines). Other model parameters are: $a_1 = -0.2$ As/m^2, $a_2 = 0.2$ As/m^2, $T = 298$ K, concentration of water $n_{0w}/N_A = 55$ mol/l and dipole moment of water $p_0 = 3.1$ Debye, where N_A is the Avogadro number.

(see also Fig. 1), so the probabilities that a single lattice site is occupied by a particle of one of the three kinds should be corrected by the corresponding Boltzmann factors, leading to ion and water dipole distribution functions in the form [46]:

$$n_+(x) = n_s \frac{n_0 e^{-e_0 \phi}\breve{}}{n_0 e^{e_0 \phi}\breve{} + n_0 e^{-e_0 \phi}\breve{} + n_{0w}(e^{-y p_0 E}\breve{}^{\cos(\omega)})_\omega}, \quad (32)$$

$$n_-(x) = n_s \frac{n_0 e^{e_0 \phi}\breve{}}{n_0 e^{e_0 \phi}\breve{} + n_0 e^{-e_0 \phi}\breve{} + n_{0w}(e^{-y p_0 E}\breve{}^{\cos(\omega)})_\omega}, \quad (33)$$

$$n_w(x) = n_s \frac{n_{0w}(e^{-y p_0 E}\breve{}^{\cos(\omega)})_\omega}{n_0 e^{e_0 \phi}\breve{} + n_0 e^{-e_0 \phi}\breve{} + n_{0w}(e^{-y p_0 E}\breve{}^{\cos(\omega)})_\omega}, \quad (34)$$

where n_s is the number density of lattice sites defined as $2n_0 + n_{0w}$ and

$$(e^{-y p_0 E}\breve{}^{\cos(\omega)})_\omega = \frac{2\pi \int_0^\pi d(\cos\omega) e^{-y p_0 E}\breve{}^{\cos(\omega)}}{4\pi} = \frac{\sinh(y p_0 E\breve{})}{y p_0 E\breve{}}, \quad (35)$$

is the dipole Boltzmann factor after rotational averaging over all possible angles ω. Eqs. (32)–(34) can be rewritten as [46]:

$$n_+(x) = n_0 e^{-e_0 \phi}\breve{} \frac{n_s}{D(\phi, E)}, \quad (36)$$

$$n_-(x) = n_0 e^{e_0 \phi}\breve{} \frac{n_s}{D(\phi, E)}, \quad (37)$$

$$n_w(x) = \frac{n_{0w} n_s}{D(\phi, E)} \frac{\sinh(y p_0 E\breve{})}{y p_0 E\breve{}}. \quad (38)$$

where $D(\phi, E) = 2n_0 \cosh(e_0\phi\check{}) + (n_{0w}/yp_0E\check{})\sinh(yp_0E\check{})$. Combining Eq. (10)

$$P(x) = -n_w(x)\frac{2+n^2}{3} p_0 L(yp_0E\check{}), \quad (39)$$

and Eq. (38) gives the polarization in the form:

$$P(x) = -\frac{2+n^2}{3}\frac{p_0 n_{0w} n_s}{D(\phi, E)}\frac{L(yp_0E\check{})}{yp_0E\check{}}\sinh(yp_0E\check{}). \quad (40)$$

Using the definition of the function $F(u)$: $F(u) = L(u)(\sinh u/u)$, Eq. (40) transforms into:

$$P = -p_0 n_{0w} n_s \frac{2+n^2}{3}\frac{F(yp_0E\check{})}{D(\phi, E)}. \quad (41)$$

Combining $\varepsilon_r(x) = n^2 + |P|/\varepsilon_0 E$ and Eq. (41) yields the relative (effective) permittivity [46]:

$$\varepsilon_r(x) = n^2 + n_{0w} n_s \frac{p_0}{\varepsilon_0}\frac{2+n^2}{3}\frac{F(yp_0E\check{})}{D(\phi, E)E}. \quad (42)$$

Using the above expression for $\varepsilon_r(x)$, we can then write the Poisson equation into the Gongadze-Iglič (GI) equation in the form [16,46]:

$$\frac{d}{dx}\left(\frac{1}{\varepsilon_0\varepsilon_r(x)}\frac{d\phi}{dx}\right) = 2e_0 n_s n_0\frac{\sinh(e_0\phi\check{})}{D(\phi, E)}, \quad (43)$$

where the macroscopic (net) volume charge density of co-ions and counterions $p_{free}(x)$ (Eqs. (36) and (37)) [46] was taken into account:

$$p_{free}(x) = e_0 n_+(x) - e_0 n_-(x) = -2e_0 n_s n_0\frac{\sinh(e_0\phi\check{})}{D(\phi, E)}. \quad (44)$$

The boundary conditions are (see also Fig. 1):

$$\frac{d\phi}{dx}(x = 0) = -\frac{a_1}{\varepsilon_0\varepsilon_r(x = 0)}, \quad (45)$$

$$\frac{d\phi}{dx}(x = H) = +\frac{a_2}{\varepsilon_0\varepsilon_r(x = H)}, \quad (46)$$

where $\varepsilon_r(x)$ is defined by Eq. (42).

In the limit of vanishing electric field strength ($E \to 0$) and zero potential ($\phi \to 0$), the above derived expression for relative permittivity (Eq. (42)) gives the well-known Onsager expression for permittivity [62]:

$$\varepsilon_{r,b} \cong n^2 + \frac{2+n^2}{3}\frac{^2 n_{0w} p_0^{2\check{}}}{2\varepsilon_0}. \quad (47)$$

It is worth noting that using Eq. (42) the value of the dipole moment $p_0 = 3.1$ D predicts a bulk permittivity of $\varepsilon_r = 78.5$.

In Fig. 7 we show the number density of counter ions $n_+(x)$ and water dipoles $n_w(x)$ as a function of the distance from a negatively planar charged surface x. The predicted depletion of water molecules near the charged surface is due to accumulation of counterions close to to the charged surface in accordance with the excluded volume principle taken into account in the Langevin–Bikerman model.

In Fig. 8 we demonstrate the spatial dependences of the electric potential $\phi(x)$ and relative permittivity $\varepsilon_r(x)$. The decrease of relative permittivity $\varepsilon_r(x)$ towards the charged surface is a consequence of the increased orientational ordering of water dipoles (saturation effect) close to the charged surface (Fig. 4) and the increased depletion of water molecules near the charged surface due to accumulation of counterions (see Fig. 7). The decrease of $\varepsilon_r(x)$ near the charged surface is more pronounced for larger magnitudes of the surface charge density (a) (Fig. 9) due to stronger water ordering at larger |a|, as presented in Fig. 4.

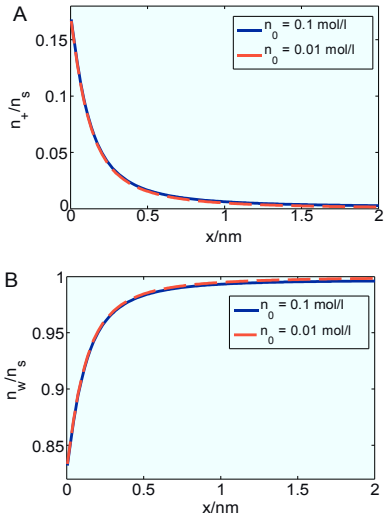

Fig. 7. The relative number density of counterions (n_+/n_s) (upper panel) and water dipoles (n_w/n_s) (lower panel) (calculated using Eqs. (36) and (38)) as a function of the distance from a planar charged surface x calculated for two values of the bulk concentration of counterions and coions n_0/N_A: 0.1 mol/l (full lines) and 0.01 mol/l (dashed lines). Values of parameters assumed: $a = -0.2$ As/m^2, dipole moment of water $p_0 = 3.1$ D, optical refractive index $n = 1.33$, bulk concentration of water $n_{ow}/N_A = 55$ mol/l, where N_A is the Avogadro number. The GI equation (43) was solved numerically as described in [46]).

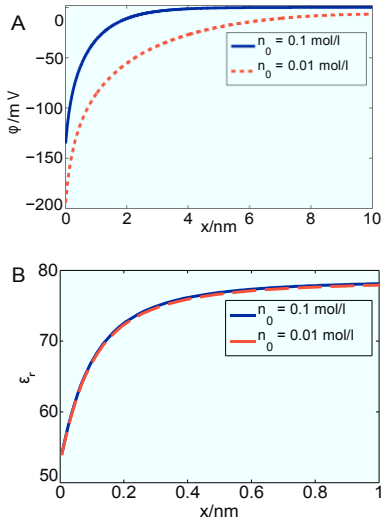

Fig. 8. Electric potential $\phi(x)$ (upper panel) and relative permittivity $\varepsilon_r(x)$ (lower panel) as a function of the distance from the negatively charged surfaces at $x = 0$ (see Fig. 1) and at large H calculated for two values of the bulk concentration of counterions and coions n_0/N_A: 0.1 mol/l (full lines) and 0.01 mol/l (dashed lines). The values of model parameters are the same as given at Fig. 7. The GI equation (43) was solved numerically as described in [46]).

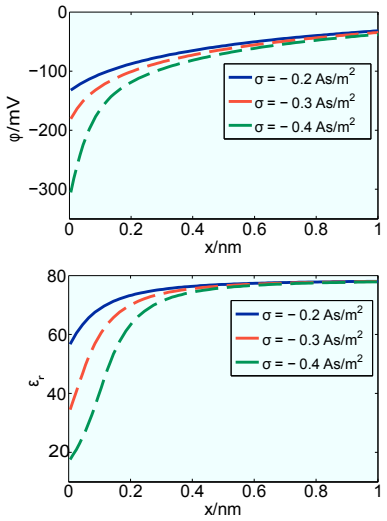

Fig. 9. Electric potential $\phi(x)$ (upper panel) and relative permittivity $\varepsilon_r(x)$ (lower panel) as a function of the distance from the negatively charged surfaces at $x=0$ (see Fig. 1) and at large H calculated for three values of the surface charge density $a=-0.2$ As/m^2 (full lines), $a=-0.3$ As/m^2 (dashed lines) and $a=-0.4$ As/m^2 (dashed-dotted lines) at the bulk concentration of counterions and coions $n_0/N_A = 0.15$ mol/l and $p_0 = 4.79$ D. The values of other model parameters are the same as given at Fig. 7. The LB equation (48) was solved numerically as described in [46]).

Comparing the decrease of relative permittivity at the charged surface $\varepsilon_r(x \approx 0)$ shows that at same (and large enough) a in the MLB model (Fig. 9) $\varepsilon_r(x \approx 0)$ attains a much lower value than in the MLPB model Fig. 5. The observed difference in the predictions of the MLB and MLPB models is the consequence of the depletion of the number density of water molecules in the vicinity of the negatively charged surface ($n_+(x \approx 0)$) (see Fig. 7), which is then reflected in a substantial decrease of the magnitude of polarization (see Eq. (39)) and therefore also in a decrease of $\varepsilon_r(x \approx 0)$.

To estimate experimentally the spatial dependence of the dielectric permittivity ($\varepsilon_r(x)$), an appropriate theoretical model and model parameters should be adopted [66,67]. This means that the experimentally obtained value of $\varepsilon_r(x)$ depends substantially on the type of theoretical model selected. To this end it is debatable whether the thickness of the oriented water layer near the charged surface is around or below 1 nanometre or a few tens of nanometres (see for example [67] and references therein). Teschke et al. [67] used atomic force microscopy and an appropriate theoretical analysis in order to determine the permittivity of an electrolyte solution at a negatively charged mica surface, i.e. at $x=0$. The value $\varepsilon_r(x=0) \leq 10$ was obtained for different kinds of electrolyte solutions in contact with the mica surface [67]. The measured permittivity $\varepsilon_r(x)$ increased with distance from the mica surface to reach a bulk value of ~80 at about 10 nm from the mica surface [66,67]. The estimated value $\varepsilon_r(x=0) \sim 10$ [67] is larger than the corresponding values predicted within the LPB and LB models calculated for $a \simeq -0.1$ to -0.2 As/m^2 as assumed by Teschke et al. [67]. Also the theoretically predicted (by the GI model) thickness of the region of oriented water molecules (coinciding with the region of spatial variation of ε_r) is considerably thinner than the experimental value determined by Teschke et al. [67]. A value of $\varepsilon_r(x=0)$ around 10 can be predicted by the GI equation, but only for $|a| > 0.2$ As/m^2. It is possible that the $|a|$ value adopted in [67] is too small, since it may be influenced by different factors such as, for example, adhesion of ions to the charged surface [5]. However, it is also possible that the simplifications adopted in the theoretical models discussed, such as for example neglecting direct interactions between water dipoles, are the partial origin of these discrepancies. Interestingly, the smaller value of $\varepsilon_r(x=0)$ (around 10) can be predicted within the theoretical approach presented by taking into account the quadrupole moment of water molecules [59] (see also Fig. 2).

4.2. Langevin–Bikerman equation

The above described GI equation (Eq. (43)) [46] may be written in the limit of $y \to 1$ and $n \to 1$ [16,42] to obtain the Langevin–Bikerman equation [42,64]:

$$\frac{d}{dx}\left(\frac{1}{\varepsilon_0 \varepsilon_r(x)} \frac{d\phi}{dx}\right) = 2 e_0 n_s n_0 \frac{\sinh(e_0 \phi^{\sim})}{H(\phi, E)}, \tag{48}$$

where the macroscopic (net) volume charge density of co-ions and counterions $p_{free}(x)$ in the form:

$$p_{free}(x) = -2 e_0 n_s n_0 \frac{\sinh(e_0 \phi^{\sim})}{H(\phi, E)}, \tag{49}$$

is taken into account, while the relative permittivity $\varepsilon_r(x)$ is [16,63,64]:

$$\varepsilon_r(x) = 1 + n_{0w} n_s \frac{p_0 \, F(p_0 E^{\sim})}{\varepsilon_0 \, E \, H(\phi, E)}, \tag{50}$$

where

$$H(\phi, E) = 2 n_0 \cosh(e_0 \phi^{\sim}) + \frac{n_{0w}}{p_0 E^{\sim}} \sinh(p_0 E^{\sim}). \tag{51}$$

The corresponding number densities of counterions, coions and water molecules are [16,64]:

$$n_+(x) = n_0 e^{-e_0 \phi^{\sim}} \frac{n_s}{H(\phi, E)}, \tag{52}$$

$$n_-(x) = n_0 e^{e_0 \phi^{\sim}} \frac{n_s}{H(\phi, E)}, \tag{53}$$

$$n_w(x) = \frac{n_{0w} n_s}{H(\phi, E)} \frac{1}{p_0 E^{\sim}} \sinh(p_0 E^{\sim}). \tag{54}$$

In the limit of vanishing electric field strength ($E \to 0$) and vanishing electric potential ($\phi \to 0$) Eq. (50) transforms into:

$$\varepsilon_{r,b} \cong 1 + \frac{n_{0w} p_0^{2 \sim}}{3 \varepsilon_0}. \tag{55}$$

Comparison between the space dependence of the relative permittivity within the GI equation and within its limiting LB equation for $y \to 1$ and $n \to 1$ shows that consideration of the cavity field and electronic polarizability of water molecules makes the reduction of the permittivity of the electrolyte solution near the charged surface stronger in the case of the GI equation. More importantly, in the LB equation the value $p_0 = 4.79$ D [63,64,68] (similarly as in the LPB model [16,42]) should be used in order to get $\varepsilon_r(x \to \infty) = 78.5$.

4.3. Bikerman equation

In the limit of $p_0 \to 0$ the particle distribution functions (Eqs. (52), (53) and (54)) transform into the Bikerman distribution functions [3,25–28,31,69,70]:

$$n_+(x) = \frac{n_0 n_s}{n_{0w}} \frac{e^{-e_0 \phi^{\sim}}}{1 + (2 n_0 / n_{0w}) \cosh(e_0 \phi^{\sim})}, \tag{56}$$

$$n_-(x) = \frac{n_0 n_s}{n_{0w}} \frac{e^{e_0\phi\breve{}}}{1 + (2n_0/n_{0w})\cosh(e_0\phi\breve{})}, \quad (57)$$

$$n_w(x) = \frac{n_s}{1 + (2n_0/n_{0w})\cosh(e_0\phi\breve{})}, \quad (58)$$

while Eq. (48) transforms into the Bikerman equation [3,25–28,31,69,70]:

$$\varepsilon_0 \varepsilon_{r,b} \frac{d^2\phi}{dx^2} = 2 e_0 n_s n_0 \frac{\sinh(e_0\phi\breve{})}{H(\phi, E)}, \quad (59)$$

where we transformed $\varepsilon_0 \to \varepsilon_{r,b}\varepsilon_0$ with $\varepsilon_{r,b} = 78.5$, while $p_{free}(x)$ is defined by Eq. (49). Eq. (56) predicts a Fermi–Dirac-like distribution for counterions if the lattice constant a is large enough. For higher values of the surface charge density (|a|), the counter-ion density saturates near the charged surface to its close packing value, while the well-known GC model [12,17,18] predicts unreasonably high values beyond the close-packing values (see also [3,25,70]).

4.4. Limiting Poisson–Boltzmann equation

In the limit of very dilute solution everywhere in the electrolyte solution:

$$\sum_{j=+,-} n_j(x) \ll n_w(x), \quad (60)$$

and by taking into account the approximation $n_{0w} \simeq n_s$, we can neglect the second term in the denominator of Eqs. (56) and (57), so the particle distribution functions (Eqs. (56) and (57)) transform into Boltzmann distribution functions within the GC model [2,4,12,17,18,58]:

$$n_+(x) = n_0 e^{-e_0\phi\breve{}}, \quad (61)$$

$$n_-(x) = n_0 e^{e_0\phi\breve{}}, \quad (62)$$

while the number density of water molecules (Eq. (58)) becomes constant [3,70]:

$$n_w(x) = n_{0w}. \quad (63)$$

The Bikerman equation (Eq. (59)) transforms into the Poisson–Boltzmann equation (Eq. (21)) within GC model [12,17,18]:

$$\varepsilon_0 \varepsilon_{r,b} \frac{d^2\phi}{dx^2} = 2 e_0 n_0 \sinh(e_0\phi\breve{}). \quad (64)$$

4.5. Osmotic pressure

Following a similar procedure (presented in Section 3.4) in the derivation of Eqs. (24) and (29), we multiply the LB equation (Eq. (48)) by ϕ' and then integrate it [11,47,63] to get an expression for the osmotic pressure in the form:

$$\breve{}_{LB} = -\frac{1}{2}\varepsilon_0 E(x)^2 - \breve{} \ln \frac{n_s}{H(\phi, E)} - n_w(x) p_0 E(x) L(p_0 E(x)\breve{}). \quad (65)$$

where $H(\phi, E)$ is defined by Eq. (51) and the number density of water $n_w(x)$ by Eq. (54).

For small $p_0 E(x)\breve{}$ and $e_0\phi\breve{}$ we can expand the 2nd and 3rd terms in Eq. (65) into Taylor series to get:

$$\breve{}_{LB} \approx -\frac{1}{2}\varepsilon_0 \left(1 + \frac{n_{0w} p_0^2 \breve{}}{3\varepsilon_0}\right) E(x)^2 + \frac{2n_0}{\breve{}}(\cosh(e_0\phi(x)\breve{}) - 1). \quad (66)$$

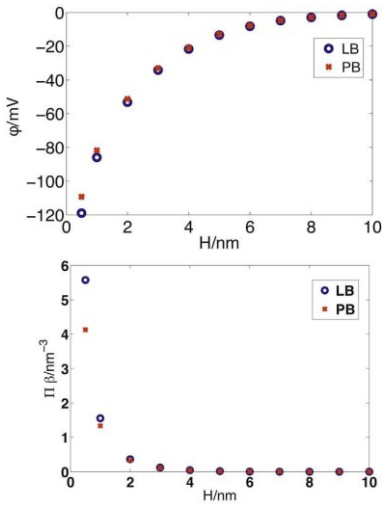

Fig. 10. Electric potential $\phi(x = H/2)$ (upper panel) and osmotic pressure $\breve{}\breve{}$ (lower panel) between two negatively charged surfaces, calculated within the PB model (Eq. (31)) (saltires) and the LB model (Eq. (70)) (empty circles) as a function of the distance between charged surfaces (H) (see Fig. 1) for a bulk salt concentration $n_0/N_A = 0.1$ mol/l. Other model parameters are: $a_1 = -0.3$ As/m^2, T = 298 K, concentration of water $n_{0w}/N_A = 55$ mol/l and dipole moment of water $p_0 = 4.79$ Debye, where N_A is the Avogadro number.

Taking into account Eq. (55) above, Eq. (66) attains the PB form of the equation for osmotic pressure:

$$\breve{}_{PB} = -\frac{1}{2}\varepsilon_0 \varepsilon_{r,b} E(x)^2 + \frac{2n_0}{\breve{}}(\cosh(e_0\phi(x)\breve{}) - 1). \quad (67)$$

In thermodynamic equilibrium the value of the osmotic pressure is equal everywhere in the space between the two charged surfaces (Fig. 1). In the case of like-charged surfaces where a_1 (at x = 0) and a_2 (at x = H) are both negative or positive and equal ($a_1 = a_2$), the electric field strength at x = H/2 is zero, therefore the expression for osmotic pressure within the LB model (Eq. (65)) in the special case of $a_1 = a_2$ simplifies to:

$$\breve{}_{LB}(x = H/2) = \frac{n_s}{\breve{}} \ln \frac{n_{0w}}{n_s} - 2\frac{n_0}{n_{0w}} \cosh(e_0 \phi_{LB}(x = H/2)\breve{}) + 1, \quad (68)$$

where $\phi_{LB}(x = H/2)$ is calculated from LB equation. Adopting the approximation $(n_s/\breve{})\ln(n_{0w}/n_s) = (n_s/\breve{})\ln((n_s - 2n_0)/n_s) = (n_s/\breve{})\ln(1 - 2n_0/n_s) \simeq -2n_0/\breve{}$ Eq. (68) transforms into:

$$\breve{}_{LB}(x = H/2) = -\frac{2n_0}{\breve{}} + \frac{n_s}{\breve{}} \ln 2\frac{n_0}{n_{0w}} \cosh(e_0 \phi_{LB}(x = H/2)\breve{}) + 1. \quad (69)$$

For $2(n_0/n_{0w})\cosh(e_0\phi_{LB}(x = H/2)\breve{}) \ll 1$ Eq. (68) can be further simplified to get:

$$\breve{}_{LB}(x = H/2) = \frac{2n_0}{\breve{}}(\cosh(e_0\phi_{LB}(x = H/2)\breve{}) - 1). \quad (70)$$

In order to shed light on the influence of water polarization and the finite size of molecules on the osmotic pressure in an electrolyte solution confined by two charged surfaces, we compared it within the PB model and the LB model calculated at x = H/2 using Eqs. (31) and (70), respectively (Fig. 10). Since in Eqs. (31) and (70) the electric potential at x = H/2 is the only input data, Fig. 10 shows the

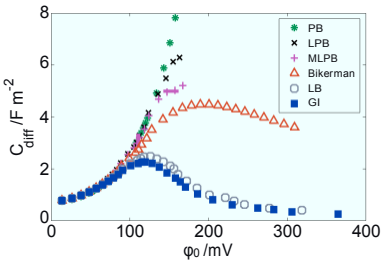

Fig. 11. Differential capacitance as a function of the surface potential ϕ_0 using Gouy–Chapman Eq. (72) (PB), LPB, MLPB, Bikerman, LB and GI model.

corresponding values of $\phi(x = H/2)$ in the PB and LB models. We can see that the osmotic pressure within the like-charged surfaces as a function of the decreasing separation between the surfaces (H) increases more in the LB than in the PB model. The difference between the predictions of the two models is much more significant for small separations $H < 2$ nm, where the influence of water ordering and the excluded volume effect in the LB model becomes important.

5. Differential capacitance

To ascertain whether the described LB mean-field approach which includes the orientational ordering of water, the cavity field, the electronic polarizability of water and the finite size of molecules has improved the agreement between theory and experiments with respect to the classical GC model and the Bikerman model, one should compare the measured and predicted values of electric potential and differential capacitance of the EDL in both models. Using the GI equation, the predicted values of the electric potential at higher surface charge densities a are substantially more negative than the corresponding values within the GC model using the PB equation or Bikerman equation (see also [71,72] and references therein).

Within the GC model, we can estimate the electric potential ϕ_0 at the surface (of an electrode for example) by applying the Grahame equation [5]:

$$a = \sqrt{8 n_0 \varepsilon_0 \varepsilon_r} \cdot \sinh\left(\frac{e_0 \phi_0}{2}\right), \quad (71)$$

where ϕ_0 is the surface potential, i.e. $\phi(x = 0)$. The corresponding GC differential capacitance is [5,72]:

$$C_{GC} = \frac{da}{d\phi^0} = \sqrt{\frac{2 e_0^2 n_0 \varepsilon_0 \varepsilon_r}{2}} \cdot \cosh\left(\frac{e_0 \phi_0}{2}\right). \quad (72)$$

The GC model provides relatively good predictions for monovalent salts at concentrations below 0.2 mol/l in aqueous solutions and magnitudes of the surface potentials between 50 and 80 mV [5].

As can be seen in Fig. 11, the GC differential capacitance C_{GC} monotonously increases as a function of the increasing surface potential ϕ_0. On the contrary, the differential capacitances calculated by the Bikerman, LB and GI equations start to decrease after reaching a maximal value, as shown in Fig. 11. At high ϕ_0 values the calculated LB and GI differential capacitances drop to very small values of the order of magnitude of 10 F/m^2 and smaller, in accordance with the experimental results [71,72] (see also Refs. [5–7,20]). Comparison of the differential capacitance (C_{diff}) calculated using the LB and GI equations shows that the GI equation predicts lower differential capacitances in the region of ϕ_0 values larger than 100 mV (Fig. 11). In the same region of ϕ_0 the values of

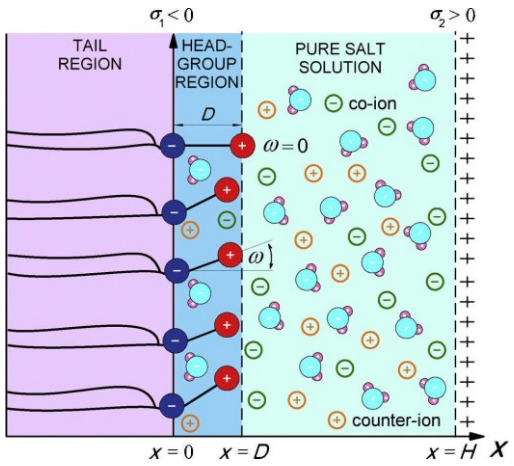

Fig. 12. Negative charges of dipolar (zwitterionic) lipid headgroups are described by a surface charge density a_1 at $x = 0$. The positive charges of the headgroups of the dipolar lipids protrude into the electrolyte solution. Here D is the distance between the charges within a single dipolar lipid headgroup and ω describes the orientational angle of the dipole within a single headgroup. The positive charge of an interacting nanoparticle (macroion) is described by a surface charge density a_2.

C_{diff} calculated using the Bikerman equation are much higher than LB and GI C_{diff}, and exceed the experimental values (see [71,72] and references therein).

The calculated dependences of $C_{diff}(\phi_0)$ in Fig. 11 are presented only for positive values of ϕ_0. The corresponding $C_{diff}(\phi_0)$ curves for negative values of ϕ_0 are the mirror images of the $C_{diff}(\phi_0)$ curves given in Fig. 11 (with respect to the vertical ($\phi_0 = 0$) axis). The Bikerman, LB and GI $C_{diff}(\phi_0)$ curves therefore have a so-called camel (or saddle-like) shape, as also observed experimentally [71,72], in Monte-Carlo simulations [73] and in molecular dynamic simulations [74].

Obviously, the GI equation can also be applied at higher surface charge densities (i.e. high voltage), where the classical PB equation within the GC model completely fails, as the differential capacitance C_{GC} (unlike the experimental results [72]) strongly and monotonously increases with increasing ϕ_0, while in this region of ϕ_0 the Bikerman equation predicts too high values of C_{diff} (see Fig. 11). To conclude, the GI differential capacitance decreases with increasing $\phi_0 > 0$ (after first reaching its maximum) and at large ϕ_0 attains the smallest values of all the models (Fig. 11), similar to that obtained experimentally.

Note that the predicted values of GI differential capacitance at high values of $|\phi_0|$ are also smaller than the corresponding values of C_{diff} predicted by the empirical formula for ε(x) given in [7]. Moreover, if the GI equation is modified by taking into account the distance of closest approach for ions (see also [9,16,75]), the predicted values of C_{diff} would even closely approach the experimental values.

6. Dipolar surface in contact with an electrolyte solution within the modified Langevin–Poisson–Boltzmann model

6.1. Modified Langevin–Poisson–Boltzmann for a dipolar surface

In this section one of the flat surfaces that confines the electrolyte solution (as shown in Fig. 1) is replaced by a flat lipid layer composed of lipid molecules with zwitterionic dipolar headgroups (Fig. 12). Zwitterionic dipolar headgroups composed of a positively

charged trimethylammonium group and a negatively charged carboxyl group (at neutral pH) are described by two charges at a fixed distance D (Fig. 12). The negative charges of the phosphate groups of the dipolar (zwitterionic) lipids are described by a negative surface charge density a_1 at x = 0; the positive surface charge is distributed in the plane at x = H as in previous sections and described by surface charge density $a_2 > 0$. The positively charged surface can, for example, be the surface of a charged nanoparticle (macroion) [65].

The corresponding Poisson's equation in planar geometry can be then written in the form [61]:

$$\frac{d}{dx}\left(\varepsilon_0 \varepsilon_r(x)\frac{d\phi}{dx}\right) = 2e n_0 \sinh(e_0\phi\tilde{}) - p_{Zw}(x), \quad (73)$$

where $p_{Zw}(x)$ is the macroscopic (net) volume charge density of the positive charges of the dipolar (zwitterionic) headgroups:

$$p_{Zw}(0 < x \le D) = \frac{|a_1|P(x)}{D} \quad \text{and} \quad p_{Zw}(x > D) = 0, \quad (74)$$

P(x) is the probability density function indicating the probability that the positive charge of a dipolar lipid headgroup is located at the distance x from the negatively charged surface at x = 0. Here the probability P(x) is defined as [61]:

$$P(x) = A_\zeta \frac{\exp(-e_0\phi(x)\tilde{})}{\exp(-e_0\phi(x)\tilde{})+1}, \quad (75)$$

where A is determined from the normalization condition

$$\frac{1}{D}\int_0^D P(x)\,dx = 1. \quad (76)$$

The parameter ζ is equal to the ratio between the average volume of the positively charged parts of dipolar (zwitterionic) headgroups and the average volume of the salt solution in the headgroup region. The boundary conditions are (see also [16,61]):

$$\frac{d\phi}{dx}(x = 0) = -\frac{a_1}{\varepsilon_0 \varepsilon_r(x = 0)}, \quad (77)$$

$$\phi(x = D_-) = \phi(x = D_+), \quad (78)$$

$$\frac{d\phi}{dx}(x = D_-) = \frac{d\phi}{dx}(x = D_+), \quad (79)$$

$$\frac{d\phi}{dx}(x = H) = +\frac{a_2}{\varepsilon_0 \varepsilon_r(x = H)}. \quad (80)$$

Fig. 13 shows the electric potential ϕ and relative permittivity ε_r as a function of the distance from the negatively charged carboxyl groups at x = 0 (see Fig. 12). It can be seen in Fig. 13 that the relative permittivity $\varepsilon_r(x)$ is considerably decreased within the lipid headgroup region. At the negatively charged plane of the carboxyl groups the value of $\varepsilon_r(x)$ drops to 53 mV. The effect of the negatively charged plane of the carboxyl groups is already very weak at the distance x = D. Far away from the x = 0 surface the value of $\varepsilon_r(x)$ is 78.5 mV.

6.2. Comparison with MD simulations

In recent years molecular dynamics (MD) simulations have given an insight into the interactions between the lipid membrane and the surrounding electrolyte [76–78]. The basis of the MD simulation method is the force field, which determines the behaviour of the studied system. AMBER, CHARMM and GROMOS, for example, are independent descriptions that are widely used for simulations of biological macromolecules. We constructed an MD model of the DPPC planar lipid bilayer in 450 mM KCl using the NAMD program and the all molecule performance CHARMM 36 force field. The model consists of 256 lipid units and 20174 water molecules. The

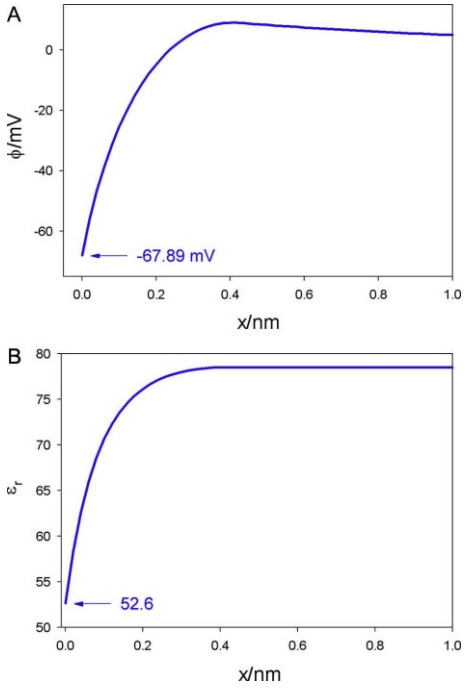

Fig. 13. Calculated electric potential $\phi(x)$ (upper panel)and relative permittivity $\varepsilon_r(x)$ (lower panel) as a function of the distance from the charged planar surface of negatively charged carboxyl groups at x = 0 (see Fig. 12) for large H. The model parameters are: $a_1 = -0.3$ As/m^2, T = 298 K, $p_0 = 3.1$ Debye, D = 0.42 nm bulk concentration of salt $n_0/N_A = 0.1$ mol/l, concentration of water $n_{0w}/N_A = 55$ mol/l, where N_A is the Avogadro number. The MLPB Eq. (73) was solved numerically as described in [61]).

solvent was modelled by 153 K^+ and 153 Cl^- ions [79,80]. Chemical bonds between hydrogen and heavy atoms were constrained to their equilibrium value. Long-range electrostatic forces were taken into account using a fast implementation of the particle mesh Ewald (PME) method [81,82]. The model was examined at constant pressure (1.013×10^5 Pa) and constant temperature (323 K) employing Langevin dynamics and the Langevin piston method. The equations of motion were integrated using the multiple time-step algorithm. A time step of 2.0 fs was employed. Short- and long-range forces were calculated every first and second time steps, respectively. The model was equilibrated and followed for 30 ns. The last 15 ns of the simulation were used for extraction of the dipole orientation angle. From the positions of the P and N atoms the dipole was determined for all 256 lipids in each of 1500 simulation frames and exported to Matlab2012b. The distribution of the vector amplitude corresponding to distance D between the charges was extracted, as well as the distribution of the angle ω between the dipole and the normal vector to the planar lipid bilayer plane (Fig. 12). To obtain the probability density P(x), the projection of each headgroup dipole on the normal vector to the planar lipid bilayer plane was calculated. The average distance between P and N atoms (0.42 nm) was used as a parameter D in the MLPB model (Eq. (73)).

A comparison between the probability density P(x) calculated within the MLPB model (Eq. (75)) and P(x) obtained in the MD simulations is presented in Fig. 14. Fig. 14 shows the space dependence of P(x) calculated by using Eq. (75) for different values of the parameter ζ. As can be seen in Fig. 14, the MLPB model predicts

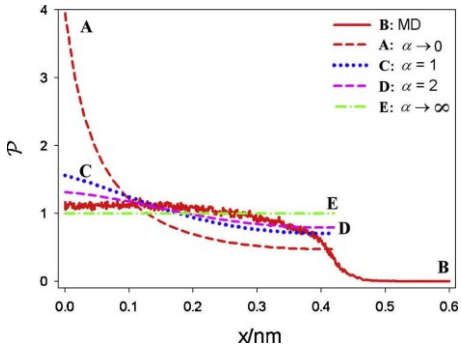

Fig. 14. Probability density P(x) that the positive charge of the lipid dipolar headgroup (see also Fig. 12) is located at distance x from the negatively charged surface calculated by the MLPB model (A,C,D,E) and obtained from MD simulations (B) for $a_1 = -0.27$ As/m^2 and very large H. The values of MLPB model parameters are: T = 323 K, $p_0 = 3.1$ Debye, D = 0.42 nm, bulk concentration of salt $n_0/N_A = 0.1$ mol/l and the concentration of water $n_{0w}/N_A = 55$ mol/l, where N_A is the Avogadro number.

Adapted from [61].

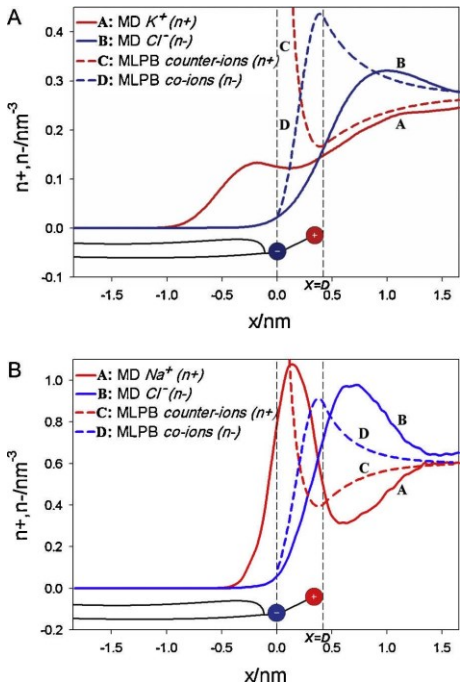

Fig. 15. The calculated number densities of coions (n_-) and counterions (n_+) in the electrolyte solution within the MLPB model (dashed lines) and MD simulations (full lines). Upper panel: $a_1 = -0.27$ As/m^2, $n_0/N_A = 0.45$ mol/l, T = 323 K. The values of other parameters within the MLPB model are the same as in Fig. 13. Lower panel: $a_1 = -0.23$ As/m^2, $n_0/N_A = 1$ mol/l, T = 310 K.

The MD results in the lower panel are adapted from [83].

saturation of the probability density function P(x), corresponding to close packing of the lipid headgroups in accordance with the results of the MD simulations.

It can therefore be concluded that taking into account the finite volume of the lipid headgroups leads to a better agreement between the predicted P(x) dependences within the MLPB model and the MD simulations [61]. In the limit of $\to \infty$ (when all lattice sites are occupied by headgroups) the probability density function P(x) becomes constant as expected. On the other hand, in the limit of small values of (i.e. negligible volume of the headgroups) the probability density P(x), calculated using Eq. (75), approaches the probability density P(x) determined by equation $P(x) = A \exp(-e_0 \phi(x)^{\sim})$ (see also [61]). Fig. 15 shows the number densities of co-ions ($n_-(x)$) and counter-ions ($n_+(x)$) of the electrolyte solution in the vicinity and within the lipid headgroup region calculated within the MLPB model. For comparison, the spatial dependences of K^+, Na^+ and Cl^- determined within the MD simulation are also presented in the same figure. Ion number density profiles of the DPPC planar lipid bilayer in 450 mM KCl were calculated using the presented MD model, while ion number density profiles of the DOPC planar lipid bilayer in 1 M NaCl were kindly provided by Vacha et al. [83–85]. On comparison of $n_-(x)$ and the spatially dependent number density of the Cl^- ion, qualitatively good agreement between the MLPB and both MD predictions can be observed in the region $x > D$ and partially also in the region $0 \le x < D$.

The depletion of negatively charged coions and Cl^- near the negatively charged surface at x = 0 appears in both the MD model and in the MLPB model. The peaks in the number density of coions ($n_-(x)$) and in the spatially dependent number density of Cl^- are predicted within the MD and MLPB models (Fig. 15). The peak in the number density of coions ($n_-(x)$) obtained by the MLPB model is located at a distance D, close to the positive charges of the lipid dipolar headgroups, which is obviously due to the consideration that molecules of electrolyte solution are point-like particles. Both MD simulations showed a peak in the number density of Cl^- ions in the electrolyte solution nearby, but outside the region of the lipid headgroups. Regarding the number density of counter-ions ($n_+(x)$) and the spatial dependence of Na^+ and K^+, a difference in the predictions of the MD model and MLPB model can be observed in the vicinity of the phosphate groups at both sides of the x = 0 plane (Fig. 15, lower panel). Unlike the predictions of the MLPB model, which shows strong accumulation of positively charged counter-ions, the results of MD simulations exhibit a decrease of the number density of Na^+ and K^+. The number density of K^+ ions [83] is maximal in the electrolyte solution. It continuously decreases in the vicinity of the positive charges of the lipid dipolar headgroups. It exhibits a local peak at the distance $x \approx -0.2$ nm which is already in the tail (hydrophobic) region. In the case of Na^+ a strong maximum in number density appears at $x \approx 0.2$ nm, i.e. in the region of the lipid headgroups (Fig. 15). Non-hydrated Na^+ ions are smaller than K^+ ions and therefore also accompanied by a larger ionic surface charge. This could be the reason that they probably penetrate rather deeply into the headgroup region and accumulate near the negative charges of the phosphate groups, while the larger (non-hydrated) K^+ ions prefer to be located in the electrolyte solution. The difference in the number densities of Na^+ and K^+ in the MD model as shown in Fig. 15 (see also [83–85]) is not predicted in the MLPB model. In order to introduce this difference in Na^+ and K^+ number densities into the MLPB model, a different distance of closest approach for different cation species could be introduced in the MLPB model (see also [16]). The observed differences in the predictions of the MD and MLPB models in the vicinity of the x = 0 charged plane partially spring from the fact that within the MLPB model the counterions are treated as point-like particles. Consideration of the finite-size of ions (described within the LB model in Section 4 of this review) would lead to better agreement between the predictions of the MD simulation and the results of theoretical modelling, i.e. lower values of ($n_+(x = 0)$) (see also Fig. 7). In addition, within the MD models Na^+ and K^+ ions may penetrate into the region of the hydrocarbon

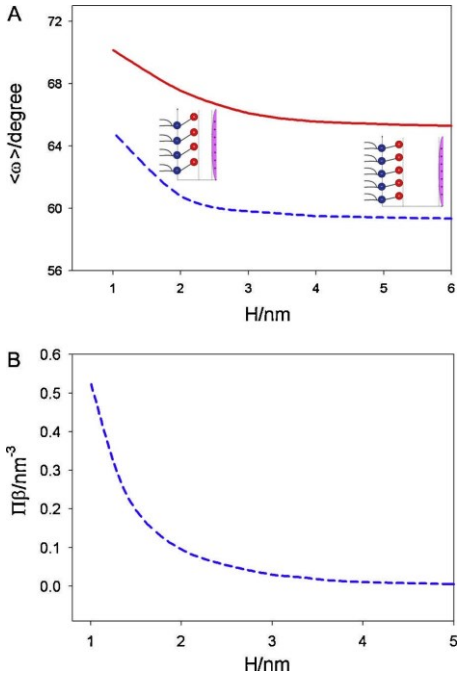

Fig. 16. Average lipid dipolar headgroup (zwitterionic) orientation angle (ω) (for definition see also Fig. 12) (upper panel) and osmotic pressure (lower panel) between the dipolar headgroups and the positively charged surface of macroions as a function of the distance between the plane of the lipid phosphate groups and the surface of the macroion (H) for two values of parameter : 0.5 (full line) and 5 (dotted line). The values of model parameters are: T = 298 K, a_1 = −0.3 As/m², the dipole moment of water p_0 = 3.1 Debye, bulk concentration of salt n_0/N_A = 0.1 mol/l and concentration of water n_{0w}/N_A = 55 mol/l.

Adapted from [65].

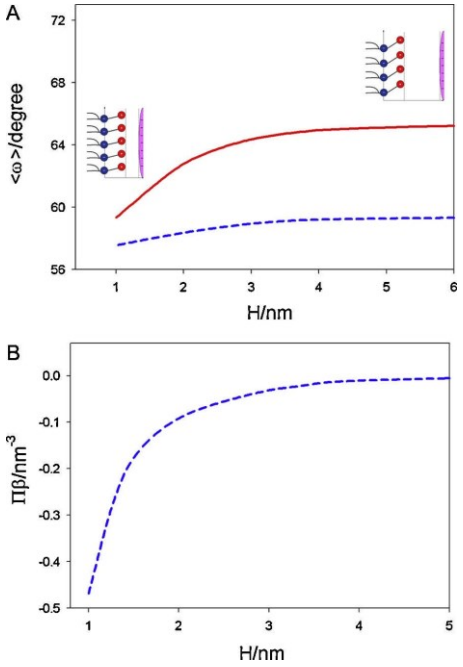

Fig. 17. (A) Average lipid dipolar (zwitterionic) headgroup orientation angle (ω) (for definition see also Fig. 12) and (B) osmotic pressure between the dipolar headgroups and negatively charged surface of macroion as a function of the distance between the plane of the lipid phosphate groups and the surface of macroion (H) for two values of parameter : 0.5 (full line) and 5 (dotted line). The values of model parameters are: T = 298 K, a_1 = −0.30 As/m², the dipole moment of water p_0 = 3.1 Debye, bulk concentration of salt n_0/N_A = 0.1 mol/l and concentration of water n_{0w}/N_A = 55 mol/l.

tails of lipid molecules x < 0, a feature which is not possible within the MLPB model since in the latter case the model boundary conditions prevent cations (as well as anions) from penetrating into the tail region of the lipid molecules x < 0. The predicted maxima and minima in the spatially dependent number densities of ions in the MD are broader and more shallow than those predicted in the MLPB model. This difference may spring from the thermal fluctuations of the lipid bilayer which are considered in MD simulations but not in the MLPB mean-field model. Far away from the charged planar surface, the number density of counter-ions equals the number density concentration of co-ions in the MD and MLPB models.

6.3. Average lipid dipolar headgroup orientation angle and osmotic pressure

Fig. 16 shows the influence of the approaching positively charged surface of a macroion to the surface of a zwitterionic (dipolar) lipid layer on the average orientation of the lipid headgroup orientation angle (< ω >). As expected the value of (ω) increases with decreasing H due to electrostatic repulsion between the positively charged parts of the lipid headgroups and the positively charged macroion. Accordingly also the osmotic pressure between the headgroups and the positively charged macroion increases with decreasing H.

Fig. 17 shows the influence of the approach of the negatively charged surface of a macroion on the average orientation of the lipid dipolar headgroup angle ((ω)). Unlike the previous case presented in Fig. 14, the value of (ω) decreases with decreasing H due to electrostatic attraction between the positively charged parts of the lipid headgroups and the positively charged surface of the macroion. Accordingly the osmotic pressure between the headgroups and the negatively charged macroion surface is also increased with decreasing H.

7. Attraction between like-charged surfaces mediated by macroions with internal charge distribution

In biological systems charged membrane surfaces are surrounded by charged macromolecules, such as DNA and various proteins. Experiments with giant phospholipid vesicles indicated that certain charged plasma proteins [49,86] may induce the coalescence of like-charged lipid vesicles. In this section a mean-field theory is presented to explain the experimentally observed macroion-mediated attraction between like-charged lipid vesicles and other like-charged biological surfaces [87].

As shown in previous sections of this review, classical mean-field EDL theories always predict electrostatic repulsion between like-charged surfaces separated by a solution of dimensionless or finite-sized ions with a single point charge (Figs. 6 and 16) [4,11,47,58,88]. On the other hand, it was shown that the attraction between like-charged biological surfaces may be

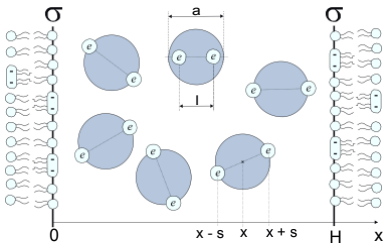

Fig. 18. Schematic illustration of two negatively charged planar lipid bilayer surfaces with surface charge density a separated by a solution containing spherical macroions (counterions) with spatially distributed positive charge. Large spheroidal multivalent macroions are modelled as spheres having average diameter a. The space charge distribution of the macroion is described by two effective poly-ions of charge $e = Ze_0$ located at different well-separated positions (i.e. at a distance $l \le a$) [49]. The main axis of the macroion coincides with the line connecting the two poly-ions. In this particular study charges within a macroion are separated by a fixed distance $l = a$, where a is the diameter of the macroions.

explained by inter-ionic correlations, i.e. particle-particle correlations [57,89–92]. Additionally, other non-electrostatic forces can also contribute to the attraction between biological surfaces, such as van der Waals attraction forces [47], or forces of entropic nature such as oscillatory forces [4,93] or depletion forces [94–96] which become increasingly important in the strong coupling regime. Orientational ordering (intra-ionic correlation) of macroions with internal charge distribution may also lead to attractive forces between like-charged surfaces [49–51,97].

In this section a generalization of the mean-field theory of the EDL is presented by explicitly taking into account the internal space charge distribution [98] of multivalent spheroidal macroions (Fig. 18). Using mean-field density functional theory it is then shown that the orientational ordering of spheroidal macroions with internal charge distribution may give rise to attraction between neighbouring like-charged biological surfaces [49,99]. To assess the limitations of the described mean field theory its predictions are tested using Monte Carlo simulations.

7.1. Spheroidal macroions

In this model we describe two like-charged flat surfaces, each of area A, separated by a distance H. The charge distribution of both membrane surfaces is described by uniform surface charge density a at $x = 0$ and $x = H$ (Fig. 18). The space between the charged surfaces is filled with a solution of charged macromolecules of a single species (counterions). Charged macromolecules are treated in the most simple way as spheroidal macroions (Fig. 18) freely moving in the solution [49,99]. The spheroidal macroion is described as a sphere of diameter a (globular protein) within which two equal positive point charges, each of valency Z ($e = Ze_0$), are separated by distance $l = a$ (Fig. 18). The distance of closest approach of the spherical macroions to the charged surfaces is taken into account, while the direct particle-particle hard core interactions are completely ignored.

The charged spheroidal macroions are subject to positional and orientational degrees of freedom. For each macroion the centre of charge distribution (also its geometric centre) is located at x and n(x) is the corresponding number density of the macroions. The two point charges are located at geometrically opposite points on the surface of the sphere such that, when projected on to the x−axis, their positions are at $x + s$ and $x - s$ respectively, as shown in Fig. 18.

Taking into account that the two point charges of the macroions are indistinguishable, all possible orientations of the macroion can be described by values of s in the interval $0 < s < l/2$ (see Fig. 18).

Therefore, the orientation of the spherical macroion is specified by the conditional probability p(s|x) which must satisfy the relation [58,99]:

$$\frac{2}{l}\int_0^{l/2} p(s|x)\,ds = 1, \tag{81}$$

where $p(s|x) = 0$ for any x and $|s| > l/2$.

The equilibrium configuration of the system can be determined by minimizing the free energy. The free energy of the system per unit area is [49]:

$$\frac{F}{A} = kT\int_0^H dx\,[\varepsilon_0\,\varepsilon_{r,b}\,\phi'(x)^2 + [n(x)\,\ln(n(x)\,v_0) - n] + n(x)(p(s|x)\,\ln p(s|x))], \tag{82}$$

where the first term is the electrostatic contribution to the free energy. The prime denotes the first derivative of the electric potential ϕ with respect to x. The second term is the contribution due to configurational entropy [3,13,16], where v_0 is the volume of a single lattice site. The third term denotes the contribution of orientational ordering of the macroions. The centres of the macroions are allowed to be distributed in the region $l/2 \le x \le H - l/2$, i.e. the distance of closest approach is taken into account to ensure that the spheroidal macroions are confined within the region defined by the charged walls. The average of an arbitrary function g(x) is defined as:

$$(g(x)) = \frac{2}{l}\int_0^{l/2} g(x,s)ds. \tag{83}$$

In the following, the limits of integration in the free energy expression are extended to infinity in both directions:

$$\frac{F}{A} = kT\int_{-\infty}^{\infty} dx[\varepsilon_0\varepsilon_{r,b}\,\phi'(x)^2 + [n(x)\,\ln(n(x)\,v_0) - n] + n(x)\,(p(s|x)\,\ln p(s|x))], \tag{84}$$

where the values of n(x) and $\phi'(x)$ are assumed to be zero outside the space between the two charged surfaces.

The equilibrium state of the system is determined by the minimum of the total free energy F, subject to the constraints that (a) the orientational probability of the spheroidal charged macroions integrated over all possible projections (Eq. (81)) is equal to one, and that (b) the total number of charged macroions is conserved [3,49]. To solve this variational problem, a functional $\int_{-\infty}^{\infty} \ldots dx$ is constructed:

$$\int_{-\infty}^{\infty} Fdx = \frac{F}{AkT} + \int_{-\infty}^{\infty} A(x)\,n(x)\left[\frac{2}{l}\int_0^{l/2} p(s|x)ds - 1\right]dx + f_L\int_{-\infty}^{\infty} n(x)\,dx, \tag{85}$$

where A(x) and f_L are the local and global Lagrange multipliers, respectively.

Taking into account Eq. (84), we can rewrite Eq. (85) in the form:

$$\int_{-\infty}^{\infty} Fdx = \int_{-\infty}^{\infty} dx\,[\varepsilon_0\,\varepsilon_{r,b}\,\phi'(x)^2/kT + n(x)\,\ln(n(x)\,v_0) - n(x) + n(x)(p(s|x)\ln p(s|x))] + \int_{-\infty}^{\infty} dx\,n(x)A(x)[(p(s|x)) - 1] + f_L\int_{-\infty}^{\infty} n(x)\,dx. \tag{86}$$

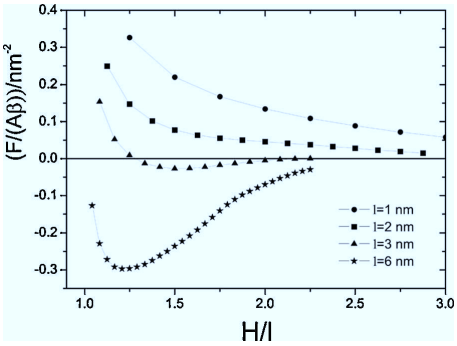

Fig. 19. The normalized free energy F/AkT as a function of the distance between two negatively charged surfaces H calculated for four different extensions between charges l within the charged macroions. Other model parameters are Z = 1, a = −0.033 As/m^2 and l_B = 0.7 nm (adapted from [49]). The hard core interaction between the macroions and charged walls is taken into account by means of the distance of closest approach (l/2), while the hard core interaction between charged macroions is not considered.

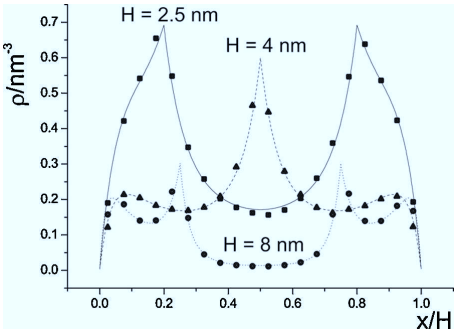

Fig. 20. Profile of the volume charge density due to positively charged divalent macroions (Z = 1) between two negatively charged surfaces. Lines represent the solutions of the integro-differential Eq. (89), points represent results of the Monte Carlo simulations. Model parameters: l = 2 nm, a = −0.07 As/m^2. The hard core interaction between the macroions and charged walls is taken into account by means of the distance of closest approach (l/2), while the hard core interaction between charged macroions is not considered.
Adapted from [49].

In equilibrium, the first variation of the functional $\int_{-\infty}^{\infty} F dx$ should be zero which, after some rearrangements, yields the equation for the number density [49]:

$$n(x) = \frac{e^{-fL}}{V_0}\left(e^{-Ze_0\phi(x+s)-Ze_0\phi(x-s)}\right) \quad (87)$$

and the volume charge density [49]:

$$p(x) = \frac{2Ze_0}{V_0}\left(e^{-Ze_0\phi(x)-Ze_0\phi(x+2s)-fL}\right). \quad (88)$$

The averaging is performed over s. The derived expression Eq. (88) for the volume charge density p(x) and the Poisson equation yield the integro-differential equation for the reduced electric potential in the form [49]:

$$\phi''(x) = -\frac{2Ze_0}{\varepsilon_0\varepsilon_{r,b}V_0}\left(e^{-Ze_0\phi(x)-Ze_0\phi(x+2s)-fL}\right). \quad (89)$$

The boundary conditions for Eq. (89) at the two charged surfaces x = 0 and x = H are:

$$\phi'(x=0) = -\frac{a}{\varepsilon_0\varepsilon_{r,b}}, \quad \phi'(x=H) = \frac{a}{\varepsilon_0\varepsilon_{r,b}}. \quad (90)$$

In this theoretical model, the finite size of the charged macroions is taken into account only by considering the distance of closest approach of the centre of the macroions to the charged surface (l/2). Eq. (89) was solved numerically as described in [49]. The solution of the integro-differential Eq. (89) yields the equilibrium potential $\phi(x)$, and the corresponding equilibrium distribution n(x) and probability density p(s|x). When the charged macroions are uniformly distributed between the charged surfaces, the free energy is independent of the distance between the charged surfaces and can therefore be taken as a reference value in determining the values of the equilibrium free energy [3,49]. Fig. 19 shows the electrostatic free energy (Eq. (84)) as a function of the distance between the two negatively charged surfaces for different distances between the charges within a single macroion (see also Fig. 18). For small surface charge density |a| and small separation between the charges within the charged macroion, the interaction was found to be repulsive for all distances between the charged surfaces [49]. However, large enough |a| and l yield non-monotonous behaviour of the free energy f with a minimum representing the equilibrium distance between the charged membrane surfaces (Fig. 19).

We now discuss a comparison of the results obtained from the above presented theoretical analysis and Monte Carlo (MC) simulations. The results of solving the integro-differential Eq. (89) and the results of Monte-Carlo simulation were shown to be in excellent agreement [49,99]. Monte Carlo simulations are widely used to describe solutions of point-like ions [58,100,101], finite-sized ions [102–104], or ions with internal charge distribution [49–51,99] in contact with charged surface(s). In the MC simulation presented in this section, the standard MC Metropolis algorithm [105] with Lekner periodic boundary conditions [106] in directions parallel to the charged walls was used [49,99]. In each MC step, a spherical macroion is chosen at random to be rotated around its centre or linearly displaced [105] as described in [49,99]. Computation of the potential in a periodic system with 2-D symmetry is performed by the Leckner–Sperb method [101,106,107], which is an alternative to the Ewald summation [108].

Fig. 20 shows the results obtained from solutions of the integro-differential equation and MC simulations for the volume charge density p(x) in an aqueous solution of divalent charged spherical macroions (Z = 1) confined between two negatively charged planar surfaces separated by a distance H. The excellent agreement between the calculated volume charge density profiles (curves) and the results of Monte Carlo simulations (points) is evident [49,99]. For a value of H which is comparable to the separation of charges within a single charged macroion (l), i.e. for H = 2.5 nm (squares), the charge density profile in the solution exhibits a single peak at each side, indicating that the macroions (on the average) orient to form electrostatic bridging between the two charged planar surfaces. On the other hand, for somewhat larger distances (H = 4 nm) between the charged surfaces, we see a peak in the middle (triangles), which corresponds to partial overlapping of the ordered macroions in the middle of the space between the two like-charged surfaces (see Fig. 21). The charges on the macroions of both layers contribute to p(x) at x = H/2, so a central peak in the volume charge density p(x) is formed. For even larger distances (H = 8 nm), the profile exhibits twin-peaks close to the two charged surfaces due to orientational ordering of the macroions, with one charge close to the charged surface.

The concept of a free energy decrease due to orientational ordering we previously used in determination of the equilibrium shapes of phospholipid bilayers (Refs. [109–111]), where it was shown that the in-plane orientational ordering of anisotropic membrane

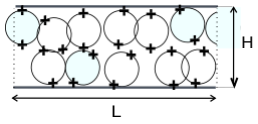

Fig. 21. Schematic representation of spherical divalent macroion positions and orientations at distance H ≈ 4 nm, where the diameter of the macroion is l = 2 nm. At the distance H = 4 nm, a peak in the density distribution of charges appears in the middle between the surfaces, as seen in Fig. 20.

constituents can decrease the free energy of a phospholipid vesicle by stabilizing shapes with larger area regions having unequal principal membrane curvatures. The in-plane ordering of membrane components was later generalized to three-dimensional ordering of ions in the EDL [49,51,97]. The results presented in this section show that internal degrees of freedom (orientational and positional ordering of constrained charges), coupled with fixed distance imposed on pairs of charges within the macroions, may contribute to the decrease of the free energy of the system of spherical macroions confined between two charged surfaces. As shown in Fig. 19 the effect may be strong enough to cause an attractive interaction between the like-charged surfaces. This attractive interaction completely vanishes when the two charges within a single macroion are brought towards the centre of the ion, as happens in the standard GC theory, to which our equations reduce when the parameter l approaches zero [49].

Fig. 19 shows that the interaction between the charged surfaces changes from attractive to repulsive as the distance between the charges in a single charged macroion (l) decreases at a fixed a. This result indicates that the attraction between the like-charged surfaces presented in Fig. 19 originates from the imposed inter-charge interaction expressed by the fixed distance between the charges within a single macroion (Fig. 18), i.e. from intra-particle charge interactions.

7.2. Spheroidal and rod-like macroions

Another interesting feature of the problem of macroions as mediators of attractive interactions between like-charged surfaces is a comparison between the orientational ordering of spherical and rod-like macroions near charged surfaces and/or between charged surfaces. The origin of the bridging attraction in the system of spherical charged macroions with quadrupolar internal charge distribution (Fig. 19) [49,99] is identical to that in the system of rod-like charged macroions [50,51,97]; namely, the energetically favourable orientational ordering of the quadrupoles in the spatially varying electric field. A comparison of the orientational ordering of rod-like macroions, spherical macroions without hard core interactions between the macroions (overlapping of the macroions is allowed) and spherical macroions with hard core interactions between macroions (overlapping of the macroions is not allowed) is presented in Fig. 22. The volume charge distribution of rod-like and spherical positively charged quadrupolar macroions, confined in the space between two like-charged surfaces with separation H > 2l, was calculated using MC simulations for different values of the valency of the macroions (Z) and different values of the surface charge density (a) of the negatively charged surfaces (Fig. 22).

The calculated volume charge distribution p(x) and the average order parameter S (Fig. 22) show distinctive differences in the average orientation of rod-like and spherical macroions near the charged surfaces for a distance between the two charged surfaces H = 10 nm. It can be seen in Fig. 22 that for low values of the surface charge density (|a|) and small valency of the macroions (Z), the rod-like macroions are not oriented in a direction orthogonal to the charged plates, but predominantly in a direction parallel to the charged surfaces, i.e. they are predominantly attached to the two charged planar surfaces (see also Fig. 23). Accordingly, the distribution peak of the volume charge density of the rod-like macroions is located at x = 0 (the other one at x = H). On the other hand, for higher values of (|a|) and Z both kinds of spherical macroions are predominantly oriented orthogonally to the charged surface and

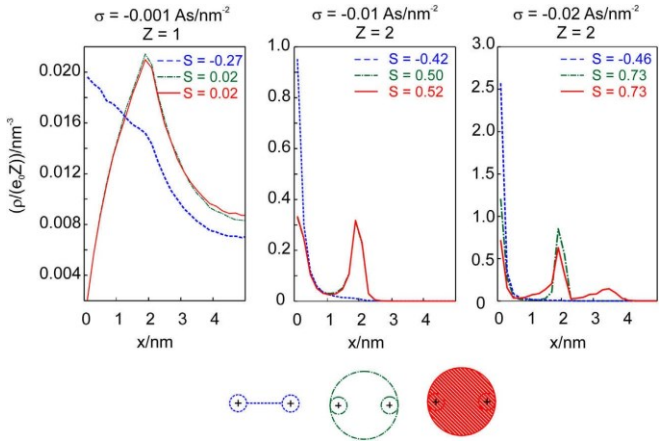

Fig. 22. Volume charge distribution between two charged surfaces for three different kinds of macroions: rod-like macroions (blue), spherical macroions without a hard core interaction between the macroions (green), and spherical macroions with a hard core interaction between the macroions effect (red), predicted by MC simulation for H = 10 nm, l = 2 nm and different valency of the macroions (Z) and different surface charge density (a). Because of symmetry, only half of the space between the two charged surfaces is plotted. H = 10 nm, l = 2 nm. The nematic order parameter S is defined as $S = (\langle 3\cos^2(\vartheta) - 1\rangle/2)$, where the angle ϑ describes the orientation of the axis connecting the two charges of the nanoparticle with respect to the x axis. S = 0 means that the nanoparticles are not oriented, while S = 1 corresponds to the nanoparticles being fully oriented with respect to the x-axis. The hard core interaction between the macroions and charged walls is taken into account by means of the distance of closest approach (l/2).

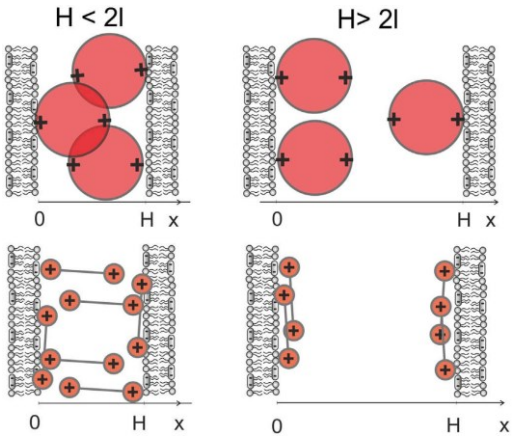

Fig. 23. Schematic figure representing the different orientational ordering of rod-like and spherical macroions at large and small distance between two like-charged surfaces. Due to their stronger average orientation in the orthogonal direction spherical macroions are better mediators of attractive interactions between like-charged surfaces than rod-like macroions.

therefore exhibit two peaks in their volume charge distribution. The excluded volume effect (i.e. hard core interactions between spherical macroions) is important only in the third case for $Z = 2$ and $a = -0.02\,As/m^2$, i.e. in the stronger coupling regime. In the third (extreme right) panel of Fig. 22 it can also be seen that considering hard core interactions between the macroions results in the appearance of the third peak in the volume charge distribution of the spherical macroions as the consequence of the exclusion volume effect. Namely, in this case the spherical macroions close to the charged surface completely fill the space in the first row (saturation) and the rest of them are forced to find the energetically most favourable location further away from the charged surface. Nevertheless, the average order parameter of the spherical macroions is the same if we take into account the hard core interactions between macroions or not.

The average orientation of macroions in the solution between two like-charged surfaces may have a strong influence on the system's free energy and consequently also on the attractive/repulsive interaction between like-charged surfaces as indicated in [49–51,99]. Stronger orientation of the macroions in the orthogonal direction with respect to the charged surface contributes to stronger attraction between the like-charged surfaces. Based on the results presented in [10,49,112], Fig. 23 shows schematically the difference in orientational ordering between rod-like and spherical macroions for different distances between the two like-charged surfaces (H). For small H ($l < H < 2l$) some of the rod-like macroions are oriented orthogonally to the charged surfaces and some in a direction parallel to the charged surfaces (Fig. 23). On the other hand, for larger H ($H > 2l$) all rod-like macroions are oriented in a direction parallel to the charged surfaces (Fig. 23). In accordance with our observation, a rod-like macroion-mediated attractive interaction between two like-charged surfaces was predicted in the range $l < H < 2l$, but not in the range $H > 2l$ [50].

On the other hand, at high enough ($|a|$) and Z spherical macroions are mostly oriented orthogonally even for higher surface separations $H > 2l$ (Fig. 23) leading to the conclusion that spherical macroions are better mediators of attractive interactions between like-charged surfaces than rod-like macroions (see also [49–51,99]).

To conclude, it is shown in this section that the density functional theory described (which does not include direct interactions between macroions) and the Monte Carlo simulation (which in contrast does include direct interactions between macroions) show remarkably good agreement between their predictions (Fig. 20). We may thus conclude that the bridging effect arising from the orientational ordering of macroions with internal charge distribution may explain the observed attractive interaction between like-charged surfaces [49–51,99]. Direct interaction between charged macroions may give rise to additional effects.

8. Conclusions

The results presented in this review provide an interesting perspective on the importance of modelling the relative permittivity in understanding EDL phenomena. A key feature that contributes to better agreement between theory and experiment is the inclusion of space-dependent permittivity, which is in general a function of the electric potential and electric field. Analytical expressions for its space dependence are derived within both models, i.e. within the LPB and LB models. Importantly, the EDL models presented in this work take into account the excluded-volume effect, orientational ordering of water in the saturation regime, the electronic polarizability of water and the concept of the cavity field. All these enable us to understand the mechanisms responsible for the spatial dependence of permittivity.

As an example of the application of the EDL models described, we calculated the differential capacitance of a charged surface in contact with an electrolyte solution as a function of the surface potential within the MLB model. Unlike the prediction of classical GC theory where the differential capacitance is a monotonous increasing function of the surface potential, in the MLB model, after reaching its maximal value, the differential capacitance decreases with increasing surface potential in accordance with experimental results. As another possible application we presented a model of a zwitterionic lipid surface in contact with an electrolyte solution of monovalent salt ions and water dipoles. It was shown that the permittivity in the zwitterionic headgroup region is decreased, while the corresponding electric potential becomes strongly negative.

The osmotic pressure of an electrolyte solution between a zwitterionic lipid surface and a charged particle (macroion) was also considered theoretically. It was indicated that in the close vicinity of the positively charged macroion the zwitterionic lipid headgroups are less extended in the direction orthogonal to the membrane surface, which coincides with the increase of osmotic pressure between the lipid surface and the macroion. In the case of a negatively charged macroion the effect is the opposite, i.e. the zwitterionic lipid headgroups are more extended, while the osmotic pressure between the lipid surface and the macroion is decreased.

Using the LPB and LB model equations described predicts that the attractive interaction between like-charged surfaces with an intermediate solution of monovalent ions is always repulsive. Therefore we hypothesized that the charged particles with a quadrupolar internal charge distribution may act as mediators, resulting in attraction between the like-charged surfaces. The above hypothesis was proved within the density functional theory (which is a mean field approach) and also by using Monte Carlo (MC) simulations. A remarkably a good agreement between the predictions of both methods was demonstrated.

Nowadays, numerical simulations provide a new window into the theoretical description of different physical phenomena where analytical solutions do not exist. The sophistication of the GC model and its PB equation allowed us to include additional properties of

the EDL, in an attempt to better characterize its complex behaviour; this would not be possible without the use of numerical simulations which were crucial in the validation of the models with high surface charge density regimes. Some of the predictions of the EDL mean-field theoretical considerations were also evaluated by molecular dynamics (MD) simulation and Monte Carlo (MC) simulations.

But finally there still remains the question of which important physical properties of the EDL are not yet considered in existing theoretical models of the EDL. This formidable task and further refinement and understanding of EDL behaviour remain the long-term goal.

Acknowledgements

This work was supported by Slovenian Research Agency (ARRS) grants J3-2120, J1-4109, J1-4136, J3-4108 and P2-0232. A.V. was also supported by the European Social Fund and SMARTEH. P.B.S., and E.G. partially by a grant from the Slovenian Human Resources Development and Scholarship Fund.

References

[1] S.W. Kenkel, J.R. Macdonald, A lattice model for the electrical double layer using finite-length dipoles, Journal of Chemical Physics 81 (1984) 3215–3222.
[2] G. Cevc, Membrane electrostatics, Biochimica et Biophysica Acta 1031 (3) (1990) 311–382.
[3] V. Kralj-Iglič, A. Iglič, A simple statistical mechanical approach to the free energy of the electric double layer including the excluded volume effect, Journal of Physics II (1996) 477–491.
[4] J.N. Israelachvili, Intermolecular and Surface Forces, Academic Press, London, 1997.
[5] H.J. Butt, K. Graf, M. Kappl, Physics and Chemistry of Interfaces, Wiley-VCH, Weinheim, 2003.
[6] A.A. Kornyshev, Double-layer in ionic liquids: paradigm change? Chemical Physics Letters 111 (2007) 5545–5557.
[7] M. Bazant, M. Kilic, B. Storey, A. Ajdari, Towards an understanding of induced-charge electrokinetics at large applied voltages in concentrated solutions, Advances in Colloid and Interface Science 152 (2009) 48–88.
[8] Z. Arsov, M. Rappolt, J. Grdodolnik, Weakened hydrogen bonds in water confined between lipid bilayers: the existence of a long-range attractive hydration force, ChemPhysChem 10 (9) (2009) 1438–1441.
[9] T. Nagy, D. Henderson, D. Boda, Simulation of an electrical double layer model with a low dielectric layer between the electrode and the electrolyte, Journal of Physical Chemistry B (2011) 11409–11419.
[10] D. Kabaso, E. Gongadze, Š Perutkova, V. Kralj-Iglič, C. Matschegewski, U. Beck, U. van Rienen, A. Iglič, Mechanics and electrostatics of the interactions between osteoblasts and titanium surface, Computer Methods in Biomechanics and Biomedical Engineering 14 (5) (2011) 469–482.
[11] R. Misra, S. Das, S. Mitra, Electric double layer force between charged surfaces: effect of solvent polarization, Journal of Chemical Physics 138 (2013) 114703.
[12] S. McLaughlin, The electrostatic properties of membranes, Annual Review of Biophysics and Biophysical Chemistry 18 (1989) 113–136.
[13] A. Safran, Statistical Thermodynamics of Surfaces, Interfaces, and Membranes, Addison-Wesley Publishing Company, 1994.
[14] C.W. Outhwaite, A treatment of solvent effect in the potential theory of electrolyte solution, Molecular Physics 31 (5) (1976) 1345–1357.
[15] C.W. Outhwaite, Towards a mean electrostatic potential treatment of an ion-dipole mixture or a dipolar system next to a plane wall, Molecular Physics 48 (3) (1983) 599–614.
[16] E. Gongadze, U. van Rienen, V. Kralj-Iglič, A. Iglič, Spatial variation of permittivity of an electrolyte solution in contact with a charged metal surface: a mini review, Computer Methods in Biomechanics and Biomedical Engineering 16 (2013) 463–480.
[17] M.G. Gouy, Sur la constitution de la charge electrique à la surface d'un electrolyte, Journal de Physique et Le Radium (1910) 457–468.
[18] D.L. Chapman, A contribution to the theory of electrocapillarity, Philosophical Magazine 6 (1913) 475–481.
[19] R. Heinrich, M. Gaestel, R. Glaser, The electric potential profile across the erythrocyte membrane, Journal of Theoretical Biology 96 (1982) 211–231.
[20] E. Gongadze, Influence of the surface structure of a biomaterial on the field distribution in the neighbouring biosystem, Dr. Ing. Thesis, University of Rostock, Rostock, 2011.
[21] O. Stern, Zur theorie der elektrolytischen doppelschicht, Zeitschrift fur Elektrochemie 30 (1924) 508–516.
[22] H. Helmholtz, Studien über elektrische grenzschichten, Annals of Physics 243 (7) (1879) 337–382.
[23] J.N. Israelachvili, H. Wennerstrom, Role of hydration and water structure in biological and colloidal interactions, Nature 379 (1996) 219–225.
[24] E. Gongadze, U. van Rienen, A. Iglič, Generalized Stern models of an electric double layer considering the spatial variation of permittivity and finite size of ions in saturation regime, Cellular and Molecular Biology Letters 16 (2011) 576–594.
[25] J. Bikerman, Structure and capacity of electrical double layer, Philosophical Magazine 33 (1942) 384–397.
[26] T. Grimley, N. Mott, The contact between a solid and a liquid electrolyte, Discussions of the Faraday Society 1 (1947) 3–11.
[27] T. Grimley, The contact between a solid and a liquid electrolyte, Proceedings of the Royal Society of London Series A 201 (1950) 40–61.
[28] V. Freise, Zur theorie der diffusen doppelschicht, Zeitschrift fur Elektrochemie 56 (1952) 822–827.
[29] M. Eigen, E. Wicke, Zur theorie der starken elektrolyte, Naturwissenschaften 38 (1951) 453–454.
[30] E. Wicke, M. Eigen, Über den einfluß des raumbedarfs von ionen in wässriger lösung auf ihre verteilung im elektrischen feld und ihre aktivitätskoeffizienten, Zeitschrift fur Elektrochemie 56 (1952) 551–561.
[31] M. Eigen, E. Wicke, The thermodynamics of electrolytes at higher concentrations, Journal of Physical Chemistry 58 (1954) 702–714.
[32] M. Manciu, E. Ruckenstein, Lattice site exclusion effect on the double layer interaction, Lamgmuir 18 (2002) 5178–5185.
[33] I. Borukhov, Charge renormalization of cylinders and spheres: ion size effect, Journal of Polymer Science Part B: Polymer Physics 42 (2004) 3598.
[34] E. Trizac, J.L. Raimbault, Long-range electrostatic interactions between like-charged colloids: steric and confinement effects, Physical Review E 60 (1999) 6530–6533.
[35] G. Barbero, L.R. Evangelista, D. Olivero, Asymmetric ionic adsorption and cell polarization in liquid crystals, Journal of Applied Physics 87 (2000) 2646–2648.
[36] L. Lue, N. Zoeller, D. Blankschtein, Incorporation of nonelectrostatic interactions in the Poisson–Boltzmann equation, Langmuir 15 (1999) 3726–3730.
[37] S. Lamperski, C.W. Outhwaite, Exclusion volume term in the inhomogeneous Poisson–Boltzmann theory for high surface charge, Langmuir 18 (2002) 3423–3424.
[38] I. Bivas, Y.A. Ermakov, Elasticity and electrostatics of amphiphilic layers, Advances in Planar Lipid Bilayers and Liposomes 5 (2007) 313–343.
[39] A. Silalahi, A. Boschitsch, R. Harris, M. Fenley, Comparing the predictions of the nonlinear Poisson–Boltzmann equation and the ion size-modified Poisson–Boltzmann equation for a low-dielectric charged spherical cavity in an aqueous salt solution, Journal of Chemical Theory and Computation 6 (12) (2010) 3631–3639.
[40] D.W.R. Gruen, S. Marčelja, Spatially varying polarization in water, Journal of the Chemical Society, Faraday Transactions II (79) (1983) 225–242.
[41] J.J. Lopez-Garcia, J. Horno, C. Grosse, Poisson–Boltzmann description of the electrical double layer including ion size effects, Langmuir 27 (23) (2011) 13970–13974.
[42] E. Gongadze, U. van Rienen, V. Kralj-Iglič, A. Iglič, Langevin–Poisson–Boltzmann equation: point-like ions and water dipoles near a charged membrane surface, General Physiology and Biophysics 30 (2) (2011) 130–137.
[43] A. Bandopadhyay, S. Chakraborty, Combined effects of interfacial permittivity variations and finite ionic sizes on streaming potentials in nanochannels, Langmuir 28 (17552) (2012) 13970–13974.
[44] I. Szalai, S. Nagy, S. Dietrich, Nonlinear dielectric effect of dipolar fluids, Journal of Chemical Physics 131 (2009) 154905.
[45] I. Szalai, S. Dietrich, Magnetization and susceptibility of ferrofluids, Journal of Physics: Condensed Matter (2008) 204122.
[46] E. Gongadze, A. Iglič, Decrease of permittivity of an electrolyte solution near a charged surface due to saturation and excluded volume effects, Bioelectrochemistry 87 (2012) 199–203.
[47] E. Verwey, J. Overbeek, Theory of the Stability of Lyophobic Colloids, Elsevier Publishing Company Inc., Weinheim, 1948.
[58] D.F. Evans, H. Wennerström, The Colloidal Domain: Where Physics, Chemistry, Biology, and Technology Meet, 2nd ed., Wiley-VCH, New York, 1999.
[49] J. Urbanija, K. Bohinc, A. Bellen, S. Maset, A. Iglič, V. Kralj-Iglič, P.S. Kumar, Attraction between negatively charged surfaces mediated by spherical counterions with quadrupolar charge distribution, Journal of Chemical Physics 129 (2008) 105101.
[50] Y. Kim, J. Yi, P. Pincus, Attractions between like-charged surfaces with dumbbell-shaped counterions, Physical Review Letters 101 (2008) 208305.
[51] S. May, A. Iglič, J. Reščič, S. Maset, K. Bohinc, Bridging like-charged macroions through long divalent rod-like ions, Journal of Physical Chemistry B 112 (2008) 1685–1692.
[52] V. Bloomfield, DNA condensation, Current Opinion in Structural Biology 6 (1996) 334–341.
[53] J. Urbanija, N. Tomšič, M. Lokar, A. Ambrožič, S. Čučnik, B. Rozman, M. Kandušer, A. Iglič, V. Kralj-Iglič, Coalescence of phospholipid membranes as a possible origin of anticoagulant effect of serum proteins, Chemistry and Physics of Lipids 150 (2007) 49–57.
[54] V. Šuštar, J. Zelko, P. Lopalco, S. Lobasso, A. Ota, N.P. Ulrih, A. Corcelli, V. Kralj-Iglič, Morphology, biophysical properties and protein-mediated fusion of archaeosomes, PLoS ONE 7 (2012) e39401.
[55] V. Kralj-Iglič, Stability of membranous nanostructures: a possible key mechanism in cancer progression, International Journal of Nanomedicine 7 (2012) 3579–3596.

[56] A. Grosberg, T. Nguyen, B. Shklovskii, The physics of charge inversion in chemical and biological systems, Reviews of Modern Physics 74 (2002) 329–345.
[57] R. Netz, Electrostatistics of counter-ions at and between planar charged walls: from Poisson–Boltzmann to the strong-coupling theory, European Physical Journal E 5 (2001) 557–574.
[58] J. Zelko, A. Iglič, V. Kralj-Iglič, S.P.B. Kumar, Effects of counterion size on the attraction between similarly charged surfaces, Journal of Chemical Physics 133 (2010) 204901.
[59] E. Gongadze, A. Velikonja, T. Slivnik, V. Kralj-Iglič, A. Iglič, The quadrupole moment of water molecules and the permittivity of water near a charged surface, Electrochimica Acta 109 (2013) 656–662.
[60] H. Fröhlich, Theory of Dielectrics, Clarendon Press, 1964.
[61] A. Velikonja, Š Perutkova, E. Gongadze, P. Kramar, A. Polak, A. Maček-Lebar, A. Iglič, Monovalent ions and water dipoles in contact with dipolar zwitterionic lipid headgroups – theory and MD simulations, International Journal of Molecular Sciences 14 (2013) 2846–2861.
[62] L. Onsager, Electric moments of molecules in liquids, Journal of the American Chemical Society 58 (1936) 1486.
[63] A. Abrashkin, D. Andelman, H. Orland, Dipolar Poisson–Boltzmann equation: ions and dipoles close to charge interfaces, Physical Review Letters 99 (7) (2007) 077801.
[64] A. Iglič, E. Gongadze, K. Bohinc, Excluded volume effect and orientational ordering near charged surface in solution of ions and Langevin dipoles, Bioelectrochemistry 79 (2010) 223–227.
[65] A. Velikonja, P.B. Santhosh, E. Gongadze, M. Kulkarni, K. Eleršič, Š. Perutkova, V. Kralj-Iglič, N.P. Ulrih, A. Iglič, Interaction between charged or dipolar lipid headgroups and charged nanoparticles mediated by water dipoles and ions, International Journal of Molecular Sciences 14 (8) (2013) 15312–15329.
[66] O. Teschke, G. Ceotto, E. de Souza, Interfacial aqueous solutions dielectric constant measurements using atomic force microscopy, Chemical Physics Letters 326 (2000) 328–334.
[67] O. Teschke, G. Ceotto, E. de Souza, Interfacial water dielectric-permittivity-profile measurements using atomic force microscopy, Physical Review E 64 (2001) 011605.
[68] E. Gongadze, D. Kabaso, S. Bauer, T. Slivnik, P. Schmuki, U. van Rienen, A. Iglič, Adhesion of osteoblasts to a nanorough titanium implant surface, International Journal of Nanomedicine 6 (2011) 1801–1816.
[69] F. Wiegel, P. Strating, Distribution of electrolytes with excluded volume around a charged DNA molecule, Modern Physics Letters B 7 (1993) 483–490.
[70] A. Iglič, V. Kralj-Iglič, Influence of finite size of ions on electrostatic properties of electric double layer, Electrotechnical Review (Slovenia) 61 (1994) 127–133.
[71] V. Lockett, R. Sedev, J. Ralston, M. Horne, T. Rodopoulos, Differential capacitance of the electrical double layer in imidazolium based ionic liquids – influence of potential, cation size, and temperature, Journal of Physical Chemistry C 1124 (2008) 7486–7495.
[72] V. Lockett, M. Horne, R. Sedev, T. Rodopoulosb, J. Ralstona, Differential capacitance of the double layer at the electrode/ionic liquids interface, Physical Chemistry Chemical Physics 12 (2010) 12499–12512.
[73] M.V. Fedorov, N. Georgi, A.A. Kornyshev, Double layer in ionic liquids: the nature of the camel shape of capacitance, Electrochemistry Communications 12 (2010) 296–299.
[74] M.V. Fedorov, A.A. Kornyshev, Towards understanding the structure and capacitance of electrical double layer in ionic liquids, Electrochimica Acta 53 (2008) 6835–6840.
[75] K.B. Oldham, A Gouy–Chapman–Stern model of the double layer at a (metal)/(ionic liquid) interface, Journal of Electroanalytical Chemistry 613 (2008) 131–138.
[76] A.A. Gurtovenko, I. Vattulainen, Effect of NaCl and KCl on phosphatidylcholine and phosphatidylethanolamine lipid membranes: insight from atomic-scale simulations for understanding salt-induced effects in the plasma membrane, Journal of Physical Chemistry B 112 (2008) 1953–1962.
[77] M. Yi, H. Nymeyer, H.X. Zhou, Test of the Gouy–Chapman theory for a charged lipid membrane against explicit-solvent molecular dynamics simulations, Physical Review Letters 101 (2008) 038103.
[78] S. Lee, S. Yuhua, N. Baker, Molecular dynamics simulations of asymmetric NaCl and KCl solutions separated by phosphatidylcholine bilayers: potential drops and structural changes induced by strong Na+-lipid interactions and finite size effects, Biophysical Journal 94 (2008) 3565–3576.
[79] L. Kale, R. Skeel, M. Bhandarkar, R. Brunner, A. Gursoy, N. Krawetz, J. Phillips, A. Shinozaki, Greater scalability for parallel molecular dynamics, Journal of Computational Physics 151 (1999) 283–312.
[80] J. Phillips, R. Braun, W. Wang, J. Gumbart, E. Tajkhorshid, E. Villa, C. Chipot, R. Skeel, L. Kale, K. Schulten, Scalable molecular dynamics with NAMD, Journal of Combinatorial Chemistry 26 (2005) 1781–1802.
[81] T. Dardenn, D. York, L. Pedersen, Particle mesh Ewald: an n·log(n) method for Ewald sums in large systems, Journal of Chemical Physics 98 (1993) 10089.
[82] U. Essmann, L. Perera, M. Berkowitz, The origin of the hydration interaction of lipid bilayers from MD simulation of dipalmitoylphosphatidylcholine membranes in gel and liquid crystalline phases, Langmuir 11 (1995) 4519–4531.
[83] R. Vácha, S.W.I. Siu, M. Petrov, R.A. Böckmann, P.J.J. Barucha-Kraszewska, M. Hof, M. Berkowitz, P. Jungwirth, Effects of alkali cations and halide anions on the DOPC lipid membrane, Journal of Physical Chemistry A 113 (2009) 7235–7243.
[84] R. Vácha, P. Jurkiewicz, M. Petrov, M. Berkowitz, R. Böckmann, J. Barucha-Kraszewska, M. Hof, P. Jungwirth, Mechanism of interaction of monovalent ions with phosphatidylcholine lipid membranes, Journal of Physical Chemistry B 114 (2010) 9504–9509.
[85] P. Jurkiewicz, L. Cwiklik, A. Vojtíšková, P. Jungwirth, M. Hof, Structure, dynamics, and hydration of POPC/POPS bilayers suspended in NaCl, KCl, and CsCl solutions, Biochimica et Biophysica Acta 1818 (2012) 609–616.
[86] J. Urbanija, N. Tomšič, M. Lokar, A. Ambrožič, S. Čučnik, B. Rozman, M. Kandušer, A. Iglič, V. Kralj-Iglič, Coalescence of phospholipid membranes as a possible origin of anticoagulant effect of serum proteins, Chemistry and Physics of Lipids 150 (2007) 49–57.
[87] E. Raspaud, M.O. de la Cruz, J. Sikorav, F. Livolant, Precipitation of DNA by polyamines: a polyelectrolyte behavior, Biophysical Journal 74 (1998) 381–393.
[88] J. Sadar, D. Chan, Long-range electrostatic attractions between identically charged particles in confined geometries and the Poisson–Boltzmann theory, Langmuir 16 (2000) 324–331.
[89] S. Carnie, S. McLaughlin, Large divalent cations and electrostatic potentials adjacent to membranes. A theoretical calculation, International Journal of Molecular Sciences 44 (1983) 325–332.
[90] J. Kirkwood, J. Schumaker, Forces between protein molecules in solution arising from fluctuations in proton charge and configuration, Proceedings of the National Academy of Science 38 (1952) 863–871.
[91] R. Kjellander, Ion-ion correlations and effective charges in electrolyte and macro-ion systems, Berichte der Bunsen-Gesellschaft Physical Chemistry Chemical Physics 100 (1996) 894–904.
[92] F. Oosawa, Interactions between parallel rodlike macro-ions, Biopolymers 6 (1968) 1633–1647.
[93] F. Porcheron, B. Rousseau, M. Schoen, A. Fuchs, Structure and solvation forces in confined alkane films, Physical Chemistry Chemical Physics 3 (2001) 1155–1159.
[94] A. Yodh, K.-H. Lin, J. Crocker, A.D. Dinsmore, R. Verma, P.D. Kaplan, Entropically driven self-assembly and interaction in suspension, Philosophical Transactions: Mathematical, Physical and Engineering Sciences 359 (2001) 921–937.
[95] Y. Mao, M. Cates, H. Lekkerkerker, Depletion force in colloidal systems, Physica A 222 (1995) 10–24.
[96] S. Asakura, F. Oosawa, On interaction between two bodies immersed in a solution of macromolecules, Journal of Chemical Physics 22 (1954) 1255–1256.
[97] K. Bohinc, A. Iglič, S. May, Interaction between macroions mediated by divalent rod-like ions, Europhysics Letters 68 (2004) 494–500.
[98] J. Jackson, Classical Electrodynamics, Wiley and Sons Inc., New York, 1999.
[99] v. Perutková, M. Frank, K. Bohinc, K. Bobojevič, J. Zelko, B. Rozman, V. Kralj-Iglič, A. Iglič, Interaction between equally charged membrane surfaces mediated by positively and negatively charged nanoparticles, Journal of Membrane Biology 236 (2010) 43–53.
[100] M. Hatlo, L. Lue, A field theory for ions near charged surfaces valid from weak to strong couplings, Soft Matter 5 (2009) 125–133.
[101] A.G. Moreira, R.R. Netz, Simulations of counterions at charged plates, European Physical Journal E 8 (2002) 33–58.
[102] G. Tresset, Generalized Poisson–Fermi formalism for investinating size correlation effects with multiple ions, Physical Review E 78 (2008) 061506.
[103] L.B. Bhuiyan, C.W. Outhwaite, Comparison of exclusion volume corrections to the Poisson–Boltzmann equation for inhomogeneous electrolytes, Journal of Colloid and Interface Science 331 (2009) 543–547.
[104] J. Ibarra-Armenta, A. Martín-Molina, M. Quesada-Pérez, Testing a modified model of the Poisson–Boltzmann theory that includes ion size effects through Monte Carlo simulations, Physical Chemistry Chemical Physics 11 (2009) 309–316.
[105] D. Frenkel, B. Smith, Understanding Molecular Simulation, Academic press, San Diego, 1996.
[106] J. Lekner, Summation of Coulomb fields in computer-simulated disordered systems, Physica A 176 (1991) 485–498.
[107] R. Sperb, An alternative to Ewald sums part I: Identities for sums, Molecular Simulation 20 (1998) 179–200.
[108] P. Ewald, Evaluation of optical and electrostatics lattice potentials, Annalen der Physik (Leipzig) 64 (1921) 253–287.
[109] V. Kralj-Iglič, V. Heinrich, S. Svetina, B. Žekš, Free energy of closed membrane with anisotropic inclusions, European Physical Journal B 10 (1999) 5–8.
[110] V. Kralj-Iglič, B. Babnik, D.R. Gauger, S. May, A. Iglič, Quadrupolar ordering of phospholipid molecules in narrow necks of phospholipid vesicles, Journal of Statistical Physics 125 (2006) 727–752.
[111] J. Jorgačevski, N.V.M. Fošnarič, M. Stenovec, M. Potokar, M. Kreft, V. Kralj-Iglič, A. Iglič, R. Zorec, Fusion pore stability of peptidergic vesicles, Molecular Membrane Biology 27 (2010) 65–80.
[112] Š Perutková, M. Frank-Bertoncelj, B. Rozman, M. Fošnarič, V. Kralj-Iglič, A. Iglič, Influence of ionic strength on agglutination of like-charged phospholipid membranes induced by beta2-glycoprotein I – Experimental and theoretical study, Colloids and Surfaces B 111 (2013) 699–706.

E Članek 5: Interactions of Divalent Calcium Ions with Head Groups of Zwitterionic Phosphatidylcholine Liposomal Membranes

Polno ime revije:	Acta chimica Slovenica
Okrajšava:	Acta Chim Slov
ISSN (tiskana izdaja):	1318-0207
Založnik:	Slovensko kemijsko društvo
Naslov založnika:	Slovensko kemijsko društvo, Ljubljana, Slovenija
Pogostost izdaje:	četrtletno
Medij:	tiskana verzija
Spletna stran revije:	http://acta.chem-soc.si/
Prvo leto izdaje:	1993
Faktor vpliva:	1.135 (2012)
Faktor vpliva (5 let):	1.05 (2012)
Naslov članka:	Interactions of Divalent Calcium Ions With Head Groups of Zwitterionic Phosphatidylcholine Liposomal Membranes
Avtorji:	Santhosh, Poornima Budime; Velikonja, Aljaž; Gongadze, Ekaterina; Iglič, Aleš; Kralj-Iglič, Veronika; Poklar Ulrih, Nataša
Izdaja:	61
Številka:	-
Strani:	215–222
Leto objave:	2014
DOI:	-

Acta Chim. Slov. **2014,** *61,* 215–222

Scientific paper

Interactions of Divalent Calcium Ions With Head Groups of Zwitterionic Phosphatidylcholine Liposomal Membranes

Poornima Budime Santhosh,[1] Alja` Velikonja,[2,3] Ekaterina Gongadze,[4] Ale{ Igli~,[4,*] Veronika Kralj-Igli~[4,5] and Nata{a Poklar Ulrih[1,6]

[1] *Department of Food Science and Technology, Biotechnical Faculty, University of Ljubljana, Jamnikarjeva 101, SI-1000 Ljubljana, Slovenia*

[2] *Laboratory of Biocybernetics, Faculty of Electrical Engineering, University of Ljubljana, Tr`a{ka 25, SI-1000 Ljubljana, Slovenia*

[3] *SMARTEH Research and Development of Electronic Controlling and Regulating Systems, Poljubinj 114, SI-5220 Tolmin, Slovenia*

[4] *Laboratory of Biophysics, Faculty of Electrical Engineering, University of Ljubljana, Tr`a{ka 25, SI-1000 Ljubljana, Slovenia.*

[5] *Laboratory of Clinical Biophysics, Faculty of Health Sciences, University of Ljubljana, Zdravstvena 5, SI-1000 Ljubljana, Slovenia*

[6] *Centre of Excellence for Integrated Approaches in Chemistry and Biology of Proteins (CipKeBiP), Jamova 39, 1000 Ljubljana, Slovenia*

** Corresponding author: E-mail: ales.iglic@fe.uni-lj.si*
Tel: (01) 4768 825: Fax: (01) 4768 850

Received: 03-10-2013

Paper based on a presentation at the 4th RSE-SEE 2013 Symposium on Electrochemistry in Ljubljana, Slovenia

Abstract

The interaction of the divalent calcium ions with the zwitterionic lipid membranes was studied by measuring the lipid order parameter which is inversely proportional to the membrane fluidity. Small unilamellar lipid vesicles were prepared from 1-palmitoyl-2-oleoyl-sn-glycero-3-phosphocholine and then treated with different concentrations of divalent calcium ions. An increase in the order parameter and decrease in the fluidity of the liposomal membranes were observed after treatment with the calcium ions. The presence of positively charged iron oxide nanoparticles in the suspension of liposomes negligibly changed the results. The results of experiments were discussed theoretically within modified Langevin-Poisson-Boltzmann (MLPB) model leading to the conclusion that the membrane fluidity and ordering of the membrane lipids are primarily altered by the accumulation of calcium ions in the region of negatively charged phosphate groups within the head groups of the membrane lipids.

Keywords: Anisotropy, liposomes, bilayer fluidity, iron oxide nanoparticles, electric double layer theory

1. Introduction

Liposomes encapsulating nanoparticles (NPs) with magnetic properties termed as "magnetoliposomes" have attracted a great interest in the recent past due to their potential biomedical applications especially in targeted drug delivery,[1] hyperthermia[2] and as contrast agents in magnetic resonance imaging (MRI).[3] Among the magnetic NPs, iron oxide (Fe_2O_3) NPs gains special importance in various clinical applications due to their non-toxicity and biodegradability.[4,5] As the usage of Fe_2O_3 NPs is tremendously increasing in the medical fields, it becomes impor-

tant to study the consequences of interactions of the NPs with the membrane which may alter the physical properties of the bilayer such as fluidity, phase transition temperature, morphology, mechanical stability and permeability.

Membrane fusion is an essential process which accounts for various biological events such as fertilization, embryogenesis, neuronal signalling and endocrine hormone secretion. The fusion process includes inter membrane contact, mixing of the membrane lipids and pore formation to mix the inner lipid contents to form large multilamellar vesicles.[6] Membrane fusion is generally induced *in vitro* and *in vivo* conditions[7, 8] by fusogenic agents called fusogens such as proteins and peptides. Apart from these larger molecules, divalent cations such as Ca^{2+}, Mg^{2+}, $Mn^{2+}$and Zn^{2+} have the potential to induce membrane fusion.[9] Since calcium is known to be an essential biological component and a key player in inducing membrane fusion, we have chosen divalent calcium ions to study their effect on liposomes which serve as a simple model system to understand the complex fusion process in cells.

Membrane fluidity characterizes the viscosity of the lipids in the plasma membrane. The cells maintain the optimal level of fluidity so that the mobility of the lipoproteins in the membrane is large enough to perform different biological functions.[10] Alterations in the fluidity level of the liposomal membranes can be conveniently studied by anisotropy measurements using the fluorescent probes such as 1, 6-diphenyl-1,3,5 hexatriene (DPH) (Fig. 1a).[11] Membrane fluidity can be altered by various factors such as temperature, cholesterol, lipid composition including the hydrocarbon chain length, degree of saturation and interaction of NPs.[12] Since Ca^{2+} interacts with the cell membrane, it induces alterations in the ordering of the membrane lipids and therefore affects the bilayer fluidity. Ca^{2+} may also promote the adhesion and fusion of the adjacent cells/liposomes and therefore mixing of the different lipid components.

A lot of work has been done on the study of the interaction of negatively charged membranes mediated by positively charged calcium ions but very less work was carried on with the zwitterionic liposomes. Hence in this work we intended to study the effect of Ca^{2+} on liposomes prepared with a zwitterionic lipid such as 1-palmitoyl-2-oleoyl-*sn*-glycero-3-phosphocholine (POPC) (Fig. 1b). In order to study the effect of electrostatic interactions of Ca^{2+} with the NPs in detail, we have used in this work the positively charged Fe_2O_3 NPs functionalized with amino groups. Through mathematical modeling using the modified Langevin-Poisson-Boltzmann (MLPB) model of electric double layer, we aim to discuss the theory and the obtained experimental results. The scope of the present study is to gain more knowledge for better understanding of the role of Ca^{2+} (also in the presence of Fe_2O_3 NPs) in altering the membrane lipid bilayer fluidity which is important to consider prior to their biomedical applications.

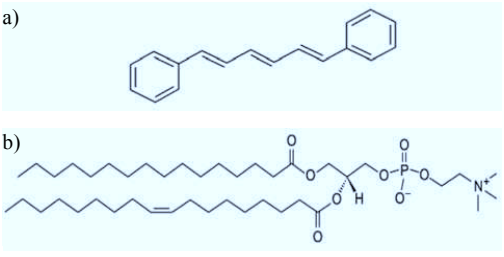

Figure 1. Structure of (a) DPH (1,6-diphenyl-1,3,5-hexatriene) and (b) POPC (1-palmitoyl-2-oleoyl-*sn*-glycero-3-phosphocholine).

2. Materials and Methods

POPC (1-palmitoyl-2-oleoyl-*sn*-glycero-3-phosphocholine) was purchased from Avanti Polar Lipids Inc., USA. DPH (1,6-diphenyl-1,3,5-hexatriene) and anhydrous calcium chloride were obtained from Sigma-Aldrich Chemie GmbH, Steinheim, Germany. All the chemicals obtained have high purity (> 99%) and used without any further purification. Iron oxide amine (Fe_2O_3-NH_2) NPs were obtained from J. Stefan Institute, Ljubljana, Slovenia.

2. 1. Preparation of Small Unilamellar Vesicles

Small unilamellar vesicles (SUVs) were prepared by the thin film method using the rotary evaporator. The POPC lipid (2 mg) was dissolved in 1 ml of chloroform in a round bottomed flask. The argon gas was bubbled through the lipid-chloroform mixture in the flask to avoid the oxidation of lipids. The organic solvent in the flask was slowly evaporated by the rotary evaporator under reduced pressure (1.7 kPa) to obtain a thin lipid film. The control liposomes containing pure POPC lipid were prepared by hydrating the obtained lipid film with double distilled water at pH 5.5. A thin lipid film was prepared in a similar way and hydrated with the Fe_2O_3-NH_2 NPs suspended in distilled water. The hydrodynamic radius of the Fe_2O_3-NH_2 NPs was 180 nm and their zeta potential value was 4 mV respectively.

The lipid suspensions in the flasks were vortexed vigorously with the glass beads for 10 min to obtain multilamellar vesicles (MLVs). The obtained vesicles were sonicated for 30 min total time with 10 s on-off cycles at 40% amplitude using a Vibracell Ultrasonic Disintegrator VCX 750 (Sonics and Materials, Newtown, USA) to form SUVs. In order to remove the debris formed after sonication, the sample containing SUVs were then centrifuged for 10 min at 212554 g (Eppendorf centrifuge 5415C). The SUVs were incubated with appropriate amount of calcium chloride ($CaCl_2$) solution to reach a final concen-

Acta Chim. Slov. **2014,** *61,* 215–222

tration of 10 mM and 100 mM in 2.5 ml of 20 mM HEPES buffer and left for 30 min before measuring the anisotropy values.

2. 2. Fluorescence Anisotropy Measurements

DPH is one of the widely used fluorescent probes for measuring viscosity, lipid order and polarity of the membrane.[13] Being a hydrophobic probe, DPH intercalates between the tail regions of the lipid bilayer and is distributed throughout the membrane. It is almost non-fluorescent in aqueous environment but shows intense fluorescence signals after incorporation into the hydrophobic core of the membrane bilayer.[14]

Temperature dependent anisotropy values were measured following the incorporation of the fluorescent dye DPH in the POPC liposomes treated with divalent calcium ions. The measurements were carried out in a 10 mm-path-length cuvette using the Cary Eclipse fluorescence spectrophotometer (Varian, Mulgrave, Australia). In the quartz cuvette, 10 μL of DPH was added to 2.5 mL 100 μM solutions of SUVs prepared from POPC to reach a final concentration of 0.5 μM DPH. The anisotropy measurements were performed within the temperature range from 15 °C to 50 °C by gradually increasing the temperature by 5 °C for every measurement, with a time interval of 8 min with constant mixing at pH 7.0. Varian autopolarizers having the slit widths with a nominal band-pass of 5 nm was used for both the excitation and emission spectra. The fluorescent probe DPH was excited at 358 nm with the excitation polarizer oriented in the vertical position. The emitted polarized light in both the vertical and horizontal planes were recorded by a monochromator and measured at 410 nm. The anisotropy $\langle r \rangle$ values were measured using the built-in software of the instrument by applying the below formula:

$$\langle r \rangle = \frac{I_{\parallel} - GI_{\perp}}{I_{\parallel} + 2GI_{\perp}}, \quad (1)$$

where $I_{\parallel}$ and $I_{\perp}$ are the parallel and perpendicular emission intensities, respectively. The G-factor value (ratio of the sensitivities of the detection system for vertically [IHV] and horizontally [IHH] polarized light) was determined separately for each sample. The lipid-order parameter S was calculated from the anisotropy values using the following expression:[15]

$$S = \frac{\left[1 - 2\left(\frac{r}{r_0}\right) + 5\left(\frac{r}{r_0}\right)^2\right]^{\frac{1}{2}} - 1 + \frac{r}{r_0}}{2\left(\frac{r}{r_0}\right)}, \quad (2)$$

where r_0 is the fluorescence anisotropy of DPH in the absence of any rotational motion of the probe. The theoretical value of r_0 for DPH is 0.4, while experimental values of r_0 lie between 0.362 and 0.394.[15] In our calculation, the experimental value of r_0 was 0.370 for DPH in POPC at 5 °C.

To conclude, the anisotropy values obtained using DPH are directly proportional to lipid-order parameter (S) in the membrane, which can be calculated using the formula shown in Equation 2. Lipid-order parameter is inversely proportional to the fluidity and hence from the obtained lipid-order parameter results, bilayer fluidity can be estimated.[16]

2. 3. Theoretical Model

2. 3. 1. Pure Salt Solution in Contact With the Zwitterionic Lipid Bilayer

POPC lipid is a common representative of the zwitterionic (dipolar) lipids. Dipolar head group consists of a phosphate (negative) and amino (positive) group in the head region. Due to amphiphilic effect, the negative part of the lipid head group bounded to the lipid tails (phosphate group) is in contact with the salt solution forming negatively charged surface at $x = 0$ (see Fig. 2). The positive part of the lipid head group (amino group) penetrates into the salt solution and can be partially movable inside head group region (see Fig. 2).

In this work the contact of the zwitterionic lipid bilayer (e.g. POPC) with the salt solution containing divalent counter-ions and monovalent co-ions (e.g. $CaCl_2$) is

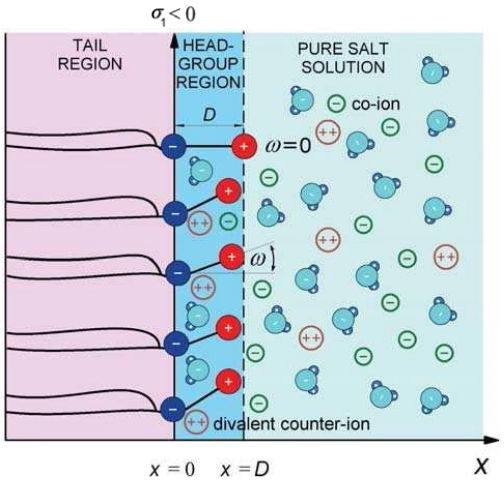

Figure 2. Schematic presentation of zwitterionic lipid bilayer in contact with the salt solution containing monovalent co-ions and divalent counter-ions (e.g. Calcium ions). Phosphate groups in the head group region are described by negatively charged surface at $x = 0$ with negative surface charge density σ_1. D is the distance between the charges in the single lipid head group, while ω describes the orientation angle of the single head group.

theoretically described by using the modified Langevin-Poisson-Boltzmann (MLPB) model.[17–19] The MLPB model takes into account the finite volumes of lipid head groups[17], the cavity field in saturation regime, and the electronic polarization of the water dipoles.[18–23] The finite volume of ions and water molecules in the solution was not taken into the account. Schematic presentation of the model system can be seen in Fig 2.

The Poisson equation describing the system presented in Fig. 2 can be written in the form:

$$\frac{d}{dx}\left[\varepsilon_0\varepsilon_r(x)\frac{d\phi(x)}{dx}\right] = -\rho_{ion}(x) - \rho_{zw}(x), \quad (3)$$

where $\varphi(x)$ is the electric potential, ε_0 is permittivity of the free space, $\varepsilon_r(x)$ is the relative permittivity of the salt solution, $\rho_{ion}(x)$ is the volume charge density of ions in the salt solution and $\rho_{zw}(x)$ is the volume charge density of the positive charges of zwitterionic lipid head groups. In the model the salt solution is composed of calcium chloride ($CaCl_2$) and water. In the water solution the single $CaCl_2$ molecule dissociates into one divalent counter-ion Ca^{2+} and two monovalent co-ions Cl^-, therefore the volume charge density of ions $\rho_{ion}(x)$ can be written as:

$$\rho_{ion}(x) = -e_0 n_-(x) + 2e_0 m(x), \quad (4)$$

where $n_-(x)$ is the number density of Cl^-, $m(x)$ is the number density of Ca^{2+}.and e_0 is the elementary charge. Considering the Bolztmann distribution function for co-ions (Cl^-) and counter-ions (Ca^{2+}):

$$n_- = n_0 e^{+e_0\phi(x)\beta} \quad ; \quad m = m_0 e^{-2e_0\phi(x)\beta}, \quad (5)$$

where n_0 is bulk concentration of monovalent chloride co-ions, m_0 the bulk concentration of divalent calcium counter-ions, $\beta = 1/kT$, kT is the thermal energy. The electro neutrality condition:

$$-n_0 + 2m_0 = 0, \quad (6a)$$

yields

$$n_0 = 2m_0 \ . \quad (6b)$$

Equation 4 can be further rewritten as:

$$\rho_{ion}(x) = -e_0 n_0 e^{+e_0\phi(x)\beta} + 2e_0 m_0 e^{-2e_0\phi(x)\beta} = \\ = -2e_0 m_0\left[e^{+e_0\phi(x)\beta} - e^{-2e_0\phi(x)\beta}\right]. \quad (7)$$

The volume charge density of the positive charges of zwitterionic lipid head groups $\rho_{zw}(x)$ can be expressed as:[17]

$$\rho_{zw}(x) = \frac{e_0 P(x)}{Da_0}, \qquad 0 \le x \le D, \quad (8)$$

where $P(x)$ is the probability density function for angle ω, D is the distance between charges in zwitterionic lipid head group (see Fig. 2) and a_0 is the area per lipid molecule. Inserting the Equation 7 and 8 into Equation 3 yields the Poisson equation in MLPB model:

$$\frac{d}{dx}\left[\varepsilon_0\varepsilon_r(x)\frac{d\phi(x)}{dx}\right] = \\ = 2e_0 m_0\left[e^{e_0\phi(x)\beta} - e^{-2e_0\phi(x)\beta}\right] - \frac{e_0 P(x)}{Da_0}, \quad (9)$$

where the last term in Equation 9 is different from zero only in the region $0 \le x \le D$ and the boundary conditions are:

$$\frac{d\phi}{dx}(x=0) = -\frac{\sigma_1}{\varepsilon_0\varepsilon_r(x=0)}, \quad (10)$$

$$\frac{d\phi}{dx}(x\to\infty) = 0, \quad (11)$$

$$\phi(x=D_-) = \phi(x=D_+), \quad (12)$$

$$\frac{d\phi}{dx}(x=D_-) = \frac{d\phi}{dx}(x=D_+). \quad (13)$$

The surface charge density σ_1 describes the negative surface charge density of the phosphate groups of lipid head groups at $x = 0$: $\sigma_1 = -e_0/a_0$ (see Fig. 2), where a_0 is the area per lipid molecule. Equation 9 was solved by using the standard implemented function for the multiboundary value problems (bvp4c) in Matlab2012b where the values $\varepsilon_r(x)$ and $P(x)$ were calculated in the iteration process outside of bvp4c function. The space dependent permittivity $\varepsilon_r(x)$ within MLPB model is[17,18]:

$$\varepsilon_r(x) = n^2 + \frac{n_{0w}p_0}{\varepsilon_0}\left(\frac{2+n^2}{3}\right)\frac{L(\gamma p_0 E(x)\beta)}{E(x)}, \quad (14)$$

where n is refractive index of water, n_{0w} is bulk concentration of water, p_0 is the dipole moment of water molecule, $L(u) = (\coth(u) - 1/u)$ is the Langevin function, $\gamma = (3/2)((2 + n^2)/3)$ and $E(x)$ is the magnitude (absolute value) of the electric field strength, while the probability density function $P(x)$ (taking into account the finite volumes of lipid head groups) is:[17]

$$P(x) = \Lambda\frac{\alpha e^{-e_0\phi(x)\beta}}{\alpha e^{-e_0\phi(x)\beta} - 1}, \qquad 0 \le x \le D, \quad (15)$$

where α is a model parameter (see also ref. 17) and the value of Λ is calculated in iterative procedure until the normalization condition is met:

$$\frac{1}{D}\int_0^D P(x)dx = 1. \quad (16)$$

2. 3. 2. Positively Charged Nanoparticles Added to Salt Solution

In the case when in the system are present also positively charged NPs (see Fig. 5) the boundary condition described by Equation 11 is replaced by equation:

$$\frac{d\phi}{dx}(x = D_{np}) = -\frac{\sigma_2}{\varepsilon_0 \varepsilon_r (x = D_{np})}, \quad (17)$$

where σ_2 is the surface charge density of nanoparticle located at the distance $x = D_{np}$ from the negatively charged plane in the lipid head group region (see Fig. 5).

2. 3. 3. Osmotic Pressure

Osmotic pressure between the zwitterionic lipid bilayer and nanoparticle can be derived by using the procedure described elsewhere[19] by integrating the Poisson equation (Equation 9 in our case) and subtracting the corresponding bulk osmotic pressure value between the lipid surface and nanoparticle surface located at $x = D_{np}$ (see Fig. 5). To this end, Equation 9 is first rewritten in the form:

$$-\frac{d}{dx}\left[\varepsilon_0 n^2 \frac{d\phi}{dx}\right] - n_{0w} p_0 \left(\frac{2+n^2}{3}\right) \frac{d}{dx} L(\gamma p_0 E(x)\beta) + \\ + 2e_0 m_0 \left(e^{e_0\phi(x)\beta} - e^{-2e_0\phi(x)\beta}\right) - \frac{e_0 P(x)}{Da_0} = 0, \quad (18)$$

where Equation 14 was taken into account. Multiplying equation 18 by $d\varphi = \varphi' dx$ followed by integration leads to:

$$-\frac{1}{2}\varepsilon_0 n^2 E(x)^2 - n_{0w} p_0 \left(\frac{2+n^2}{3}\right) L(\gamma p_0 E(x)\beta) E(x) + \\ + \left(\frac{2+n^2}{3}\right) \frac{n_{0w}}{\gamma\beta} \ln\left[\frac{\sinh(\gamma p_0 E(x)\beta)}{\gamma p_0 E(x)\beta}\right] + \\ + \frac{m_0}{\beta}\left(2e^{e_0\phi(x)\beta} + e^{-2e_0\phi(x)\beta}\right) = const., \quad (19)$$

where the integration of the last term in Equation 18 (with non-zero value only in the region $0 \leq x \leq D$) was omitted since the osmotic pressure was always calculated outside the lipid head group region in the region $x > D$. The osmotic pressure difference $\Pi = \Pi_{inner} - \Pi_{bulk}$ can be therefore written as:

$$\Pi = -\frac{1}{2}\varepsilon_0 n^2 E(x)^2 - E(x)\left(\frac{2+n^2}{3}\right) n_{0w} p_0 L(\gamma p_0 E(x)\beta) + \\ + \left(\frac{2+n^2}{3}\right) \frac{n_{0w}}{\gamma\beta} \ln\left(\frac{\sinh(\gamma p_0 E(x)\beta)}{\gamma p_0 E(x)\beta}\right) + \\ + \frac{m_0}{\beta}(2e^{e_0\phi(x)\beta} + e^{-2e_0\phi(x)\beta} - 3). \quad (20)$$

3. Results and Discussion

The calculated number density profile of divalent calcium counter-ions (m(x)) and monovalent chloride co-ions (n(x)) of the salt solution as a function of the distance x from the negatively charged surface at $x = 0$ for two different bulk concentrations of divalent counter-ions can be seen in Fig. 3. Within the head group region the concentration of counter-ions decreases and the con-

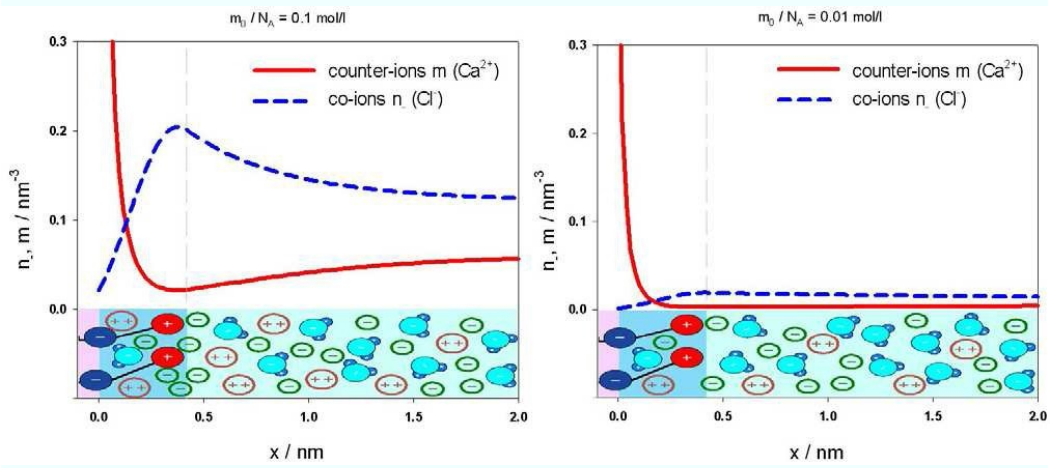

Figure 3. Number density profile of divalent counter-ions (full red line) and monovalent co-ions (dashed blue line) of the salt solution as a function of the distance x from negatively charged surface at $x = 0$ with two different bulk concentration of divalent calcium counter-ions m_0/N_A (0.1 mol/l – left panel and 0.01 mol/l – right panel). Other MLPB model parameters are: the dipole moment of water $p_0 = 3.1$ Debye, $D = 0.42$ nm, T = 298 K, $\sigma_1 = -e_0/a_0$, $a_0 = 0.60$ nm^2, $\alpha = 0.5$, bulk concentration of water $n_{0w}/N_A = 55$ mol/l, where N_A is Avogadro number.

centration of co-ions increases towards the positive charge of the lipid head groups. Near the negatively charged region of the head groups at $x = 0$ there is high accumulation of divalent counter-ions (Ca^{2+}) and the lack of monovalent co-ions (Cl^-). Far away from the zwitterionic lipid surface, concentration of co-ions is two times higher than the concentration of divalent counter-ions in accordance with the electro neutrality condition in the bulk solution (Fig.3).

The lipid-order parameter of POPC SUVs without NPs (Fig. 4A) and SUVs with adhered Fe_2O_3- NH_2 NPs (Fig. 4B) was measured for two different concentrations of Ca^{2+}. In comparison with the control, the lipid-order parameter values were highest after the treatment with $CaCl_2$ (with or without NPs). The initial order parameter values for control SUVs without NPs and SUVs with adhered positively charged Fe_2O_3-NH_2 NPs are nearly the same. Our results indicate that Ca^{2+} played a predominant role in altering the membrane fluidity. As the temperature increased, the order parameter values decreased in all the cases.

The presented experimental results can be interpreted by the calculated (relative) osmotic pressure between the zwitterionic lipid bilayer and the positively charged NPs presented in Fig. 5. At larger distances between the bilayer and the positive nanoparticle the osmotic pressure is practically equal to zero. Osmotic pressure increases with decreasing the distance between the bilayer and positive nanoparticle and practically does not depend on the bulk number density of calcium (m_0). The repulsion between the zwitterionic lipid bilayer and positively charged NPs prevent the positive NPs to interact strongly with the zwitterionic lipid bilayer. As a consequence also the membrane order parameter and fluidity are not expected to be changed by the positively charged NPs. Accordingly, the difference in the measured order parameter values is almost negligible for the control SUVs and Fe_2O_3-NH_2 NPs loaded SUVs (Fig. 4).

In SUVs treated with 10 mM and 100 mM $CaCl_2$ the order parameter is substantially increased, i.e. the fluidity is decreased. This result indicates that the accumulation of divalent calcium in the phosphate group region of the lipid head groups (Fig. 4) strongly influence the membrane order parameter and membrane fluidity. Our theoretical results presented in Fig. 3 also coincides with the results from the literature indicating that the positively charged Ca^{2+} has a strong affinity to accumulate in the region of negatively charged phosphate groups in the head region of the zwitterionic phospholipids, which may influence the fusion of the adjacent vesicles.[24–26] The accumulation of Ca^{2+} in the region of phosphate groups may reduce the repulsion between the neighbouring lipid molecules in the lipid bilayer and in this way reduce the area per lipid molecule and therefore also the membrane fluidity. Boss et al.[27] reported that addition of $CaCl_2$ to the carrot protoplast cell cultures reduced the membrane fluidity and high calcium concentrations dramatically altered the membrane structure and induced phase transition of the membrane lipids. We hypothesize that the accumulation of Ca^{2+} in the region of the negatively charged phosphate groups in the lipid head group region (Fig.3), the mobility of DPH and Fe_2O_3 NPs in the lipid bilayer is affected leading to alterations in the bilayer fluidity.

Ca^{2+} ions may play an important role also in the fusion of vesicle membranes, altering the shape of the vesicles and causes lipid mixing thereby disturbing the ordering of lipids in the membrane bilayer and the bilayer fluidity. The rotational mobility of DPH in the bila-

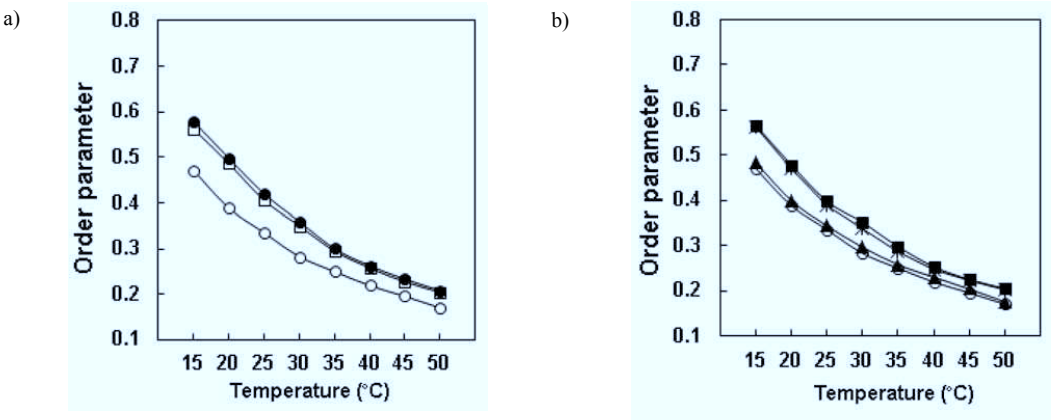

Figure 4. Effect of divalent calcium ions on the lipid-order parameter of zwitterionic POPC liposomes (A) SUVs without NPs (B) SUVs with adhered positively charged Fe_2O_3-NH_2 NPs (o Control – SUVs without NPs; D SUVs with 10 mM $CaCl_2$; - SUVs with 100 mM $CaCl_2$; ▲ SUVs with adhered Fe_2O_3-NH_2 NPs; * NPs loaded SUVs treated with 10 mM $CaCl_2$; - NPs loaded SUVs treated with 100 mM $CaCl_2$). SUVs without NPs were incubated with 10 mM and 100 mM $CaCl_2$ for 30 min before measuring the anisotropy of DPH.

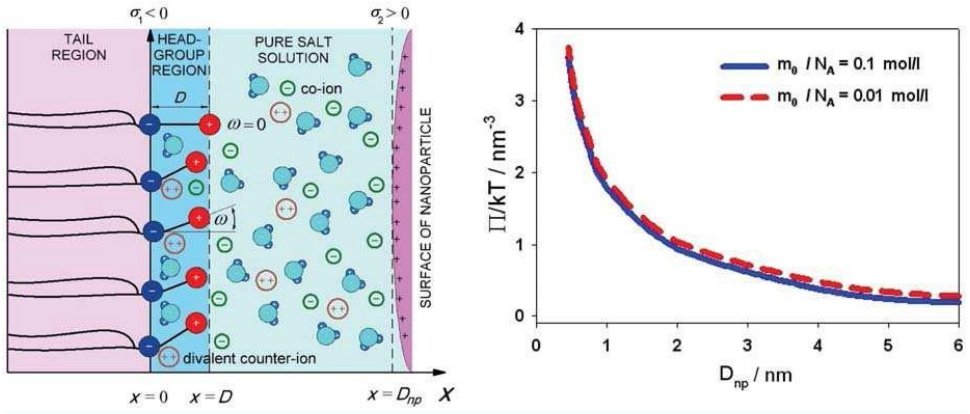

Figure 5: Left: Schematic presentation of the model for studying the interaction between zwitterionic (dipolar) lipid layer and positively charged NPs suspended in salt solution containing monovalent co-ions, and divalent counter-ions (e.g. calcium ions). D_{np} presents the distance of the nanoparticle from negatively charged surface at x = 0. **Right:** Osmotic pressure as a function of the distance (D_{np}) between negatively charged surface at $x = 0$ and positively charged NP ($\sigma_2 = -0.5\sigma_1$) calculated for two bulk concentration of divalent counter-ions (Ca^{2+}): $m_0/N_A = 0.1$ mol/l (full red line) and $m_0/N_A = 0.01$ mol/l (dashed blue line). Osmotic pressure was calculated using MLPB model. Parameter $\alpha = 1$, while all other parameters are the same as in Fig.3.

yer correlates with the ordering of lipids in the membrane. The mobility of the probe in the bilayer is affected by factors such as viscosity, temperature, size and shape of the vesicles. Taking into account of the experimental conditions, the results presented in Fig. 4 could be partially also interpreted on the basis of an increase in the size and shape of the liposomes due to fusion after incubation with Ca^{2+} which is a well-known fusogen. Mishra et al.[28] reported variation in the size and the shape of the zwitterionic phosphotidylcholine liposomal matrix due to the fusion induced by divalent cations such as Ca^{2+} and Mg^{2+}, reduced the membrane fluidity.

4. Conclusions

Our results provide information on the effect of Ca^{2+} on the bilayer fluidity of zwitterionic liposomes. The effect of Ca^{2+} on POPC SUVs adhered with and without Fe_2O_3 NPs bound with positively charged amino group on the membrane fluidity was investigated. The increase in the order parameter values of the SUVs after incubation with calcium ions can be explained by the accumulation of Ca^{2+} in the region of the negatively charged phosphate groups within the lipid head groups as shown in the presented theoretical consideration. Further studies on the influence of divalent cations on the negatively charged liposomes are needed in the future in order to gain more knowledge on the membrane electrostatic interactions, size and stability of the liposomes.

5. Acknowledgements

P.B.S.and E.G. would like to thank the Slovene Human Resources Development and Scholarship Fund for financial support. A.V. was also supported by the European Social Fund and SMARTEH.

6. References

1. A. Marcu, S. Pop, F. Dumitrache, M. Mocanu, C. M. Niculite, M. Gherghiceanu, C. P. Lungu, C. Fleaca, R. Ianchis, A. Barbut, C. Grigoriu, I. Morjan, *Appl. Surf. Sci.* **2013**, *281*, 60–65.
2. J. P. Williams, P. Southern, A. Lissina, H. C. Christian, A. K. Sewell, R. Phillips, Q. Pankhurst, J. Frater, *Int J Nanomedicine*. **2013**, *8*, 2543–54.
3. D. Frascione, C. Diwoky, G. Almer, P. Opriessnig, C. Vonach, K. Gradauer, G. Leitinger, H. Mangge, R. Stollberger, R. Prassl, *Int J Nanomedicine*. **2012**, *7*, 2349–2359.
4. P. B. Santhosh, N. P. Ulrih, *Cancer Lett*. **2013**, *336*, 8–17.
5. H. M. Yang, C. W. Park, P. K. Bae, T. Ahn, B. K. Seo, B. H. Chung, J. D. Kim, *J. Mater. Chem. B.* **2013**, *1*, 3035–3043.
6. S. M. Roy, M. Sarkar, *J. Lipids*. **2011**, 528784, 2011.
7. J. M. Hernandez, A. Stein, E. Behrmann, D. Riedel, A. Cypionka, Z. Farsi, P. J. Walla, S. Raunser, R. Jahn, *Science.* **2012**, *336*, 1581–1584.
8. J. A. Read, R. Duncan, *Methods*. **2011**, *55*, 122–126.
9. Y. H. Wang, S. Dupont, F. Gai, T. Svitkina, P. A. Janmey, *J. Am. Chem. Soc.* **2012**, *134*, 3387–3395.
10. R. Mercier, P. Dominguez-Cuevas, J. Errington, *Cell Rep.* **2012,** *1*, 417–23.

11. V. Sreekanth, A. Bajaj, *J Phys Chem B*. **2013**, *117*, 2123–33.
12. M. A. Casadei, P. Manas, G. Niven, E. Needs, B. M. Mackey, *Appl. Environ. Microbiol*. **2002,** *68,* 125965–5972.
13. A. P. Demchenko, Y. M. G. Duportail, A. S. Klymchenko, *Biophys. J*, **2009**, 3461–3470.
14. B. Aricha, V. Fishov, V. Cohen, N. Sikron, S. Pesakhov, I. Khozin-Goldberg, R. Dagan, N. Porat. *J. Bacteriol*. **2004**, *186*, 4638–4644.
15. H. Pottel, W. Vandermeer, W. Herreman, *Biochim. Biophys. Acta*. **1983**, *730*, 181–186.
16. M. N. Giraud, C. Motta, D. Boucher, G. Grizard, *Hum. Re- prod,* **2000**, *15*, 2160–2164.
17. A. Velikonja, [. Perutkova, E. Gongadze, P. Kramar, A. Polak, A. Ma~ek-Lebar, A. Igli~, *Int. J. Mol. Sci.* **2013,** *14*, 2846–2861.
18. E. Gongadze, U. V. Rienen, V. Kralj-Igli~, A. Igli~, *Gen. Physiol.* Biophys. **2011**, *30*, 130–137.
19. A. Velikonja, P. B. Santhosh, E. Gongadze, M. Kulkarni, K. Eler{i~, [. Perutkova, V. Kralj- Igli~, N. Poklar Ulrih, A. Igli~, *Int. J. Mol. Sci*, **2013,** *14*, 15312–15329.
20. E. Gongadze, U. V. Rienen, A. Iglic, Cell. Mol. Biol. Lett. **2011**, *16*, 576–549.
21. E. Gongadze, A. Iglic*, Bioelectrochemistry,* **2012,** *87*, 199–203.
22. H. Frohlich, Theory of dielectrics, Clarendon Press, Oxford, UK, **1964**.
23. E. Gongadze, A. Velikonja, [. Perutkova, P. Kramar, A. Ma~ek-Lebar, V. Kralj-Igli~, A. Igli~, *Electrochimica Acta*, **2013**, http://dx.doi.org/10.1016/j.electacta.2013.07.147
24. S. Ohnishi, T. Ito, *Biochem Biophys Res Commun*, **1973**, *51,* 132–138.
25. S. Ohnishi, T. Ito, *Biochemistry*, **1974**, *13,* 881–887.
26. D. Papahadjopoulos, *J Coil Interface Sci*, **1976**, *58*, 459–470.
27. W. F Boss, R. L. Mott, *Plant Physiol*. **1980,** *66*, 835–837.
28. R. K. Mishra, G. S. Singhal, *J. Biosci.* **1990**, *3*, 193–197.

Povzetek

Obravnavali smo interakcijo divalentnih kalcijevih ionov z lipidno dvojno plastjo majhnih liposomov, pripravljenih iz elektri~no nevtralnih lipidov 1-palmitoil-2-oleoil-sn-glicero-3-fosfoholina, ki imajo zaradi notranje porazdelitve elektri~nega naboja hidrofilne glave z od ni~ razli~nim elektri~nim dipolnim momentom. Pokazali smo, da pri ve~jih koncentracijah kalcija naraste vrednost ureditvenega parametra membrane, fluidnost membrane liposomov pa se zmanj{a. Prisotnost pozitivno naelektrenih nanodelcev `elezovega oksida v suspenziji liposomov zanemarljivo vpliva na rezultate meritev ureditvenega parametra in fluidnosti lipidne dvojne plasti membrane liposomov. Rezultate eksperimentov smo ovrednotili s pomo~jo modificiranega Langevin-Poisson-Boltzmannovega modela elektri~ne dvojne plasti in pri{li do zaklju~ka, da je izmerjena variacija ureditvenega parametra in fluidnosti lipidne dvojne plasti liposomov predvsem posledica akumulacije kalcijevih ionov v podro~ju negativno naelektrenih fosfatnih skupin v hidrofilnih glavah lipidnih molekul.

F Članek 6: Charge Dependent Capacitance of Stern Layer and Capacitance of Electrode/Electrolyte Interface

Polno ime revije:	International Journal of Electrochemical Science
Okrajšava:	Int. J. Electrochem. Sci
ISSN (elektronska izdaja):	1452-3981
Založnik:	ESG
Naslov založnika:	ESG, Belgrade, Serbia
Pogostost izdaje:	mesečno
Medij:	elektronska verzija
Spletna stran revije:	http://www.electrochemsci.org/
Prvo leto izdaje:	2006
Faktor vpliva:	1.956 (2013)
Faktor vpliva (5 let):	-
Naslov članka:	Charge Dependent Capacitance of Stern Layer and Capacitance of Electrode/Electrolyte Interface
Avtorji:	Velikonja, Aljaž; Gongadze, Ekaterina; Kralj-Iglič, Veronika; Iglič, Aleš;
Izdaja:	9
Številka:	-
Strani:	5885–5894
Leto objave:	2014
DOI:	-

Int. J. Electrochem. Sci., 9 **(2014)** 5885 - 5894

333International Journal of
ELECTROCHEMICAL
SCIENCE
www.electrochemsci.org

Short communication

Charge Dependent Capacitance of Stern Layer and Capacitance of Electrode/Electrolyte Interface

Aljaž Velikonja[1], Ekaterina Gongadze[1], Veronika Kralj-*Iglič*[2] and *Aleš Iglič*[1,*]

[1] Faculty of Electrical Engineering, University of Ljubljana, Tržaška 25, SI-1000 Ljubljana, Slovenia
[2]Faculty of Health Studies, University of Ljubljana, Zdravstvena 5, SI-1000 Ljubljana, Slovenia
[*]E-mail: ales.iglic@fe.uni-lj.si

Received: 2 July 2014 / Accepted: 8 August 2014 / Published: 25 August 2014

The influence of potential dependent relative permittivity of Stern layer on the capacitance of electrode-electrolyte interface is studied theoretically. A decrease of capacitance at larger magnitudes of electrode surface potential is predicted. At large electrode surface potentials the capacitance of metal-electrolyte interface is determined solely by the capacitance of Stern layer, whereas the contribution of the capacitance of diffuse layer is negligible.

Keywords: capacitance, electric double layer, Stern layer, relative permittivity, water ordering

1. INTRODUCTION

When metal electrode comes into contact with electrolyte solution an electric double layer (EDL), composed of charged surface of electrode and counter-ions is created (Figure 1). Counter-ions, i.e. ions with the sign of charge opposite to that of electrode surface, are accumulated at electrode surface, while co-ions, having the same sign of the charge as the electrode metal surface, are depleted from the metal-electrolyte interface. As a consequence the potential difference over the metal-electrolyte interface is generated [1,2]. The drop of electric potential at metal-electrolyte interface occurs mostly in electrolyte [2].

Int. J. Electrochem. Sci., Vol. 9, 2014 5886

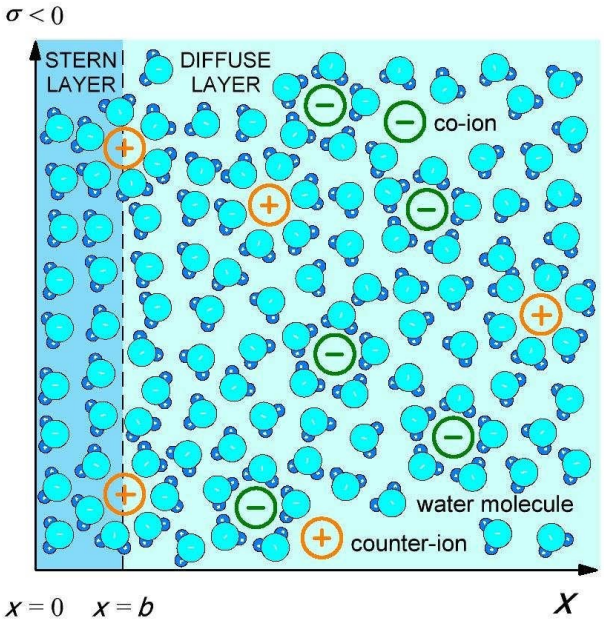

Figure 1. Schematic figure of the Stern layer ($0 \leq x \leq b$) and diffuse electric double layer ($b \leq x \leq \infty$) . Outer Helmholtz plane (OHP) is located at the distance of closest approach (b) which is approximately equal to the hydrated radius of the counter-ions. The water dipoles are oriented within Stern layer as well as around counter-ions and co-ions in the bulk solution. The symbol σ denotes the surface charge density of the metal surface.

Most of the theoretical models of electrolyte solution in contact with charged surface assume that the relative (dielectric) permittivity is constant everywhere in the electrolyte solution [2-7] and do not consider the space dependence of relative permittivity of electrolyte solution near the charged surface [1] . Therefore the classical Gouy-Chapman theory of electric double layer [8,9] has been generalized by taking into account the water polarization in electrolyte solution near the charged surface resulting in spatial decay of relative permittivity in close vicinity of the charged surface [10-16] .

In this work we adopted Stern model [17] as a combination of Gouy-Chapman and Hemholtz models [18] where the outer Helmholtz plane (OHP) define a border between Stern layer and diffuse layer (Figure 1). The relative permittivity of Stern layer is calculated for different values of surface charge density of the metal surface within a simple theoretical model of orientational ordering of water. The total (differential) capacitance of the metal-electrolyte interface (C_{diff}) is calculated using the formula [19]:

$$\frac{1}{C_{diff}} = \frac{1}{C_{DL}} - \frac{1}{C_S} \quad , \tag{1.1}$$

Int. J. Electrochem. Sci., Vol. 9, 2014 5887

assuming that C_{diff} is the capacitance of two capacitors in series, i.e. Stern layer capacitor (C_S) and diffuse layer capacitor (C_{DL}).

2. THEORETICAL MODEL

2.1. Capacitance of metal-electrolyte interface

In the above Equation 1.1 the influence of the final size of molecules is taken into account only by the distance of closest approach (b) (Figure 1) in the first term for the capacitance of Stern layer $C_S = \varepsilon_S \varepsilon_0 / b$. Here ε_0 is the permittivity of the free space and ε_S the electric field dependent relative permittivity of the Helmholtz/Stern layer. The capacitance of the diffuse layer ($x > b$) in the second term (C_{DL}) also depends on the size of molecules, which can be described within different theoretical approaches [20-21,10,11,5]. However, in this work we would like to keep all formulas analytical and simple. To this end C_{DL} is calculated within Gouy-Chapman model for point-like ions[1] from Grahame equation [1,16,19]:

$$C_{DL} = \frac{d\sigma}{d(x-b)} = \sqrt{2\varepsilon e^2 n_r \varepsilon_0 \varepsilon_r} \cosh(\beta e_0 (x-b)/2) \quad (2.1)$$

Hence

$$\frac{1}{C_{diff}} = \frac{b}{\varepsilon_S \varepsilon_0} + \frac{1}{\sqrt{2\varepsilon e^2 n_0 \varepsilon_0 \varepsilon_r}} \frac{1}{\cosh(\beta e_0 (x-b)/2)} \quad (2.2)$$

Here n_0 is the bulk number density of salt ions, e_0 is the unit charge, ε_r is the constant permittivity of diffuse electric double layer in the region $b < x < \infty$ and $\beta = 1/kT$, where kT is the thermal energy.

Close to the charged metallic surface, i.e. for small values of x, the relative permittivity ε_r strongly depends on the distance from the charged metallic surface [10,11,13-16]. For simplicity reasons in this work the permittivity of diffuse layer (for $x > b$) in Equation 2.1 (ε_r) is considered independent on the electric field strength [1,19], while due to strong orientation of water molecules in Stern layer the dependence of relative permittivity of Stern layer (ε_S) on the electric field strength [15] is taken into account. This means that also the capacitance of Stern layer (1st term on the right hand side of the Equation 2.2) depends on the electric field strength.

2.2. Capacitance of Helmholtz/Stern layer

In this subsection we shall first derive the electric field dependence of relative permittivity in Stern layer (ε_S). In the second step the dependence of capacitance of Stern layer $C_S = \varepsilon_S \varepsilon_0 / b$ on the electric field strength will be determined.

Int. J. Electrochem. Sci., Vol. 9, 2014 5888

In the model a single water molecule is considered as the sphere with the point-like rigid (permanent) water dipole located at its centre [13,16]. The permittivity of the sphere is n^2, where $n \approx 1.33$ is the optical refractive index of water [13]. The polarization of water molecules P in Stern layer ($0 \le x \le b$) can be expressed as [13,16]:

$$P(E) = n_{0w} p_0 \left[\frac{2 n^2 + 1}{3} \right] L(p_0 E), \quad (2.3)$$

where n_{0w} is the constant (bulk) number density of water molecules, E is the magnitude of the electric field strength, n^2 is the optical refractive index of water, p_0 is the magnitude of the water external dipole moment, $L(u) = \coth(u) - 1/u$ is the Langevin function and $u = (2 n^2 + 1)/2$. In Stern layer ($0 \le x \le b$) the magnitude of electric field strength E is constant for given σ, therefore also relative permittivity (ε_S) is constant for given σ. The relative permittivity in Stern layer can then be written as (see also [13]):

$$\varepsilon_S = n^2 + \frac{|P|}{\varepsilon_0 E} = n^2 + n_{0w} p_0 \left[\frac{2 n^2 + 1}{3} \right] \frac{L(p_0 E)}{\varepsilon_0 E}, \quad (2.4)$$

and finally the capacitance of Stern layer in the region $0 \le x \le b$:

$$\frac{1}{C_S} = \frac{b}{\varepsilon_0 \left(n^2 + n_{0w} p_0 \left[\frac{2 n^2 + 1}{3} \right] \frac{L(p_0 E)}{E} \right)}. \quad (2.5)$$

For $x \ge b$ we assume constant relative permittivity $\varepsilon_r \approx 78.5$ at room temperature.

2.3. Boundary conditions

The boundary conditions at $x = 0$ and $x = b$ are:

$$\left. \frac{d\varphi}{dx} \right|_{x=0} = -\frac{\sigma}{\varepsilon_S \varepsilon_0}, \quad \varepsilon_S \varepsilon_0 \left. \frac{d\varphi}{dx} \right|_{x=b} = \varepsilon_r \varepsilon_0 \left. \frac{d\varphi}{dx} \right|_{x=b}, \quad \varphi|_{x=b^-} = \varphi|_{x=b}, \quad (2.6)$$

where σ is the surface charge density of the metallic surface at $x = 0$. Due to constant electric field strength in Stern layer $\left. \frac{d\varphi}{dx} \right|_{x=0} = \left. \frac{d\varphi}{dx} \right|_{x=b}$ it follows from Equations 2.6:

$$\left. \frac{d\varphi}{dx} \right|_{x=b} = -\frac{\sigma}{\varepsilon_r \varepsilon_0}. \quad (2.7)$$

The boundary condition 2.7 can be used in the region $b \le x \le \infty$ to solve Gouy-Chapman equation and calculate the value of electric potential $\varphi(x \ge b)$.

3. RESULTS AND DISCUSSION

Boundary condition at $x = 0$ (see Equation 2.6) and Equation 2.4 together yields the non-linear equation for the magnitude of electric field (E) in Stern layer:

$$\varepsilon_0 \varepsilon_S E = n_{0w} p_0 \left[\frac{2n^2 + L(\mu_0 p_0 E / kT)}{n^2} \right] \quad (3.1)$$

Inserting the calculated value of E in Equation 2.4 yields the value of relative permittivity in Stern layer (ε_S) for given surface charge density σ. Figure 2 shows the relative permittivity ε_S as a function of surface charge density σ. It can be seen that ε_S strongly decreases with increasing magnitude of σ, which can be explained by saturation of orientational ordering of water dipoles in strong electric field at large values of σ [16,24,25]. For illustration Figure 3 shows the space dependence of relative permittivity for three different values of σ.

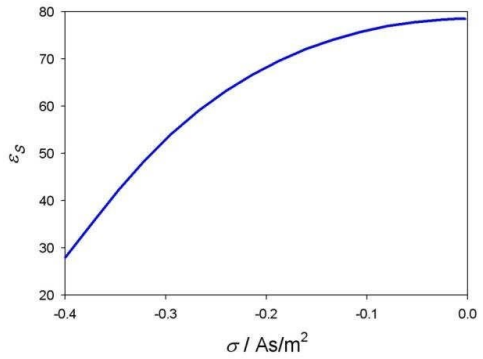

Figure 2. The relative permittivity ε_S in Stern layer $0 \le x \le b$ as a function of the magnitude of the surface charge density of electrode surface (σ). The values of model parameters are : distance of closest approach b = 0.4 nm, p_0 = 3.1 D and concentration of water n_{0w} / N_A = 55 mol/l.

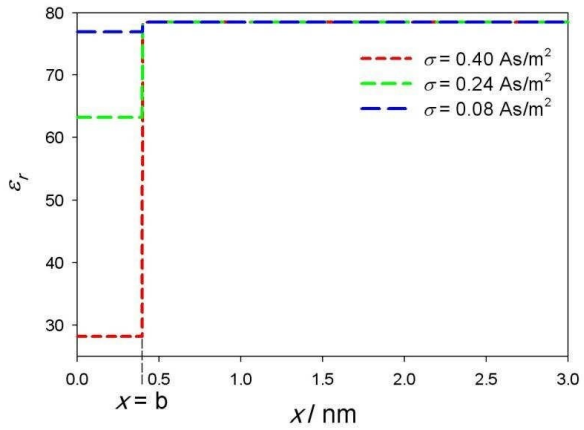

Figure 3. The space dependence of relative permittivity in Stern ($0 \le x \le b$) and diffuse layer ($b \le x \le \infty$) calculated for three values of electrode surface charge density (σ). The values of other parameters are the same as in Figure 2.

Int. J. Electrochem. Sci., Vol. 9, 2014 5890

The electric potential dependence in the diffuse region $b \le x \le \infty$ is calculated from Gouy-Chapman equation [1,3,4]:

$$\frac{d^2\phi}{dx^2} = -\frac{2e_0 n_0}{\varepsilon_r \varepsilon_0} \sinh(e_0 \phi(x)), \quad (3.2)$$

where the volume charge density of electrolyte solution $\rho = -2e_0 n_0 \sinh(e_0 \phi(x))$ is taken into account. To calculate from Equation 3.2 the dependence $\phi(x)$ for $x \ge b$, the boundary condition defined by Equation 2.7 should also be considered.

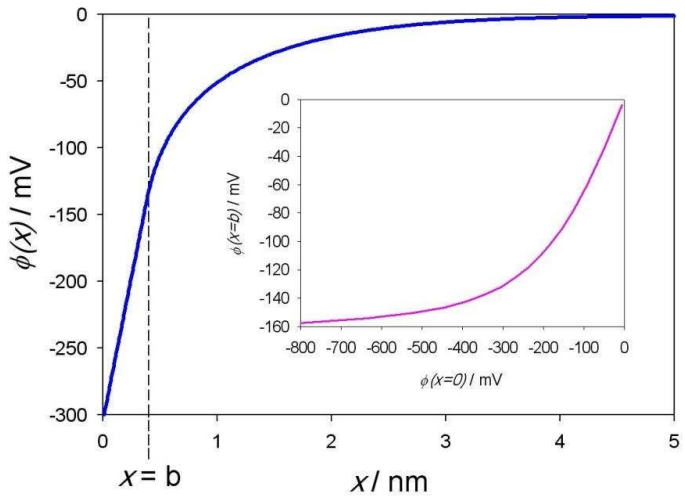

Figure 4. The calculated electric potential $\phi(x)$ as a function of the distance from the charged metallic surface. The model parameters are: surface charge density $\sigma = -0.21\ As/m^2$, bulk concentration of ions $n_0 / N_A = 0.1$ mol/l, distance of closest approach $b = 0.4$ nm, $p_0 = 3.1$ D and concentration of water $n_{0w} / N_A = 55$ mol/l. The inset shows the interdependence between the potentials $\phi(x = b)$ and $\phi(x = 0)$ calculated for different σ.

Figure 4 shows the space dependence of the electric potential $\phi(x)$. The linear space dependence of electric potential in Stern layer $0 \le x \le b$ was determined by integration from the boundary conditions $x = 0$ (first Equation 2.6) and not from Eqution 3.2. The inset in Figure 4 shows the interdependence between electric potentials at $x = 0$ and $x = b$. Note that in Equation 2.1 for capacitance of diffuse layer C_{DL} appears the potential $\phi(x = b)$ [19] and not $\phi(x = 0)$. For better understanding Figure 5 shows also the dependences of the surface potentials $\phi(x = 0)$ and $\phi(x = b)$ on surface charge density σ.

Int. J. Electrochem. Sci., Vol. 9, 2014 5891

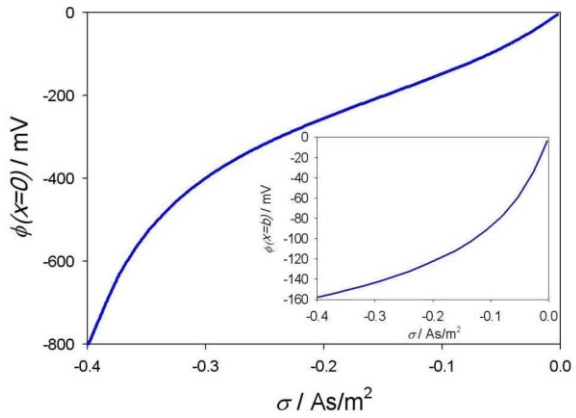

Figure 5. The calculated electric potential $\Delta\phi(x=0)$ as a function of the electrode surface charge density σ. Inset shows the dependence of $\Delta\phi(x=0)$ on σ. The values of model parameters n_0 / N_A, b, p_0 and n_{0w} / N_A are the same as in Figure 4.

Figure 6 shows the capacitances of Stern (C_S) and diffuse layer (C_{DL}) and the total capacitance (C_{diff}) as functions of the surface potential $\Delta\phi(x=0)$. It can be seen in Figure 6 that diffuse layer capacitance C_{DL} increases, while Stern layer capacitance C_S decreases with increasing magnitude of $\Delta\phi(x=0)$. As the capacitance C_{diff} is calculated by Equation 1.1, this explains why at larger magnitudes of surface potential $\Delta\phi(x=0)$ the contribution of C_{DL} to C_{diff} is negligible and $C_{diff} \approx C_S$ as presented in Figure 6.

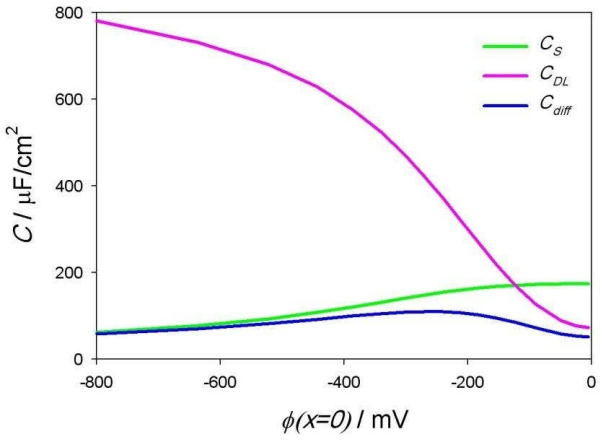

Figure 6. Differential capacitance of Stern (C_S) and diffuse layer (C_{DL}) and the total capacitance (C_{diff}) as a function of the surface potential $\Delta\phi(x=0)$. The values of model parameters n_0 / N_A, b, p_0 and n_{0w} / N_A are the same as in Figure 4.

Int. J. Electrochem. Sci., Vol. 9, 2014 5892

Figure 7 shows the calculated capacitance of electrode-electrolyte interface (C_{diff}) for relative permittivity in Stern layer which depends on surface charge density of electrode ($\varepsilon_S(\sigma)$) , determined as described above, and for the case of constant value of relative permittivity in Stern layer ($\varepsilon_S = 30$). It can be seen that in the first case of $\varepsilon_S(\sigma)$ the capacitance C_{diff} exhibit a maximum and subsequent monotonous decreasing of C_{diff} with increasing magnitude of $\phi(x=0)$. On the contrary, for constant $\varepsilon_S = 30$ there is no maximum in C_{diff} and its decrease at large magnitudes of $\phi(x=0)$. The maximum in dependence of C_{diff} on surface potential $\phi(x=0)$ and decrease of C_{diff} at large magnitudes of $\phi(x=0)$ can be predicted also at constant relative permittivity by taking into account the finite size of ions (volume excluded effect) within Bikerman model [6,16,23]. In accordance, it was shown recently [16], that combination of volume excluded effect [20] and space dependence of relative permittivity in electrolyte solution [13] predict stronger decrease of C_{diff} at large magnitudes of $\phi(x=0)$ as predicted within pure Bikerman model .

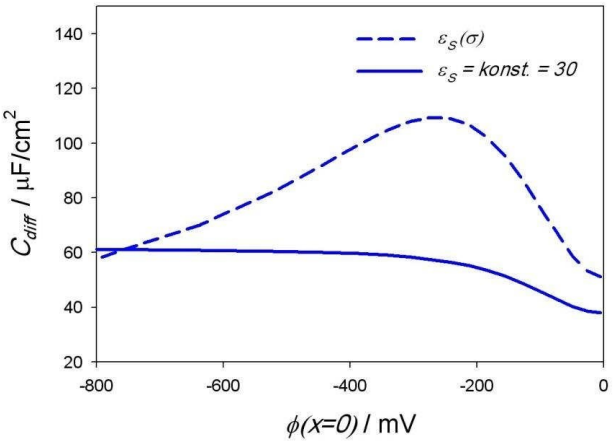

Figure 7. Differential capacitance of metal-electrolyte interface (C_{diff}) as a function of the surface potential $\phi(x=0)$ for the case voltage/surface charge dependent relative permittivity of Stern layer (Figures 2 and 3) and constant permittivity in Stern layer. The values of the model parameters are the same as in Figure 4.

4. CONCLUSIONS

Water is one of the most important molecules in biological systems [26]. In this work we attempt to uncover the relation between the electric potential dependent orientational ordering of water molecules in Stern layer and the capacitance of metal electrode-electrolyte interface. In order to keep our theory analytical and appropriate for analysis of experimental results as much as possible the finite volume of molecules was taken into account by the distance of closest

approach only. In addition, also the transport phenomena in Stern and diffuse layers [27] are totally neglected . To this end the influence of conductivity of diffuse layer on the capacitance of Stern layer can not be described within the presented model.

Obtaining the charge/potential dependence of relative permittivity in Stern layer, the capacitance of electrode-electrolyte interface as a function of electrode charge/potential is calculated. A decrease of capacitance at larger magnitudes of electrode surface potential is predicted. It is also shown that at large electrode surface potentials the capacitance of metal-electrolyte interface is determined solely by the capacitance of Stern layer, whereas the contribution of the capacitance of diffuse layer becomes negligible.

ACKNOWLEDGEMENTS
This work was in part supported by the Slovenian Research Agency (ARRS).

References

1. H. Butt, K. Graf and M. Kappl, Physics and Chemistry of Interfaces, Wiley-VCH, Weinheim (2003).
2. W. Schmickler and E. Santos, Interfacial Electrochemistry, Springer, Heidelberg (2010).
3. S. McLaughlin, Annual Review of Biophysics and Biophysical Chemistry, 18 (1989) 113-136.
4. G. Cevc, Biochimica et Biophysica Acta, 1031 (1990) 311–382.
5. V. Kralj-Iglič and A. Iglič, Journal of Physics II, 6 (1996) 477–491.
6. M.Z. Bazant, M.S. Kilic, B. Storey and A. Ajdari, Advances in Colloid and Interface Science, 152 (2009) 48-88.
7. I. Bivas and Y.A. Ermakov, Advances in Planar Lipid Bilayers and Liposomes 5 (2007) 313–343.
8. M.G. Gouy, Journal de Physique et Le Radium (France), 9 (1910) 457-468.
9. D.L. Chapman, Philosophical Magazine, 25 (1913) 475-481.
10. C.W. Outhwaite, Molecular Physics, 31 (1976) 1345–1357.
11. C.W. Outhwaite, Molecular Physics, 48 (1983) 599–614.
12. T. Nagy, D. Henderson and D. Boda, Journal of Physical Chemistry B, 115 (2011) 11409–11419.
13. E. Gongadze and A. Iglič, Bioelectrochemistry, 87 (2012) 199–203.
14. R. Misra, S. Das and S. Mitra, Journal of Chemical Physics, 138 (2013) 1147
15. E. Gongadze and A. Iglič, Acta Chimica Slovenica, 61 (2014) 241–245.
16. E. Gongadze, A. Velikonja, Š. Perutkova, P. Kramar, A. Maček-Lebar, V. Kralj-Iglič and A. Iglič, Electrochimica Acta, 126 (2014) 42-60.
17. O. Stern, *Zeitschrift für Elektrochemie*, 30 (1924) 508-516.
18. H. Helmholtz, Annals of Physics, 7 (1879) 337-382.
19. V. Lockett, M. Horne, R. Sedev, T. Rodopoulos and J. Ralston, Physical Chemistry Chemical Physics, 12 (2010) 12499–12512.
20. J. Bikerman, Philosophical Magazine, 33 (1942) 384–397.
21. T. Grimley and N. Mott, Discussions of the Faraday Society, 1 (1947) 3–11.
22. M. Eigen and E. Wicke, Journal of Physical Chemistry, 58 (1954) 702–714.
23. A. A. Kornyshev, Journal of Physical Chemistry B, 111 (2007), 5545-5557.
24. F. Booth, Journal of Chemical Physics, 19 (1951) 391-394.
25. H. Fröhlich, Theory of Dielectrics, Clarendon Press, Oxford (1964).

26. Z. Arsov, M. Rappolt and J. Grdodolnik, ChemPhysChem, 10 (2009) 1438–1441.
27. H. Wang and L. Pilon, Electrochimica Acta, 64 (2012) 130– 139.